UNIVERSITÀ DEGLI STUDI DI PADOVA
Dipartimento di Scienze Biomediche Sperimentali

Scuola di Dottorato di Ricerca in Bioscienze
Indirizzo Biologia Cellulare
Ciclo XX

From mitochondrial morphology to apoptosis: Genetic analysis of OPA1 function and regulation

Direttore della Scuola: Ch.mo Prof. Tullio Pozzan
Supervisore: Ch.mo Prof. Luca Scorrano

Dottoranda: Sara Cipolat

31 gennaio 2008

Table of contents:

1. Riassunto dell'attività svolta

I mitocondri svolgono un ruolo fondamentale nella fisiopatologia delle cellule eucariote: producono gran parte dell'energia necessaria per le reazioni endoergoniche (Danial et al., 2003) e partecipano attivamente ad importanti vie di traduzione del segnale, dall'apoptosi (Rizzuto et al., 2000) all'omeostasi del Ca^{2+} (Rizzuto et al., 2000). La versatilità funzionale di questi organelli è rispecchiata dalla loro complessità strutturale (Griparic and van der Bliek). A livello ultrastrutturale, i mitocondri possono essere divisi in tre compartimenti: matrice, spazio intermembrana e *cristae,* strutture pleomorfe, a sacchetto, connesse ad uno spazio intermembrana estremamente assottigliato tramite una stretta giunzione tubulare del diametro di circa 20 nm (Frey and Mannella, 2000). Inoltre, nel citoplasma i mitocondri possono esistere come un reticolo molto interconnesso di organelli fusi tra loro, oppure possono esistere come singole entità tra loro distinguibili. La forma del reticolo mitocondriale e la struttura interna dei singoli mitocondri è determinata dall'equilibrio fra eventi di fusione e fissione. Tali processi sono finemente regolati da numerose proteine, tra cui le proteine simili a dinamine. Il loro ruolo nel controllo della morfologia mitocondriale è stato identificato inizialmente nel lievito, dove la delezione di specifiche dinamine mitocondriali esita in alterazioni del reticolo mitocondriale e quindi in anomalie funzionali come perdita del DNA mitocondriale, difetti di proliferazione cellulare e generazione di ceppi *petite* (Dimmer et al., 2002; Shaw and Nunnari, 2002). Le dinamine sono meccanoenzimi, ubiquitari, ad elevato peso molecolare, che idrolizzano il GTP per regolare fusione, tubulazione e vescicolazione delle membrane (McNiven et al., 2000). Nei mammiferi la fissione del reticolo mitocondriale è regolata da Drp-1 (Smirnova et al., 2001) che trasloca dal citosol alla membrana mitocondriale esterna dove interagisce durante la fissione attraverso l'adattatore specifico FIS1 (Yoon et al., 2003) (James et al., 2003), La fusione mitocondriale è regolata dalla mitofusina-1 (MFN1) e mitofusina-2 (MFN2), proteine integrali della membrana mitocondriale esterna (Rapaport et al., 1998). Più recentemente è stata caratterizzata una proteina localizzata nella membrana mitocondriale interna, OPA1, mutata in individui affetti da atrofia ottica dominante, una malattia genetica caratterizzata da perdita delle cellule gangliari retiniche e atrofia del nervo ottico (Alexander et al., 2000; Delettre et al., 2000).
Scopo del mio progetto di Dottorato è stato la generazione, l'utilizzo ed in seguito l'analisi di modelli genetici per comprendere e caratterizzare la funzione biologica di OPA1, così come la sua regolazione funzionale.
Per comprendere la funzione biologica di OPA1, abbiamo utilizzato approcci genetici e di visualizzazione di immagini di microscopia confocale per analizzare il suo ruolo nella regolazione dell'equilibrio tra i processi di fusione e fissione mitocondriali.
Fibroblasti embrionali di topo (cellule MEFs) sono stati trasfettati con una variante spettrale della *green fluorescent protein*, la *cyan fluorescent protein* (mtCFP) specificatamente diretta ai mitocondri. La visualizzare in microscopia confocale della morfologia mitocondriale in stato

stazionario di queste cellule ha rivelato che i mitocondri appaiono singoli e separati, di forma bastoncellare o rotondeggiante, con una lunghezza media di 3±0.34 μm lungo l'asse maggiore. L'analisi morfometrica del reticolo mitocondriale ha confermato queste osservazioni: solo il 23% delle cellule analizzate presentavano mitocondri allungati, cioè nelle quali più del 50% dei mitocondri hanno una lunghezza media maggiore di 5 μm ed un indice di rotondità minore di 0.5. In cellule co-trasfettate con OPA1 e mtCFP i mitocondri apparivano come strutture tubolari allungate, interconnesse e ramificate a formare un reticolo. L'analisi morfometrica ha confermato la capacità di OPA1 di indurre allungamento del reticolo mitocondriale; infatti, più del 50% delle cellule che sovraesprimevano OPA1 presentavano mitocondri allungati. Abbiamo inoltre analizzato gli effetti di mutazioni patogenetiche di OPA1 sulla forma del reticolo mitocondriale. Abbiamo introdotto due mutazioni in OPA1: una mutazione *missense* nel dominio GTPasico, che riduce l'attività GTPasica di più dell'80%, (K301AOPA1) (Misaka et al., 2002) ed una mutazione *nonsense* nel dominio C-terminale, che elimina la regione *coiled-coil*, richiesta per le interazioni proteina-proteina (R905stopOPA1). Mitocondri di cellule MEFs trasfettate con entrambi i mutanti erano isolati, piccoli e rotondeggianti, indicando che OPA1 richiedeva un dominio GTPasico e *coiled coil* terminale funzionali per indurre allungamento del reticolo mitocondriale. Per studiare gli effetti di una diminuzione dei livelli di espressione di OPA1 sulla forma del reticolo mitocondriale abbiamo generato e selezionato cloni di cellule MEFs che stabilmente esprimessero un plasmide codificante per uno *short hairpin* diretto contro la sequenza di OPA1. I mitocondri delle cellule in cui OPA1 era stato silenziato apparivano rotondeggianti e frammentati quando comparati ai mitocondri allungati e bastoncellari dei cloni di controllo. La tubulazione indotta da OPA1 non era il risultato di una semplice giustapposizione di mitocondri, ma rappresentava un vero e proprio aumento di fusione mitocondriale, come indicato da saggi specifici di fusione in eteropolicarii generati per fusione indotta da PEG. L'espressione di OPA1 accelerava in modo significativo il mescolamento del contenuto della matrice, mentre la diminuzione dei suoi livelli di espressione riduceva la fusione mitocondriale.

Studi condotti nel lievito *S. cerevisiae* avevano dimostrato che Mgm1p, l'ortologo di OPA1, partecipa ad un complesso multiproteico che comprende anche Fzo1p (l'ortologo delle mitofusine). Abbiamo quindi voluto esplorare se OPA1 esercitasse la sua funzione in maniera autonoma o se necessitasse di altre proteine mitocondriali. Per capire se la fusione mitocondriale indotta da OPA1 dipendesse dalle mitofusine, abbiamo utilizzato un approccio genetico nel quale abbiamo sovraespresso OPA1 in cellule MEFs prive della *Mfn1* o *Mfn2*. OPA1 promuoveva tubulazione e fusione del reticolo mitocondriale in cellule wt e *Mfn2*$^{-/-}$, ma non in cellule *Mfn1*$^{-/-}$. Tale difetto era complementato dalla reintroduzione della MFN1, ma non della MFN2, identificando in maniera inequivocabile la MFN1 come un partner essenziale per la funzione mediata da OPA1. Inoltre, l'espressione di MFN2, ma non di MFN1 causava fusione

mitocondriale anche in cloni con bassi livelli di OPA1, indicando quindi una differenza funzionale fra le due mitofusine. Quindi OPA1 e MFN1 erano funzionalmente dipendenti l'una dall'altra. Per capire se cellule MEFs *Mfn1*$^{-/-}$ presentassero difetti a livello degli eventi preparatori della fusione, come la giustapposizione e l'ancoraggio, abbiamo condotto esperimenti di microscopia confocale a quattro dimensioni, cioè acquisendo nel tempo ricostruzioni tridimensionali del reticolo mitocondriale. Il numero totale di contatti tra mitocondri non era modificato né dall'espressione di OPA1, né dall'ablazione della MFN1. OPA1 facilitava il processo di fusione che seguiva il contatto tra mitocondri di cellule *wt* e *Mfn2*$^{-/-}$, ma non in cellule *Mfn1*$^{-/-}$. I nostri dati suggeriscono che OPA1 richiede la MFN1 per indurre fusione delle membrane di due mitocondri giustapposti e non per aumentare il numero e la frequenza di contatti inter-mitocondriali. Nel loro complesso questi risultati hanno evidenziato per la prima volta una differenza funzionale fra le due mitofusine, suggerendo l'esistenza di un asse funzionale tra OPA1 e MFN1(Cipolat et al., 2004).

La scoperta che OPA1 era una proteina pro-fusogena ha aperto nuove domande sulla sua capacità di partecipare alla regolazione dell'apoptosi, durante la quale la fusione mitocondriale è alterata. Abbiamo quindi deciso di differenziare il ruolo di OPA1 in fusione e apoptosi. Abbiamo dimostrato che OPA1 svolge un'attività antiapoptotica, controllando il processo di rimodellamento delle *criste* in corso di apoptosi e che questa funzione era indipendentemente dalla sua capacità di indurre fusione mitocondriale. OPA1 non interferiva con l'attivazione delle vie essenziali di apoptosi, come l'attivazione di BAX e BAK. OPA1 era però in grado di inibire il rilascio di citocromo *c*, prevenendo il rimodellamento delle *cristae* e la ridistribuzione del citocromo *c* stesso. Mutazioni che inattivavano il dominio GTPasico della proteina, alteravano la sua attività antiapoptotica aumentando la scuscettibilità all'apoptosi indotta da stimoli che utilizzano la via mitocondriale di morte.

I nostri risultati hanno contribuito a chiarire la funzione biologica di OPA1, ma, allo stesso tempo, hanno lasciato aperte numerose domande. In particolare, dal momento che attività di fusione mitocondriale e di protezione dall'apoptosi risultavano essere tra loro indipendenti, come potevano essere controllate?

Era stato precedentemente dimostrato che in lievito la proteasi di tipo romboide, localizzata nella IMM, Rbd1/Pcp1p taglia Mgm1p e genera una forma più corta della proteina, che risulta essere la forma attiva nella regolazione della forma mitocondriale (Herlan et al., 2003; McQuibban et al., 2003). Ci siamo quindi chiesti se PARL, l'ortologo di mammifero di Rbd1p, fosse ugualmente in grado di regolare le funzioni biologiche di OPA1, cioè la sua capacità di indurre fusione mitocondriale e la sua attività antiapoptotica. Per rispondere a queste domande abbiamo deciso di caratterizzare il fenotipo del modello murino di delezione di *Parl*. Il topo *Parl*$^{-/-}$ nasceva in normali rapporti mendeliani e si sviluppava in modo normale fino alla quarta settimana di vita. Successivamente il topo manifestava ritardo nella crescita e atrofia di vari

organi, in particolare timo, milza e muscoli e moriva per cachessia generale tra l'ottava e la dodicesima settimana di vita. L'atrofia di timo, milza e muscoli dei topi *Parl*$^{-/-}$ era causata da massiva apoptosi di linfociti timici T doppi positivi ($CD4^{+}CD8^{+}$), splenici B ($B220^{+}$) e mioblasti, rispettivamente. Abbiamo successivamente analizzato in che modo disfunzionalità mitocondriale e disregolazione della morfologia potessero contribuire all'atrofia multisistemica del modello murino di *Parl*. PARL non era richiesta per una normale funzionalità mitocondriale: mitocondri privi di *Parl* non presentavano disfunzione mitocondriale latente né difetti respiratori in epatociti, MEFs, e colture primarie di mioblasti e miotubi. Inoltre PARL non era richiesta per il mantenimento della forma e fusione mitocondriali, anche in tessuti molto colpiti dall'assenza della proteasi come i muscoli. Inoltre PARL non era richiesta per regolare la funzione profusogena di OPA1. Ci siamo quindi chiesti se PARL fosse in grado di regolare l'apoptosi analizzando la risposta di cellule MEFs dopo trattamento con vari stimoli che utilizzano la via mitocondriale di morte. MEFs *Parl*$^{-/-}$ manifestavano un'aumentata suscettibilità all'apoptosi indotta da stimoli intrinseci rispetto alle cellule *wt*. La reintroduzione di PARL cataliticamente attiva ha dimostrato che il difetto era specifico. PARL svolgeva la sua funzione a livello mitocondriale: in assenza di *Parl* il rilascio di citocromo *c* e la disfunzione mitocondriale ad esso associata avvenivano prima. PARL non alterava i meccanismi molecolari fondamentali dell'apoptosi, come l'attivazione di BAX e BAK. PARL era invece richiesta per controllare il rimodellamento delle *cristae* e prevenire la mobilizzazione del citocromo *c* durante l'apoptosi, come abbiamo confermato analizzando immagini di microscopia elettronica a trasmissione. Questi risultati suggerivano un possibile ruolo di PARL nella via di rimodellamento delle *cristae*, regolata da OPA1; a questo punto era naturale chiedersi se PARL fosse in grado di regolare l'attività antiapoptotica di OPA1. La sovra-espressione di OPA1 era in grado di proteggere dall'apoptosi le cellule *wt*, ma non quelle *Parl*$^{-/-}$: inoltre l'espressione di OPA1 in cellule *Parl*$^{-/-}$ non riduceva il rilascio di citocrome *c*, né la depolarizzazione mitocondrale associata, dopo trattamento con stimoli apoptotici intrinseci. L'espressione di PARL in cellule MEFs *Parl*$^{-/-}$ in cui fosse stato silenziato il gene *Opa1* non permetteva di ripristinare la normale suscettibilità alla morte cellulare programmata. PARL era quindi situato a monte rispetto a OPA1 nella via di controllo dell'apoptosi. Questa interazione genetica è stata successivamente confermata a più livelli: OPA1 e PARL interagivano in saggi *yeast two-hybrid* e esperimenti di co-immunoprecipitazione. PARL era richiesta per produrre una forma solubile, rilasciata nello spazio intermembrana di OPA1. L'attività catalitica di PARL era richiesta per un'efficiente produzione di tale forma solubile. L'espressione di questa forma solubile di OPA1, indirizzata allo spazio intermembrana, proteggeva cellule *Parl*$^{-/-}$ dall'apoptosi, senza avere peraltro attività fusogena (Cipolat et al., 2006). Abbiamo successivamente dimostrato che la forma di OPA1 integrale di membrana e quella solubile localizzata nello spazio intermembrana partecipano nella formazione di oligomeri ad elevato peso molecolare, che sono precocemente distrutti

durante il processo di rimodellamento delle *cristae*. La diminuzione dell'entità di tali oligomeri in cellule *Parl*$^{-/-}$ spiegherebbe il più veloce rimodellamento e la maggior mobilizzazione di citocromo *c* osservati in assenza della proteasi (Frezza et al., 2006).

OPA1 controlla funzioni cellulari complesse oltre all'apoptosi, come è stato dimostrato in studi che mostrano come la sovraespressione di OPA1 controlla il movimento di leucociti (Campello et al., 2006) e la formazione di spine dendritiche (Li et al., 2004). Inoltre modelli *knock out* di *Opa1* mostrano che OPA1 è richiesta per un corretto sviluppo embrionale. Mutanti omozigoti di *Opa1* muoiono in utero 13.5 *dpc* ed i primi segni di ritardo nello sviluppo sono già presenti a 8.5 *dpc* (Alavi et al., 2007; Davies et al., 2007). Ci siamo quindi chiesti se i livelli di epsressione di OPA1 fossero in grado di regolare sviluppo e funzionalità di vari organi, modulando la fusione o l'apoptosi mitocondriali. Nell'ultima parte di questa Tesi, ci siamo dedicati allo studio degli effetti dell'ablazione di OPA1 sul differenziamento di cellule embrionali staminali di topo in vitro, utilizzando il metodo della goccia pendente. A questo scopo abbiamo analizzato una linea di cellule ES dove *Opa1* è stata *gene-trapped*, dando origine ad un fenotipo eterozigote. Abbiamo confrontato la capacità di cellule *Opa1*^{gt} rispetto alle relative *wt* di differenziare in cardiomiociti e neuroni. Cellule *Opa1*^{gt} presentavano una diminuita capacità di differenziare in cardiomiociti pulsanti, mentre mantenevano un normale differenziamento neuronale. Questi risultati preliminari indicano che OPA1 è un buon candidato per la regolazione del differenziamento di cellule staminali embrionali in vitro. Vogliamo ora comprendere quali sono i meccanismi molecolari attraverso i quali OPA1 influenza il differenziamento di cellule staminali embrionali in cardiomiociti.

In conclusione, i dati presentati in questa Tesi dimostrano che OPA1 svolge due funzioni geneticamente distinte tra loro nel controllare la forma del reticolo mitocondriale e l'apoptosi. L'individuazione che l'asse funzionale tra OPA1 e la MFN1 (che regola la fusione mitocondriale) e il meccanismo di regolazione nella IMM, che comprende la coppia substrato-proteasi OPA1-PARL, potrebbero anche controllare il differenziamento embrionale, ha aperto nuove, inaspettate strade, che permetteranno di meglio comprendere il ruolo dei mitocondri nella vita e nella morte della cellula.

2. Summary

Mitochondria are essential organelles for life and death of the cell: they produce most of the cellular ATP (Danial et al., 2003), regulate cytosolic Ca^{2+} signalling (Rizzuto et al., 2000), and integrate and amplify different apoptotic stimuli (Green and Kroemer, 2004). Such a functional versatility is matched by a complex and dynamic morphology, both at the ultrastructural and at the cellular level (Griparic and van der Bliek). At the ultrastructural level, the mitochondrial *cristae* constitute a separate compartment connected to the thin intermembrane space by narrow tubular junctions (Frey and Mannella, 2000). In the cytosol, mitochondria are organized in a network of individual organelles that dynamically fuse and divide. Mitochondrial morphology results from the equilibrium between fusion and fission processes, controlled by a family of "mitochondria-shaping" proteins, many of which are dynamin-related proteins initially identified by genetic screens in buddying yeast (Dimmer et al., 2002; Shaw and Nunnari, 2002). Dynamins are ubiquitous mechano-enzymes that hydrolyze GTP to regulate fusion, fission, tubulation and elongation of cellular membranes (McNiven et al., 2000). In mammalians, mitochondrial fission is controlled by a cytosolic dynamin related protein DRP-1 (Smirnova et al., 2001) that translocates to sites of mitochondrial fragmentation where it binds to FIS1, its adapter in the outer membrane (Yoon et al., 2003) (James et al., 2003). Fusion is controlled by mitofusin-1 (MFN1) and-2 (MFN2), two large GTPases of the outer mitochondrial membrane, orthologues of *S. cerevisiae* Fzo1p (Rapaport et al., 1998). OPA1, the mammalian homologue of *S. cerevisiae* Mgm1p, is the only dynamin-related protein of the inner mitochondrial membrane (Olichon et al., 2002). Loss-of-function or dominant-negative mutations in *Opa1* are associated with autosomal dominant optic atrophy (DOA), the leading cause of inherited optic neuropathy, characterized by retinal ganglion cells degeneration followed by ascending atrophy of the optic nerve (Alexander et al., 2000; Delettre et al., 2000).

The aim of my PhD has been to generate, use and analyze genetic models in order to unravel the biological function of OPA1 as well as its regulation.

In order to dissect the biological function of OPA1, we undertook a combination of genetics and imaging to address its role in regulating mitochondrial fusion/fission equilibrium. Imaging of *wild type* mouse embryonic fibroblasts (MEFs) cotransfected with a mitochondrially targeted cyan fluorescent protein (mtCFP) showed mitochondria as individual organelles, rod or round-shaped, with an average length of 3±0.34 μm along their major axis. Morphometric analysis confirmed that only 23% of the analyzed cells displayed elongated mitochondria, *i.e.* cells with axial length >5 μm and roundness index <0.5 in more than 50% of mitochondria. Cotransfection of OPA1 with mtCFP induced visible changes in the shape of the mitochondrial reticulum. The rod-shaped mitochondria appeared now to be interconnected in a branched network. Morphometric analysis confirmed this mitochondria-shaping effect of OPA1, with more than 50% of the cells analyzed showing elongated mitochondria. Furthermore, we analyzed the effect of

pathogenic mutations of OPA1 on its ability to elongate mitochondria. A missense mutation in the GTPase domain (K301A) that reduces the GTPase activity of more than 80%, as well as a truncative one in the coiled coil domain (R905stop), which eliminates the C-terminal coiled-coil domain required in protein-protein interactions, abolished the ability of OPA1 to elongate mitochondria, indicating that it requires a functional GTPase and coiled-coil domain.

To address the effect of reduced OPA1 levels on mitochondrial morphology we turned to stable, plasmid-generated RNA interference (RNAi). In cell clones where OPA1 was ablated, mitochondria appeared globular and fragmented as opposed to the rod, elongated organelles of the control clones. Tubulation induced by OPA1 is not the results of simple juxtaposition of mitochondria, but it represents the steady state appearance of increased mitochondrial fusion events, as substantiated by assays of mitochondrial fusion in polykarions induced by PEG treatment. Expression of OPA1 significantly speeded up mixing of matricial content, whereas its downregulation reduced mitochondrial fusion.

In yeast, the pro-fusion activity of Mgm1p, the orthologue of OPA1, depends on the outer membrane mitochondria-shaping protein Fzo1p. We therefore wished to ascertain whether this paradigm was maintained in higher eukaryotes. We turned to a genetic approach, testing the ability of overexpressed OPA1 to promote mitochondrial tubulation in MEFs deficient for either *Mfn1* or *Mfn2*. Expression of OPA1 induced mitochondrial tabulation and fusion in *wt* and in *Mfn2*$^{-/-}$ but not in *Mfn1*$_{-/-}$ cells. This defect was complemented by re-introduction of MFN1 but not MFN2, unequivocally identifying outer membrane MFN1 as an essential functional partner of OPA1. Moreover, MFN1 was unable to promote mitochondrial elongation if OPA1 had been ablated. Thus, OPA1 and MFN1 appear to functionally depend one on each other. To address whether *Mfn1*$^{-/-}$ MEFs displayed any defect in the preparatory events of mitochondrial juxtaposition and docking, we performed 4D-imaging of mitochondria, *i.e.* time series of *z*-stacks of mitochondrial images. The total number of contacts between mitochondria was not affected by OPA1 overexpression or by MFN deficiency. OPA1 facilitated fusion following contacts between *wt* and *Mfn2*$^{-/-}$ but not *Mfn1*$^{-/-}$ mitochondria. Taken together, our results suggested that OPA1 requires MFN1 to fuse the membranes of two juxtaposed mitochondria and not to produce inter-mitochondrial contacts. Our genetic analysis provided the first evidence of a functional diversity between MFN1 and MFN2, suggesting a functional axis between OPA1 and MFN1 (Cipolat et al., 2004).

The discovery that OPA1 is a pro-fusion protein raised the question of whether this protein participated in the regulation of apoptosis, during which fusion is impaired. We therefore decided to genetically dissect the role of OPA1 in fusion and apoptosis. We could demonstrate that OPA1 has an antiapoptotic activity, controlling the *cristae* remodelling pathway of apoptosis, independently of mitochondrial fusion. OPA1 did not interfere with the activation of the core mitochondrial apoptotic pathway of BAX and BAK activation. Yet OPA1 inhibited the

release of cytochrome *c* by preventing the remodelling of the *cristae* and the intramitochondrial redistribution of cytochrome *c.* Inactivating mutations in the GTPase domain of OPA1 impaired its anti-apoptotic activity, enhancing susceptibility to apoptosis induced by stimuli that recruit the mitochondrial pathway.

While our results contributed to clarify the biological function of OPA1, they left open a number of questions. In particular, if the pro-fusion activity of OPA1 was dispensable for the inhibition of apoptosis, how was this function controlled? In yeast Mgm1p is processed by the inner mitochondrial membrane rhomboid protease Rbd1/Pcp1 into a short active form, responsible for the effects of Mgm1p on mitochondrial morphology (Herlan et al., 2003; McQuibban et al., 2003). The mammalian orthologue of Rbd1p, PARL, could similarly play a role in the regulation of one of the two biological functions we ascribed to OPA1, *i.e.* its effect in mitochondrial fusion and its anti-apoptotic activity. In order to address this issue, we decided to analyze the phenotype of a mouse model of *Parl* deletion. *Parl*$^{-/-}$ mice were born with normal Mendelian frequency and developed normally up to 4 weeks. From then on, mice displayed severe growth retardation and progressive atrophy in multiple tissues, leading to cachexia and death. The atrophy of *Parl*-/- tymi, spleens and muscular tissues was caused by an increased apoptosis of double-positive ($CD4^+CD8^+$) thymic lymphocytes, splenic B lymphocytes ($B220^+$) and myoblasts, respectively. We investigated to what extent mitochondrial dysfunction and morphology dysregulation contributed to this multisystemic atrophy. PARL was not required for normal mitochondrial function: *Parl*$^{-/-}$ mitochondria did not display primary respiratory defects or latent mitochondrial dysfunction in hepatocytes, MEFs, primary myocytes and myotubes. Mitochondrial dysfunction therefore did not explain *Parl*$^{-/-}$ muscular atrophy and multisystem failure. Moreover *Parl* was not required for maintenance of mitochondrial shape and fusion, even in tissues severely affected by *Parl* ablation like muscle, and *Parl* was dispensable for regulation of mitochondrial dynamics by OPA1. We therefore investigated whether PARL regulates mitochondrial apoptotic machinery by analyzing apoptosis in MEFs treated with different intrinsic mitochondria utilizing stimuli. *Parl*$^{-/-}$ MEFs were more sensitive to all the stimuli tested as compared to their *wt* counterparts. Reintroduction of a catalytically active PARL showed that the defect was specific. PARL exerted its antiapoptotic effect at the mitochondrial level, since cytochrome *c* release and mitochondrial dysfunction following treatment with an apoptotic stimulus occurred faster in *Parl*-/- fibroblasts than in their relative wt counterparts. PARL did not regulate activation of the core BAX, BAK dependent apoptotic pathway, but it was required to keep in check the *cristae* remodelling pathway and to prevent mobilization of the *cristae* stores of cytochrome *c* during apoptosis. Since these results pointed to a role for PARL in the *cristae* remodelling pathway, regulated by OPA1, we ought to understand whether OPA1 required PARL to regulate apoptosis. OPA1 protected *wt* but not *Parl*$^{-/-}$ MEFs from apoptosis; furthermore, expression of OPA1 in *Parl*$^{-/-}$ MEFs did not reduce cytochrome *c* release, or

mitochondrial depolarization following intrinsic stimuli. When *Opa1* was silenced by siRNA in *Parl*$^{-/-}$ cells, they were no longer rescued by re-expression of PARL, demonstrating that PARL is genetically positioned upstream of OPA1. This genetic interaction was confirmed at multiple levels, since PARL and OPA1 interacted in a yeast two-hybrid and co-immunoprecipitation assays. PARL participated in the production of a soluble, IMS located, "anti-apoptotic" form of OPA1. The catalytic activity of PARL was required for the efficient production of soluble OPA1 and the re-introduction of a form of OPA1 in the IMS rescued the pro-apoptotic phenotype of *Parl*$^{-/-}$ cells. Thus, this IMS form resulted pivotal in controlling the pathway of *cristae* remodelling and cytocrome *c* redistribution. IMS and integral IM OPA1 indeed were both found to participate in the assembly of OPA1-containing oligomers that are early targets during *cristae* remodelling and greatly reduced in *Parl*$^{-/-}$ mitochondria. The reduced level of OPA1 oligomers could account for the faster remodelling and cytochrome *c* mobilization observed in the absence of PARL.

OPA1 affects complex cellular functions other than apoptosis, as substantiated in overexpression studies showing a role for this protein in movement of leukocytes (Campello et al., 2006) and formation of dendritic spines (Li et al., 2004). Furthermore, *Opa1* knockout mice demonstrated that OPA1 is required for embryonic development. Homozygous mutant mice die in uterus at 13.5 dpc, with first notable developmental delay at E8.5 (Alavi et al., 2007). We therefore reasoned that levels of OPA1 are likely to affect development and function of multiple organs, by regulating mitochondrial fusion or apoptosis. In the last part of this Thesis, we therefore decided to study whether ablation of OPA1 influences differentiation of embryonic stem (ES) cells *in vitro* using a hanging-drop differentiation system. To this end, we analyzed an ES cell line where *Opa1* had been gene trapped (*Opa1*^{gt}), resulting in an *Opa1*$^{+/-}$ genotype. We compared the differentiation potential into cardiomyocytes and neurons of this *Opa1*^{gt} ES cell line to its relative *wt* ES cell line. *Opa1*^{gt} ES cells displayed a decreased capacity to differentiate into beating cardiomyocytes, while they retained a normal neuronal differentiation potential. These preliminary results indicate that OPA1 is a good candidate to regulate differentiation of ES cells *in vitro*. We now aim at understanding the molecular mechanism by which levels of OPA1 influence differentiation into cardiomyocytes.

In conclusion, the data presented in this Thesis demonstrate genetically distinct roles of the mitochondrial dynamin related protein OPA1 in the regulation of organellar shape and apoptosis. The individuation that the functional axis between OPA1 and MFN1 (that regulates mitochondrial fusion) and the regulatory IMM network comprised of the couple substrate-protease Parl-Opa1 could perhaps even control embryonic differentiation opens novel, unexpected avenues to investigate the role of mitochondria in life and death of the cell.

3. Introduction

Eukaryotic cells are surrounded by a plasma membrane (PM) and contain extensive internal membranes that enclose specific compartments, the organelles, and separate them from the rest of the cytoplasm, the region of the cell lying outside the nucleus. Most eukaryotic cells contain many mitochondria, which occupy up to 25% of the cytoplasmic volume.

Mitochondria are the main site of ATP production. In addition to supplying cellular energy, mitochondria are involved in a range of other processes, such as signalling, cellular differentiation and death, as well as the control of the cell cycle and cell growth. Finally, mitochondria have been implicated in several human diseases, such as degenerative disorders and cancer and may play a role in the aging process.

Mitochondria are complex organelles and their elaborate structure is very important to their function. In certain cell types they are organized in networks of interconnected mitochondria. Ultrastructurally, the IM can be further subdivided in an inner boundary membrane and in the *cristae* compartment, bag-like folds of the IM connected to it *via* narrow tubular junctions. The ultrastructure and the reticular organization of the organelle are determined by mitochondria-shaping proteins that impinge on the equilibrium between fusion and fission processes.

We will now discuss the mechanisms involved in the regulation of mitochondrial dynamics, apoptosis and the possible role of mitochondria in development. More specifically, we will focus on OPA1, one component of the family of mitochondria- shaping proteins

3.1. Mitochondria

Mitochondria are crucial organelles in life and death of eukaryotic cells. In the last few decades their role in cellular physiology and function has been reconsidered and the number of processes in which they are involved is likely to increase in the future.

They produce most of the ATP needed for endoergonic processes and convey it to the sites of greater energy demand. They participate to and shape complex signalling processes such as cytosolic Ca^{2+} transients (Jouaville et al., 1995). During apoptosis they integrate diverse stimuli by releasing protein cofactor needed in the cytosol to grant the efficient activation of the caspases that execute cell destruction (Wang, 2001). Defects in any of these processes can be detrimental for the cell: several diseases are indeed consequences of, or are aggravated by, mitochondrial dysfunction (Schapira, 2006). Moreover evidences have been accumulating in favour of a direct implication of mitochondria in oncogenesis. Mitochondria exert a dual function in carcinogenesis: cancer cells display changes in cellular metabolism (the so called Warburg effect) (WARBURG, 1956) and tend to disable the mitochondrial pathway of apoptosis (Hanahan and Weinberg, 2000). Unlike any other organelle, except for chloroplasts, mitochondria appear to originate only from other mitochondria. They contain their own circular DNA (mtDNA), along with their own transcriptional and translational machinery. Mitochondrial ribosomes and transfer RNA molecules are similar to those of bacteria, as are components of their membrane. These and related observations led L. Margulis, in the 1970s, to propose an extracellular origin for mitochondria, the endosymbiotic theory (Margulis, 1971). Mutations in mtDNA are associated with a number of genetic, multisystemic diseases that highlight the importance of this organelle in physiology of multiple organs.

3.2. The metabolic role of mitochondria

Pioneering biochemical studies have long forged the concept that the mitochondrion is the “energy powerhouse” of the cell. It is the centre of cellular energetic metabolism being the principal source of ATP for eukaryotic cells: only 5% of ATP generate by glucose is provided by glycolysis. ATP is required to drive most energy-dependent intracellular processes. Due to their function, mitochondria display very well-characterized mechanisms to regulate production, consumption and conservation of cellular energy.

The three major processes leading to ATP synthesis are:

- The tricarboxylic acid cycle, located in the mitochondrial matrix, in which NADH and $FADH_2$ are produced from organic compounds
- The mitochondrial respiratory chain, in which electrons are sequentially transferred to oxygen by electron carriers, the respiratory chain complexes. To limit free energy dissipation, electrons from NADH are transferred stepwise from the IM-associated

respiratory chain complexes with higher redox potential to the ones with lower. The complex I (NADH dehydrogenase) catalyzes the transfer of electrons from NADH to CoQ. Complex II (succinate dehydrogenase) transfers electrons directly from succinate to CoQ. Electrons are transferred by complex III (ubiquinone-cytochrome *c* reductase) from reduced CoQ to cytochrome *c*, which in turns shuttle them to complex IV (cytochrome *c* oxidase). Complex IV finally catalyzes the electron transfer from cytochrome *c* to O_2. Electrons transfer in complexes I, III and IV is coupled to proton pumping from the matrix to the intermembrane space.

- The phosphorilating system, which uses the energy supplied by the respiratory chain to catalyze the synthesis of ATP from ADP and P_i.

In 1961 Mitchell proposed that the fundamental mechanism of energy transduction in mitochondria is chemiosmosis (Mitchell, 1979), in which the free energy of oxidation of carboxylic acids is used to pump protons from the matrix to the intermembrane space establishing an electrochemical gradient. Since the inner mitochondrial membrane displays an extremely low passive permeability to ions in general and protons in particular, the result is the buildup of a proton electrochemical gradient ($\Delta\mu H^+$) across the membrane. The electrochemical gradient is the sum of two components: the proton concentration difference across the membrane (ΔpH) and the electrical potential difference across the membrane ($\Delta\psi_m$). The estimated magnitude of the proton electrochemical gradient is about -220 mV (negative inside) and under physiological conditions most of the gradient is in the form of $\Delta\psi_m$. The proton gradient is utilized to synthesize ATP: the F_1F_0-ATPase synthase couples the transport of these protons back across the inner membrane into the matrix with the phosphorylation of ADP to produce ATP.

Mitochondria are the site of many other metabolic processes, such as biosynthesis and degradation of fatty acids and amino acids, and synthesis of ketone-bodies and heme. They also play a major role in generation and detoxification of reactive oxygen species and in H^+ and Ca^{2+} homeostasis

3.3. Mitochondrial biogenesis

Mitochondria perform essential cellular functions, yet can not be synthesized *de novo* (Attardi and Schatz, 1988). Instead, these organelles are derived from pre-existing mitochondria and specific cellular mechanisms act to ensure their faithful transmission to the progeny.

A growing list of key protein components of the inheritance process emerged from analysis of conditional mutants of the budding yeast *Saccharomyces cerevisiae* that were defective for mitochondrial distribution and morphology (the mdm mutants) (Berger and Yaffe, 1996; Koehler et al., 1999; Hermann and Shaw, 1998).

Mitochondria consist of four distinct compartments. The mitochondrial outer and inner membranes serve as barriers for the maintenance and integrity of two soluble compartments, the mitochondrial intermembrane space (IMS) and mitochondrial matrix. The outer membrane is composed of about half lipid and half protein, contains specific transports and pores that render the membrane permeable to molecules having molecular weights as high as 10 KDa. The OMM is similar to the outer membrane of gram-negative bacteria. The inner membrane is less permeable, constituted for approx. 80% of proteins, a higher proportion than that occurring in other cellular membranes.

Mitochondria contain their DNA: in vertebrates, mtDNA consists of a double stranded covalently closed circular DNA molecule of about 16.5 kb. Many mtDNA molecules are packaged within mitochondria into small clusters called nucleoids (Jacobs et al., 2000), that vary in size and number in response to physiological conditions (Nosek and Tomaska, 2003; Legros et al., 2004; Malka et al., 2006). Nucleoid structure is stabilized by TFAM, or mtTFA, which binds to mtDNA and regulates its abundance (Kanki et al., 2004). The maintenance of the mtDNA integrity is important for keeping proper cellular functions both under physiological and pathological conditions (Kang et al., 2007)

Mitochondria contain about 1500 different proteins, only half of which have been identified (Calvo et al., 2006). mtDNA encodes 13 mRNAs for subunits of the oxidative phosphorylation complexes (OXPHOS) (Anderson, 1981; Fernandez-Silva et al., 2003). Proteins of mitochondrial origin are translated on mitochondrial ribosomes bound to the matrix side of the inner membrane, and cotranslationally inserted into the proper compartment (Allen et al., 2005; Poyton and McEwen, 1996). 99% of the ~1,000 different mitochondrial proteins are produced on cytosolic ribosomes and are imported into the organelle (Sickmann et al., 2003; Prokisch et al., 2004). The correct delivery and sorting of nuclear encoded mitochondrial precursors to each of these four compartments is pivotal in the maintenance of normal organelle function and structure. However, in addition to be delivered to the correct submitochondrial location, many proteins have to be further assembled into homo- or hetero-oligomeric structures in order to fulfill their functions. Translocation machineries within the outer and inner membranes in addition to translocation mediators within the organelle's soluble regions exist and execute these delicate tasks (Koehler, 2004).

Nuclear-encoded mitochondrial proteins are imported by the TOM complex. Subsequently, they follow different pathways. Presequence-carrying proteins are transported by the TIM23 complex and the motor PAM into the matrix, where mitochondrial processing peptidase (MPP) cleaves off the presequences. Small proteins of the intermembrane space (IMS) are imported via the mitochondrial intermembrane space assembly machinery (MIA). β-barrel precursors of the outer membrane (OM) are transferred by the Tim9–Tim10 chaperone complex from TOM to SAM.

Precursors of inner membrane (IM) carriers use Tim9–Tim10 for transfer to the TIM22 complex that drives insertion into the inner membrane.

The protein translocases in the four mitochondrial compartments do not function as independent complexes but cooperate in a dynamic manner. This includes transient contacts between translocases located in different compartments and the involvement of protein complexes that have previously been thought not to be related to protein biogenesis, such as the respiratory chain and mitochondrial morphology components.

3.4. Mitochondrial ultrastructure

Since the 1950s, electron microscopy (EM) has provided otherwise unreachable glimpses into the substructure of the cell. Sjöstrand and Palade led pioneering work on electron microscopy of mitochondria. They both recognized that mitochondria have two very different membranes, an outer (OMM) and a highly convoluted inner (IMM) membrane. It was proposed that mitochondria consist of two compartments: the intermembrane space (IMS), between the OM and the IM, and the matrix, the central electrodense space. Palade's model evolved into that currently depicted in textbooks in which the inner mitochondrial membrane is one continuous closed surface with a complex morphology, folded in ridges called *cristae* (Figure 1, A). This model, sometimes called the baffle model, shows the *cristae* with broad openings to the intermembrane space on one side of the mitochondrion and protruding across the matrix nearly to the other side (Palade, 1952).

Some years later Hackenbrock demonstrated that the structure of mitochondrial membrane is linked to the metabolic state of mitochondria. For example, the matrix contracts during changes in osmotic or metabolic state, producing a 'condensed' conformation in which the inner membrane is pulled away from the outer membrane except at loci he called 'contact sites' (Hackenbrock, 1966). By contrast, mitochondria observed in situ are usually found in the 'orthodox' conformation, characterized by a relatively large matrix volume and the non-cristal component of the inner membrane closely apposed to the outer membrane with a small intermembrane space.

The need to reinvestigate the issue of mitochondrial compartmentation provided the impetus to apply a new 3D imaging technology, EM tomography, to this problem. In EM tomography, multiple projection images representing many different views are collected from a specimen whose thickness can range from 0.25 to 1.5 μm or larger. Imaging of these thick specimens is obtained using electron microscopes operating at high accelerating voltages (400–1200 kV) equipped with precision tilting stages. The first applications of EM tomography to mitochondria were performed by Mannella and co-workers on rat-liver mitochondria (Mannella et al., 1994). Sections used were 0.5 μm thick, representing a large segment of the intact, isolated organelles, typically ellipsoids, 0.5–2 μm in size. The resulting tomograms provided striking

evidence that the standard baffle model was incorrect, at least for isolated rat-liver mitochondria, which are among the most commonly used for bioenergetic investigations.

When Frey, Perkins and co-workers applied high-voltage electron tomography coupled with three-dimensional image reconstruction *in situ* in several different tissues, they identified the *cristae* as a novel compartment. *Cristae* are separated from the inner boundary membrane, shaped like bags and connected by narrow tubular junctions (with a diameter of approximately 28 nm) to the thin intermembrane space (Perkins et al., 2001) (Figure 1, B).

In contrast to the standard baffle model for mitochondrial structure, this new structural organization strongly suggest that diffusion between internal compartments is restricted, which has profound functional implications. Because oxidative phosphorylation relies on rapid diffusion of ions and substrates to sites of transport or reaction on the mitochondrial inner membrane, the number and shape (diameter and length) of *cristae* junctions could regulate rates of ATP phosphorylation under certain conditions (Perotti et al., 1983; D'Herde et al., 2001). Likewise, the shape and volume of *cristae* can be expected to affect the diffusion of cytochrome *c* between intracristal and intermembrane compartments (Bernardi and Azzone, 1981; Scorrano et al., 2002).

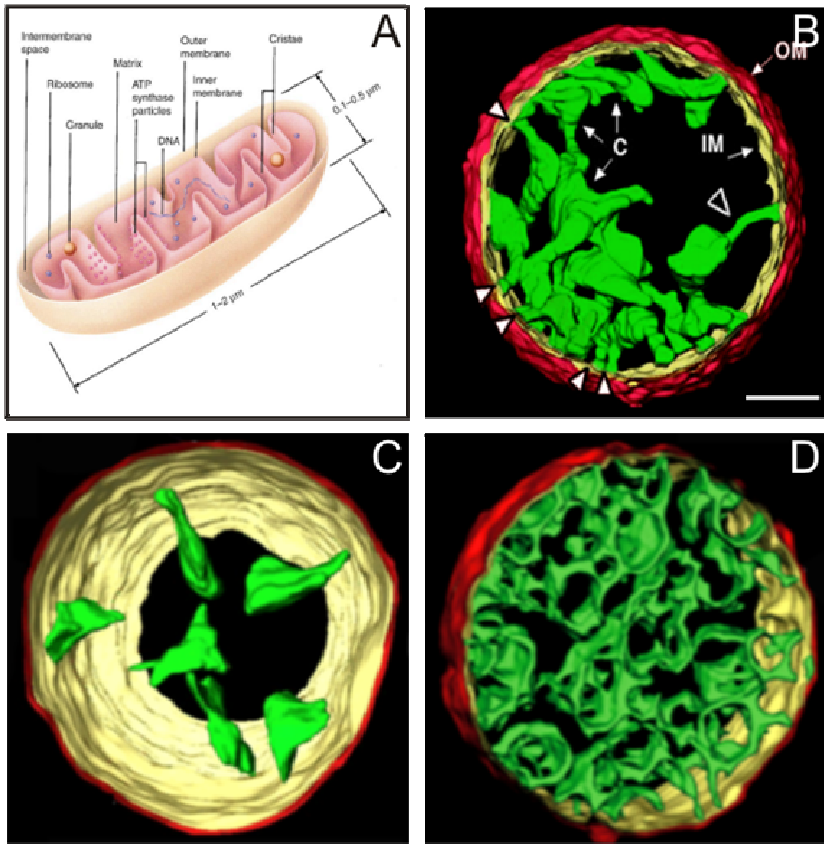

Figure 1: Mitochondrial ultrastructure. (A) A text book like representation of the buffle model adapted from (Frey and Mannella, 2000) (**B**) Three-dimensional reconstructions of isolated rat liver mitochondria obtained by high-voltage electron microscopic tomography. OM: outer membrane, IM: inner membrane, C: selected cristae; arrowheads point to narrow tubular regions that connect cristae to periphery and to each other. Bar, 0.4 µm. Adapted from (Frey and Mannella, 2000). (**C-D**) Representative surface-rendered views of electron microscopy tomography reconstructions of class I (**C**) and II mitochondria (**D**). The OM is depicted in red, the inner boundary membrane in yellow, and the cristae in green.

3.5. Mitochondrial reticulum

Mitochondria are dynamic organelles able to change number and shape in living cells during development, mitosis -when they co-ordinately divide into daughter cells (Catlett and Weisman, 2000)- and in response to physiological or toxic conditions.

Mitochondrial structure is very heterogeneous and can range from small, individual spheres to interconnected and branched tubules. The different and dynamic changes in mitochondrial shapes were already noticed in early times by cytologists who observed living cells under light microscopy: due to the high heterogeneity of mitochondrial shape, they christened this organelle "mitochondrion", a combination of the Greek word for *μίτος* or *mitos*, "thread" and *χονδρίον* or *khondrion*, "grain".

In the cytosol of certain cell types, mitochondria can be organized in a net, where individual organelles dynamically fuse and divide (Legros et al., 2002) to generate functional units of fused mitochondria, where a stimulus or a signal hitting one end of the mitochondrial wire can be readily transmitted to other distal components of the net (Amchenkova et al., 1988). This property is useful to rapidly convey signals across the cytoplasm, especially in large cells such as cardiomyocytes (Pacher and Hajnoczky, 2001). On the other hand, in other cell types both shape and function of individual mitochondria are heterogeneous, with limited interconnectivity of the organelles (Collins et al., 2002).

The morphological plasticity of mitochondria results from the equilibrium between fusion and fission events. Even more remarkably, imaging studies in live cells indicate that mitochondria constantly move and undergo structural transitions. Individual mitochondria move back and forth along their long axes on radial tracks. Occasionally two distinct mitochondria can encounter each other during these movements and undergo fusion, head to head or side to head. Conversely, long tubules can divide by fission events, giving rise to two or more distinct units. Mitochondria are organelles surrounded by two membranes making the fusion and fission complicated processes. Any fusion or fission event requires the coordinate fusion-division of four lipid bilayers in a coordinate and complete manner.

Dynamic control of mitochondrial structure is performed by a growing set of "mitochondria-shaping" proteins that include both pro-fusion and pro-fission members.

3.6. Mitochondrial movement and transport

Mitochondria distribution and transport inside a cell is likely to be a very well-regulated process. These organelles are often enriched at cellular sites where energy demand is greater, or where their metabolic function is required, like at the level of the synaptic button. This implies that mitochondria are (i) mobile; (ii) use cytoskeletal proteins as tracks for their directional movement; (iii) are transiently or permanently stopped where their presence is required *via* interactions with specialized cellular structures.

Mitochondrial transport depends on the actin cytoskeleton in budding yeast (Fehrenbacher et al., 2004) and on both actin and microtubules in mammalian cells (Morris and Hollenbeck, 1995; Hollenbeck and Saxton, 2005). Depending on the cellular context, these transport processes can ensure proper inheritance of mitochondria or can recruit mitochondria to active regions of

the cell. For example, in budding yeast, mitochondria are transported into and retained in the developing bud to ensure mitochondrial inheritance to the daughter cell (Fehrenbacher et al., 2004).

Energy-dependent molecular motors transport mitochondria along cytoskeletal filaments. Along microtubules, multiple kinesin family members and cytoplasmic dynein have been implicated in anterograde and retrograde mitochondrial transport, respectively (Hollenbeck and Saxton, 2005).

Recent work has clarified the linkage between mitochondria and kinesin-1. Genetic screens in *D. melanogaster* identified milton and miro, both of which are required for anterograde mitochondrial transport in neurons (Guo et al., 2005; Stowers et al., 2002). Milton interacts directly with kinesin and miro, which is a mitochondrial outer membrane protein that has GTPase and Ca^{2+} binding EF-hand domains (Glater et al., 2006). It is very likely that miro is not only an adaptor for milton, but is also a critical regulator of kinesin-dependent mitochondrial transport: either the GTPase activity or calcium binding can regulate miro's conformation and, therefore, its ability to recruit milton or arrange the milton–kinesin complex at the surface of mitochondria. In yeast, disruption of the Miro orthologue Gem1p results in abnormalities in mitochondrial morphology and poor respiratory activity (Frederick et al., 2004). Both GTP-binding and Ca^{2+}-binding motifs are essential for Gem1 function, which appears not to be involved in fusion or fission.

Depending on the cell type, mitochondria can also travel along actin filaments under the control of myosin motors (Hollenbeck and Saxton, 2005).

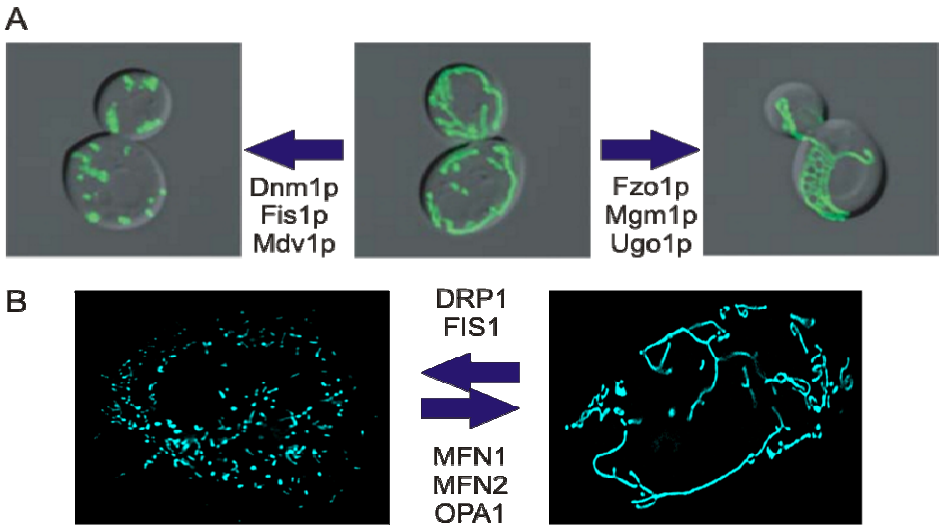

Figure 2 Fusion and fission of mitochondrial network. (A) Cartoon depicting the structure of mitochondrial network in *S. cerevisiae* and the relative mitochondria-shaping protein regulating fusion or fission processes. **(B)** Cartoon depicting the different shape of mitochondrial network in mammals and the

3.7. Mitochondria-shaping proteins: fusion

Dynamic control of mitochondrial structure is performed by a growing family of “mitochondria-shaping” proteins that include both pro-fusion and pro-fission members. Several players

involved in the control of mitochondrial are dynamins-related proteins. Dynamins are ubiquitous mechano-enzymes that hydrolyze GTP to regulate fusion, fission, tubulation and elongation of cellular membranes (McNiven et al., 2000). The role of dynamins in controlling mitochondrial shape was initially identified by genetic screens in budding yeast, where deletion of specific genes resulted in gross alterations of the mitochondrial network, and ultimately in functional abnormalities including loss of mitochondrial DNA, growth defects and petite strains (Dimmer et al., 2002; Shaw and Nunnari, 2002).

3.7.1. Fzo1/Mitofusin1-2

The first mediator of mitochondrial fusion identified was the *D. Melanogaster* Fuzzy onions protein (Fzo1), an evolutionarily conserved, large transmembrane GTPase localized in the outer mitochondrial membrane. In *Drosophila* Fzo gene is activated during spermatogenesis and mutations in the gene are responsible of male fly sterility (Hales and Fuller, 1997). Fzo1 mediates the formation of two giant mitochondria (Nebenkern structure) in the spermatide required to give energy to the flagellum.

The *S. cerevisie* orthologue of Fzo1 mediates mitochondrial fusion events during mitotic growth and mating and is it required for long-term maintenance of mitochondrial DNA (Hermann et al., 1998; Rapaport et al., 1998) (Figure 2, A). Fzo1p has two homologues in mammals, MFN1 and MFN2 (Santel and Fuller, 2001), which both control mitochondrial fusion (Figure 2, B). MFN1 and -2 display high (81%) homology and similar topologies, both residing in the OM (Rojo et al., 2002; Chen et al., 2003; Santel et al., 2003). They possess an N-terminal GTPase domain, two transmembrane domains spanning the outer mitochondrial membrane and two coiled coil motifs crucial for protein–protein interaction (Rojo et al., 2002; Santel and Fuller, 2001)(Figure 3).

Despite their highly similarity, the two mitofusins display some structural and functional divergences. MFN2 possesses a p21ras-binding domain at its N-terminal, which is not retrieved in MFN1 (Chen et al., 2004). Moreover, in silico analysis of MFN2 reveals that this protein also has a proline-rich-domain between aminoacids 576 and 590, which is poorly conserved in MFN1. Proline-rich domains are involved in the binding to other proteins (Kay et al., 2000). MFN1 and MFN2 are believed to dock two juxtaposed mitochondria *via* their coiled coil domains (Koshiba et al., 2004). However, MFN2 seems to have a different role from MFN1. First, it has been shown that MFN1 has a higher GTPase activity than MFN2, although its affinity for GTP is lower (Ishihara et al., 2004). In agreement with this, MFN1 exhibits a higher capacity to induce fusion (Ishihara et al., 2004). The differential role played by the two mitofusins during mitochondrial fusion was first demonstrated by directly measuring mitochondrial fusion rates in *Mfn1*$^{-/-}$ and *Mfn2*$^{-/-}$ cells. These experiments substantiated that cells containing only MFN1 retain more fusion activity than those that contain only MFN2 (Chen et al., 2003). Extending these cell biological observations, genetic ablation of the two genes in the mouse does not result in the

same phenotype: *Mfn1*$^{-/-}$ mice die in midgestation, whereas *Mfn2*$^{-/-}$ embryos display deficient placentation (Chen et al., 2003).

Overall, these observations suggest that if mitofusins can obviously share a common role in mitochondrial fusion, they appear probably to regulate this process in different manners and to have additional functions. In particular, increasing experimental evidence is mounting on the role of MFN2 in different pathologic and physiologic conditions (de Brito and Scorrano, 2007).

3.7.2. Mgm1p/Msp1p

Mgm1p has been identified in a genetic screen for nuclear genes required for the maintenance of mtDNA in the budding yeast *S. Cerevisae* (Jones and Fangman, 1992). Years later, Pelloquin and colleagues isolated Msp1p, the *S. Pombe* orthologue (Pelloquin et al., 1999). Mgm1p is a conserved dynamin related GTPase essential for fusion, morphology, inheritance, and genome maintenance of mitochondria in yeast (Sesaki et al., 2003b; Wong et al., 2003; Jones and Fangman, 1992) (Figure 2, A). The human orthologue of Mgm1p is Opa1, which was identified in 2000 by two independent groups (Delettre et al., 2000; Alexander et al., 2000). Albeit Mgm1p and Opa1 display a sequence identity of approximately 20%, they maintain a highly conserved secondary structure, consisting of a N-terminal mitochondrial targeting sequence (MTS) composed of scattered positively charged amino acid residues, two consecutive hydrophobic segments, a GTPase domain, a middle domain, and a C-terminal coiled-coil domain that may correspond to GTPase effector domain GED (Satoh et al., 2003). The pleckstrin homology and proline-rich domains, found in classical dynamins, are missing (Figure 3).

3.7.3. Ugo1p

A third mitochondrial fusion protein named Ugo1p has only been identified in fungi (Ugo means fusion in Japanese) (Sesaki and Jensen, 2001) (Figure 2, A). Ugo1p contains at least one transmembrane segment in the middle of the protein and two motifs similar to those found in mitochondrial carrier proteins that transport small molecules across the inner membrane. However, unlike characterized carrier proteins, Ugo1p is embedded in the outer membrane with its N terminus exposed to the cytoplasm and its C terminus in the intermembrane space. Since the outer mitochondrial membrane contains large pores that allow free passage of small molecules and proteins, it seems unlikely that Ugo1p functions as a classical carrier protein. Mammalian homologue of Ugo1p is yet unidentified.

3.7.4. LETM1

LETM1 is an inner-membrane protein, deleted in Wolff-Hirschhorn syndrome, a complex genetic condition, homologue to the yeast regulator of mitochondrial morphology Mdm38p (Dimmer et al., 2002). Its ablation results in mitochondrial fragmentation (Dimmer et al., 2008). However, it appears that LETM1 does not impinge on the core mechanism of mitochondrial morphology,

because its downregulation cannot be complemented by inhibition of the fission machinery. Work performed in yeast suggests that Letm1/Mdm38p is involved in the regulation of mitochondrial K^+/H^+ exchange, indicating possible crosstalk between ion homeostasis and regulation of mitochondrial shape (Nowikovsky et al., 2004).

3.7.5. Regulatory proteins in fusion process

The regulation of mitochondrial fusion is poorly understood. However, recent discoveries point to a role for ubiquitination, for lipid remodelling and for proapoptotic members of the BCL-2 family in this process.

Membrane-associated 'really-interesting-new-gene-'cystein/histidine (RING-CH) V (MARCH)-V is a novel ubiquitin ligase integrated in the OM. MARCH-V is a E3 ubiquitin ligase and catalyses polyubiquitination in the presence of the E2 enzymes UbcH6 or UbcH5 (Nakamura et al., 2006). MARCH-V interacts with MFN2 and promotes mitochondrial elongation in a MFN2-dependent manner. On the other side, MARCH-V promotes ubiquitination of DRP1 (Karbowski et al., 2007). MARCH5 RING mutants and MARCH5 RNA interference induce an abnormal elongation and interconnection of mitochondria indicative of an inhibition of mitochondrial division (Karbowski et al., 2007). Altogether, it seems that MARCH-V controls mitochondrial morphology by regulating the activity of mitochondria-shaping proteins (Nakamura et al., 2006).

A recent work has reported the involvement in mitochondrial dynamics of a novel phospholipase D isoform (mitoPLD), possessing a MTS directing it to the external face of mitochondria. This lipid-modifying enzyme participates in mitochondrial fusion by hydrolyzing cardiolipin to generate phosphatidic acid (Choi et al., 2006). Interestingly, phosphatidic acid is thought to play a part in generating the membrane curvature that is required for sNARE-mediated fusion. This indicates for the first time the existence of a common mechanism between SNARE-mediate vesicle fusion and MFN-mediated mitochondrial fusion

Mitofusin-binding protein (MIB) regulates mitochondrial morphology by its interaction with MFN1 (Eura et al., 2003). MIB is a member of the medium-chain dehydrogenase/reductase protein superfamily and has a conserved coenzyme binding domain (CBD). MIB needs an intact CBD domain to interact with MFN1, this interaction resulting in inhibition of MFN1 function and mitochondrial fragmentation. The subcellular localization of MIB is not very clear, since only ~50% of the cellular protein associates with mitochondria; the rest is in the cytosol or seems to be associated with microsomes. However, the association of MIB with other membranes does not seem to affect their morphology (Eura et al., 2003). Whether MIB regulates morphology in response to the supply of fatty acids to mitochondria remains an intriguing possibility that waits experimental testing.

Finally, the proapoptotic BCL-2 family members BAX and BAK seem to play an additional role during life of the cell in controlling mitochondrial fusion. They are retrieved in a high-molecular weight complex with MFN2 and their ablation reduces the rate of mitochondrial fusion, implying

these multidomain proapoptotics also in the control of mitochondrial morphology (Karbowski et al., 2006).

3.8. Mitochondria-shaping proteins: fission

3.8.1. Dnm1p/Dlp1/Drp1

The two proteins FIS (fission) 1 and DRP1 regulate mitochondrial fission in mammals. The dynamin-like-protein (Dlp) 1p in yeast, DRP-1 in *C. elegans*, and DLP1/DRP1 in mammals are homologues (Figure 2, A and B). DRP1 exists largely in a cytosolic pool, but a fraction is found in spots on mitochondria at sites of constriction (Labrousse et al., 1999b; Smirnova et al., 2001). DRP1 contains a dynamin-like-central domain and a C-terminal GTPase effector domain (GED), in addition to its N-terminal GTPase (Figure 3). DRP1 can oligomerize, in vitro, into ring-like structures and intermolecular oligomerization is observed at membrane constriction sites. Given these similarities with dynamin, DRP1 has been proposed to couple GTP hydrolysis with mitochondrial membrane constriction and fission (Hinshaw, 1999; Smirnova et al., 2001).

3.8.2. Fis1p/hFis1

Fis1p is a 17-kDa integral protein of the outer mitochondrial membrane (James et al., 2003). Its N-terminal domain is exposed to the cytoplasm and forms a tetratricopeptide (TPR)-like fold (Suzuki et al., 2003). The C-terminal domain of FIS1 possesses a predicted TM domain and a short stretch of amino acids facing the IMS (Figure 3). FIS1 is thought to recruit DRP1 to punctuate structures on mitochondria during mitochondrial fusion. It is therefore considered the limiting factor in the fission reaction (Stojanovski et al., 2004). Moreover it has been shown that hFis1 is a bifunctional protein which independently regulates fission and apoptosis (Alirol et al., 2006).

3.8.3. Endophilin B1

Endophilin B1, a member of the endophilin family of fatty acid acyl transferases that participate in endocytosis, has been shown to play a role in mitochondrial fission (Karbowski et al., 2004b). During endocytosis, endophilin 1 builds complexes with dynamin I, the dynamin responsible for the severing of the neck of the nascent endocytic vesicle, and provides the required lipid modification (Schmidt et al., 1999).

Endophilin B1 partially colocalizes and cofractionates with mitochondria and its downregulation by siRNA leads to changes in mitochondrial shape, as well as the formation of OM-bound structures resembling those formed by vesicles in neuronal terminals after inactivation of endophilin 1.

Members of the endophilin family, which are all Bin-Amphiphysin-Rvs(BAR)-domain proteins (like for example amphiphysin and endophilin 1), are supposed to participate in the regulation of membrane curvature, a process required for membrane scission during dynamin-mediated

endocytosis (Gallop et al., 2006). However, the mechanism by which BAR-domain proteins and related components regulate membrane scission has recently been questioned. First, it has been proposed that BAR-domain proteins have an acyl transferase activity that promotes membrane fission by altering membrane curvature from positive to negative (Schmidt et al., 1999). Later studies by the laboratory of H. McMahon demonstrated that BAR-domain proteins have no fatty acyl transferase activity as previously believed (Gallop et al., 2005). The amphipathic helices of BAR domains alter membrane curvature by inserting into the phospholipids bilayers and not by displaying a fatty acyl transferase activity (Gallop et al., 2006). Similarly, endophilin B1 seems to participate in the control of the morphology of OM by altering membrane curvature. Whether this is a direct effect, or it requires the recruitment of other proteins, such as phospholipase D and/or other mitochondria-shaping proteins, remains to be elucidated.

3.8.4. MTP18

MTP18, a nuclear-encoded mitochondrial membrane protein, is suggested to be a novel component required for mitochondrial fission in mammalian cells (Tondera et al., 2004; Tondera et al., 2005). MTP18 is supposed to be an intramitochondrial protein exposed to the IMS, however it is still not clear whether MTP18 is an OM or IM protein. Interestingly MTP18 is a downstream effector of phosphatidyl-inositol 3-kinase (PI3-K) signalling. It has been reported that overexpression of MTP18 leads to mitochondrial fragmentation. On the other hand, after downregulation of MTP18 levels by siRNA, mitochondria appear filamentous. Thus, MTP18 could be a regulator of mitochondrial shape that responds to activation of PI3-K, coupling morphology of the reticulum to cellular cues.

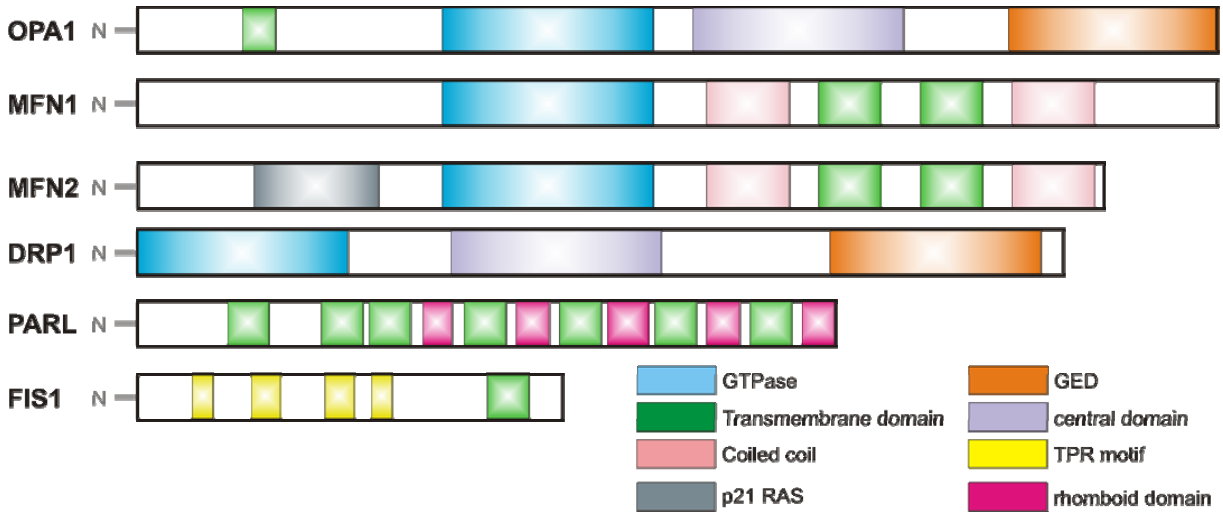

Figure 3: Mitochondria-shaping proteins in mammals and their domains

3.9. Proteins that mediate inner membrane morphology

In addition to changes in the overall shape of mitochondrial network, the internal structure of mitochondria is also dynamic. The pleomorphic, tubular *cristae* constitute highly sequestered compartments, where the majority of cytochrome *c* (80-85% of the total pool) is located, separated from the IM space by narrow cristae junctions (Figure 1 B).

Several proteins have been implied in the regulation of the IMM topology. In the buddying yeast, mitochondrial F_1F_oATP synthase, is essential for normal *cristae* structure (Paumard et al., 2002). This role in inner membrane structure involves a dimeric form of ATP synthase that contains the additional subunits ε and γ. As visualized by electron microscopy, the ATP synthase dimer has a dimeric interface with a sharp angle that could distort the local lipid membrane. This distortion might contribute to the high membrane curvature that characterizes *cristae* tubules (Dudkina et al., 2005; Minauro-Sanmiguel et al., 2005). Along this line, Mgm1p is required for the oligomerization of ATP synthase, suggesting a link between these two proteins in mitochondrial morphology (Amutha et al., 2004).

In yeast, Mdm33 is required for normal mitochondrial morphology and its overexpression leads to septation and vesiculation of the inner membranes (Messerschmitt et al., 2003). Because of these phenotypes, Mdm33 has been suggested to play a role in inner membrane fission. Depletion of Mmm1, Mdm31 and Mdm32, yeast proteins implicated in mitochondrial DNA maintenance, also cause aberrant cristae morphologies (Hobbs et al., 2001; Dimmer et al., 2005). Knockdown of mitofilin, a 90-KDa inner-membrane protein with a predicted membrane anchor and a coil-coiled domain, causes dramatic abnormalities of the *cristae* in mammalian cells, resulting in the formation of complex layers of inner membrane (John et al., 2005).

A study by the group of G. Shore shows DRP1-dependent remodelling of the IM during apoptosis, demonstrating for the first time a connection between mitochondrial fragmentation and *cristae* remodeling (Germain et al., 2005). The signal leading to DRP1-mediated *cristae* remodelling was identified in the release of Ca^{2+} from the ER. Since this by itself is not enough to induce the egress of cytochrome *c* from mitochondria, another yet unknown signal, like another proapoptotic member of the BCL-2 family, carries on this second task. In conclusion, the *cristae* morphology derives from a balance between intra-mitochondrial membrane fusion and fission events, raising the possibility that proteins controlling the inter-mitochondrial fusion and fission events control also IMM topology.

3.10. Mechanisms of mitochondrial fusion and fission

Several important characteristics of mitochondria make their fusion mechanism particularly intriguing. First, unlike almost all other intracellular fusion events, neither SNAREs nor the AAA-ATPase NSF have been implicated in the fusion reaction. Indeed, there are specific, dedicated

mitochondrial fusion molecules, suggesting that the machinery evolved independently and is uniquely tailored for this organelle. Second, mitochondria have two membranes: therefore, the fusion of four sets of lipid bilayers must be coordinated. Third, unlike viral fusion and most SNARE-mediated fusion, mitochondrial fusion is homotypic. Finally, mitochondrial fusion it is likely to be influenced by cellular energetic demands, apoptotic stimuli and developmental cues. Taken together, these characteristics suggest that mitochondria fuse through a novel mechanism that reflects their unique endosymbiontic origin and double membrane architecture.

Why do mitochondria continually fuse and divide? Recent studies show that these processes have important consequences for the morphology, function and distribution of mitochondria. First, fusion and fission control the shape, length and number of mitochondria. The balance between these opposing processes regulates mitochondrial morphology. Second, fusion and fission allow mitochondria to exchange lipid membranes and intramitochondrial content. Such exchange is probably crucial for maintaining the health of a mitochondrial population. When mitochondrial fusion is abolished, a large fraction of the mitochondrial population loses nucleoids (Chen et al., 2007). In addition to mtDNA, other components, such as substrates, metabolites or specific lipids, can be restored in defective mitochondria by fusion. Third, the shape of mitochondria affects the ability of cells to distribute their mitochondria to specific subcellular locations. This function is especially important in highly polarized cells, such as neurons. Mitochondrial fusion and fission affect the mitochondrial distribution in dendrites. In hippocampal neurons, mitochondria accumulate at dendritic spines following neuronal stimulation. Inhibition of mitochondrial fission causes elongation of the mitochondria and decreases the abundance of dendritic mitochondria and the density of dendritic spines. Conversely, increased fission facilitates the mobilization of dendritic mitochondria and leads to an increased spine number (Li et al., 2004). Mitochondrial dynamics appears to be important for proper mitochondrial redistribution in lymphocytes during chemotaxis (Campello et al., 2006). Finally, mitochondrial fission facilitates apoptosis by regulating the release of intermembrane-space proteins into the cytosol. Moreover mitochondria actively participate in the regulation of Ca^{2+} signalling by taking up and releasing Ca^{2+} in response to physiological, inositol triphosphate coupled agonists. This process relies on the relative position of mitochondria in the cytosol, as well as on their juxtaposition to the ER, required for the production of microdomains of high [Ca^{2+}], essential for the activation of the low affinity mitochondrial Ca^{2+} uniporter (Rizzuto et al., 2000). It is therefore conceivable that changes in mitochondrial shape influence mitochondrial participation in the Ca^{2+} game. This hypothesis is substantiated by the finding that excessive fission by Drp1 blocks propagation of Ca^{2+} waves (Szabadkai et al., 2004), while Fis1 reduces refilling of ER Ca^{2+} stores, probably by impairing capacitative Ca^{2+} entry from the plasma membrane (Frieden et al., 2004). Surprisingly, Fis1 promotes higher degrees of fragmentation than Drp1, yet its effect on the propagation of mitochondrial Ca^{2+} waves are

apparently much lower. A possibility is that Drp1 has a specific but yet not characterized function on mitochondrial Ca^{2+} propagation, in addition to its effect on mitochondrial morphology.

3.10.1. Yeast

3.10.1.1. Fusion

Fusion of mitochondria can be divided in at least 3 steps: docking, fusion of the OM and fusion of the IM. During docking, two or more Fzo1p on juxtaposed mitochondria interact via their coiled coil domains. Fzo1p, Mgm1p and Ugo1p form a fusion complex that connects the IM and the OM and can be immunoprecipitated from isolated mitochondria (Sesaki and Jensen, 2004; Sesaki et al., 2003b; Wong et al., 2003). This is possible because Ugo1p contains domains that permit the formation of bridges between Fzo1p and Mgm1p in the fusion complex. A series of in vitro pull-down experiments demonstrated that the cytoplasmic and intermembrane space domains of Ugo1p bind Fzo1p and Mgm1p, respectively (Sesaki and Jensen, 2004).

A recently developed in vitro assay showed that fusion of the OM can be separated from fusion of IM. OM requires guanosin triphosphate (GTP) and a pH gradient across the IM. On the other hand, fusion of the IM requires the electrical component of the electrochemical gradient and high concentrations of GTP (Meeusen et al., 2004).

Mitochondrial fusion is regulated by proteolytic processing in yeast. Mgm1p processing by the rhomboid-like protease Pcp1p is required to maintain the tubular network, although only the non-cleaved long form of Mgm1p (l-Mgm1p) is essential for mitochondrial fusion (Sesaki et al., 2003a). Further, Mgm1p processing by Pcp1p depends on mitochondrial membrane potential, meaning that the energetic status of the cell influences mitochondrial morphology (Herlan et al., 2004). In agreement with this, it has been shown that only l-Mgm1p and not its short form (s-Mgm1p) interacts with Fzo1p (Sesaki and Jensen, 2004). This means that s-Mgm1p may play a role that is different from the coupling between IM and OM fusion. The relative amount of these two forms of Mgm1p seems to be regulated by Ups1p, the homologue of the protein of lymphoid interest (PRELI) and an evolutionarily conserved IMS protein, by controlling the insertion into the IM of the Pcp1p-sensitive rhomboid-cleavage site of Mgm1p (Sesaki et al., 2006)

Another regulation mechanism of mitochondrial morphology may be given by the activity of Mdm30p. This protein is localized mostly in the cytoplasm, but can be also retrieved on mitochondria where it regulates mitochondrial fusion. Mdm30p possesses a F-box motif, typical of Skp1-cullin-F-box(SCF)-E3 ubiquitin ligases on its N-terminal (Dimmer et al., 2002; Fritz et al., 2003). Mdm30p is able to target Fzo1p for degradation and by doing this it may regulate mitochondrial fusion (Escobar-Henriques et al., 2006).

3.10.1.2. Fission

The current model of fission in yeast is based on a trimer complex of Dnm1p, Mdv1p, and Fis1p (Tieu et al., 2002). Upon its activation Dnm1p translocates to mitochondria, where it functions as

a mechanoenzyme constricting mitochondrial membranes like its homolog dynamin I constricts the nascent endocytotic vescicle. Two models for yeast mitochondrial fission have been proposed (Okamoto and Shaw, 2005).

In one model, a stable Fis1p-Mdv1p complex is essential to recruit Dnm1p, which then homo-oligomerizes (Tieu et al., 2002; Shaw and Nunnari, 2002). In this model, Mdv1p is stably associated with mitochondria *via* interaction with Fis1p. After homo-oligomerization of Dnm1p on mitochondria, the Mdv1p-Fis1p incorporates into the Fis1p-Dnm1p complex. The association of the two complexes triggers, or mechanically induces membrane scission.

The second model is similar to the first one, except that assembly of Dnm1p in spots on mitochondria is proposed to be both Fis1p- and Mdv1p-independent. The Dnm1p homo-oligomers subsequently recruits Fis1p and Mdv1p into a ring structure that induces fission (Cerveny and Jensen, 2003; Cerveny and Jensen, 2003).

In a recently revised model, Dnm1p recruitment to mitochondria is catalysed both by Fis1p, Mdv1p and Caf4p (Karren et al., 2005; Griffin et al., 2005). At an early stage of fission, Fis1p recruits Dnm1p to the outer mitochondrial membrane *via* interaction with Mdv1p and Caf4p. In the absence of Mdv1p, Caf4p mediates formation of punctuate Dnm1p complexes on the mitochondrial surface. However, these Dnm1p complexes are not functional and cannot complete fission. On the other hand, Mdv1p can recruit Dnm1p and complete fission efficiently also in the absence of Caf4p (Okamoto and Shaw, 2005).

The role of the GTPase cycle of Dnm1p is still not completely understood. Since Dnm1p interacts with Mdv1p in a GTPase-dependent manner, it is possible that the GTPase cycle regulates this interaction (Cerveny and Jensen, 2003; Okamoto and Shaw, 2005). There is also the possibility that constriction is Dnm1p independent, but generated by local interactions of one or more mitochondrial proteins. Such a function has been proposed for the IM protein Mdm33p (Messerschmitt et al., 2003). Another possibility is that cytoskeletal movement generates tension along the mitochondrial axis and stretches it out, resulting in local constrictions along the tubule. This mechanism could be Dnm1p-dependent and the assembled Dnm1p complexes would generate mechanical forces for the constriction. Alternatively, like dynamin during endocytosis, Dnm1p could recruit yet unidentified proteins that change membrane lipid composition and curvature.

Remarkably, blockage of fission is not lethal to yeast, suggesting that mitochondria can still divide during cytokinesis as well as during meiosis and sporulation of diploid yeast cells (Gorsich and Shaw, 2004).

3.10.2. Mammals

3.10.2.1. Fusion

Fusion of mammalian mitochondria is thought to occur in a similar way as in yeast. The mammalian orthologues of Fzo1p, MFN1 and MFN2, are believed to dock two juxtaposed mitochondria via their coiled coil domains (Koshiba et al., 2004).

In the case of MFNs, two molecules on opposing membranes can bind in trans to bridge mitochondria, maintaining a distance of 95 Å between the two membranes (Koshiba et al., 2004). It has been recently reported that MFN2 forms high molecular weight complexes with stomatin-like protein 2 (Stoml2), a novel protein associated to the IM, facing the IMS. The function of this protein remains unknown, albeit it does not seem to have a role in regulating mitochondrial morphology (Hajek et al., 2007).

The role of Opa1 in mitochondrial fusion was questioned, as it was originally proposed that Opa1 participated in fission of the organelle (Misaka et al., 2002; Misaka et al., 2002). Aim of this Thesis has therefore been to investigate the potential role of OPA1 in mitochondrial morphology and to verify if it required partners on the outer mitochondrial membrane like its yeast orthologue Mgm1p.

3.10.2.2. Fission

Also mitochondrial fission in mammalian cells seems to follow the same mechanism in yeast. Drp1 is recruited to spots on mitochondria and it seems that constriction of the membranes takes place via interaction with Fis1, since it has been shown that recombinant Drp1 and recombinant Fis1 interact *in vitro* (Yoon et al., 2003). However, this association has never been shown *in vivo* and reduction of Fis1 levels by siRNA does not disrupt Drp1 localization to mitochondria (Lee et al., 2004). Yet, the residual level of Fis1 could still be sufficient to recruit Drp1 to mitochondria.

Recent findings discovered new regulatory mechanisms that control mitochondrial fission in response to a variety of cellular events, including cell division, metabolic flux and cell differentiation. Most of these processes seem to regulate the localization, dynamics and activity of Drp1.

A recent paper demonstrated a direct link between the cell-cycle and the mitochondrial-division machinery. During mitosis Drp1 is specifically activated upon phosphorylation by Cdk1/cyclin B on Ser-585 in the GTPase-effecter domain (GED) of Drp1 (Taguchi et al., 2007). Another recent study showed that cyclic-AMP-kinase-dependent phosphorylation of a different serine (Ser637) in the same domain inhibits Drp1 GTPase activity (Chang and Blackstone, 2007). Although these studies indicate that Drp1 phosphorylation can modulate the frequency of mitochondrial division, it remains to be determined if fission competent Drp1 is always phosphorylated or if this is a mechanism exploited only during the cell cycle.

DRP1 is modified post-transcriptionally by sumoylation (Harder et al., 2004). Sumoylation is a process that involves the covalent binding of the small protein SUMO to the substrate, protecting it from binding to ubiquitin and therefore from degradation by the proteasome (Johnson, 2004). Along this line, the ubiquitin ligase of the OM MARCH-V regulates targeting of DRP1 for degradation (Nakamura et al., 2006). The conjugation of the 76-amino acid protein ubiquitin to substrate proteins is involved in the regulation of a variety of cellular processes (Welchman et al., 2005) ranging from selective protein degradation to DNA repair (Huang and D'Andrea, 2006) and membrane protein trafficking (Staub and Rotin, 2006). Recent findings indicate that ubiquitylation plays a direct role in mitochondrial membrane remodeling (Escobar-Henriques et al., 2006; Nakamura et al., 2006; Yonashiro et al., 2006; Neutzner and Youle, 2005). Thus, DRP1 turnover is controlled by the equilibrium between ubiquitination and sumoylation, affecting mitochondrial fission.

3.11. Mitochondria-shaping proteins in health and disease

In the past years, mitochondrial defects have been implicated in a number of degenerative diseases, aging and cancer. Mitochondrial diseases involve mainly tissues with high energetic demands, such as muscle, heart, endocrine and renal systems. More recently, mutations in genes coding for pro-fusion proteins have been associated with genetic disorders.

In 2004, work by Zuchner et al. mapped the mutations responsible for Charcot-Marie-Tooth 2A (CMT2A), and identified *MFN2* as being the gene responsible for the disorder. CMT is one of the most common inherited disorders in humans, with an estimated prevalence of one in 2500 individuals. CMT neuropathies can be divided into 2 main groups, type 1 and type 2. In CMT1, nerve conduction velocities are considerably reduced. In CMT2, the nerve conduction velocities are normal but conduction amplitudes are decreased, due to the loss of nerve fibres (Zuchner et al., 2004).

CMT2A is a neurodegenerative disorder characterized by the loss of sensory and motor axons at early stages of the disease and resulting in the degeneration of the neurons themselves during a later stage of the disease. The clinical symptoms of CMT are distal weakness of the lower limbs, sensory loss, decreased reflexes and foot deformities. Other symptoms include cranial nerve involvement, scoliosis, vocal cord paresis and glaucoma (Lawson et al., 2005). Mutations in *MFN2* account for around 20% of CMT2 cases, making this the most prevalent axonal form of CMT. Most *MFN2* mutations in CMT2A cluster within the GTPase and the RAS-binding domains and are missense mutations (Zuchner et al., 2004; Lawson et al., 2005; Kijima et al., 2005). Recently, a *de novo* truncation mutation in MFN2 has been associated to CMT2 and optic atrophy (also known as hereditary motor and sensory neuropathy VI, HMSN VI) (Zuchner and Vance, 2006).

Mfn2 is up-regulated in the skeletal muscle of obese patients (Bach et al., 2003) and its over-expression suppresses vascular muscle cells proliferation in animal models of hypertension via sequestration of p21RAS, inhibition of the ERK/MAPK cascade and cell cycle arrest (Chen et al., 2004).

3.12. OPA1

Optic Atrophy 1 (Opa1), the homologue of *S. cerevisiae* Mgm1p, is the only dynamin-related protein identified in the inner membrane so far (Olichon et al., 2002).

3.12.1. Gene and protein structure

The human *OPA1* gene is composed of 30 coding exons distributed across more than 90 kb of genomic DNA on chromosome 3q28-q29. *OPA1* is expressed ubiquitously with the highest levels in retina, brain, testis, heart and muscle (Alexander et al., 2000). Alternative splicing of exons 4, 4b and 5b leads to eight differentially expressed isoforms with open reading frames for polypeptides of 960–1015 amino acids (Delettre et al., 2001). The protein contains a mitochondrial leader sequence within the highly basic N-terminal targeting the protein to the outer surface of the mitochondrial inner membrane, a GTPase domain, a central dynamin domain that is conserved across all dynamins, and a carboxy-terminus coiled-coil domain responsible of protein-protein interactions (Figure 3). Its splicing region corresponds to a part of the protein with unknown function located between the mitochondrial leader sequence and the GTPase domain.

Domain 4, corresponding to exon 4 shares broad homologies among vertebrates, but restricted similarities with invertebrate and yeast sequences. Exon 4b and exon 5b, are found only in vertebrate genomes, and are absent from *Drosophila*, *Caenorhabditis* and lower eukaryote genomic sequences. The 17 amino acids of domain 4b are well conserved, but do not display any specific motif or structure. The first 24 residues of the 37-amino-acid long domain 5b are highly conserved and the whole domain displays a highly conserved coiled-coil structure predicted to homooligomerize.

Mouse OPA1 shares 97% overall identity with the human sequence. Human and mouse sequences are somewhat divergent in the first 200 N-terminal amino acids (83 % identity) that mostly contains the mitochondrial leading sequence and the alternative splicing region.

The initially identified Opa1 corresponds to isoform 1 lacking both exons 4b and 5b, and encodes 960 amino acid residues. Isoforms 1 and 7 of *OPA1* gene are predominantly expressed in human cells. The difference between the two proteins of isoforms 1 and 7 is the addition of exon 5b, which encodes a major part of the N-terminal coiled-coil domain (Satoh et al., 2003).

The submitochondrial localization of Opa1 protein has been a controversial subject. Mgm1p/Msp1p were detected in the outer membrane (van der Bliek, 2000), intermembrane space (Pelloquin et al., 1999), or matrix (Alexander et al., 2000). Delettre and collaborators reported human Opa1 localized in the intermembrane space and associated with the inner membrane; the immunocytochemical electron microscopic analysis indicated the strong signals against anti-Opa1 antibody close to cristae (Delettre et al., 2000). A more detailed analysis showed that both Mgm1p and Opa1 are localized in the IMS, tightly associated with the IM (Olichon et al., 2002; Wong et al., 2000; Herlan et al., 2003; Sesaki et al., 2003b).

3.12.2. Role in mitochondrial shape

After the discovery of Opa1, its function was unclear as well as its proteolytic cleavage or its interaction with other mitochondria shaping proteins. It had been proposed that overexpression of Opa1 promotes fission and perinuclear clustering of mitochondria (Satoh et al., 2003; Misaka et al., 2002). It is difficult to reconcile the proposed pro-fission role of Opa1 with the known function of its yeast orthologue Mgm1p in mitochondrial fusion. One should hypothesize that Mgm1p drastically diverged during evolution from being a pro-fusion to become Opa1, a pro-fission mitochondria shaping protein. Concurrently, it was unclear whether mitochondrial fission following Opa1-specific RNAi was an epiphenomenon of mitochondrial dysfunction, often associated with increased fission (Griparic and van der Bliek, 2001; Frank et al., 2001; Karbowski et al., 2004a), or the specific consequence of the ablation of a protein pivotal for mitochondrial fusion. In the first part of this Thesis we therefore investigated the role of OPA1 in controlling mitochondrial shape.

Specific analysis of *OPA1* splice variants revealed a functional role of exon 4 in the maintenance of mitochondrial membrane and fusion of the mitochondrial network, (Olichon et al., 2007). Silencing of Opa1 variants containing exon 4, which encode the most abundant isoforms in HeLa cells, induces mitochondrial fragmentation and $\Delta\psi_m$ dissipation, without consequence on cytochrome *c* release and apoptosis.

3.12.3. Role in apoptosis

To ensure the complete release of cytochrome *c*, the ultrastructure of mitochondria changes in the early stages of apoptosis; individual *cristae* fuse and *cristae* junction widen. These morphological changes support the mobilization of cytochrome *c* from the *cristae* to the IMS, and eventually to the cytosol (Scorrano et al., 2002) (Figure 1, C and D). Opa1, the first discovered mitochondria-shaping protein located at the level of the IMM, seems a natural candidate to regulate this pathway. As expected, down regulation of Opa1 leads to mitochondrial fragmentation. This is accompanied by organelle dysfunction and cytochrome *c* release and interestingly by changes in mitochondrial ultrastructure (Olichon et al., 2003). These results raised the possibility that Opa1 could as a matter of fact participate in the biogenesis of the *cristae* and regulate the *cristae* remodelling pathway. The increased apoptosis observed

after specific down regulation of exons 4b or 5b, prompted to speculate a specific and restricted function of Opa1 isoforms including these domains in trapping cytochrome *c* inside the *cristae* compartment (Olichon et al., 2007).

3.12.4. Role in development

OPA1 plays an important role during early embryogenesis since homozygous mice are not viable, which is consistent with an essential requirement for mitochondrial fusion during embryonic development (Alavi et al., 2007; Davies et al., 2007).

Opa1$^{-/-}$ embryos are smaller compare with the relative *wt* and die during late gastrulation. Blastocysts at embryonic stage E3.5 do not show any apparent morphological differences compared to heterozygous or wild type blastocytes. First defects of embryogenesis appeared in E8.5 homozygous mutant embryos. This retarded development becomes more obvious at E9.5 and embryos are finally resorbed at E12.5. Analysis of *Mfn1* and *Mfn2* knockout mice demonstrated that they die in midgestation, similar to *Opa1* homozygous mutant mice (Chen et al., 2003).

Mouse embryonic fibroblasts derived from *Opa1*$^{-/-}$ embryos have lost their ability to undergo mitochondrial fusion, being completely fragmented; and many cells succumb to apoptosis. They contain enlarged mitochondria without *cristae*, but single septum-like and round-shaped double membrane structures. Mitochondria in *Opa1*$^{-/-}$ embryos are loosing their DNA. Heterozygous mice are viability and fertility with a normal behavior and a comparable size to wild-type littermates.

3.12.5. Role in homeostasis of adult tissues

OPA1 affects complex cellular functions, as substantiated in overexpression studies showing a role for this protein in movement of leukocytes (Campello et al., 2006) and formation of dendritic spines (Li et al., 2004).

Mitochondrial dynamic appears to be important for proper mitochondrial redistribution in lymphocytes during chemotaxis. Mitochondria are transported to the uropod along microtubules and concentrated in the trailing edge in lymphocyte cell lines that migrate in response to chemical attractants. Modulation of mitochondrial fusion or fission affects both mitochondrial redistribution and cell migration. OPA1 blocked mitochondrial and cell polarization in response to the chemokine. OPA1, MFN1, and a dominant-negative mutant of DRP1 (K38A-DRP1) prevented migration of T lymphocytes towards chemoattractant gradients (Campello et al., 2006).

It has been demonstrated that a small fraction of mitochondria are present within dendritic protrusion of cultured neurons and there is a positive physical association between this mitochondrial pool and dentritic spines and synapses morphogenesis. Importantly, normal synaps density and activity-dependent synapse formation depend critically on the proper distribution and function of mitochondria in dendrites. OPA1 overexpressio, reduces the amount

of dendritic mitochondria and leads to a decrease density of spines and synapses (Li et al., 2004). Since abnormal mitochondrial morphology and function are associated with neurodegenerative diseases, like Alzheimer's and Parkinson's disease (Castellani et al., 2002; Dawson and Dawson, 2003), these findings raise the possibility that the characteristic synapse loss of such disorders arises in part from mitochondrial dysfunction.

3.12.6. DOA

Heterozygous mutations of *OPA1* cause autosomal dominant optic atrophy (ADOA), the most common form of inherited optic neuropathy, with an estimated prevalence of 1:50000 (Alexander et al., 2000; Delettre et al., 2000). Linkage analysis has revealed that *OPA1*, mapping to 3q28-q29, is the major locus (Trimmer et al., 2000; Votruba et al., 1997). A positional cloning approach similarly identified this gene as being responsible for OPA1-type DOA (Alexander et al., 2000).

ADOA is a specific disease of the retina characterized by retinal ganglion cells (RGC) degeneration followed by ascending atrophy of the optic nerve. Very little is known on the pathogenesis of ADOA; the lack of pain and inflammation during the development of the disease suggest that apoptosis may play key a role in the loss of RGC. More than 117 different pathogenic mutations in Opa1 have been described (Ferre et al., 2005). The vast majority results in a truncated protein or affects the GTPase domain crucial for the biological activity of dynamins. Since the disease is transmitted as a dominant trait, it has been suggested that these mutations either act as dominant negative or induce a condition of haploinsufficiency leading to the clinical phenotype; however the heterozygous mouse mutants described above do not display overt symptoms, challenging this hypothesis.

DOA is characterized by decrease in visual acuity, tritanopia (dyschromatopsia characterized by confusion in the blue-yellow hues), sensitivity loss in the central visual fields, and pallor of the optic nerve (Votruba et al., 1998; Ferre et al., 2005). Classic DOA usually begins before 10 years of age, with a large variability in the severity of clinical expression, which may range from non-penetrant unaffected cases up to very severe, early onset cases, even within the same family carrying the same molecular defect (Delettre et al., 2002; Carelli et al., 2004). Histopathology studies have shown diffuse atrophy of the ganglion cell layer that predominates in the central retina and loss of myelin and nerve tissue within the optic nerve (Kjer et al., 1996).

It remains unclear why Opa1-ADOA manifests with an apparently restricted clinical ocular phenotype, comprising RGC loss. Opa1 is ubiquitously expressed throughout the body: in the heart, skeletal muscle, liver, testis, and most abundantly in the brain and retina. In the human retina, Opa1 is present in the cells of the RGC layer, nerve fibre layer, the photoreceptor layer, and the inner and outer plexiform layers (IPL & OPL). RGC display high expression levels of Opa1 and a "threshold" effect can be an explanation for the specificity of the disease.

How Opa1 mutations cause the clinical symptoms of ADOA remains to be clarified. Non-neuronal cells from patients with ADOA can have aggregated, fragmented or normal mitochondria (Delettre et al., 2000; Olichon et al., 2007); however, because data from only a few patients have been reported, it is not clear whether these findings are the norm. In addition, Opa1 mutations have been associated with reduced ATP production and reduced mtDNA content (Lodi et al., 2004; Kim et al., 2005; Lodi et al., 2004). The defects that have been documented in human ADOA diseased tissue are not as severe as those observed in experimental cells in which OPA1 is depleted.

It has been also proposed an involvement of Opa1 in regulating the amount of mtDNA, as suggested by a study showing that DOA patients may have slightly reduced mtDNA copy number in blood lymphocytes (Kim et al., 2005). Miss-sense point mutations in the highly conserved GTPase domain are responsible for a syndromic form of DOA associated with sensori-neural deafness, ataxia, axonal sensory-motor polyneuropathy, chronic progressive external ophthalmoplegia and mitochondrial myopathy. These patients all harboured multiple deletions of mitochondrial DNA (mtDNA) in their skeletal muscle, thus revealing an unrecognized role of the Opa1 protein in mtDNA stability (Kim et al., 2005).

Mouse models of ADOA that contain OPA1 mutations develop the features of ADOA in an age-dependent manner (mati-Bonneau et al., 2007; Alavi et al., 2007). A small proportion of heterozygous mice show a progressive decline in retinal ganglion cell number and aberrations of axons in the optic nerve. Though variable in expression, the pathology in mutant mice eventually advances to a stage of nearly complete loss of RGCs and gliosis of the optic nerve that is very similar to histopathological studies in patients with severe ADOA. Ageing effects, as well as the effects of physiologically relevant stressors, such as light and intra-ocular pressure, may have important roles in the full manifestation of the phenotype. The mild phenotype of the heterozygous models, and the increased manifestation of anomalies with age, is therefore, not surprising.

3.12.7. Cleavage of Opa1

Both Opa1 and Mgm1p undergo extensive post-translational processing, but processing of the yeast protein is less complex and better characterized.

At steady state, Mgm1p exists in a long l-Mgm1p and a short s-Mgm1p form (Esser et al., 2002; Herlan et al., 2003). Biochemical studies support a model of alternative topogenesis of Mgm1p (Herlan et al., 2004). L-Mgm1p is produced by targeting of the precursor, which contains a mitochondrial targeting sequence (MTS), to the mitochondrial inner membrane and cleavage of the MTS by the mitochondrial processing peptidase (MPP). At the time of MTS cleavage, the precursor is presumably associated with the translocase of the inner membrane (TIM). Lateral exit from the TIM complex would generate l-Mgm1p, associated with the inner membrane through the first hydrophobic segment (upstream TM1). Alternatively, if exit from the TIM

complex were delayed, the Mgm1p precursor would be further pulled into the matrix, by the pulling force provided by ATP and the mitochondrial import motor complex, until the second hydrophobic segment is anchored in the inner membrane (more C-terminal TM2). At that point, the mitochondrial rhomboid protease, Rbd1p/Pcp1p, cleaves Mgm1p at a second site to produce s-Mgm1p (Herlan et al., 2004; McQuibban et al., 2003). Both l-Mgm1p and s-Mgm1p are necessary for mitochondrial fusion, and deletion of Rbd1/Pcp1 results in loss of fusion activity. Ups1p, a mitochondrial protein peripherally associated with the inner membrane, regulates this bifurcate sorting of Mgm1p (Sesaki et al., 2006) .

Because OPA1 has a key role in regulating mitochondrial morphology and mitochondrial *cristae* remodelling, it was of major interest to identify the protease responsible of its cleavage and regulation. Apparently contradicting results have been reported in the respect of the protease responsible of OPA1 cleavage.

In contrast to the two electroforetic forms of Mgm1p, Opa1 exists at least in 5 bands in human cells and tissues. Opa1 is encoded by a complicated set of at least eight mRNA splice forms that are produced by differential splicing (Delettre et al., 2001). All Opa1 variants are synthesized with a bipartite-type mitochondrial targeting sequence; during import, the matrix-targeting signal is removed and processed forms (L-forms) are anchored to the inner membrane in type I topology (residue 87–88 of the pre-proteins). L-forms undergo further processing to produce short forms. In principle, therefore, each mRNA splice variant can produce a long form (produced by cleavage with MPP alone) and one or more short forms, deeply complicating the analysis.

The quest for the protease(s) involved in the cleavage of Opa1 is far from complete. Several groups proposed at least four different proteases to be involved. Mihara and colleagues demonstrated that in mammalian cells the m-AAA protease paraplegin is involved in a metal-binding site-dependent processing of OPA1 (Ishihara et al., 2006). Paraplegin is an ATP-dependent metallo-protease located in the mitochondrial inner membrane with its catalytic site exposed to the matrix (Ishihara et al., 2006). Dissipation of membrane potential, paraplegin overexpression, or induction of apoptosis, stimulated OPA1 processing along with mitochondrial fragmentation (produced by cleavage at S1, in exon 5, or S2 in exon 5b).

More recently, Duvezin-Caubet and collaborators have reconstituted Opa1 processing in yeast. They demonstrated that homo-oligomeric m-AAA protease complexes composed of murine AFG3L1, AFG3L2, or human Afg3l2 subunits cleaved Opa1 with higher efficiency than paraplegin-containing m-AAA proteases, and Opa1 processing proceeded normally in murine cell lines lacking paraplegin. Notably, certain Opa1 processing products are preferentially formed depending on the splice variant analyzed and on the subunit composition of the m-AAA protease (Langer et al., 2001). Tissue-specific differences in the subunit composition of m-AAA protease isozymes as well as in the expression of OPA1 isoforms could explain why

deficiencies in paraplegin in mouse and human do result in cell type specific mitochondrial defects.

Using *Opa1*-null cells, the group of D. Chan showed that only Opa1 mRNA splice forms that generates a long form in addition to one or more short forms support substantial mitochondrial fusion activity. By themselves, long and short Opa1 forms have little activity, but, when coexpressed they functionally complement each other. Loss of mitochondrial membrane potential destabilizes the long isoforms and enhances the cleavage of Opa1, regulated by the i-AAA protease Yme1L (Song et al., 2007). These data were confirmed by Rojo and collaborators in a recent paper, where they showed that metalloprotease-mediated processing of Opa1 is modulated by the inner membrane potential and is likely mediated by the YME1L protease (Guillery et al., 2007).

The issue of OPA1 processing is crucial if one thinks that Opa1 could be a central molecular player linking mitochondrial dysfunction with changes in mitochondrial morphology. Dissipation of the mitochondrial membrane potential leads to fast induction of proteolytic processing of Opa1 and concomitant fragmentation of mitochondria. Proteolysis of Opa1 is observed in patients and in various model systems of human disorders associated with mitochondrial dysfunction: in cybrid cells from a patient with myoclonus epilepsy and ragged-red fibers syndrome, in mouse embryonic fibroblasts harbouring an error-prone mitochondrial mtDNA polymerase γ, in heart tissue derived from heart-specific TFAM knock-out mice and in skeletal muscles from patients suffering from mitochondrial myopathies. (Duvezin-Caubet et al., 2006). In principle, mitochondrial dysfunction and depletion of mitochondrial ATP levels could lead to Opa1 processing, inhibition of mitochondrial fusion, and therefore to segregation of damaged mitochondria from the network of intact mitochondria (Duvezin-Caubet et al., 2006)(Baricault et al., 2007).

What is the role of the most likely candidate to process OPA1, the mammalian orthologue of yeast Rbd1p PARL, in the cleavage of OPA1? In order to address this issue, in this Thesis we analyzed a genetic model of *Parl* ablation in the mouse and its effect on OPA1 cleavage and function. At this point is therefore essential that we introduce the family of rhomboid proteases and their function in regulated intramembrane proteolysis.

3.13. Regulated intramembrane proteolysis

Regulated intramembrane proteolysis (RIP) is a signal transduction mechanism which appears to be prominent in all forms of life. Under RIP, membrane bound proteins undergo site-specific proteolysis within their transmembrane helix (TMH). This processing releases a moiety of the protein that through intracellular relocation or extracellular release, executes a signalling function. The RIP processing is executed by a class of proteases, named intramembrane-cleaving proteases (I-Clips), which are able to hydrolyze their TM substrates in a water

excluding environment such as the lipid bilayer (Brown et al., 2000). Intramembrane proteases are found in all forms of life, and their functions influence diverse processes, including transcriptional control, lipid metabolism, cellular signalling and differentiation, mitochondrial morphology, parasite invasion, and bacterial protein translocation (Urban and Freeman, 2002). They have also been implicated in a wide range of human diseases, from Alzheimer's to infection by pathogens including *hepatitis C virus*, *M. tuberculosis*, and the malaria parasite *P. falciparum*, making them potentially valuable new drug targets.

Up to date only three families of I-Clip proteins have been discovered. The first is composed by a group of metalloproteases whose prototypic member is the human site-two protease that cleaves and activates sterol regulatory element binding proteins (Rawson et al., 1997). The second class includes aspartic proteases like γ-secretase, which catalytic component is presenilin, involved in the cleavage of the amyloid β protein precursor (AβPP) and Notch (De Strooper et al., 1998; De Strooper et al., 1999). The third and most recently discovered I-clip family is the rhomboid superfamily, which is the most evolutionary conserved one and, by implication, the first to emerge in life (Koonin et al., 2003).

3.13.1. Rhomboids

Rhomboid proteases constitute probably the most widely conserved polytopic-membrane-protein family identified until now (Koonin et al., 2003). Seven rhomboids have been identified in *D. melanogaster* (Freeman, 2004). Rhomboids are essential activators of the epidermal growth factor (EGF) signalling pathway, proteolytically cleaving the EGF receptor ligands Spitz, Gurken and Keren. Since all Rhomboids share a conserved serine protease catalytic dyad (Lemberg et al., 2005; Urban et al., 2001), it has been suggested that they are all able to cleave proteins in the transmembrane domain. Our knowledge of the mammalian rhomboids is extremely scarce. For example, they are unlikely involved in EGF signalling, since TGFα, the major mammalian ligand of the EGFR pathway, is released by metalloproteases of the ADAM family (Freeman, 2004).

Rhomboids differ from all the other families of intramembrane proteases because they do not require prior trimming of the substrate. Since rhomboids cleave intact membrane proteins, without a regulated prior cleavage, how is rhomboid activity controlled?

The best-characterized mode of rhomboid regulation is cellular compartmentalization, a case exemplified by the couple Spitz /Rhomboid-1. Before cleavage, Spitz is kept at the endoplasmic reticulum, while Rhomboid-1 resides in Golgi. By analogy with other secretases in the secretory pathway, it seems likely that rhomboid enzymatic activity itself is also directly regulated, and although there is no evidence yet to confirm this, there are some novel observations. For example, it has been suggested that the activity of the mammalian mitochondrial rhomboid PARL may be regulated by phosphorylation and autoproteolytic processing in the N-terminal tail (Jeyaraju et al., 2006). Equally, some rhomboids have putative calcium-binding EF hands

(Koonin et al., 2003) or a lipid-binding domain (Del Rio et al., 2007); these could represent regulatory sites. Even more speculatively, a class of highly conserved, catalytically inactive rhomboid homologs (termed iRhoms) could regulate rhomboid activity.

In the last years several intramembrane cleaving proteases have been identified, overturning the dogma that proteolysis (a hydrolyzing reaction) occurs only in aqueous environments (Annaert and De Strooper, 2002; Brown et al., 2000; Freeman, 2004; Kopan and Ilagan, 2004). All doubts that hydrolysis can occur in the hydrophobic environment of the membrane have now completely evaporated, and we have real mechanistic insights into how rhomboids work. In a landmark paper, Ha and colleagues published the first high-resolution structure of an intramembrane protease: the 2.1 Å crystallographic structure of the *E. coli* rhomboid GlpG (Wang et al., 2006; Wang et al., 2006). The hydrophilic cavity surrounding the rhomboid active site suggests an aqueous microenvironment suitable for a hydrolysis reaction to occur in the plane of the membrane.

Several studies show that rhomboids across evolution recognize related substrate features (Urban et al., 2001; Urban and Freeman, 2003; Urban and Wolfe, 2005; Lemberg et al., 2005). For example, rhomboids that localize in the eukaryotic secretory pathway cleave type I membrane proteins with helix-destabilizing residues, like glycine, near their cleavage site (Urban and Freeman, 2003).

In 2006 the group of Freeman showed that in *Drosophila*, the mitochondrial rhomboid 7 is required for mitochondrial fusion during fly spermatogenesis and muscle maturation. Rhomboid-7 mutant flies have severe neurological defects, evidenced by compromised signalling across the first visual synapse, as well as light-induced neurodegeneration of photoreceptors that resembles the human ADOA disease. Rhomboid-7 mutant flies also have a greatly reduced lifespan (McQuibban et al., 2006).

3.13.2. Rbd1/Pcp1p

Saccharomyces cerevisiae has two rhomboids, named Rbd1p and Rbd2p. Rbd1p has two substrates: cytochrome *c* peroxidase (Ccp1p); and a dynamin-like GTPase (Mgm1p). (McQuibban et al., 2003)

∆rbd1 cells display fragmented mitochondria and impaired growth on non-fermentable carbon sources, similar to the phenotype caused by deletion of one of the substrate of Rbd1p, the dynamin related protein Mgm1p (Esser et al., 2002; Herlan et al., 2003; McQuibban et al., 2003; Sesaki et al., 2003). The short isoform of Mgm1p produced by Rbd1p is required to maintain mitochondrial morphology (Herlan et al., 2003; McQuibban et al., 2003). Thus, rhomboids and intramembrane proteolysis appear to control mitochondrial dynamics and function in yeast.

The dynamin-like GTPase Mgm1p and the rhomboid protease Rbd1p constitute a substrate-protease couple in yeast (Herlan et al., 2003; McQuibban et al., 2003). Mgm1p is pulled by the mitochondrial import machinery further into mitochondrial matrix until the second TM domain,

harbouring the rhomboid cleavage site, becomes integrated into the inner mitochondrial membrane (Herlan et al., 2004). This second translocation requires ATP, thereby coupling Mgm1p processing with the mitochondrial bioenergetic state. The balance between the membrane-anchored and the rhomboid-released isoforms of Mgm1p is crucial for the control of mitochondrial membrane dynamics in yeast (Herlan et al., 2003; McQuibban et al., 2003). A similar process occurs with yeast cytochrome *c* peroxidase (Ccp1), the second known substrate of Pcp1/Rbd1: the primary TM domain has to be dislocated by the m-AAA protease subunits Yta10 (Afg3) and Yta12 (Rca1) in order to allow rhomboid cleavage (Esser et al., 2002; Tatsuta et al., 2007).

3.13.3. PARL

PARL, presenilin-associated rhomboid-like, originally identified in a yeast two-hybrid screen as an interactor of presenilin (Pellegrini et al., 2001), is a rhomboid protease of the inner mitochondrial membrane (IMM).

Despite of the functional and structural conservation of Pcp1p, rhomboid-7, and PARL, their N-terminal domain are unrelated (Sik et al., 2004). The N-terminal region of PARL, which is in the matrix (Jeyaraju et al., 2006), spans the first 100 amino acids of the protein and shows no detectable similarity to any other available protein sequences.

The matrix N-terminal domain of PARL (Pβ) undergoes two consecutive cleavage events, termed α and β. The proximal α-cleavage (52Gly↓Phe53) is a constitutive processing associated with the protein import in the mitochondria (Sik et al., 2004). Therefore, it is probably executed by one of the two proteases that typically are responsible for the import of most IMM proteins, the mitochondrial processing peptidase (MPP) and the innermembrane peptidase (IMP) (Gakh et al., 2002). The distal β-cleavage (77Ser↓Ala78) is regulated through a mechanism of proteolysis requiring PARL activity supplied in trans (Sik et al., 2004). The identity of the matrix protease that cleaves PARL at the β-cleavage site remains elusive. However, PARL β-cleavage is unlikely to be executed by PARL itself since the cleavage site is not embedded within a hydrophobic helix. β-Cleavage confers a gain of function in PARL-mediated regulation of mitochondria morphology. Mitochondrial fragmentation by overexpressed PARL is reduced when β-cleavage is abolished by removing or mutating the cleavage site. PARL is constitutively and completely phosphorylated at three residues placed in close proximity to the β-cleavage site (Ser65, Thr69, Ser70). Since hyperphosphorylation of PARL blocks β–cleavage, (Jeyaraju et al., 2006) dephosphorylation appears to be required to allow this processing, thereby implicating a matrix phosphatase in the regulation of mitochondrial morphology.

The 25-amino acid-long peptide released in the matrix by PARL β-cleavage, termed Pβ peptide, can be found in the nucleus (Sik et al., 2004), suggesting a role for it in mitochondria-to-nucleus signalling. Although further studies are required to confirm this possibility, participation of the Pβ

peptide in retrograde regulation (nuclear responses to changes in the functional state of mitochondria) would bring PARL within the mainstream concept of RIP, whereby a signalling protein is subjected to highly regulated release. Unlike other I-CliPs, however, the case of PARL would be the first example of RIP where the putative signalling moiety is part of the I-CliP itself.

3.14. Apoptosis

The term apoptosis was first coined by Currie and colleagues in 1972 to describe a common, conserved, programmed type of cell death that the authors repeatedly observed in various tissues and cell types, morphological distinct from necrotic cell death (Kerr et al., 1972).

In multicellular organisms, apoptosis ensures the precise and orderly elimination of surplus or damaged cells. Cell death during embryonic development is essential for successful organogenesis and crafting of complex multicellular tissues: elimination of the webbing between digits in humans and mice, and the deletion of mammary tissue in males are good examples of this. During adulthood, it ensures the maintenance of normal cellular homeostasis and regulation of immunity. Conditions that increase or decrease normal cell death levels in different tissues can result in disease: insufficient apoptosis manifests as cancer or autoimmunity, while accelerated cell death is evident in acute and chronic degenerative diseases (Meier et al., 2000; Kroemer and Zitvogel, 2007; Kerr et al., 1972).

The fact that apoptosis is characterized by a stereotyped series of morphological and biochemical changes (Krammer, 2000) suggests that a common intracellular pathway ultimately leads to cell demise in a coordinated fashion, independently of the specific activating event. Depending on the cell type and the death stimulus, two main apoptotic pathways are activated: the intrinsic pathway, which is triggered by intracellular apoptotic signals and is almost always mediated by mitochondria; and the extrinsic pathway, which is triggered by activation of specific death receptors at the cell surface [reviewed in (Hacker, 2000)], and leads to pro-caspase 8 recruitment and activation. Caspase 8 can cleave other caspases (type I cells), or generate truncated Bid (tBid) that in turn triggers the mitochondrial amplification loop (type II cells).

3.14.1. Mitochondrial involvement in apoptosis

Mitochondrial involvement in apoptosis has been well characterized in the last 10 years. Its two main features include the release of proteins from the intermembrane space (IMS) and the initiation of a programme of dysfunction that includes the loss of the proton electrochemical gradient across the inner membrane. Molecular mechanisms are still under investigation and probably crosstalk mediate these two events (Bernardi et al., 2001).

The mitochondrion is at the core of the intrinsic apoptosis pathway, and provides a reservoir for protein factors that induce caspase activation. Mitochondria release into the cytosol a plethora of pro-apoptotic factors, such as cytochrome *c*, Smac/DABLO and Omi/HtrA2, which inhibit the

cytosolic inhibitor of apoptosis proteins (IAPs) responsible for caspase inhibition; AIF and endonuclease G, which migrate in the nucleus to induce chromatin cleavage and condensation (Kroemer et al., 2007).

The most studied protein cofactor released by mitochondria in response to an apoptotic stimulus is cytochrome *c* (Liu et al., 1996). Nevertheless, the precise mechanism whereby cytochrome *c* and other mitochondrial intermembrane space proteins are released is still under active investigation.

Several hypothesis have been proposed to explain the egress of cytochrome *c* from mitochondria; these mechanisms may either function on their own or in cooperation: (i) in response to an apoptotic stimulus, the “BH3-only” subset of proapoptotic BCL-2 family members senses death signals and transmits them to the “multidomain” proapoptotics like Bax and Bak. These ultimately oligomerize in the mitochondrial outer membrane and form pores permitting the physical efflux of cytochrome *c* and of the other mitochondrial apoptotic cofactors. (ii) proapoptotic BCL-2 family members interact with intrinsic proteins of mitochondria, triggering mitochondrial dysfunction and permeability transition. (iii) Mitochondrial membrane permeabilization may result from an alteration in membrane curvature or from the formation of lipidic pores in the OM. Anyway, permeabilization of the MOM alone results only in the partial release of cytochrome *c* into the cytosol: the complete release of cytochrome *c* occurring during apoptosis requires the structural remodelling of the mitochondrial *cristae*.

Independently from the precise mechanism of cytochrome *c* egress from mitochondria, the BCL-2 family proteins appear as critical death regulators. This family of proteins, consisting of both pro- and antiapoptotic members, possesses conserved α-helices with sequence conservation clustered in BCL-2 homology (BH) domains. Antiapoptotic members exhibit the homology in all segments from BH1 to 4, while proapoptotic molecules lack stringent sequence conservation of the first α-helical BH4 domain. Proapoptotic molecules can be further subdivided into multidomain and BH3-only proteins. Multidomain proapoptotic members such as BAX and BAK display sequence conservation in BH1-3 domains. BH3- only members display sequence conservation solely in the amphipathic α-helical BH3 region (Scorrano and Korsmeyer, 2003). Nowadays it is clear that the decision to die or not depends on the balance resulting from the activation of proapoptotic and antiapoptotic members of the BCL-2 family (Danial and Korsmeyer, 2004).

In a widely accepted model, the BH3-only members connect upstream proapoptotic signals to the mitochondrial pathway. Once activated, BH3-only proteins function as ligands for the multidomain proapoptotics BAX and BAK, induce their homo/heterooligomerization and ultimately release cytochrome *c* from mitochondria (Scorrano and Korsmeyer, 2003). As mentioned above, other mechanisms (for example: permeability transition or alteration of

membrane curvature) may cooperate with multidomain proapoptotics during cytochrome c release.

While such a model appears substantiated by several evidences, how antiapoptotic BCL-2 family members oppose their proapoptotic counterparts is less clear. It has been proposed that BCL-2 and BCL-XL sequester BH3-only molecules, preventing activation of the multidomain proapoptotics (Cheng et al., 2001). Alternatively, antiapoptotic proteins could keep BAX and BAK in an inactive conformation, antagonizing binding to the incoming BH3-only proteins (Willis et al., 2005).

Once released, cytosolic cytochrome *c* binds to APAF-1, increasing its affinity for dATP/ATP. The complex composed by APAF-1, cytochrome *c*, dATP and ATP forms the apoptosome. The apoptosome is able to recruit procaspase-9, facilitate its auto-activation and subsequently leads to the activation of downstream executioner caspases, cysteine proteases, that effect cell demise (Zou et al., 1999; Rodriguez and Lazebnik, 1999). Executioner caspases then cleave other intracellular substrates leading to the characteristic morphological changes in apoptosis such as chromatin condensation, nucloesomal DNA fragmentation, nuclear membrane breakdown, externalization of phosphatidylserine (PS) and formation of apoptotic bodies (Hengartner, 2000).

While the cell death machinery is well conserved from worm to mammals, it remains uncertain whether mitochondria play an active role in caspase activation during developmental apoptosis of *C. elegans*. If we go back to more ancient multicellular organisms like *C. elegans* and *D. melanogaster*, we would see that despite conservation of Bcl-2 family members, mitochondria appear to be dispensable or just platforms where the reactions that regulate apoptosis happen to take place. In *C. elegans* the BCL-2 related protein CED-9 localizes to mitochondria through its C-terminal transmembrane domain and inhibits programmed cell death by inactivating the function of the caspase activating protein CED-4. EGL-1, a pro-apoptotic BH3-only protein of the Bcl-2 family, promotes dell death by binding to CED-9 and displacing it from CED-4; CED4 is thereby able to translocate to perinuclear membranes resulting in activation of the *C. elegans* caspase CED-3 (Lettre and Hengartner, 2006).

3.14.2. Mitochondrial morphology and apoptosis

Early in the course of programmed cell death, mammalian mitochondria coordinately fragment and undergo a reorganization of their *cristae*, called "*cristae* remodeling", in order to release most of their cytochrome *c* content (Frank et al., 2001; Scorrano et al., 2002; Germain et al., 2005). Mitochondrial fission is an early trait of apoptosis, occurring simultaneously to BAX translocation from the cytosol, and before activation of caspases (Frank et al., 2001). Although mitochondrial fragmentation is a common event during cell death, it is not yet clear whether fragmentation of the mitochondrial network is necessary and sufficient for induction of cell death. The fragmented appearance of mitochondria is caused by a combination of activation of

the fission machinery and inhibition of the fusion one (Lee et al., 2004). The importance of mitochondria-shaping proteins and of mitochondrial shape changes in regulating mammalian apoptosis is substantiated by genetic evidences showing that inhibition of fission, as well as promotion of fusion counteract apoptosis by intrinsic, mitochondria utilizing stimuli [reviewed in (Youle and Karbowski, 2005)]. The dynamin-related protein Drp-1 and endophilin B1, a fatty acil transferase, translocate from the cytosol to foci on mitochondria early during apoptosis and they probably mediate mitochondrial apoptotic fission (Frank et al., 2001; Breckenridge et al., 2003; Germain et al., 2005). On the other hand, apoptosis can be inhibit by antagonizing the fission process. The down regulation of Drp-1 activity by RNAi or by overexpression of a dominant negative mutant Drp-1K38A, inhibits apoptosis and mitochondrial fragmentation, although Bax was traslocated to mitochondria and coalesced into foci with Bak (Karbowski and Youle, 2003; Frank et al., 2001). Inhibition of FIS1 also protects from apoptosis (Sugioka et al., 2004), while its overexpression induced apoptosis (James et al., 2003; Alirol et al., 2006).

Recent works show that early in the course of cell death, MFN1 mediated fusion is suppressed and the concomitant overexpression of both mitofusins protects from apoptosis induced by intrinsic stimuli like BID and etoposide (Sugioka et al., 2004). Down regulation of OPA1 levels induces fragmentation of mitochondrial network, release of cytochrome *c* and apoptosis (Olichon et al., 2003).

Interestingly, one of the most prominent mitochondrial traits of developmental apoptosis in the worm as well as in *Drosophila* cells are their morphological changes. Jagasia et al. showed that the fragmentation of the mitochondrial network during developmental apoptosis of *C. elegans* is enhanced by EGL-1 and independent of caspase activation, suggesting that it occurs before of, or simultaneously to caspase activation (Jagasia et al., 2005). Expression of Debcl in Drosophila as well as in mammalian cells causes a similar fragmentation of the mitochondrial network (Igaki et al., 2000). These probably represent the only mitochondrial change that we found conserved during apoptosis of invertebrate and mammalian cells.

Moreover, studies in yeast confirm a role for mitochondrial fragmentation and for Drp1 in apoptosis (Fannjiang et al., 2004). On the other hand, fragmentation can also negatively regulate the progression of the apoptotic cascade, as suggested by data from the laboratory of R. Rizzuto. While Drp1 can enhance staurosporine-mediated apoptosis, it slows down the amplification of Ca^{2+}-mediated cell death (Szabadkai et al., 2004).

3.15. The role of mitochondria in development and differentiation

Mitochondria display a unique behaviour during embryonic development. They are maternally transmitted, with little (if any) paternal contribution, and they originate from a restricted founder population, which is amplified during oogenesis. Then, having established the full complement of mitochondria in the fully grown oocyte, there is no further increase of the mitochondrial

population during early development. For example, murine oocytes possess 10^5 mtDNA copies immediately prior to fertilisation and there is no increase in mtDNA copy number until post-implantation, each newly divided blastomere within the pre-implantation embryo will possess fewer copies of the genome at each stage of post-fertilization cell division. This persists until the blastocyst (Shoubridge and Wai, 2007), the final stage of pre-implantation development.

Localization of mitochondria in the fertilized egg and their segregation to blastomeres in the cleaving embryo are strictly regulated (Thundathil et al., 2005). Gradients in the distribution of mitochondria present in the egg have the potential to give rise to blastomeres receiving different numbers of mitochondria. Such maternally inherited differences in mitochondrial distribution are thought to play roles in defining the long-term viability of the blastomere in some cases and embryonic axes and patterning in others. This is probably a consequence of the direct involvement of these organelles in the reproductive and development processes, by modulating Ca^{2+} signalling, production of ATP, reactive oxygen species, and intermediary metabolites. Besides these multiple functions, the dual role for mitochondria in controlling life and death of the cell may influence the quality control system of the early embryo, that will determine whether the embryo proceeds further into development or is quickly eliminated (Lonergan et al., 2006).

Mitochondrial dynamics seems to play an essential role in the early stages of development. Reports demonstrate a rearrangement of mitochondrial network during early fertilisation of the hamster oocyte, when nearly all the mitochondria move from a totally homogeneous or dispersed configuration to a location around the pronuclei, (Dumollard et al., 2007) and deficits in mitochondria shaping proteins result in specific developmental defects. Both MFN1 and MFN2 are essential for embryonic development and loss of either MFN1 or MFN2 results in mid-gestational lethality (Chen et al., 2003). *Mfn1*$^{-/-}$ embryos die at embryonic day E10.5. However, by E12.5, most mutant embryos are absorbed. It is also noteworthy that by E8.5 most mutant embryos are smaller than the relative wt. In *Mfn2*$^{-/-}$, normal numbers of live homozygous mutant embryos are recovered up to E9.5, however, after E10.5 embryos start to be absorbed. The live mutant embryos at E9.5 and E10.5 are slightly smaller than the wt ones, but otherwise well developed and show no obvious malformation. Lethality in *Mfn2*$^{-/-}$ embryos results from an improper development of the placenta. The trophoblast giant cell layer is sparse and incomplete, resulting in placental insufficiency and trophoblast cells present a fragmented mitochondrial network (Chen et al., 2003). Beyond defects in mitochondrial fusion, worms deficient in mitochondrial division die before adulthoodd (Labrousse et al., 1999b) and an infant patient with a dominant negative Drp1 allele has been reported. This patient died at ~1 month of age and had a wide range of abnormalities, including reduced head growth, increased lactic acid and optic atrophy. Fibroblasts from this patient showed elongated mitochondria and peroxisomes (Labrousse et al., 1999a).

3.15.1. ES cells

In 1981 two independent groups of scientists successfully isolated and cultured proliferative cells derived from mouse embryos (Waterham et al., 2007; Evans and Kaufman, 1981) . Prior to that day, *in vitro* model systems to study the developing embryo used cell lines derived from teratocarcinomas (Martin, 1980). Teratocarcinoma cell lines shared many morphological, biochemical, and immunological properties with pluripotent ES cells, but had undergone transformation and karyotypic changes prior to establishment as cultured cell lines.

In 1985, O. Smithies and colleagues (Smithies et al., 1985) demonstrated gene targeting using homologous recombination in a mammalian cell line. At the same time Thomas and Capecchi (Thomas and Capecchi, 1987) applied site-directed mutagenesis in a mouse ES cell establishing homologous recombination as a resource to systematically modify the mouse genome. Several years earlier, it was demonstrated that, when they were injected into mouse blastocysts, genetically altered ES cells could generate transgenic offspring (Gossler et al., 1986; Robertson et al., 1986). The application of these techniques with homologous recombination technology thus provided scientists with a controlled process to generate an unlimited variety of transgenic and knock-out mice with engineered, predetermined genomes. The technology developed rapidly, and the first viable chimeric mice were reported in 1989 (Thompson et al., 1989). The isolation of murine ES cell lines in 1981 enabled a plethora of research opportunities. From gene targeting by homologous recombination to new insights on cell cycle regulation and development, ES cells provided researchers with the toolkit needed to better understand the genetic basis of many diseases.

ES cells are derived from the inner cell mass of preimplantation blastocysts and exhibit three particularly useful properties. First, they are totipotent: ES cells maintained in culture remain competent to contribute to all tissues, including germ cells, after introduction into mouse blastocysts. Second, targeted mutations in ES cells may be created readily through homologous recombination and introduced into the mouse germ line to study their effects in vivo. Third, wild-type or mutant ES cells can differentiate *in vitro* to form a variety of cell types in a sequence that recapitulates the first stages of embryogenesis. Therefore ES cells are the most available and simplest system to analyze the genetic pathways that regulate embryonic development and to identify novel genes that control differentiation.

Stem cells have been recently implicated in the origin of cancer: according to the cancer stem cell hypothesis, a tissue-specific adult stem cell might acquire a malignant phenotype and initiate a tumour. Therefore, cancer can be considered to be a disease of un-regulated self-renewal. This theory is based on three similarities between stem cells and tumour cells: the resemblance of the mechanisms regulating self-renewal; the possibility that tumour cells can arise from normal stem cells; and the notion that tumours can contain cancer stem cells (Reya et al., 2001a). Evidences show that many pathways classically associated with cancer may also

regulate normal stem cell development. Adult stem cells and their malignant counterparts share almost all of the same intrinsic and extrinsic factors to regulate self-renewal, differentiation and proliferation pathways. In addition, normal and cancer stem cells exhibit an active telomerase expression, migratory properties, resistance to apoptosis (Reya et al., 2001b; Peters et al., 1998), enhanced activity of membrane transport (Feuerhake et al., 2000; Zhou et al., 2001), and can growth under anchorage-independent in vitro conditions. Stem cells have been identified in a number of solid tumours, ranging from breast (Terskikh et al., 2001) to colon (O'Brien et al., 2007) and prostate (Liu et al., 2005; Reiter et al., 1998) and have been shown to be able to self maintain the tumour population. Part of this phenotype could be ascribed to changes in the mitochondrial pathways of apoptosis.

3.15.2. In vitro differentiation of ES cells

In vitro differentiation of ES cells offers a unique approach to examine what occurs during *in vivo* embryonic development and complements gene knockout studies in whole animals. The identification of genes that regulate ES cells self-renewal, pluripotential, and differentiation to specific subtypes is essential to understand the same processes in adult and progenitor cells and therefore to clarify the pathogenetic mechanisms of many diseases.

ES cells can be maintained and expanded *in vitro* as a poor population of pluripotent cells under conditions that inhibit differentiation, e.g. on the surface of growth inactivated embryonic fibroblasts or in complete medium supplemented with leukemia inhibitory factor (LIF). Differentiation of ES is typically carried out by removing LIF from the medium and allowing cultures to overgrow, by plating cells in suspension on non-adhesive substrates, in ‘‘hanging drop’’ (to control cell number and force cell-cell contact), or in low-substrate adhesion conditions such as in methylcellulose. After 4–8 days in vitro, cells aggregate into irregular clumps, which, because they grossly resemble early embryo with an endoderm exterior, mesoderm and ectoderm interior, surrounding a large cystic yolk sac–like cavity, have been called ‘‘embryoid bodies’’ (EBs). Haematopoiesis within EBs has been studied most extensively, although vasculogenesis, myogenesis, and development of neuronal- like cells have also been observed [reviewed in (Weiss and Orkin, 1996)].

In vitro differentiation of murine ES cells gives rise to the three primary germ layers – the endoderm, mesoderm and ectoderm – that characterize early stages of embryonic development (Weiss and Orkin, 1996). This is then followed by the expression of stage specific markers, associated with certain lineages, such as vimentin, nestin and β-tubulin III during neuronal differentiation (Leahy et al., 1999; Rolletschek et al., 2001) and brachyury and Nkx2,5 during cardiac differentiation (Bouhon et al., 2006; Wilkinson et al., 1990a).

3.15.3. Mitochondrial contribution to stem cells

The distribution and functions of mitochondria in stem cells have not been extensively examined, yet the contributions of these organelles to stem cell viability and differentiation must be vitally important in view of their critical roles in all other cell types.

A large number of studies on both adult and embryonic stem cells have been accumulated until now. Many of these studies have addressed the functionality and pluripotency of stem cells by examining their behaviour in culture, sometimes under very non-physiological conditions, or by injecting them into immuno-compromised mice. Functional cellular markers, such as mitochondrial properties, have been greatly neglected during the rush to study stem cells. Parameters of mitochondrial activity, both genomic and bioenergetic, might serve as useful markers of the quality of 'stemness' that would help identify the most dependable and reliable stem cell lines for basic research and eventually for clinical transplantation studies. Furthermore, commitment into a specific lineage, regulated by lineage-specific transcription factors (Wilkinson et al., 1990b; Pevny et al., 1998) is likely to initiate the expansion of the number of mitochondria and mtDNA molecules per cell according to the specific metabolic demands of individual cells.

It has been recently demonstrated that the loss of pluripotency and the induction of cell fate commitment, upon differentiation of ES cells occur in the presence of low levels of mtDNA replication. A decrease in expression of pluripotency markers and increasing numbers of committed ES cells proceed in the presence of low levels of expression of POLG, POLG2 and TFAM, which ensure that sufficient mtDNA is preserved within proliferating mESCs for subsequent transmission. After ES cells have committed to a specific lineage, mtDNA is extensively replicated, leading to the enrichment of the mitochondrial content to provide the higher levels of ATP required for further differentiation (Facucho-Oliveira et al., 2007). Low number of mtDNA copies reported in undifferentiated mESCs could be related to the requirements of the cell for high glycolytic metabolism and low oxygen consumption, which are needed to maintain their proliferative capacity (Kondoh et al., 2007).

Transition from anaerobic metabolism, which characterizes undifferentiated ESCs, into a more efficient mitochondrial, aerobic metabolism is crucial for successful differentiation of mouse and human ESCs (St John et al., 2005; Chung et al., 2007; Kondoh et al., 2007). Activation of the electron transport chain and Krebs' cycle as part of this switch involves an increase in mtDNA content and expression of proteins involved in aerobic metabolism and ATP production (Chung et al., 2007; Cho et al., 2006). Indeed, inhibition of the ETC with antimycin A or rotenone during mESCs differentiation has been shown to decrease mitochondrial volume (Spitkovsky et al., 2004; Chung et al., 2007), whereas disrupted mitochondrial networks lead to a dramatic reduction in the number of beating embryoid bodies (EBs; up to 80%) and sarcomere content of differentiating cardiomyocytes (Chung et al., 2007).

In conclusion, mitochondria appear to be crucial also in the regulation of ES cell differentiation; moreover, a specific layer of control appear to be exerted by mitochondria-shaping proteins, whose levels are tightly regulated for example during differentiation into cardiomyocytes. A last part of this Thesis has therefore been devoted to the development of an in vitro ESC differentiation protocol to analyse the effect of the ablation of *Opa1* on cardiac and neuronal differentiation.

4. Results

Frezza C, Cipolat S, Scorrano L.
Organelle isolation: functional mitochondria from mouse liver, muscle and cultured fibroblasts.
Nat Protoc. 2007;2(2):287-95.

Frezza C, Cipolat S, Scorrano L Frezza C, Cipolat S, Scorrano L
Measuring mitochondrial shape changes and their consequences on mitochondrial involvement during apoptosis.
Methods in Molecular Biology 2007, 372

Cipolat,S., de Brito,O.M., Dal Zilio,B., and Scorrano,L.
OPA1 requires mitofusin 1 to promote mitochondrial fusion.
Proc. Natl. Acad. Sci. U. S. A. 2004 (101) 15927-15932.

Cipolat S, Rudka T, Hartmann D, Costa V, Serneels L, Craessaerts K, Metzger K, Frezza C, Annaert W, D'Adamio L, Derks C, Dejaegere T, Pellegrini L, D'Hooge R, Scorrano L, De Strooper B.
Mitochondrial rhomboid PARL regulates cytochrome c release during apoptosis via OPA1-dependent cristae remodeling.
Cell. 2006 Jul 14;126(1):163-75.

Frezza C, Cipolat S, Martins de Brito O, Micaroni M, Beznoussenko GV, Rudka T,Bartoli D, Polishuck RS, Danial NN, De Strooper B, Scorrano L.
OPA1 controls apoptotic cristae remodeling independently from mitochondrial fusion.
Cell. 2006 Jul 14;126(1):177-89.

Cipolat S, Scorrano L.
To fuse and to protect: a novel role of CED-9 in mitochondrial morphology reveals an ancient function.
Cell Death and Differentiation. 2006 (13): 1833-1834

Cipolat S, Scorrano L.
OPA1 participates in differentiation of embryonic stem cells into cardiomyocytes

Organelle isolation: functional mitochondria from mouse liver, muscle and cultured filroblasts

Christian Frezza, Sara Cipolat & Luca Scorrano

Dulbecco-Telethon Institute, Venetian Institute of Molecular Medicine, Via Orus 2, 35129 Padova, Italy. Correspondence should be addressed to L.S. (luca.scorrano@unipd.it).

Published online 22 February 2007; doi:10.1038/nprot.2006.478

© 2007 Nature Publishing Group http://www.nature.com/natureprotocols

Mitochondria participate in key metabolic reactions of the cell and regulate crucial signaling pathways including apoptosis. Although several approaches are available to study mitochondrial function *in situ* are available, investigating functional mitochondria that have been isolated from different tissues and from cultured cells offers still more unmatched advantages. This protocol illustrates a step-by-step procedure to obtain functional mitochondria with high yield from cells grown in culture, liver and muscle. The isolation procedures described here require 1–2 hours, depending on the source of the organelles. The polarographic analysis can be completed in 1 hour.

INTRODUCTION

Mitochondria are central organelles controlling the life and death of the cell. They participate in key metabolic reactions, synthesize most of the ATP and regulate a number of signaling cascades, including apoptosis[1].

Since the early years of "hard-core" bioenergetics when mechanisms behind energy conservation were avidly investigated, mitochondrial research has benefited from the availability of preparations of organelles isolated from tissues. We owe this to the pioneering work of George Palade and coworkers, who in the late 1940s developed a protocol to isolate mitochondria, based on differential centrifugation[2]. They built on the earlier work of Bensley and Hoerr[3], who isolated a mixed membranous fraction by centrifugation from freeze-thawed guinea-pig liver that was probably enriched in mitochondria. The intuition of Palade was to apply differential centrifugation to allow for separation of the constituents of the cell based on their different sedimentation properties following mechanical homogenization of the tissue. This approach was a real Copernican revolution for mitochondrial research, allowing the isolation of pure organelles with high yields. As a practical consequence, in the subsequent 20 years, we saw such amazing discoveries: the mechanism of energy conservation[4]; the identification of mitochondrial DNA[5,6] and of import of mitochondrial precursor proteins[7]; the definition of mitochondrial ultrastructure, with the development of the so-called "Palade's model"[8]; and last but not least, the discovery of inner mitochondrial membrane channels[9].

After almost 15 years during which mitochondria left the center stage of biomedical research, they made their grand *reentrée* in the 1990s, following the discovery that they amplify apoptosis by releasing cytochrome *c* and other intermembrane space proteins required to activate fully effector caspases[10,11]. Although it appears clear that mitochondria play a crucial role in apoptosis, the precise mechanism by which cytochrome *c* is released remains a matter of intense debate and research[12]. Moreover, evidence is mounting on the role of this organelle in several pathophysiological processes, including neurodegeneration[13], neuronal morphogenesis and plasticity[14] and infertility[15]. These findings, added to the results of old and new areas of research, aimed at unraveling the basic biological mechanisms of mitochondrial function. From the transport of metabolites and ions, to the elucidation of the mechanisms and proteins involved in protein import, and to the dynamic behavior of mitochondria, all of these fields benefit greatly from the availability of isolated, pure organelles.

This protocol describes how to obtain functional, purified, intact mitochondria from three different sources: liver[16], skeletal muscle[17] and cultured cells[18]. These variants intend to be exemplificative and not exhaustive, as they do not cover the different sources from which mitochondria can be isolated. For example, isolation of mitochondria from yeast cells is tailored on the mechanical and osmotic characteristics of these lower eucaryotes[19]. Since our intention is to give a general framework for different organs and for cultured cells that can be in any case modified by the individual researcher, following exactly these protocols is best suited only for isolation of organelles from the described tissues and cells. However, our experience indicates that the protocol used with fibroblasts can be adopted without modification to isolate mitochondria from other cell lines such as HeLa and the prostate cancer cell line LnCaP. On the other hand, the protocols to isolate mitochondria from organs other than muscle and liver differ from the ones described here. We therefore strongly advise the reader to refer to published protocols specific for brain[20], brown adipose tissue[21], and heart[22].

It should be stressed that protocols available to isolate mitochondria are somewhat differ from ours, especially in the speeds of the differential centrifugation steps and in the sugar used as osmolyte in the isolation buffer. While in our experience small changes in the sedimentation speeds (600 vs. 800*g*, 7,000 vs. 8,000*g*) do not affect quality and yield of the mitochondrial preparation, it has been reported that the use of monosaccharides such as mannitol results in better coupled isolated mitochondria[23,24]. In our experience the use of mannitol did not improve the quality of our mitochondrial preparations. Should the reader find that quality or yield of mitochondria isolated using our protocol is unsatisfactory, it is advisable to try to substitute sucrose with a monosaccharide like mannitol. The ultimate goal of a mitochondrial isolation is to obtain organelles as pure and as functional as possible. We strongly advise, especially if mitochondria are used in functional assays (e.g., release of cytochrome *c*, mitochondrial fusion, protein import and

production of reactive oxygen species), to always measure the coupling of the preparation using an oxygen electrode. These protocols therefore end with a description of how to measure mitochondrial respiration to ascertain the quality of the preparation. Well-coupled mitochondria are the first step to achieving reliable, reproducible results in assays aimed at investigating the mechanisms of mitochondrial involvement in complex biological phenomena.

In conclusion, these protocols represent a valuable starting point to obtain pure mitochondria from tissues and cells. Isolated mitochondria can then be used to study the function of the organelle, response to apoptotic stimuli, characteristics of cytochrome *c* release, protein import and many other aspects of mitochondrial biology and pathophysiology that require a source of pure and functional organelles.

© 2007 Nature Publishing Group http://www.nature.com/natureprotocols

MATERIALS

REAGENTS

- Cell line of interest or liver or muscle isolated from mice
- Mice of the desired genetic background (Charles River or Jackson Laboratories)
- Dulbecco's phosphate-buffered saline without Ca^{2+} and Mg^{2+} (PBS, Invitrogen, cat. no. 14200-067)
- Sucrose (Sigma, cat. no. 84100)
- Potassium phosphate monobasic (Pi, Sigma, cat. no. P5379)
- Sigma7-9 (Tris, Sigma, cat. no. T1378)
- 4-Morpholinepropanesulfonic acid (MOPS; Sigma, cat. no. M1254)
- Disodium ethylenediaminetetraacetate dihydrate (EDTA; Sigma, cat. no. ED2SS)
- Ethylene-bis(oxyethylenenitrilo)tetraacetic acid (EGTA; Sigma, cat. no. E4378)
- Potassium chloride (Baker, cat. no. 0208)
- Magnesium chloride hexahydrate (Sigma, cat. no. M9272)
- Bovine serum albumin (BSA; Sigma, cat. no. A6003)
- Dulbecco's modified Eagle's medium (Invitrogen, cat. no. 11971025)
- 200 mM L-glutamine (Invitrogen, cat. no. 25030024),
- Fetal bovine serum (Invitrogen, cat. no. 10270106)
- 5,000 U ml^{-1} penicillin/5,000 µg ml^{-1} streptomycin (Invitrogen, cat. no. 15070063)
- 10 mM minimal essential medium nonessential amino-acid solution (Invitrogen, cat. no. 11140)
- 0.25% (w/v) trypsin–EDTA solution (Invitrogen, cat. no. 25200072)
- Adenosine 5′-diphosphate sodium salt (ADP; Sigma, cat. no. A2754)
- Carbonyl cyanide 4-(trifluoromethoxy)phenylhydrazone (FCCP; Sigma, cat. no. C2920)
- Glutamic acid (Sigma, cat. no. 27647)
- Malic acid (Sigma, cat. no. M1000)
- Succinic acid (Sigma, cat. no. S3674)
- Rotenone (Sigma, cat. no. R8875)
- L-Ascorbic acid (Sigma, cat. no. 255564)
- *N,N,N,N*-Tetramethyl-*p*-phenylenediamine dihydrochloride (TMPD; Sigma, cat. no. T3134)
- Antimycin A (Sigma, cat. no. A8674)

EQUIPMENT

- 500 cm^2 dishes for cell culture (Nunclon, cat. no. 16 6508)
- 18-cm cell scrapers (Falcon, cat. no. 353085)
- Motor-driven tightly fitting glass/Teflon Potter Elvehjem homogenizer (**Fig. 1**)
- Clark-type oxygen electrode (Hansatech Oxygraph; **Fig. 2**)
- 50 ml polypropylene Falcon tubes
- 14 ml polypropylene Falcon tubes
- 1.5 ml microfuge test tube
- 30 ml round-bottomed glass centrifuge tube (Kimble, cat. no. 45500-30)
- Rubber adapter sleeve for centrifuge tube (Kimble, cat. no. 45500-15)
- Refrigerated centrifuge for 50 ml Falcon tubes and glass centrifuge tube
- Hamilton syringe: 10 µl (Hamilton, cat. no. 701 N) and 50 µl (Hamilton cat. no. 705 N)

REAGENT SETUP

Cell culture medium Use the medium recommended for your favorite cell line. For the cell lines mentioned in this protocol, use Dulbecco's modified Eagle's medium supplemented with 10% (v/v) fetal bovine serum, 0.1 mM minimal essential medium nonessential amino acids, 2 mM L-glutamine, penicillin–streptomycin 50 U ml^{-1} and 50 µg ml^{-1}, respectively.

Cells Two or three days before performing the experiments, plate cells in 500 cm^2 tissue-culture dishes. Use 70 ml of cell culture medium for each plate.

▲ CRITICAL Ensure that the cells are spread thoroughly wide on the plates: for high yield of isolated mitochondria, it is crucial to reach almost 100% confluence on the day of the experiment.

1 M sucrose Dissolve 342.3 g of sucrose in 1 liter of distilled water; mix well and prepare 20 ml aliquots; store them at −20 °C.

0.1 M Tris/MOPS Dissolve 12.1 g of Tris in 500 ml of distilled water, adjust pH to 7.4 using MOPS powder, bring the solution to 1 liter and store at 4 °C.

1 M Tris/HCl Dissolve 121.14 g of Tris in 500 ml of distilled water, adjust pH to 7.4 using HCl; bring the solution to 1 liter and store at room temperature.

0.1 M EGTA/Tris Dissolve 38.1 g of EGTA in 500 ml of distilled water, adjust pH to 7.4 using Tris powder, bring the solution to 1 liter and store at 4 °C.

0.5 M $MgCl_2$ Dissolve 101.7 g of $MgCl_2$ in 1 liter of distilled water and store at 4 °C.

1 M KCl Dissolve 74.6 g of KCl in 1 liter of distilled water and store at 4 °C.

1 M EDTA Dissolve 372.2 g of EDTA in 500 ml of distilled water, adjust pH to 7.4 using Tris powder, bring the solution to 1 liter and store at 4 °C.

10% BSA Dissolve 10 g of BSA in 100 ml of distilled water and store at −20 °C.

1 M Pi Dissolve 136.1 g of KH_2PO_4 in 500 ml of distilled water, adjust pH to 7.4 using Tris powder, bring the solution to 1 liter and store at 4 °C.

10 mM ADP Dissolve 4.7 mg of ADP in 1 ml of distilled water. Adjust pH to 7.4, prepare 100 µl aliquots and store in the dark at −20 °C for up to 6 months.

20 mM FCCP Dissolve 5.1 mg of FCCP in 1 ml of absolute ethanol. The color of the solution is faint yellow. Store at −20 °C. Dilute the stock solution to 100 µM by adding 10µl of 20 mM FCCP in 2 ml of absolute ethanol, just prior to use.

Figure 1 | Glass/Teflon Potter Elvehjem homogenizers. The homogenizer on the left (5 ml) is most suitable for isolation of mitochondria from cells, whereas the one on the right (30 ml) is more appropriate for isolation from tissues.

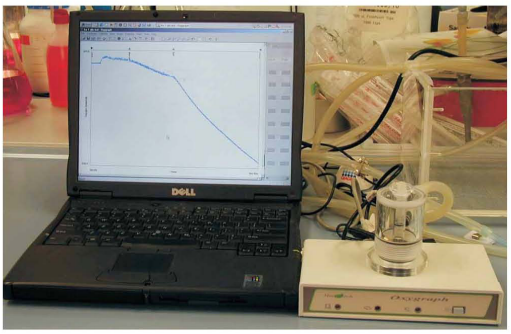

Figure 2 | A Clarke-type oxygen electrode connected to a laptop and a water bath. The trace on the screen corresponds to the recording of the experiment running when the photograph was taken.

0.25 M glutamate/0.125 M malate Dissolve 9.2 g of glutamic acid and 4.2 g of malic acid in 100 ml of distilled water. Adjust pH to 7.4 with Tris base to achieve complete dissolution of the salts. Add water to bring the volume to 250 ml, prepare 10 ml aliquots and store at −20 °C for up to 6 months.
0.5 M succinate stock solution (100×) Dissolve 3.0 g of succinic acid in 30 ml of distilled water. Adjust pH with Tris base to achieve complete solubilization of the salts. Add water to make up the volume to 50 ml, prepare 10 ml aliquots and store at −20 °C for up to 6 months.
2 mM rotenone stock solution Dissolve 4.7 mg of rotenone in 6 ml of absolute ethanol. Mix well for complete dissolution. ▲ CRITICAL Rotenone in organic solvents decomposes and is oxidized upon exposure to light and air. The solution, previously transparent, becomes brownish. It is imperative to protect the stock solution from direct light using an aluminum foil. ! CAUTION Rotenone is highly toxic: avoid skin contact and inhalation.

PROCEDURE

1| Mitochondria can be isolated from a variety of cells or tissues. Option A describes isolation of mitochondria from mouse embryonic fibroblasts (MEFs) (see **Fig. 3** for a timeline); option B describes isolation of mitochondria from mouse liver (see **Fig. 4** for a timeline); and option C describes isolation of mitochondria from mouse skeletal muscle (see **Fig. 5** for a timeline).

(A) Isolation of mitochondria from MEFs ● TIMING approximately 2 h

(i) Remove the medium from the cells and wash the cells once with PBS.
(ii) Remove PBS and detach the cells using a cell scraper.
(iii) Transfer the cell suspension to a 50 ml polypropylene Falcon tube.
(iv) Wash the plate once with PBS and scrape the dish to detach the remaining cells.
(v) Transfer the cells to the same polypropylene Falcon tube defined in Step 3. In our experience, seeding 120 × 10^6 MEFs per dish 2 days before the experiment results in a good yield of mitochondria (approximately 3 mg of mitochondrial protein).
(vi) Centrifuge cells at 600*g* at 4 °C for 10 min.
(vii) Discard the supernatant and resuspend cells in 3 ml of ice-cold IB_c.

600 mM ascorbate stock solution Dissolve 5.2 g of ascorbic acid in 50 ml of distilled water, adjust pH to 7.4 and store at −20 °C for up to 6 months.
30 mM TMPD stock solution Dissolve 0.36 g of TMPD in 50 ml of distilled water; adjust pH to 7.4; store at −20 °C for up to 6 months. The color of the solution is deep blue owing to the oxidation of the compound by oxygen.
25 mg ml^{-1} antimycin A stock solution Dissolve 50 mg of antimycin A in 2 ml of absolute ethanol. Dilute the stock solution to 25 µg ml^{-1}, by adding 2 µl of 25 mg ml^{-1} Antimycin A in 2 ml of absolute ethonal, just prior to use.
! CAUTION Antimycin A is highly toxic: avoid skin contact and inhalation.
Buffer for cell and mouse liver mitochondria isolation (IB_c) Prepare 100 ml of IB by adding 10 ml of 0.1 M Tris–MOPS and 1 ml of EGTA/Tris to 20 ml of 1 M sucrose. Bring the volume to 100 ml with distilled water. Adjust pH to 7.4.
Buffer 1 for muscle mitochondria isolation (IB_m1) Prepare 100 ml of IB_m1 by mixing 6.7 ml of 1 M sucrose, 5 ml of 1 M Tris/HCl, 5 ml of 1 M KCl, 1 ml of 1 M EDTA and 2 ml of 10% BSA. Adjust pH to 7.4. Bring the volume to 100 ml with distilled water.
Buffer 2 for muscle mitochondria isolation (IB_m2) Prepare 100 ml of IB_m12 by mixing 25 ml of 1 M sucrose, 3 ml of 0.1 M EGTA/Tris and 1 ml of 1 M Tris/HCl. Adjust pH to 7.4. Bring the volume to 100 ml with distilled water.
Experimental buffer for cell and mouse-liver mitochondria (EB_c) To prepare 100 ml of EB_c, mix 12.5 ml of 1 M KCl, 1 ml of 1 M Tris/MOPS, 10 ml of 100 µl 0.1 M EGTA/Tris and 100 µl of Pi. Adjust pH to 7.4. Bring the volume to 100 ml with distilled water.
Experimental buffer for muscle mitochondria (EB_m) To prepare 100 ml of EB_m, add 1 ml of 1 M Tris/HCl, 1 ml of 0.5 M $MgCl_2$, 200 µl of 1 M Pi and 20 µl of 0.1 M EGTA/Tris to 25 ml of 1 M sucrose. Adjust pH to 7.4. Bring the volume to 100 ml with distilled water. ▲ CRITICAL Wash all glassware three times with bidistilled water to avoid Ca^{2+} contamination. Ca^{2+} overload is the most common cause for the dysfunction of isolated mitochondria. ▲ CRITICAL Prepare all the buffers the same day of the experiment, to avoid bacterial/yeast growth in stored buffers. ▲ CRITICAL Since pH depends on temperature, measure the pH of all solutions at 25 °C.

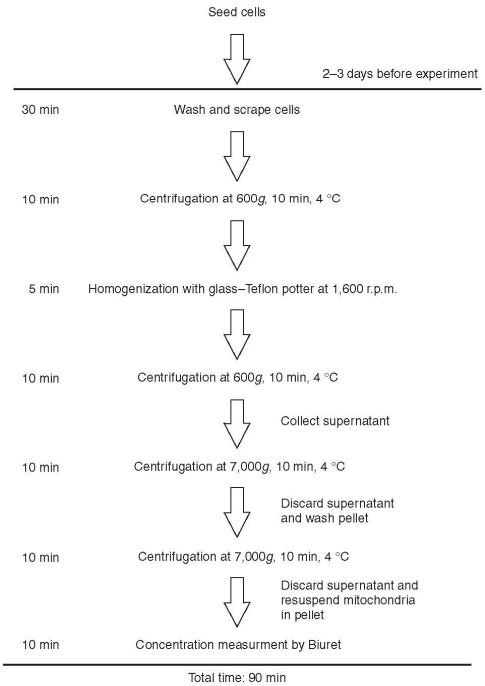

Figure 3 | Timing of isolation of mitochondria from MEFs.

© 2007 Nature Publishing Group http://www.nature.com/natureprotocols

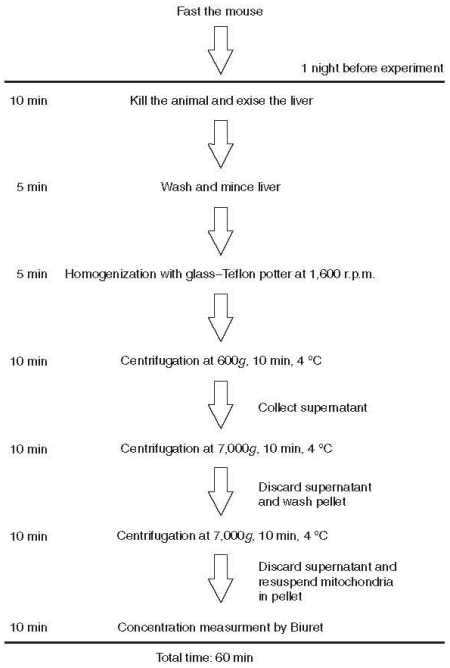

Figure 4 | Timing of isolation of mitochondria from mouse liver.

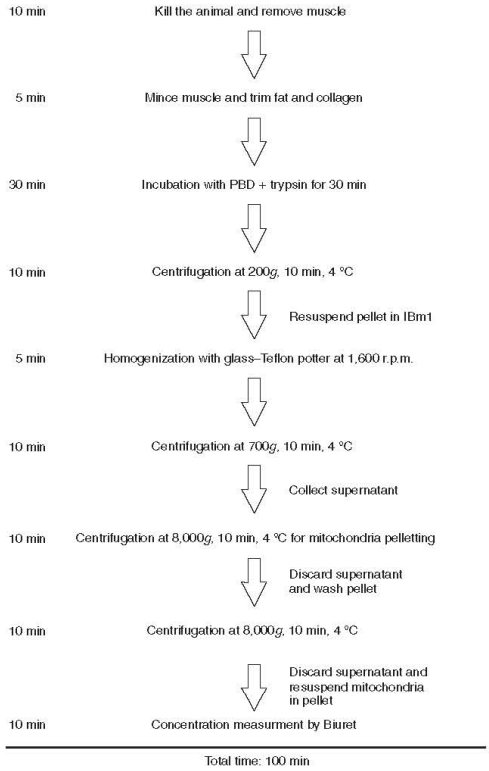

Figure 5 | Timing of isolation of mitochondria from mouse skeletal muscle.

(viii) Homogenize the cells using a Teflon pestle operated at 1,600 r.p.m.; stroke the cell suspension placed in a glass potter 30–40 times the cell suspension placed in a glass potter.
▲ **CRITICAL STEP** The Teflon–glass coupling represents the best compromise between homogenization of the cells and the preservation of mitochondrial integrity. Harsher techniques, including glass pestle in a glass potter, can easily damage mitochondria.
▲ **CRITICAL STEP** Precool the glassware in an ice-bath 5 min before starting the procedure. Homogenization as well as the following steps must be performed at 4 °C to minimize the activation of damaging phospholipases and proteases.
! **CAUTION** Wear protecting gloves while you are using the homogenizer to avoid possible injuries in the unlikely event that the potter breaks down.
? **TROUBLESHOOTING**

(ix) Transfer the homogenate to a 50 ml polypropylene Falcon tube and centrifuge at 600*g* for 10 min at 4 °C.

(x) Collect the supernatant, transfer it to a glass centrifuge tube and centrifuge it at 7,000*g* for 10 min at 4 °C.
? **TROUBLESHOOTING**

(xi) Discard the supernatant and wash the pellet with 200 µl of ice-cold IB_c. Resuspend the pellet in 200 µl of ice-cold IB_c and transfer the suspension to a 1.5 ml microfuge tube.

(xii) Centrifuge the homogenate at 7,000*g* for 10 min at 4 °C.

(xiii) Discard the supernatant and resuspend the pellet containing mitochondria. You can use a glass rod to loosen the pellet paste. Avoid adding IB and try to resuspend the mitochondria in the small amount of buffer that remains after discarding the supernatant. Use a 200 µl pipettor and avoid the formation of bubbles during the resuspension.

(xiv) Transfer the mitochondrial suspension to a microfuge and store it on ice.
▲ **CRITICAL STEP** Avoid diluting mitochondria with buffer. Mitochondria retain their functionality for a longer time, probably as a consequence of lower exposure to oxygen, when they are stored in a concentrated form.

(xv) Measure mitochondria concentration using the Biuret methods.
■ **PAUSE POINT** Mitochondria are now ready to be used in experiments: use the preparation within 1–3 h for better functional responses.
▲ **CRITICAL STEP** The typical yield of this preparation is ~50 mg ml^{-1} in a total volume of approximately 0.1 ml.

© 2007 Nature Publishing Group http://www.nature.com/natureprotocols

▲ CRITICAL STEP The Biuret method for measurement of mitochondrial concentration is accurate in the range of protein concentrations obtained from this protocol; other methods like the Bradford method can be used, but the mitochondrial lysate must be diluted in order to avoid saturation of the probe.

(B) Isolation of mitochondria from mouse liver ● TIMING approximately 1 h

(i) Starve the mouse overnight before the isolation experiment.

(ii) Kill an adult mouse (about 30 g) by cervical dislocation and rapidly explant the liver from the peritoneal cavity. Find the gallbladder and remove it using a scalpel. Immerse the liver in 50 ml of ice-cold IB_c in a small beaker.
▲ CRITICAL STEP Local and national regulations on animal care and handling vary. Check that you hold the appropriate authorization to perform animal experiments.

(iii) Rinse the liver free of blood by using ice-cold IB_c. Usually, four or five washes are sufficient to completely clarify the IB_c.

(iv) Mince the liver into small pieces using scissors. This should be performed while keeping the beaker in an ice bath.

(v) Discard the IB_c used during the mincing and replace it with 5 ml of ice-cold fresh IB_c. Transfer the suspension to the glass potter.
▲ CRITICAL STEP Homogenization, as well as the following steps, must be performed at 4 °C to minimize activation of damaging phospholipases and proteases.

(vi) Homogenize the liver using a Teflon pestle operated at 1,600 r.p.m., stroke the minced liver 3–4 times.
▲ CRITICAL STEP The optimal ratio between tissue and isolation buffer ranges between 1:5 to 1:10 (w:v).
▲ CRITICAL STEP Precool the glassware in an ice-bath 5 min before starting the procedure. Homogenization and the following steps must be performed at 4 °C to minimize activation of damaging phospholipases and proteases.
! CAUTION Wear protecting gloves while you are using the homogenizer to avoid possible injuries in the unlikely event that the potter breaks down.
? TROUBLESHOOTING

(vii) Transfer the homogenate to a 50 ml polypropylene Falcon tube and centrifuge at 600*g* for 10 min at 4 °C.

(viii) Transfer the supernatant to glass centrifuge tubes and centrifuge at 7,000*g* for 10 min at 4 °C.
? TROUBLESHOOTING

(ix) Discard the supernatant and wash the pellet with 5 ml of ice-cold IB_c.

(x) Centrifuge at 7,000*g* for 10 min at 4 °C.

(xi) Discard the supernatant and resuspend the pellet, containing mitochondria. You can use a glass rod to loosen the pellet paste. Avoid adding IB and try to resuspend the mitochondria in the small amount of buffer that remains after discarding the supernatant. Use a 1 ml pipettor and avoid the formation of bubbles during the resuspension process.

(xii) Transfer mitochondrial suspension into a 14 ml Falcon tube and store on ice.
▲ CRITICAL STEP Avoid diluting mitochondria with buffer as mitochondria retain their functionality for a longer time when kept concentrated, minimizing exposure to oxygen.
■ PAUSE POINT Mitochondria are now ready to be used in experiments; use the preparation within 1–3 h for better functional responses.

(xiii) Measure mitochondrial concentration using the Biuret methods.
▲ CRITICAL STEP The usual concentration of mitochondria in this kind of preparation is about 80 mg ml^{-1} and the total volume is about 1 ml.
▲ CRITICAL STEP The Biuret method for measurement of mitochondrial concentration is accurate in the range of protein concentrations obtained from this protocol; other methods like the Bradford method can be used, but the mitochondrial lysate must be diluted in order to avoid saturation of the probe.

(C) Isolation of mitochondria from mouse skeletal muscle ● TIMING approximately 1.5 h

(i) Kill the mouse by cervical dislocation. Using a scalpel, rapidly remove the skeletal muscles of interest and immerse them in a small beaker containing 5 ml of ice-cold PBS supplemented with 10 mM EDTA. A timeline of this protocol is outlined in **Figure 6**.
▲ CRITICAL STEP Local and national regulations on animal care and handling vary. Check that you hold the appropriate authorizations to perform animal experiments.
▲ CRITICAL STEP The use of EDTA instead of EGTA chelates also Mg^{2+}, which is extremely abundant in muscle tissue (given the high content in ATP). Mg^{2+} can influence mitochondrial function as well as the kinetics of cytochrome *c* release[25].

(ii) Mince the muscles into small pieces using scissors and trim visible fat, ligaments and connective tissue.

(iii) Wash the minced muscles twice or thrice with ice-cold PBS supplemented with 10 mM EDTA.

(iv) Resuspend the minced muscles in 5 ml of ice-cold PBS supplemented with 10 mM EDTA and 0.05% trypsin for 30 min.

(v) Centrifuge at 200*g* for 5 min and discard the supernatant.

(vi) Resuspend the pellet in IB_m1.

© 2007 Nature Publishing Group http://www.nature.com/natureprotocols

(vii) Homogenize the muscles using a Teflon pestle operated at 1,600 r.p.m.; stroke the minced muscle ten times.
▲ CRITICAL STEP The optimal ratio between tissue and isolation buffer ranges between 1:5 and 1:10 (w:v).
▲ CRITICAL STEP Precool the glassware in an ice-bath 5 min before starting the procedure. Homogenization, and the following steps, must be performed at 4 °C to minimize the activation of damaging phospholipases and proteases.
! CAUTION Wear protecting gloves while you are using the homogenizer to avoid possible injuries in the unlikely event that the potter breaks down.
Precool the glassware in an ice-bath for 5 min before starting the following steps.
? TROUBLESHOOTING
(viii) Transfer the homogenate to a 50 ml polypropylene Falcon tube and centrifuge at 700*g* for 10 min at 4 °C.
(ix) Transfer the supernatant to glass centrifuge tubes and centrifuge at 8,000*g* for 10 min at 4 °C.
? TROUBLESHOOTING
(x) Discard the supernatant and resuspend the pellet in 5 ml of ice-cold IB_m2.
(xi) Centrifuge at 8,000*g* for 10 min at 4 °C.
(xii) Discard the supernatant and resuspend the pellet containing mitochondria. You can use a glass rod to loosen the pellet paste. Avoid adding IB and try to resuspend the mitochondria in the small amount of buffer that remains after discarding the supernatant. Use a 200 µl pipettor and avoid the formation of bubbles during the resuspension process.
(xiii) Transfer mitochondrial suspension into a 14 ml Falcon tube and keep it on ice.
(xiv) Measure mitochondrial concentration using the Biuret methods.
▲ CRITICAL STEP This preparation normally yields 0.8 ml of 50 mg ml^{-1} mitochondria.
▲ CRITICAL STEP The Biuret method for measurement of mitochondrial concentration is accurate in the range of protein concentrations obtained from this protocol; other methods like the Bradford method can be used, but the mitochondrial lysate must be diluted in order to avoid saturation of the probe.

Measuring mitochondrial respiration ● TIMING approximately 1 h

2| Calibrate the Clarke-type oxygen electrode. Procedures vary from instrument to instrument. You should follow the manufacturer's instructions for the instrument you are using.

3| Equilibrate temperature and oxygen tension of EBc or EBm by placing open beakers containing the buffers in the water bath connected to the oxygraph. After 20–30 min, the temperature of the buffers is likely to be in equilibrium with that of the water bath.

4| Add an appropriate volume of EB to the oxygraph chamber. Use 0.5 ml for the mitochondria isolated from cells and 1 or 2 ml for the liver and muscle mitochondria. Close the oxygraph chamber.

5| Start the recording of the oxygen consumption.
▲ CRITICAL STEP Verify that the recording is stable and that no drifts are apparent. Drifts can mask the oxygen consumption by the mitochondrial preparation and thereby complicate the interpretation of the results.
? TROUBLESHOOTING

6| Wait for 2 min to obtain a stable baseline.

7| Using an appropriate Hamilton microsyringe, add mitochondria to obtain a final concentration of 1 mg ml^{-1}. A fast, transitory decrease in the oxygen content of the chamber will be observed, caused by anaerobiosis of the isolated mitochondria; this will be followed by a slower decrease caused by the respiration of the mitochondria. This is supported by endogenous substrates and is commonly referred to as "state 1" respiration[26].

8| Record oxygen consumption till it stops.
! CAUTION In liver mitochondria state 1 respiration commonly does not stop.

TABLE 1 | Substrates and inhibitors of the respiratory chain.

	Substrate (final concentration)	Inhibitor (final concentration)
Complexes I, III, IV	Glutamate (5 mM)/malate (2.5 mM)	///
Complexes II, III, IV	Succinate (5 mM)	Rotenone (2 µM)
Complex IV	Ascorbate (6 mM)/TMPD (300 µM)	Antimycin A (0.25 µg ml^{-1})

The span of the respiratory chain examined by each combination of substrate/inhibitor is indicated along with the final concentration to use in the oxygraphy experiments.

© 2007 Nature Publishing Group http://www.nature.com/natureprotocols

9| Using Hamilton microsyringes, add the appropriate concentrations of respiratory substrates and inhibitors for the complexes of the respiratory chain you wish to study (refer to **Table 1**). The mitochondrial suspension will now start consuming oxygen as a consequence of the basal activity of the respiratory chain in counteracting the inner mitochondrial membrane proton leak. This represents the so-called "state 2" respiration[26].

▲ CRITICAL STEP The rate of oxygen consumption should now be faster than the rate observed with buffer alone. This indicates that you have obtained functional, respiring mitochondria.

? TROUBLESHOOTING

10| Record for 5 min.

11| Add ADP to obtain a final concentration of 100–150 μM. Faster consumption of oxygen will be observed. This has been caused by proton back-diffusion through the stalk portion of the ATPase, which has been compensated by faster electron flow through the respiratory chain to the terminal electron acceptor, O_2. This is classically referred to as "state 3" respiration[26].

▲ CRITICAL STEP The rate of oxygen consumption should now be faster than the rate observed with substrates alone, indicating that we have obtained well coupled mitochondria. The increase in respiration, observed with ADP, varies from tissue to tissue and from substrate to substrate. As a general rule, and for the sole purpose of quality control of the preparation, the minimum requirements to proceed with the experiment are as follows: using glutamate malate as a substrate, maintaining a ratio of 2 in mitochondria isolated from cell lines and a ratio of 4 in mitochondria isolated from tissues.

? TROUBLESHOOTING

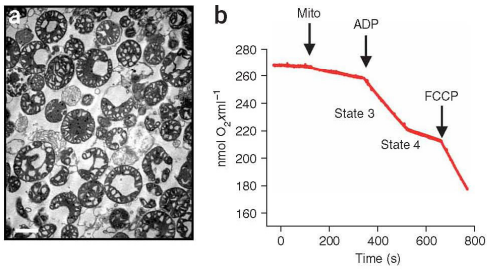

Figure 6 | Ultrastructure and oxygen consumption of mouse liver mitochondria isolated according to the protocol presented. (**a**) Mitochondrial ultrastructure. Mouse liver mitochondria (0.5 mg ml^{-1}) incubated in EB supplemented with 5 mM glutamate and 2.5 mM malate for 5 min were fixed by adding glutaraldehyde (final concentration 2.5% (v/v)). Transmission electron micrographs were acquired from randomly selected fields, as described[18]. (**b**) Oxygen consumption of 1 ml EB supplemented with 5 mM glutamate and 2.5 mM malate. Where indicated (arrows), mouse liver mitochondria (MLM, final concentration 1 mg ml^{-1}), ADP (100 μM) and FCCP (60 nM) were added. Respiration after ADP stimulation is indicated as "state 3", whereas respiration after consumption of added ADP is indicated as "state 4."

12| Wait until the respiration slows down and returns to a rate comparable to that before the addition of ADP. This is caused by the consumption of the added ADP. The respiration, which follows ADP exhaustion, is classically referred to as "state 4" respiration[26].

13| Wait for 3 min.

14| Add the uncoupler FCCP to obtain a final concentration of 60–100 nM.

15| The respiration will speed up and reach values slightly higher than those observed during the recording of state-3 respiration.

? TROUBLESHOOTING

16| Record for a further 5 min and then stop recording.

● TIMING

Step 1A: approximately 2 h, depending on the amount of cells to be used; however, cells will need to be seeded 2 or 3 d in advance to let them grow

Step 1B: approximately 1 h; however the mouse will need to be fasted from the night before

Step 1C: 1.5 h, depending on the amount of muscle to be minced

? TROUBLESHOOTING

Troubleshooting advice can be found in **Table 2**.

TABLE 2 | Troubleshooting table.

Step	Problem	Possible causes	Solution
1Aviii, 1Bvi, 1Cvii	Low yield of isolated mitochondria	Low cell density during homogenization	Low cell density may result in better homogenization. However, mitochondria are usually of lower quality, probably as a consequence of mechanical damage during preparation

© 2007 Nature Publishing Group http://www.nature.com/natureprotocols

TABLE 2 | Troubleshooting table (continued).

Step	Problem	Possible causes	Solution
1Ax, 1Bviii, 1Cix	Low quality of isolated mitochondria	Pellet after centrifugation is lost	When the supernatant is poured off, the loose upper part of the mitochondrial pellet may be detached as well. Intact mitochondria tend to sediment more quickly than damaged mitochondria. The loose part of the pellet probably contains a high proportion of damaged (uncoupled) mitochondria and can be lost without affecting the overall quality of the mitochondrial preparation
1Ax, 1Bvii	Low quality of isolated mitochondria	Lipid contamination	The white foamy material near the top of the tube consists of lipids. Mixing of lipids with the mitochondria suspension will cause some degree of uncoupling. Therefore avoid contact with mitochondria: remove the foamy material by wiping the inside of the tube with a Kimwipe
5	Oxygen consumption baseline is not stable	Bacterial or yeast contamination of your buffer	Verify if your buffers are contaminated, by repeating the recording with bidistilled water in the oxygraph chamber
		Inadequate calibration of the instrument	Re-calibrate the instrument
		Tears in the polyethylene membrane of the electrode	Check response of the oxygraph by transiently stopping stirring: due to the immediate drop in the local oxygen concentration the recording should immediately fall and return to the original baseline only when the stirrer is restarted. If this *manoeuvre* does not give the expected results, inspect and if necessary substitute the membrane of the electrode
9	Mitochondrial preparation is not consuming oxygen	Overestimation of final protein concentration (therefore added too little protein in the oxygraph chamber)	Try to double mitochondrial concentration in the chamber
		Mechanical and osmotical damage to mitochondria during isolation	Substitute 0.2 M sucrose with 0.3 M mannitol in the isolation buffer
		Contamination by other intracellular membranes, such as endoplasmic reticulum or nuclei	In steps 1Axi, 1Bix or 1Cx, wash the mitochondrial pellet with twice the amount of isolation buffer
11	ADP-stimulated respiration rate is too low	The most trivial explanation is that you omitted Pi from your buffer	Add Pi and check the respiration
		High percentage of mitochondria with ruptured outer membranes that leaked cytochrome *c*	Add exogenous cytochrome *c* and check the respiration; if respiration starts, the outer membrane is leaky. See troubleshooting for step 9 (mechanical and osmotic damage)
		Unusually high basal respiration, as a consequence of uncoupling by Ca^{2+} overload	Follow carefully all the indicated critical steps to avoid the indicated contaminations; try washing glassware with isolation buffer, supplemented with EGTA
		Unusually high basal respiration, as a consequence of uncoupling by fatty acids	Include 0.1% fatty acid free albumin in the EB; if this procedure works increase FCCP concentration since albumin binds reversibly to FCCP
15	Uncoupled respiration rate is lower than ADP-stimulated respiration	Too much FCCP used	Since at high doses FCCP is also an inhibitor of the respiratory chain, you can overcome this problem by titrating down the concentration of FCCP used

© 2007 Nature Publishing Group http://www.nature.com/natureprotocols

ANTICIPATED RESULTS

The goal of a mitochondrial preparation is to obtain a good amount of relatively pure, well coupled mitochondria. The quality of the obtained organelles can be checked by using oxygraphy to measure their oxygen consumption. For example, mitochondria isolated from mouse liver and energized with glutamate/malate respond to stimulation of ATPase by added ADP with a sixfold

increase in the rate of oxygen consumption (**Fig. 6b**). This usually reflects mitochondria that are highly pure and intact. A closer look by conventional electron microscopy at the morphology and at the purity of the organelles isolated from other intracellular membranes revealed that most of the organelles displayed an intact inner and outer membrane and that the level of contamination by other membranes was kept to a minimum (**Fig. 6a**).

ACKNOWLEDGMENTS We thank Giuliano Dodoni and members of the Scorrano lab for helpful discussions. LS is an Assistant Telethon Scientist of the Dulbecco-Telethon Institute. Research in his laboratory is supported by Telethon Italy; AIRC Italy; Compagnia di San Paolo; Human Frontier Science Program Organization; United Mitochondrial Disease Fund USA, Muscular Dystrophy Association USA.

COMPETING INTERESTS STATEMENT The authors declare that they have no competing financial interests.

Published online at http://www.natureprotocols.com
Reprints and permissions information is available online at http://npg.nature.com/reprintsandpermissions

1. Dimmer, K.S. & Scorrano, L. (De)constructing mitochondria: what for? *Physiology (Bethesda)* **21**, 233–241 (2006).
2. Hogeboom, G.H., Schneider, W.C. & Pallade, G.E. Cytochemical studies of mammalian tissues. I. Isolation of intact mitochondria from rat liver; some biochemical properties of mitochondria and submicroscopic particulate material. *J. Biol. Chem.* **172**, 619–635 (1948).
3. Bensley, R.R. & Hoerr, N. Studies on cell structure by the freezing-drying method VI. The preparation and properties of mitochondria. *Anat. Rec.* **60**, 449–455 (1934).
4. Mitchell, P. & Moyle, J. Chemiosmotic hypothesis of oxidative phosphorylation. *Nature* **213**, 137–139 (1967).
5. Schatz, G., Haslbrunner, E. & Tuppy, H. Deoxyribonucleic acid associated with yeast mitochondria. *Biochem. Biophys. Res. Commun.* **15**, 127–132 (1964).
6. Nass, M.M. & Nass, S. Intramitochondrial fibers with DNA characteristics. I. Fixation and electron staining reactions. *J. Cell Biol.* **19**, 593–611 (1963).
7. Hallermayer, G., Zimmermann, R. & Neupert, W. Kinetic studies on the transport of cytoplasmically synthesized proteins into the mitochondria in intact cells of *Neurospora crassa*. *Eur. J. Biochem.* **81**, 523–532 (1977).
8. Palade, G.E. The fine structure of mitochondria. *Anat. Rec.* **114**, 427–451 (1952).
9. Sorgato, M.C., Keller, B.U. & Stuhmer, W. Patch-clamping of the inner mitochondrial membrane reveals a voltage-dependent ion channel. *Nature* **330**, 498–500 (1987).
10. Liu, X., Kim, C.N., Yang, J., Jemmerson, R. & Wang, X. Induction of apoptotic program in cell-free extracts: requirement for dATP and cytochrome *c*. *Cell* **86**, 147–157 (1996).
11. Yang, J. *et al.* Prevention of apoptosis by Bcl-2: release of cytochrome *c* from mitochondria blocked. *Science* **275**, 1129–1132 (1997).
12. Scorrano, L. & Korsmeyer, S.J. Mechanisms of cytochrome *c* release by proapoptotic BCL-2 family members. *Biochem. Biophys. Res. Commun.* **304**, 437–444 (2003).
13. Bossy-Wetzel, E., Barsoum, M.J., Godzik, A., Schwarzenbacher, R. & Lipton, S.A. Mitochondrial fission in apoptosis, neurodegeneration and aging. *Curr. Opin. Cell Biol.* **15**, 706–716 (2003).
14. Li, Z., Okamoto, K., Hayashi, Y. & Sheng, M. The importance of dendritic mitochondria in the morphogenesis and plasticity of spines and synapses. *Cell* **119**, 873–887 (2004).
15. St. John, J.C., Jokhi, R.P. & Barratt, C.L. The impact of mitochondrial genetics on male infertility. *Int. J. Androl.* **28**, 65–73 (2005).
16. Cipolat, S. *et al.* Mitochondrial rhomboid parl regulates cytochrome *c* release during apoptosis via opa1-dependent cristae remodeling. *Cell* **126**, 163–175 (2006).
17. Fontaine, E., Eriksson, O., Ichas, F. & Bernardi, P. Regulation of the permeability transition pore in skeletal muscle mitochondria. Modulation by electron flow through the respiratory chain complex I. *J. Biol. Chem.* **273**, 12662–12668 (1998).
18. Frezza, C. *et al.* OPA1 controls apoptotic cristae remodeling independently from mitochondrial fusion. *Cell* **126**, 177–189 (2006).
19. Meeusen, S., McCaffery, J.M. & Nunnari, J. Mitochondrial fusion intermediates revealed *in vitro*. *Science* **305**, 1747–1752 (2004).
20. Stahl, W.L., Smith, J.C., Napolitano, L.M. & Basford, R.E. BRAIN MITOCHONDRIA: I. Isolation of Bovine Brain Mitochondria. *J. Cell Biol.* **19**, 293–307 (1963).
21. Cannon, B. & Lindberg, O. Mitochondria from brown adipose tissue: isolation and properties. *Methods Enzymol.* **55**, 65–78 (1979).
22. Mela, L. & Seitz, S. Isolation of mitochondria with emphasis on heart mitochondria from small amounts of tissue. *Methods Enzymol.* **55**, 39–46 (1979).
23. Siess, E.A. Different actions of mono- and disaccharides on rat liver mitochondria. *Hoppe Seylers. Z. Physiol Chem.* **364**, 835–838 (1983).
24. Siess, E.A. Influence of isolation media on the preservation of mitochondrial functions. *Hoppe Seylers. Z. Physiol Chem.* **364**, 279–289 (1983).
25. Eskes, R. *et al.* Bax-induced cytochrome c release from mitochondria is independent of the permeability transition pore but highly dependent on Mg^{2+} ions. *J. Cell Biol.* **143**, 217–224 (1998).
26. Nicholls, D.G. & Ferguson, S.J. *Bioenergetics*. Academic Press, London (2002).

© 2007 Nature Publishing Group http://www.nature.com/natureprotocols

29

Measuring Mitochondrial Shape Changes and Their Consequences on Mitochondrial Involvement During Apoptosis

Christian Frezza, Sara Cipolat, and Luca Scorrano

Summary

Mitochondria are key players in cell death following intrinsic and, in some cell types, extrinsic stimuli. The recruitment of the mitochondrial pathway results in mitochondrial dysfunction and release of intermembrane space proteins like cytochrome c that are required in the cytosol for complete activation of effector caspases. Apoptotic shape changes of this organelle and the role of "mitochondria-shaping" proteins in cell death has attracted considerable attention. We present protocols to investigate how morphological changes of the mitochondrial reticulum regulate release of cytochrome-c, as evaluated quantitatively by an in situ approach, and changes in mitochondrial membrane potential measured in real time.

Key Words: Apoptosis; cytochrome-*c* release; fission; fusion; imaging; membrane potential; OPA1.

1. Introduction

Besides providing most cellular ATP, mitochondria participate in the early stages of programmed cell death or apoptosis. Apoptosis is essential for successful development and tissue homeostasis of all multicellular organisms, and it is accomplished by evolutionarily conserved pathways that result in an orderly process of cell demise with distinct morphological and biochemical parameters *(1)*. Dysregulation of apoptosis contributes to a variety of human diseases, including cancer *(2)*. In mammalian cells, there are two main pathways downstream of death signals that appear to be linked in certain cell types: the death receptor pathway and the mitochondrial pathway *(3)*. Both culminate in the activation of caspases, cysteine proteases that cleave a number of substrates

From: *Methods in Molecular Biology, vol. 372: Mitochondria: Practical Protocols*
Edited by: D. Leister and J. M. Herrmann © Humana Press Inc., Totowa, NJ

involved in maintenance of cytoskeletal and nuclear integrity, cell cycle progression, and deoxyribonucleic acid (DNA) repair, resulting in the orderly demise of the cell.

Mitochondria participate in the competent activation of caspases by releasing cytochrome-*c* and additional apoptogenic factors from the intermembrane space into the cytosol ***(3)***. Cytochrome-*c* in complex with Apaf-1 activates caspase-9 and other downstream caspases ***(4)***. The release of cytochrome-*c* is preceded by changes in the structure of the mitochondrial network and of mitochondrial cristae ***(5,6)***.

Besides mitochondrial shape changes during cell death, a vast variety of physiological and pathological conditions, ranging from elevated intracellular Ca^{2+} levels ***(7,8)*** to mitochondrial uncoupling ***(9)*** and inhibition of autophagocytosis ***(10)***, have been reported to affect morphology of the organelle. Mitochondrial shape is regulated by the balance between fusion and fission processes ***(11)***. Several mitochondria-shaping proteins have been identified through genetic screens in yeast; their mammalian counterparts are less characterized ***(11)***.

Mitochondrial fission in mammalian cells is regulated by dynamin-related protein (DRP-1), a cytosolic dynamin that translocates to fission sites, where it interacts with its molecular adapter homolog fission (hFis1) ***(12)***, an integral protein of the outer mitochondrial membrane ***(13)***. Fusion is regulated by optic atrophy 1 (OPA1) and mitofusin (MFN) 1 and 2. MFNs are outer membrane proteins required for mitochondrial fusion ***(9,14–16)***. Interestingly, MFN1 seems to cooperate with the inner mitochondrial membrane protein OPA1 to fuse mitochondria ***(17)***.

DRP-1 has been shown to mediate mitochondrial fragmentation during developmental cell death of *Caenorhabditis elegans* ***(18)***. Moreover, an interesting crosstalk between "BH3-only" members (BCL-2 homology domain 3) of the B-cell lymphoma 2 (BCL-2) family, DRP-1, and remodeling of the cristae has been described ***(19)***.

Thus, considerable interest has developed in the relationship between mitochondrial shape and mitochondrial and cellular function, in particular, but not only in the course of apoptosis. Researchers exploiting these avenues face the major challenge of having to combine quantitative analysis of mitochondrial morphology and pathophysiology during apoptosis. How to reliably follow components of the latter process, such as depolarization and cytochrome-*c* release, is still a matter of debate (for a review, *see* **ref. *20***). A safe way that is less artifact prone is to use in situ methods accompanied by quantitative analyses. Here, we present protocols to address morphological changes of mitochondria and to verify if these changes play any role in controlling release of cytochrome-*c* and in mitochondrial depolarization in response to intrinsic apoptotic stimuli.

2. Materials

2.1. Mitochondrial Morphology

2.1.1. Seeding of Cells for Morphological Analysis

1. Sterile 75-cm^2 tissue culture flasks and six-well sterile tissue culture plates.
2. Sterile Dulbecco's modified Eagle's medium (DMEM) supplemented under sterile conditions with sterile 10% (v/v) fetal bovine serum (FBS), 50 U/mL penicillin, 50 µg/mL streptomycin, 100 µ*M* minimum essential medium (MEM) nonessential amino acids, and 2 m*M* glutamine. Filter sterilize through a 22-µm filter and store at 4°C.
3. Sterile phosphate-buffered saline (PBS): 2.7 m*M* KCl, 1.5 m*M* KH_2PO_4, 140 m*M* NaCl, 8 m*M* Na_2HPO_4. Alternatively, prepare working solution by dilution of one part of sterile 10X PBS (Gibco) with nine parts of sterile deionized water. Filter sterilize through a 22-µm filter and store at 4°C.
4. Sterile trypsin/ethylenediaminetetraacetic acid (EDTA) solution: sterile 0.25% (w/v) trypsin, 1 m*M* EDTA, pH 7.4. Divide under sterile conditions into 2-mL aliquots and store at 4°C.
5. Sterile Hanks' balanced salt solution (HBSS): prepare working solution by diluting one part sterile 10X HBSS (Gibco) with nine parts sterile deionized water; add 0.1 part sterile 100X HEPES (Gibco) and adjust to pH 7.4 with NaOH if necessary. Filter sterilize through a 0.22-µm filter and store at 4°C.
6. 24-mm Round glass grade 0 or 1 coverslips: coverslips must be ultraviolet (UV) sterilized by placing them under sterile conditions vertically inside the wells of a six-well plate (without the cover). Plates must be exposed to the UV source of a laminar flux hood for 45 min, with coverslips oriented toward the lamp (*see* **Note 1**).

2.1.2. Transfection of Cells for Morphological Analysis

1. Cationic lipid and colipid vehicle TransFectin lipid reagent (Bio-Rad) (*see* **Note 2**).
2. Plasmids for the expression of mitochondrially targeted DsRED. Always cotransfect it with the negative control plasmid (e.g., empty plasmid of the one containing the complementary deoxyribonucleic acid [cDNA] of your protein of interest) or with the one containing the cDNA of your protein of interest. In our experiments, we use pMSCV (BD-Clontech) and pMSCV containing murine *OPA1* cDNA (corresponding to human transcript variant 1) ***(17)*** (*see* **Note 3**).
3. Sterile DMEM (*see* **Subheading 2.1.1.**).

2.1.3. Confocal Imaging of Mitochondrial Morphology

1. HBSS: prepare as described in **Subheading 2.1.1., item 5** (*see* **Note 4**).
2. Coverslip holder: 25-mm round Attofluor stainless steel coverslip holders (Molecular Probes).

3. An inverted confocal microscope with HeNe laser light line and appropriate emission filters and photomultipliers, with a motorized *z*-axis connected to a computer for image storage and analysis.
4. Image analysis software: the freeware ImageJ (National Institutes of Health [NIH]) is suitable for all postacquisition image editing and analysis and three-dimensional (3D) reconstruction.

2.2. Cytochrome-c Release Immunofluorescence Assay

2.2.1. Seeding of Cells for Cytochrome-c Release Immunofluorescence Assay

1. Sterile 75-cm^2 tissue culture flasks and 6- and 24-well sterile tissue culture plates.
2. Sterile DMEM supplemented under sterile conditions with sterile 10% (v/v) FBS, 50 U/mL penicillin, 50 µg/mL streptomycin, 100 µ*M* MEM nonessential amino acids and 2 m*M* glutamine. Filter sterilize through a 22-µm filter and store at 4°C.
3. Sterile trypsin/EDTA solution: sterile 0.25% (w/v) trypsin, 1 m*M* EDTA, pH 7.4. Divide under sterile conditions into 2-mL aliquots and store at 4°C.
4. Sterile HBSS: prepare working solution by diluting one part sterile 10X HBSS (Gibco) with nine parts of sterile deionized water; add 0.1 part sterile 100X HEPES (Gibco) and adjust to pH 7.4 with NaOH if necessary. Filter sterilize through a 0.22-µm filter and store at 4°C.
5. 13-mm Round glass grade 0 or 1 coverslips: coverslips must be UV sterilized by placing them under sterile conditions vertically inside the wells of a 24-well plate (without the cover). Plates must be exposed to the UV source of a laminar flux hood for 45 min, with coverslips oriented toward the lamp (*see* **Note 1**).

2.2.2. Transfection of Cells for Cytochrome-c Release Immunofluorescence Assay

1. Cationic lipid and colipid vehicle TransFectin lipid reagent (Bio-Rad) (*see* **Note 2**).
2. Plasmids for the expression of mitochondrially targeted DsRED. Always cotransfect it with the negative control plasmid (e.g., empty plasmid of the one containing the cDNA of your protein of interest) or with the one containing the cDNA of your protein of interest. In our experiments, we use pMSCV (BD-Clontech) and pMSCV containing murine *OPA1* cDNA (corresponding to human transcript variant 1) *(17)* (*see* **Note 3**).
3. Sterile DMEM (*see* **Subheading 2.1.1.**).

2.2.3. Treatment of Cells With an Apoptosis Inducer and Immunostaining and Confocal Immunofluorescence of Cytochrome-c

1. Freshly prepared hydrogen peroxide (Sigma) dissolved in sterile HBSS at a final concentration of 1 m*M* (*see* **Note 5**).
2. PBS: 2.7 m*M* KCl, 1.5 m*M* KH_2PO_4, 140 m*M* NaCl, 8 m*M* Na_2HPO_4. Alternatively, prepare working solution by dilution of one part 10X PBS (Gibco) with nine parts of deionized water.

3. Fixing solution: prepare working solution by diluting one part 37% (v/v) formaldehyde solution (Sigma) in nine parts PBS; adjust to pH 7.4 using NaOH. Store at 4°C and prepare fresh every 4 wk (*see* **Note 6**).
4. Permeabilization solution: 0.01% (v/v) Nonidet P-40 (Sigma) in PBS; adjust to pH 7.4 using HCl or NaOH as required.
5. Blocking solution: 0.5% (w/v) bovine serum albumin (BSA) in PBS; divide into 10-mL aliquots and store at −20°C.
6. Primary antibody: purified anti-cytochrome-*c* mouse monoclonal antibody (BD-Pharmingen clone 6H2.B4), 1:200 in PBS.
7. Secondary antibody: antimouse immunoglobulin G, fluorescein isothiocyanate conjugated (Calbiochem), 1:200 in PBS.
8. Mounting medium: Prolong Antifade Gold (Molecular Probes).
9. 76 × 26 mm rectangular microscope slides.
10. An upright confocal microscope with HeNe and Xe laser light lines and appropriate emission filters and photomultipliers and connected to a computer for image storage and analysis.
11. Image analysis software: the freeware ImageJ (NIH) is suitable for all postacquisition image processing and analysis.

2.3. Imaging of Mitochondrial Membrane Potential

2.3.1. Seeding of Cells for Analysis of Mitochondrial Membrane Potential

1. Sterile 75-cm^2 tissue culture flasks and 6- and 24-well sterile tissue culture plates.
2. Sterile DMEM supplemented under sterile conditions with sterile 10% (v/v) FBS, 50 U/mL penicillin, 50 µg/mL streptomycin, 100 µ*M* MEM nonessential amino acids, and 2 m*M* glutamine. Filter sterilize through a 22-µm filter and store at 4°C.
3. Sterile trypsin/EDTA solution: sterile 0.25% (w/v) trypsin, 1 m*M* EDTA, pH 7.4. Divide under sterile conditions into 2-mL aliquots and store at 4°C.
4. Sterile HBSS: prepare working solution by diluting one part of sterile 10X HBSS (Gibco) with nine parts of sterile deionized water; add 0.1 part of sterile 100X HEPES (Gibco) and adjust to pH 7.4 with NaOH if necessary. Filter sterilize through a 0.22-µm filter and store at 4°C.
5. 24-mm round glass grade 0 or 1 coverslips: coverslips must be UV sterilized by placing them under sterile conditions vertically inside the wells of a 6- or 24-well plate (without the cover), respectively. Plates must be exposed to the UV source of a laminar flux hood for 45 min, with coverslips oriented toward the lamp (*see* **Note 1**).

2.3.2. Transfection of Cells for Analysis of Mitochondrial Membrane Potential

1. Cationic lipid and colipid vehicle TransFectin lipid reagent (Bio-Rad) (*see* **Note 2**).
2. Plasmids for the expression of cytosolic green fluorescent protein (GFP) (like pEGFP, BD-Clontech). Always cotransfect it with the negative control plasmid (e.g., empty plasmid of the one containing the cDNA of your protein of interest) or with the one containing the cDNA of your protein of interest. In our experiments,

we use pMSCV (BD-Clontech) and pMSCV containing murine *OPA1* cDNA (corresponding to human transcript variant 1) ***(17)*** (*see* **Note 3**).

2.3.3. Imaging of Mitochondrial Membrane Potential

1. HBSS: 1.3 m*M* $CaCl_2$, 0.5 m*M* $MgCl_2$, 0.4 m*M* $MgSO_4$, 5.3 m*M* KCl, 4.4 m*M* KH_2PO_4, 138 m*M* NaCl, 0.3 m*M* Na_2HPO_4, 1000 mg/L D-glucose; add 0.1 part 100X HEPES (Gibco) and adjust to pH 7.4 with NaOH if necessary. Alternatively, prepare working solution by dilution of one part 10X HBSS (Gibco) with nine parts deionized water; add 0.1 part 100X HEPES (Gibco) and adjust to pH 7.4 with NaOH if necessary.
2. 0.1 m*M* Tetramethylrodhamine methyl ester (TMRM) (Molecular Probes) in dimethyl sulfoxide. Store at –20°C in the dark.
3. 10 mg/mL Cyclosporine H (CsH) (Sigma) in dimethyl sulfoxide. Store at –20°C (*see* **Note 7**).
4. 2 m*M* carbonyl cyanide(*p*-trifluoromethoxy)-phenylhydrazone (FCCP) (Sigma) in absolute ethanol. Store at –20°C (*see* **Note 8**).
5. 1 m*M* H_2O_2 prepared freshly as described in **Subheading 2.2**.
6. An imaging workstation including an inverted microscope equipped with a fluorescent light source, proper excitation and emission filters, a shutter to avoid photobleaching of the samples, and a 12-bit charge coupled device camera for image acquisition. All must be connected to a computer with imaging software (usually provided with the imaging workstation) to set up the acquisition routine and to store the imaging sequence.
7. Image analysis software to analyze gray levels in the selected regions of interest (ROIs). The freeware ImageJ (NIH) with the MultiMeasure plugin is suitable.

3. Methods

3.1. Mitochondrial Morphology

Our method of choice to analyze the effect of a putative mitochondria-shaping protein on mitochondrial morphology is to cotransfect it with a mitochondrially targeted fluorescent protein and to compare the shape of the mitochondrial reticulum with that of cells transfected with the mitochondrially targeted fluorescent protein alone (*see* **Note 9**). We prefer to image the mitochondria in living cells confocally to avoid possible fixation artifacts. It must be kept in mind that when performing confocal imaging, tubular structures that move in and out of the focal plane can be easily mistaken for individual rod or spherical organelles. We therefore strongly advise acquiring stacks of mitochondrial images along the *z*-axis of the entire cell, followed by 3D image reconstruction to confirm the single-plane confocal images.

3.1.1. Seeding of Cells for Morphological Analysis

1. Check a 75-cm^2 flask containing mouse embryonic fibroblasts (MEFs) by using a standard inverted, transmitted light microscope. If cells are approaching confluence,

then open the flask in a laminar flux hood, sterile aspirate the medium, and wash the cells three times with sterile PBS.
2. Detach cells from flasks using a 0.25% (v/v) sterile trypsin/EDTA solution. For a 75-cm^2 flask, evenly distribute 1 mL sterile solution on top of the cells, gently swirl the flasks, and incubate for 3 min at 37°C.
3. Check cells for detachment using a standard inverted microscope. Gently tap the bottom of the flask if cells are still attached. After complete detachment, inactivate trypsin by adding 10 mL complete DMEM.
4. Count the cells using a hemocytometer (Burker chamber).
5. Seed 10^5 cells in each well of a six-well plate containing the sterile 22-mm round coverslips (*see* **Note 10**).
6. Place the plate in the tissue culture incubator and leave for 24 h.
7. Check confluence after 24 h. A 50–60% confluence will yield optimal transfection efficiency. Proceed with transfection if confluence is optimal.

3.1.2. Transfection of Cells for Morphological Analysis

1. For each well, 3 µg plasmid DNA in 250 µL serum-free medium are required: 1.5 µg of the fluorescent protein plasmid DNA and 1.5 µg of plasmid DNA of the protein of interest or empty vector for the control transfection.
2. For each well, add 3 µL TransFectin transfection reagent to 250 µL serum-free medium.
3. Mix the DNA and TransFectin solutions together. Gently mix by tapping or pipeting.
4. Incubate for 20 min at room temperature.
5. Take the plate containing cells grown on coverslips from the incubator.
6. Add 500 µL DNA–TransFectin complexes directly to cells in serum-containing medium. Swirl gently.
7. Place the plate in the tissue culture incubator and leave for 4 h.
8. Change the medium with complete DMEM 4 h after the addition of the DNA–TransFectin complexes.
9. Place the plate in the tissue culture incubator and leave for 20 h.

3.1.3. Confocal Imaging for Morphological Analysis

1. At 24 h after transfection, place coverslips with transfected cells in the coverslip holder.
2. Wash the cells free of medium, add HBSS, and place cells on the stage of a confocal microscope (*see* **Note 11**).
3. Choose the appropriate objective. Good images with a great degree of definition can be acquired using a 60×, 1.4-numerical aperture (NA) Plan Apo objective (*see* **Note 12**).
4. Using the binocular and epifluorescence illumination, rapidly find a field with transfected cells.
5. Regulate the power of the laser beam to obtain contrasted images and at the same time to minimize photobleaching and phototoxicity. It is advisable not to exceed 10% of the maximum power of the laser.

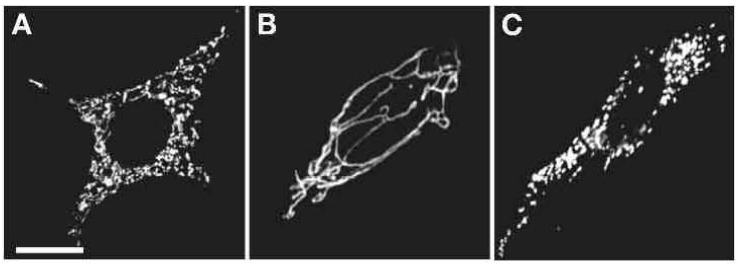

Fig. 1. Overexpression of OPA1 promotes mitochondrial elongation. Mouse embryonic fibroblasts (MEFs) grown on coverslips were cotransfected with mtRFP and empty vector (**A**), WT OPA1 (**B**), K301A OPA1 (**C**). After 24 h, confocal images of mtRFP fluorescence from randomly selected cells were acquired and stored. Bar: 10 µm.

6. Acquire and store images of transfected cells. If cells are expressing mitochondrially targeted red fluorescent protein (mtRFP), then excite using the 543-nm line of the HeNe laser and acquire emitted light through a 600-nm long-pass filter. Examples of images of MEFs expressing mtRFP and wild type (WT) or K301A *OPA1* are shown in **Fig. 1**.
7. Acquire and save stacks of images separated by 0.5 µm along the *z*-axis by using the appropriate function of your confocal microscope.
8. Open the acquired stacks with ImageJ and use the 3D reconstruction function of the program to reconstruct them.

3.2. Immunofluorescence Analysis of Cytochrome-c Release

Several methods are available to estimate the release of cytochrome *c* from mitochondria during apoptosis. Most rely on the preparation by differential centrifugation of cytosolic and mitochondrial fractions, followed by semiquantitative determination of cytochrome-*c* content in each fraction, performed by enzyme-linked immunosorbent assay or immunoblotting. Separation of subcellular fractions by differential centrifugation requires the mechanical rupture of the plasma membrane, which can cause unspecific mitochondrial disruption with cytochrome-*c* release ***(21)***. Moreover, it is always difficult to assess the effect of a transiently transfected protein at a bulk population level. On the other hand, these approaches are far more quantitative than the analysis of cytochrome-*c* subcellular localization by immunofluorescence. We therefore modified a double-immunofluorescence protocol coupled to a quantitative analysis of cytochrome-*c* distribution devised by Petronilli et al. ***(22)*** to evaluate quantitatively the effects of a transfected mitochondria-shaping protein on the release of cytochrome-*c*.

3.2.1. Seeding of Cells for Analysis of Cytochrome-c Release

1. Check a 75-cm^2 flask containing MEFs using a standard inverted, transmitted light microscope. If cells are approaching confluence, then open the flask in the hood, aspirate the medium, and wash the cells three times with sterile PBS.
2. Detach cells from flasks using the sterile trypsin/EDTA solution. For a 75-cm^2 flask, evenly distribute 1 mL sterile solution on top of the cells, gently swirl the flasks, and incubate for 3 min at 37°C.
3. Check cells for detachment. Gently tap the bottom of the flask if cells are still attached. After complete detachment, inactivate trypsin by adding 10 mL complete DMEM.
4. Count the cells using a hemocytometer (Burker chamber).
5. Seed 10^4 cells in each well of a 24-well plate containing the sterile 13-mm round coverslips (*see* **Note 10**).
6. Place the plate in the tissue culture incubator and leave for 24 h.
7. Check confluence after 24 h. A 50–60% confluence will yield optimal transfection efficiency. Proceed with transfection if confluence is optimal.

3.2.2. Transfection of Cells for Analysis of Cytochrome-c Release

1. For each well, 0.5 µg plasmid DNA in 50 µL serum-free medium is required: 0.25 µg of the fluorescent protein plasmid DNA and 0.25 µg of plasmid DNA of the protein of interest or empty vector for the control transfection.
2. For each well, add 1 µL TransFectin transfection reagent to 50 µL serum-free medium.
3. Mix the DNA and TransFectin solutions together. Gently mix by tapping or pipeting.
4. Incubate 20 min at room temperature.
5. Take the plate containing cells grown on coverslips from the incubator.
6. Add 100 µL DNA–TransFectin complexes directly to cells in serum-containing medium. Swirl gently.
7. Change the medium with complete DMEM 4 h after the addition of the DNA–TransFectin complexes.
8. Place the plate in the tissue culture incubator and leave for 20 h.

3.2.3. Treatment of Cells With an Apoptosis Inducer and Immunostaining and Confocal Immunofluorescence of Cytochrome-c

1. Seeded, transfected cells are now ready to be treated with the apoptotic stimulus of choice. We use H_2O_2, which at 1 m*M* is an intrinsic, mitochondria-utilizing apoptotic stimulus ***(23)***.
2. Aspirate medium and wash twice with PBS.
3. Add the solution of 1 m*M* H_2O_2 (freshly prepared; *see* **Note 5**) in HBSS.
4. Treat cells for 30, 60, and 90 min by placing the plate back in the tissue culture incubator (*see* **Note 13**).
5. Discard medium.
6. Add 0.3 mL 3.7% (v/v) ice-cold formaldehyde to each well.
7. Fix cells by leaving for 30 min at room temperature (*see* **Note 14**).
8. Discard formaldehyde by following your local hazardous waste regulations.

9. Wash samples twice with PBS.
10. Permeabilize cells by incubating with 0.3 mL 0.01% (v/v) ice-cold Nonidet NP40 for 20 min at room temperature.
11. Wash samples twice with PBS.
12. Block by adding 0.3 mL 0.5% (w/v) BSA for 15 min at room temperature.
13. Discard the blocking solution.
14. Add anti-cytochrome-*c* antibody (1:200) in PBS at room temperature for 30 min or at 4°C overnight.
15. Recover the primary antibody.
16. Wash samples twice with PBS.
17. Block by adding 0.3 mL 0.5% (w/v) BSA for 15 min at room temperature.
18. Add secondary antibody (1:200) in PBS at room temperature for 30 min at room temperature (*see* **Note 15**).
19. Wash samples twice with PBS and then with deionized water.
20. Add a drop (~5 µL) of mounting medium Prolong Antifade Gold to the microscopy slides.
21. Mount the coverslip on the slide with cells facing the mounting medium.
22. Remove any remaining water by blotting the coverslip against clean kimwipes.
23. When samples are completely dry, seal the coverslips with nail polish.
24. The sample can be viewed immediately after the nail polish dries or be stored in the dark at 4°C for up to a month.
25. Place slides on the stage of a confocal microscope.
26. For detection of mtRFP and of cytochrome-*c* immunodecorated with fluorescein isothiocyanate-conjugated antibodies, red and green channel images can be acquired simultaneously using two separate color channels on the detector assemblies of most confocal microscopes. Check that your microscope is equipped with 605-nm long-pass and 522- (± 25) nm band-pass filters, respectively.
27. Acquire and store RGB (red-green-blue) images of transfected, treated, and untreated cells for subsequent analysis.
28. Open the images using ImageJ.
29. Draw a line across the cell (**Fig. 2** illustrates such lines).
30. Using the Analyze >Plot Profile function of ImageJ, measure the fluorescence intensity of each pixel along the line in both the green and the red channels (**Fig. 2A′, B′** illustrates fluorescence intensity profiles along the lines drawn in **Fig. 2A,B**).
31. Export data to a spreadsheet program such as Excel™.
32. Calculate the localization index, defined as the ratio between the normalized standard deviations (SDs) of the fluorescence intensities of each channel: $(SD_{cyt\text{-}c}/\Sigma_{cyt\text{-}c})/(SD_{mtRFP}/\Sigma_{mtRFP})$. A punctuate distribution results in a higher SD; normalization allows correction for different fluorescence intensities in the two channels. A localization index of 1 indicates that cytochrome-*c* follows a mitochondrial distribution; an index lower than 1 means that cytochrome-*c* is randomly distributed (i.e., released cytochrome-*c*). In the example of **Fig. 2**, the localization index is 1 for the cell in panel A and 0.6 for the cell in panel B.
33. A macro can be conveniently recorded to repeat this calculation on several lines from different cells in separate experiments

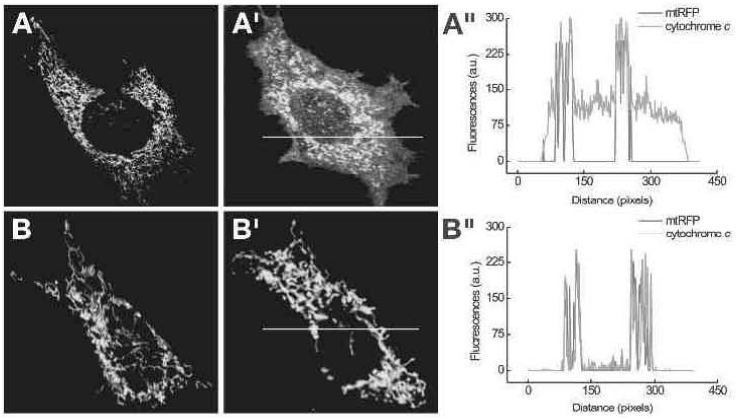

Fig. 2. Effect of the mitochondria-shaping protein OPA1 on cytochrome-*c* release evaluated by a quantitative *in situ* approach. MEFs were cotransfected with mtRFP and empty vector (**A**) or OPA1 (**B**). After 24 h, the cells were treated for 60 min with H_2O_2 (1 m*M*). Cells were then fixed, immunostained with an anti-cytochrome-*c* antibody (green), and imaged using a confocal microscope. Images of randomly selected cells before (**A**), (**B**) and after (**A′**), (**B′**) H_2O_2 treatment are shown. Sample lines are shown for the calculation of the localization index. Their fluorescence intensity profiles in the red and green channels of the lines drawn in panels **A′** and **B′** are reported in **A′** and **B′**, respectively. Bar: 10 µm.

3.3. Real-Time Imaging of Mitochondrial Membrane Potential During Apoptosis

Mitochondrial dysfunction accompanies cytochrome-*c* release during apoptosis. One of its aspects is the decrease in the mitochondrial membrane potential, which can be imaged using cationic lipophilic fluorescent dyes. To assess if overexpression of a protein of interest interferes with the apoptotic loss of mitochondrial membrane potential, transient cotransfection with a fluorescent protein such as GFP is needed to identify cells expressing the protein of interest.

3.3.1. Seeding and Transfection of Cells for Analysis of Mitochondrial Membrane Potential

Proceed exactly as indicated in the **Subheadings 3.1.1.** and **3.1.2.**

3.3.2. Imaging of Mitochondrial Membrane Potential

1. At 24 h after transfection, place coverslips with transfected cells in the coverslip holder.

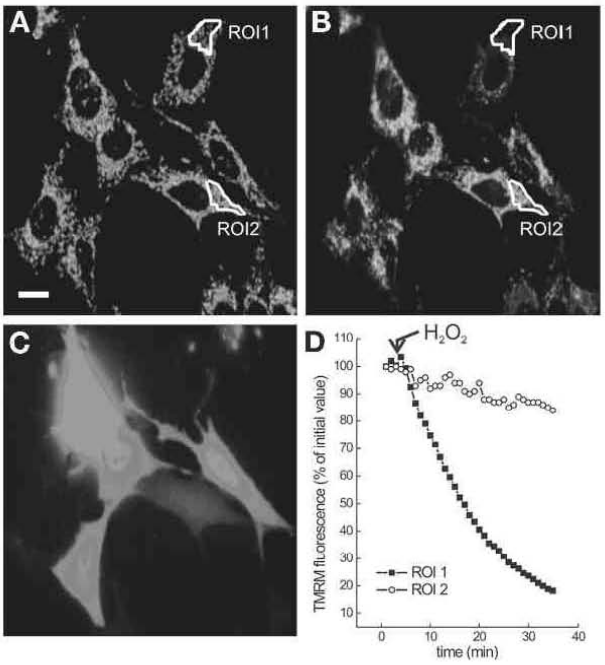

Fig. 3. Effect of the mitochondria-shaping protein OPA1 on apoptotic mitochondrial depolarization evaluated by a real-time approach. MEFs were cotransfected with GFP and OPA1. After 24 h, cells were loaded with TMRM and placed on the stage of an Olympus CellR Imaging system, and images of GFP fluorescence (**C**) were acquired and stored to identify cotransfected cells. Images of TMRM fluorescence were then acquired every 60 s for 40 min; after 3 min, cells were treated with 1 m*M* H_2O_2. Representative ROIs are drawn in images taken before (**A**) and 35 min after (**B**) addition of H_2O_2 in untransfected (ROI1) and transfected (ROI2) cells. The fluorescence intensity in the depicted ROIs was calculated, background subtracted, and normalized and is reported in (**D**). Where indicated, 1 m*M* H_2O_2 was added. Bar: 15 μm.

2. Add 1 mL 20 n*M* TMRM in HBSS supplemented with 2 μg/mL CsH.
3. Incubate for 30 min at 37°C in the dark.
4. Place coverslips on the stage of an inverted microscope (*see* **Note 11**).
5. Using the binocular and epifluorescence illumination, rapidly find a field with multiple GFP-positive cells. Check that TMRM fluorescence is stable before starting the experiment.

6. Regulate exposure times to obtain contrasted images and at the same time minimize photobleaching and phototoxicity. It is advisable not to exceed 50-ms exposure times.
7. Acquire and store the image of GFP fluorescence. This will be needed to identify the transfected cells. **Figure 3** shows GFP fluorescence in a field of transfected, TMRM-loaded MEFs.
8. Set up your imaging workstation to acquire sequential frames of TMRM fluorescence, one each 30 s to 1 min, for a total of 1–2 h.
9. After 5 min, add the apoptotic inducer.
10. Save the time series stack of images. **Figure 3** shows TMRM fluorescence before (panel B) and 35 min after (panel C) the addition of 1 m*M* H_2O_2.
11. Import the time series stack in ImageJ and proceed to analyze quantitatively the changes in mitochondrial TMRM fluorescence.
12. Open the MultiMeasure Plugin and freehand draw regions of interest on cytosolic areas comprising 10–20 mitochondria in both transfected and untransfected cells. **Figure 3** shows such ROIs. Draw a ROI on an area without cells, which will be identified as the background fluorescence.
13. Measure average fluorescence intensity values of the selected ROIs in the whole time series stack using the MultiMeasure function of ImageJ.
14. Copy the results in a spreadsheet, subtract the background, and normalize the values for the initial fluorescence. **Figure 3D** shows the quantitative analysis of changes of TMRM fluorescence in the depicted ROIs in response to 1 m*M* H_2O_2.

4. Notes

1. UV sterilization is essential for larger, 22-mm round coverslips. 13-mm round coverslips can also be sterilized by submerging them in a 1:3 isopropanol:ethanol mixture, followed by fast passage on a Bunsen flame. This protocol, however, is less safe, and free flames will disrupt the laminar flux of your sterile hood, increasing the risk of bacterial contamination.
2. Our personal experience is that this is the optimal transfection reagent for MEFs Other reagents, as well as alternative methods, such as Ca^{2+}-phosphate-mediated transfection, adenoviral infection, or electroporation, can be used successfully with this and other cell types.
3. Fluorescent proteins are essential for the morphological and functional analysis of the transfected cells. One should obtain mitochondrially targeted DsRED (mtRFP, BD-Clontech) and pEGFP (BD-Clontech) for the identification of mitochondria and the analysis of the mitochondrial morphology and for the visualization of the cotransfected cells, respectively; these fluorescent markers should be cotransfected with plasmids encoding the protein of interest. In our experiments, we use empty pMSCV and pMSCV containing murine *OPA1* cDNA. These fluorescent proteins are selected to minimize spectral interaction with other fluorescent molecules and probes exploited in the protocols presented here. Users can choose other spectral variants of GFP (like cyan and yellow fluorescent protein, for example), but it should be always kept in mind that their spectra should not overlap with those of

the other fluorescent probes used, and that the imaging workstation available to the user should have appropriate filters.

4. HBSS is used in imaging experiments to avoid spectral interference of emitting components of tissue culture media, such as phenol red. It can be replaced with phenol red-free complete media. FBS can also interfere with probes and fluorescent proteins with emission maxima around 560 nm, like TMRM and mtRFP.
5. H_2O_2 must be prepared fresh the day of the experiment as it tends to dismute spontaneously. Failure to do this will alter the formal concentration of the solution, having an impact on the reproducibility of the experiment.
6. 37% (w/v) Formaldehyde is highly toxic and a potential carcinogen, so always handle it very carefully and in a chemical hood. The use of free amines (like Tris-HCl) in the buffer will decrease the efficiency of formaldehyde, which reacts with amino groups. Efficiency will fade with time, dictating preparation of fresh solutions every month. The pH of the 3.7% (v/v) formaldehyde solution is crucial for the success of the cytochrome-*c* immunolocalization. The pH should be checked the day of the experiment.
7. CsH is an inhibitor of the P-glycoprotein multidrug resistance pump, of which all rhodamine derivatives are substrates ***(20)***. Failure to inhibit these pumps will introduce additional variables in the equilibrium distribution of TMRM, complicating the interpretation of any recorded changes. Alternatively, other multidrug resistance inhibitors, like verapamil, can be used ***(24)***.
8. FCCP is dissolved in absolute ethanol: always keep the 2 m*M* stock solution at 4°C (in an ice bath) during the whole experiment to avoid ethanol evaporation and consequent concentration of FCCP.
9. All the protocols presented in this chapter have been thoroughly tested with adherent mammalian cell lines, such as MEFs, HeLa, PC3, DU145 and several other cell lines. With minimal adjustments, they can be adapted to cells grown in suspension, such as Jurkat cells, which can adhere to coverslips in the absence of serum or once plated on polylysine-coated coverslips. We are unaware of the suitability of these protocols in cell lines derived from different organisms (i.e., insects or plants).
10. When passaging cell cultures, accurately resuspend MEFs by pipeting the suspension a few times. This will ensure an even distribution of the plated cells on the coverslips.
11. This is a delicate procedure because the coverslip is fragile. Always check that the cleft where the coverslip is placed is free of debris and use extreme caution when sealing the Attofluor chamber. Once HBSS is added, check for sealing by wiping the bottom of the coverslip with a dry kimwipe.
12. A detailed description of the optical limitations of confocal microscopy is beyond our scope, but the user should always remember that the resolution (i.e., the ability to image two adjacent fluorescent emitters as separate objects) of a confocal microscope depends on several factors, including the excitation-emission wavelength, the numerical aperture of the objective, the refraction index of the medium used by the objective (air, oil, water). When using a 60×, 1.4-NA oil immersion objective and probes emitting in the red zone of the light spectrum, the resolution can be around 200–300 nm.

13. Treatment with hydrogen peroxide may be influenced by intrinsic susceptibility of the cell type used; to assess the proper concentration and timing for treatment, a titration curve is needed; moreover, treatment with hydrogen peroxide may be influenced by cell density.
14. Immunofluorescence can be paused at this step if needed; after fixation, wash coverslips with PBS and keep at 4°C for no longer than 24 h.
15. During incubation with secondary antibody, wrap the plate with aluminum foil to protect conjugated fluorophores from light.

References

1. Hengartner, M. O. (2000) The biochemistry of apoptosis. *Nature* **407,** 770–776.
2. Thompson, C. B. (1995) Apoptosis in the pathogenesis and treatment of disease. *Science* **267,** 1456–1462.
3. Gross, A., McDonnell, J. M., and Korsmeyer, S. J. (1999) BCL-2 family members and the mitochondria in apoptosis. *Genes Dev.* **13,** 1899–1911.
4. Zou, H., Henzel, W. J., Liu, X., Lutschg, A., and Wang, X. (1997) Apaf-1, a human protein homologous to *C. elegans* CED-4, participates in cytochrome c-dependent activation of caspase-3. *Cell* **90,** 405–413.
5. Frank, S., Gaume, B., Bergmann-Leitner, E. S., et al. (2001) The role of dynamin-related protein 1, a mediator of mitochondrial fission, in apoptosis. *Dev. Cell* **1,** 515–525.
6. Scorrano, L., Ashiya, M., Buttle, K., et al. (2002) A distinct pathway remodels mitochondrial cristae and mobilizes cytochrome *c* during apoptosis. *Dev. Cell* **2,** 55–67.
7. Breckenridge, D. G., Stojanovic, M., Marcellus, R. C., and Shore, G. C. (2003) Caspase cleavage product of BAP31 induces mitochondrial fission through endoplasmic reticulum calcium signals, enhancing cytochrome c release to the cytosol. *J. Cell Biol.* **160,** 1115–1127.
8. Scorrano, L. (2003) Divide et impera: Ca^{2+} signals, mitochondrial fission and sensitization to apoptosis. *Cell Death. Differ.* **10,** 1287–1289.
9. Legros, F., Lombes, A., Frachon, P., and Rojo, M. (2002) Mitochondrial fusion in human cells is efficient, requires the inner membrane potential, and is mediated by mitofusins. *Mol. Biol. Cell* **13,** 4343–4354.
10. Terman, A., Dalen, H., Eaton, J. W., Neuzil, J., and Brunk, U. T. (2003) Mitochondrial recycling and aging of cardiac myocytes: the role of autophagocytosis. *Exp. Gerontol.* **38,** 863–876.
11. Yaffe, M. P. (1999) The machinery of mitochondrial inheritance and behavior. *Science* **283,** 1493–1497.
12. Yoon, Y., Krueger, E. W., Oswald, B. J., and McNiven, M. A. (2003) The mitochondrial protein hFis1 regulates mitochondrial fission in mammalian cells through an interaction with the dynamin-like protein DLP1. *Mol. Cell Biol.* **23,** 5409–5420.
13. James, D. I., Parone, P. A., Mattenberger, Y., and Martinou, J. C. (2003) hFis1, a novel component of the mammalian mitochondrial fission machinery. *J. Biol. Chem.* **278,** 36,373–36,379.

14. Chen, H., Detmer, S. A., Ewald, A. J., Griffin, E. E., Fraser, S. E., and Chan, D. C. (2003) Mitofusins Mfn1 and Mfn2 coordinately regulate mitochondrial fusion and are essential for embryonic development. *J. Cell Biol.* **160,** 189–200.
15. Koshiba, T., Detmer, S. A., Kaiser, J. T., Chen, H., McCaffery, J. M., and Chan, D. C. (2004) Structural basis of mitochondrial tethering by mitofusin complexes. *Science* **305,** 858–862.
16. Ishihara, N., Eura, Y., and Mihara, K. (2004) Mitofusin 1 and 2 play distinct roles in mitochondrial fusion reactions via GTPase activity. *J. Cell Sci.* **117,** 6535–6546.
17. Cipolat, S., de Brito, O. M., Dal Zilio, B., and Scorrano, L. (2004) OPA1 requires mitofusin 1 to promote mitochondrial fusion. *Proc. Natl. Acad. Sci. U. S. A.* **101,** 15,927–15,932.
18. Jagasia, R., Grote, P., Westermann, B., and Conradt, B. (2005) DRP-1-mediated mitochondrial fragmentation during EGL-1-induced cell death in *C. elegans*. *Nature* **433,** 754–760.
19. Germain, M., Mathai, J. P., McBride, H. M., and Shore, G. C. (2005) Endoplasmic reticulum BIK initiates DRP1-regulated remodelling of mitochondrial cristae during apoptosis. *EMBO J.* **24,** 1546–1556.
20. Bernardi, P., Scorrano, L., Colonna, R., Petronilli, V., and Di Lisa F. (1999) Mitochondria and cell death. Mechanistic aspects and methodological issues. *Eur. J. Biochem.* **264,** 687–701.
21. Adachi, S., Gottlieb, R. A., and Babior, B. M. (1998) Lack of release of cytochrome *c* from mitochondria into cytosol early in the course of Fas-mediated apoptosis of Jurkat cells. *J. Biol. Chem.* **273,** 19,892–19,894.
22. Petronilli, V., Penzo, D., Scorrano, L., Bernardi, P., and Di Lisa, F. (2001) The mitochondrial permeability transition, release of cytochrome c and cell death. Correlation with the duration of pore openings in situ. *J. Biol. Chem.* **276,** 12,030–12,034.
23. Hockenbery, D. M., Oltvai, Z. N., Yin, X. M., Milliman, C. L., and Korsmeyer, S. J. (1993) Bcl-2 functions in an antioxidant pathway to prevent apoptosis. *Cell* **75,** 241–251.
24. Cornwell, M. M., Pastan, I., and Gottesman, M. M. (1987) Certain calcium channel blockers bind specifically to multidrug-resistant human KB carcinoma membrane vesicles and inhibit drug binding to P-glycoprotein. *J. Biol. Chem.* **262,** 2166–2170.

OPA1 requires mitofusin 1 to promote mitochondrial fusion

Sara Cipolat, Olga Martins de Brito, Barbara Dal Zilio, and Luca Scorrano*

Dulbecco–Telethon Institute, Venetian Institute of Molecular Medicine, Via Orus 2, I-35129 Padua, Italy

Communicated by Stanley J. Korsmeyer, Dana–Farber Cancer Institute, Boston, MA, September 23, 2004 (received for review July 23, 2004)

The regulated equilibrium between mitochondrial fusion and fission is essential to maintain integrity of the organelle. Mechanisms of mitochondrial fusion are largely uncharacterized in mammalian cells. It is unclear whether OPA1, a dynamin-related protein of the inner membrane mutated in autosomal dominant optic atrophy, participates in fusion or fission. OPA1 promoted the formation of a branched network of elongated mitochondria, requiring the integrity of both its GTPase and C-terminal coiled-coil domain. Stable reduction of OPA1 levels by RNA interference resulted in small, fragmented, and scattered mitochondria. Levels of OPA1 did not affect mitochondrial docking, but they correlated with the extent of fusion as measured by polyethylene glycol mitochondrial fusion assays. A genetic analysis proved that OPA1 was unable to tubulate and fuse mitochondria lacking the outer membrane mitofusin 1 but not mitofusin 2. Our data show that OPA1 functionally requires mitofusin 1 to regulate mitochondrial fusion and reveal a specific functional difference between mitofusin 1 and 2.

Mitochondria are crucial organelles for life and death of the cell: they produce most cellular ATP, shape cytosolic Ca^{2+} transients, and integrate diverse apoptotic stimuli by releasing protein cofactors needed for the efficient activation of effector caspases (1, 2). Such a functional versatility is matched by a complex structural organization. The mitochondrial cristae have been identified as a separate compartment connected to the thin intermembrane space by narrow tubular junctions (3), which may generate gradients of ions and small molecules along the cristae (4) and are responsible for the segregation of cytochrome *c* in the cristae compartment (5, 6). In the cytosol of certain cell types, mitochondria are organized in a network of individual organelles that dynamically fuse and divide (7, 8), generating functional mitochondrial cables. This organization allows stimuli hitting one end of the mitochondrial wire to be readily transmitted to distal components of the net (9), a useful property in large cells such as cardiomyocytes (10). On the other hand, mitochondria can also behave as individual units in other cell types, such as pancreatic beta cells (11). Mitochondrial shape is not static, because during mitosis, mitochondria divide and partition into daughter cells (12). Major changes of mitochondrial morphology have been described during apoptosis, with fragmentation of the mitochondrial network, cristae fusion, and enlargement of cristae junctions (6, 13).

Dynamic control of mitochondrial structure is performed by a growing set of "mitochondria-shaping" proteins that include both pro-fusion and pro-fission members, several of which have been identified in budding yeast (14). Fission of yeast mitochondria is accomplished by the recruitment of the dynamin-related large GTPase Dnm1p to the outer membrane, where it forms a complex with the adapter Mdv1p and the integral membrane protein Fis1p (15–18). Fusion involves proteins localized at both the outer and the inner membrane. A crucial role has been ascribed to the GTPase Fzo1p (19, 20), which interplays with the adapter Ugo1p in the outer membrane (21) and associates with the inner membrane dynamin-related protein Mgm1p to coordinate the fusion of the four membranes of two juxtaposed mitochondria (22–24).

Mammalian orthologues of *DNM1* and *FIS1*, called dynamin-related protein 1 (*Drp1*) and *hFis1*, respectively, have been identified and shown to participate in mitochondrial fission (25–27). Fusion processes seem to be more complex. Two *FZO1* homologues have been identified, mitofusin (*Mfn*) 1 and 2 (28, 29). Both are required for embryonic development, as substantiated by their genetic ablation in the mouse (30), but it is unclear whether *Mfn* redundancy reflects specific functional differences between MFN1 and MFN2. The mammalian orthologue of mgm1p is the inner membrane dynamin-related protein OPA1. Mutations in *Opa1* are associated with autosomal dominant optic atrophy, the leading cause of inherited optic neuropathy (31, 32). It has been proposed that OPA1 participates in a fission/fragmentation pathway (33–35) or in the maintenance of the structural integrity of the mitochondrial reticulum (36), but, until now, function of OPA1 was unclear, as was its interaction with other mitochondria-shaping proteins.

Here we investigated the role of OPA1 in controlling mitochondrial shape. A genetic analysis revealed that OPA1 requires MFN1 but not MFN2 to induce mitochondrial fusion. Our results identify a role for OPA1 in fusion of mammalian mitochondria and reveal a functional difference between MFN1 and MFN2.

Experimental Procedures

Plasmid Construction. Murine OPA1 cDNA (33) (corresponding to human transcript variant 1; a kind gift of Y. Kubo, Tokyo University, Tokyo) was subcloned into the *Cla*I site of pMSCV (BD-Clontech). K301A and R905stop mutants of OPA1 were generated by using QuikChange (Stratagene) and confirmed by DNA sequencing. Details on other plasmids used can be found in *Supporting Materials and Methods*, which is published as supporting information on the PNAS web site.

RNA Interference (RNAi). Stable RNAi against murine OPA1 nucleotide region 1813–1831 and scrambled control was delivered by using p*Silencer*2.1-U6/hygro (Ambion, Austin, TX). Details on this and on the generation of stable clones can be found in *Supporting Materials and Methods*.

Imaging. Details on epifluorescence, real-time, and static confocal imaging systems, parameters, and operations can be found in *Supporting Materials and Methods*.

Polyethylene Glycol (PEG) Fusion Assay. For PEG fusion assay, 5×10^5 mouse embryonic fibroblasts (MEFs) of the indicated genotype were transfected with mitochondrially targeted yellow fluorescent protein (mtYFP) or with mitochondrially targeted dsRED (mtRFP) alone or contransfected with mtYFP or mtRFP plus the indicated constructs. After 24 h, cells labeled

Abbreviations: DRP1, dynamin-related protein 1; MEF, mouse embryonic fibroblast; mtCFP, mitochondrially targeted cyan fluorescent protein; mtYFP, mitochondrially targeted yellow fluorescent protein; mtRFP, mitochondrially targeted dsRED; MFN, mitofusin; PEG, polyethylene glycol; RNAi, RNA interference.

*To whom correspondence should be addressed. E-mail: luca.scorrano@unipd.it.

© 2004 by The National Academy of Sciences of the USA

with different fluorescent proteins were coplated at a 1:1 ratio onto 13-mm round coverslips. Fusion was then induced after 24 h by a 60-sec treatment with a 50% (wt/vol) solution of PEG 1500 in PBS (Sigma), followed by extensive washes in DMEM supplemented with 10% FCS. To inhibit *de novo* synthesis of fluorescent proteins, 30 min before PEG treatment cells were incubated with the protein synthesis inhibitor cyclohexymide (20 μg/ml, Sigma), which was subsequently kept in all solutions and tissue culture media until cells were fixed for 30 min with ice-cold 3.7% (vol/vol) formaldehyde in PBS. After two washes with PBS, coverslips were mounted on slides with Anti-Fade Reagent (Molecular Probes).

Results

OPA1 Induces Mitochondrial Tubulation. We addressed whether expression of OPA1 affected mitochondrial morphology. Transient transfection of WT MEFs from 129/SvEv background (30) with OPA1 (33) resulted in a several-fold elevation of OPA1 levels after 24 h, as judged by immunoblotting (Fig. 5, which is published as supporting information on the PNAS web site). Imaging of WT MEFs transfected with a mitochondrially targeted cyan fluorescent protein (mtCFP) showed mitochondria as individual, rod-shaped, or round-shaped organelles, with an average length of 3 ± 0.34 μm ($n = 100$ cells in five different experiments) along their major axis (Fig. 1*A*). Morphometric analysis confirmed that only 23% of the analyzed cells displayed elongated mitochondria, i.e., cells with axial length >5 μm and roundness index <0.5 in $>50\%$ of mitochondria (Fig. 1*I*). When mtCFP was cotransfected with OPA1, mitochondria appeared tubular and interconnected in a branched network, with axial lengths of up to 18 μm (Fig. 1*B*). More than 50% of the transfected cells displayed elongated mitochondria (Fig. 1*I*). Strong overexpression of OPA1 in HeLa (35) and COS-7 (33) cells causes clustering of small mitochondria, whereas in 3T3 fibroblasts it promotes tubulation (37). We tested whether under a strong CMV promoter OPA1 caused mitochondrial fragmentation in MEFs. Levels of OPA1 in MEFs transfected with pCDNA3.1-OPA1 were >3-fold higher than those obtained by transfection with pMSCV-OPA1. Nevertheless, pCDNA3.1-OPA1 also promoted mitochondrial elongation in MEFs (data not shown). This finding suggests that overexpression of OPA1 result in mitochondrial fragmentation only in cells where mitochondria are already organized in a network of interconnected tubuli, such as HeLa cells.

We compared the observed effects of OPA1 on mitochondrial morphology with those induced by other mitochondria-shaping proteins. After expression of MFN1 or MFN2, clusters of rod-shaped mitochondria coexisted with elongated organelles (28, 29, 38) (Fig. 1 *E* and *F*). Quantification revealed a positive effect of these proteins on mitochondrial tubulation in MEFs, albeit lower than that induced by OPA1 (Fig. 1*I*). Expression of the fission protein DRP1 resulted in the appearance of globular and dispersed mitochondria (Fig. 1 *G* and *I*), whereas its dominant negative K38A mutant (26) promoted mitochondrial elongation and formation of tubuli of interconnected mitochondria (Fig. 1 *H* and *I*). MEFs appear to be a valid model cell line to study mitochondria-shaping proteins.

Tubular structures that move in and out of the focal plane can be easily mistaken for individual rod or spherical organelles in conventional imaging. Therefore, we acquired stacks of mitochondrial images along the *z*-axis of the entire cell, followed by 3D-image reconstruction and volumetric rendering. In mock-transfected MEFs, mitochondria were separated and dispersed throughout the cytosol, with clusters of individual organelles visible at high-power magnification (Fig. 1 *J* and *K*). Cells transfected with OPA1 showed an intricate network of highly interconnected mitochondria that spanned the entire volume of the cytoplasm (Fig. 1 *L* and *M*). Thus, overexpression of OPA1 in MEFs results in efficient formation of a network of elongated mitochondria.

Function and Levels of OPA1 Determine Shape of the Mitochondrial Reticulum. *OPA1* is affected in dominant optic atrophy, its mutations clustering in the GTPase, and in the C-terminal coiled-coil domain (39). Because the disease is transmitted as a dominant trait, it has been suggested that these mutations either act as dominant negative or induce a condition of haploinsufficiency leading to the clinical phenotype (36, 40). Therefore, we tested whether pathogenetic mutants of OPA1 or reduction of OPA1 levels modified mitochondrial morphology. We generated mutants of OPA1 GTPase and coiled-coil domains by substituting Lys-301 with Ala (K301A OPA1) and Arg-905 with a stop codon (R905stop OPA1), respectively. The K301A mutation has been shown to reduce the GTPase activity of OPA1 by >80%, whereas the R905stop mutant lacks the C-terminal coiled-coil domain thought to participate in protein–protein interactions (35). Transfection with K301A or R905stop OPA1 resulted in OPA1 levels comparable with those observed after transfection with WT OPA1 (Fig. 5), suggesting that these mutations do not affect protein stability. Mitochondria of cells transfected with K301A (Fig. 1*C*) or R905stop OPA1 (Fig. 1*D*) appeared globular. The reduction in mitochondrial elongation induced by these two mutants was comparable with that observed after transfection with the fission protein DRP1 (Fig. 1*I*).

To address the effect of reduced OPA1 levels on mitochondrial morphology, we turned to stable, plasmid-generated RNAi. We generated clones of MEFs from a mixed 129/CD1 background (41) stably expressing scrambled (control) or OPA1-targeted RNAi. In the OPA1-ablated clone A7, OPA1 levels were $\approx$30% compared with those of the control clone H4 (Fig. 2*A*). Other mitochondria-shaping proteins, such as DRP1, hFIS1, and MFN2, were not affected (data not shown). Clone A7 mitochondria appeared globular and fragmented as opposed to the rod, elongated organelles of clone H4 (Fig. 2*B*; see morphometric analysis in Fig. 2*C*). Fragmentation of mitochondria could be achieved by transient RNAi against OPA1 with 19-mer duplexes RNA in clone H4, suggesting that the mitochondrial morphology observed in clone A7 does not result from long-term adaptation of this particular clone (data not shown). In other screened clones, the degree of mitochondrial fragmentation correlated with levels of expressed OPA1 (data not shown). Taken together, these data demonstrate that levels of OPA1, as well as integrity of GTPase and coiled-coil domains of OPA1, determine mitochondrial morphology.

OPA1 Participates in Mitochondrial Fusion. Mitochondrial shape is the result of the equilibrium between fusion and fission events. In principle, a shift from a rod-globular to a tubular mitochondrial shape could result from increased fusion as well as decreased fission. We addressed which direction of the fusion/fission equilibrium was controlled by OPA1. We performed PEG fusion assays on clones H4 and A7. MEFs transfected with mtYFP or mtRFP were coplated and triggered to fuse by treatment with PEG. Differential interference contrast light microscopy revealed cytoplasmic fusion as early as 30 min after treatment, with numerous polykaryons becoming apparent after 2 h. We quantified fusion events in the heteropolykaryons by measuring the fraction of mitochondria simultaneously positive for both mtYFP and mtRFP, which cannot be exchanged between mitochondria because the targeting sequences are cleaved after mitochondrial import. Double labeling thus reports only fusion of mitochondria with mixing of matricial content. Four hours after PEG treatment, polykaryons derived from control clone (H4) displayed $\approx$65% of mitochondria positive for both yellow fluorescent protein and red fluorescent protein (Fig. 2 *D* and *E*). Mitochondrial fusion increased with time, reaching 78%

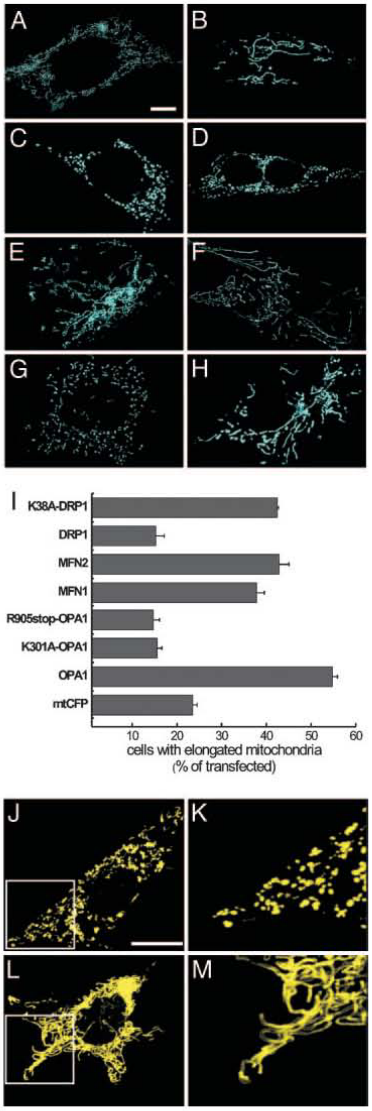

Fig. 1. Overexpression of OPA1 promotes mitochondrial elongation. (*A–H*) Effect of mutations in the GTPase and coiled-coil domains. Mitochondrial shape in MEFs transfected with mitochondria-shaping proteins is shown. WT MEFs grown on coverslips were cotransfected with mtCFP and empty vector (*A*), WT OPA1 (*B*), K301A OPA1 (*C*), R905stop OPA1 (*D*), Mfn1 (*E*), Mfn2 (*F*), WT DRP1 (*G*), or K38A DRP1 (*H*). After 24 h, images of mtCFP fluorescence from randomly selected cells were acquired, deconvoluted, and stored. (Scale bar, 15 μm.) (*I*) Morphometric analysis of mitochondrial elongation. WT MEFs grown on coverslips were cotransfected with mtCFP and empty vector or the indicated mitochondria-shaping protein. After 24 h, 20 randomly selected images of mtCFP fluorescence were acquired, deconvoluted, stored, and subsequently classified as described in *Supporting Materials and Methods*. Data represent mean ± SE of 14 different experiments. (*J–M*) Volume-rendered 3D reconstructions of mitochondrial network in MEFs. MEFs grown on coverslips were cotransfected with mtYFP and empty vector (*J*) or OPA1 (*L*), and, after 24 h, randomly selected confocal *z*-axis stacks of mtYFP fluorescence were acquired, stored, reconstructed, and volume-rendered as described in *Supporting Materials and Methods*. *K* and *M* represent 3× magnification of the boxed area in *J* and *L*, respectively. The depth of stacks was 20 μm. (Scale bar, 15 μm.)

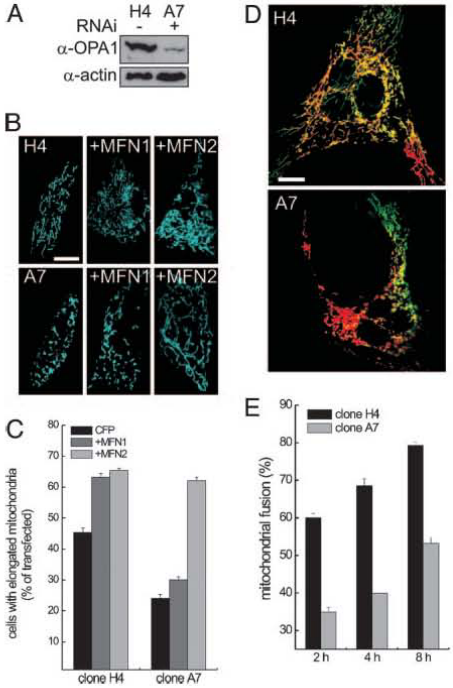

Fig. 2. Mitochondrial shape, mitochondrial fusion, and response to mitofusins after RNAi against OPA1. (*A*) Expression levels of OPA1 in MEF clones. Cells (5×10^6) from clone H4 carrying pSilencer-control and clone A7 carrying pSilencer-OPA1 were lysed, and equal amounts of protein were separated and immunoblotted with anti-OPA1 (1:2,000) antiserum and an anti-actin monoclonal antibody (1:2,000, Chemicon). (*B*) Mitochondrial shape and response to mitofusins after OPA1 ablation. MEFs from clones H4 and A7 grown on coverslips were transfected with mtCFP or cotransfected with the indicated mitofusins. After 24 h, images of mtCFP fluorescence were acquired exactly as in Fig. 1 *A–H*. (Scale bar, 15 μm.) (*C*) Morphometric analysis. H4 and A7 MEFs grown on coverslips were transfected as indicated. Experiments were performed exactly as in Fig. 1*I*. Data represent mean ± SE of four different experiments. (*D*) Representative heteropolykaryons from H4 and A7 clones. MEFs from the indicated clones were transfected with mtYFP or mtRFP, coplated on glass coverslips, fused as described in *Experimental Procedures*, and fixed after 4 h. Confocal images of representative polykaryons are shown. (Scale bar, 20 μm.) (*E*) Quantitation of the effects of ablation of OPA1 on a mitochondrial PEG fusion assay. Experiments were carried out as described in *D*, except that cells were fixed at the indicated times. Mitochondrial fusion was evaluated as described in *Experimental Procedures* from 30 randomly selected polykaryons. Data represent mean ± SE of three different experiments.

after 8 h. Ablation of OPA1 in clone A7 impaired fusion, reducing it to ≈52% even after 8 h (Fig. 2 *D* and *E*). We turned to WT MEFs to address whether increased OPA1 levels enhanced mitochondrial fusion. The number of mitochondria that were positive for both yellow fluorescent protein and red fluorescent protein increased linearly in WT MEFs after PEG treatment, reaching ≈55% after 8 h (Fig. 3 *C* and *D*, open

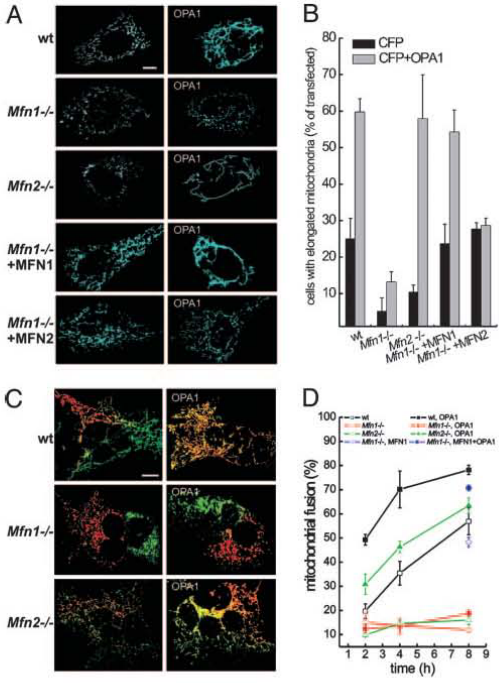

Fig. 3. OPA1 changes the shape of the mitochondrial reticulum by promoting MFN1-dependent mitochondrial fusion. (*A*) Effect of OPA1 on the shape of the mitochondrial network in WT, *Mfn1*−/−, and *Mfn2*−/− MEFs. MEFs of the indicated genotype grown on coverslips were cotransfected with mtCFP and empty vector (*Left*) or OPA1 (*Right*). When indicated, MFN1 or MFN2 were cotransfected with mtCFP in *Mfn1*−/− MEFs. After 24 h, images of mtCFP fluorescence were acquired exactly as in Fig. 1 *A–H*. (*B*) Morphometric analysis of WT, *Mfn1*−/−, and *Mfn2*−/− mitochondria. MEFs of the indicated genotype grown on coverslips were cotransfected with mtCFP and empty vectors (black bars) or with OPA1 (gray bars). Where indicated, *Mfn1*−/− cells were complemented by cotransfection with MFN1 or MFN2. Experiments were performed exactly as in Fig. 1*I*. Data represent mean ± SE of nine different experiments. (*C*) MEFs of the indicated genotype were transfected with mtYFP or mtRFP (*Left*) or cotransfected with mtYFP or mtRFP plus OPA1 (*Right*), coplated on glass coverslips, fused with PEG as described in *Experimental Procedures*, and fixed after 4 h. Confocal images of representative polykaryons are shown. (Scale bar, 20 μm.) (*D*) Quantification of the effect of OPA1 on fusion of WT, *Mfn1*−/−, and *Mfn2*−/− mitochondria. The experiments were conducted as described in *C*, except that heteropolykaryons were fixed at the indicated times. In the experiments depicted with diamonds, *Mfn1*−/− cells were cotransfected with mtYFP or mtRFP plus MFN1 (◇) and with mtYFP or mtRFP plus MFN1 and OPA1 (◆). Mitochondrial fusion was evaluated as described in *Experimental Procedures* from 30 randomly selected polykaryons. Data represent mean ± SE of four different experiments.

squares). OPA1 increased fusion to ≈50% after 2 h and to ≈80% after 8 h (Fig. 3 *C* and *D*, filled squares). On the other hand, K301A-OPA1 impaired mitochondrial fusion, reducing it to 31 ± 3.4% after 8 h (data not shown). These results show that levels and function of OPA1 regulate mitochondrial shape by impinging on organellar fusion.

Fusion by OPA1 Depends on the Outer Membrane Protein Mitofusin 1. We next wished to ascertain whether OPA1 required other mitochondria-shaping proteins to control mitochondrial morphology. We turned to a genetic approach, testing the ability of overexpressed OPA1 to promote mitochondrial tubulation in MEFs deficient for either *Mfn1* or *Mfn2*, the orthologues of yeast fzo1p. In *Mfn1*−/− MEFs, most mitochondria appeared globular, whereas in *Mfn2*−/− MEFs, the shape of mitochondria ranged from round dots to short rods (Fig. 3*A*) (30). Of note, levels and cleavage pattern of OPA1 were comparable in WT, *Mfn1*−/−, and *Mfn2*−/− MEFs (Fig. 6, which is published as supporting information on the PNAS web site), and transfection with pMSCV-OPA1 yielded similar levels of mitochondrial OPA1 in the MEFs of the different genotypes (Fig. 5). Expression of OPA1 induced mitochondrial tubulation in WT and *Mfn2*−/− but not in *Mfn1*−/− cells (Fig. 3*A*). Morphometric analysis confirmed that OPA1 can efficiently tubulate mitochondria in the absence of MFN2 but not MFN1 (Fig. 3*B*).

To address why *Mfn1*−/− cells did not respond to OPA1, we performed PEG fusion assays. In polykaryons derived from *Mfn1*−/− MEFs, mitochondria labeled with yellow fluorescent protein and red fluorescent protein sometimes segregated at the opposite sides of the cell with extremely low levels of fusion (Fig. 3*C*) that did not increase in time (Fig. 3*D*). In keeping with previous findings (30), this segregation occurred in only 20% of *Mfn1*−/− polykaryons. Mixing of differently labeled mitochondria was a constant feature of *Mfn2*−/− polykaryons, but mitochondria were still unable to fuse (Fig. 3 *C* and *D*) (30). Mitochondrial fusion in *Mfn2*−/− MEFs transfected with OPA1 was higher than in untransfected WT MEFs, whereas overexpression of OPA1 had no effect on mitochondrial fusion in polykaryons from *Mfn1*−/− cells (Fig. 3 *C* and *D*). These results show that MFN1 is required for OPA1-dependent mitochondrial fusion. Thus, OPA1, like mgm1p in *Saccharomyces cerevisiae*, requires outer membrane protein(s) to fuse mitochondria. Furthermore, our results reveal a functional difference between MFN1 and MFN2, at least in respect to OPA1-driven mitochondrial tubulation.

Specific Functional Interdependence Between MFN1 and OPA1. These results raised two crucial questions. Is the defect of *Mfn1*−/− mitochondria specific? If so, which step is affected by lack of MFN1, mitochondrial docking or the actual fusion process?

We first addressed whether the defect of *Mfn1*−/− mitochondria was specific. We checked whether reintroduction of MFN1 in *Mfn1*−/− cells corrected OPA1-induced mitochondrial elongation and fusion. Reexpression of MFN1 in *Mfn1*−/− MEFs restored mitochondrial shape (Fig. 3 *A* and *B*). Coexpression of MFN1 with OPA1 in *Mfn1*−/− cells resulted in tubular and elongated mitochondria (Fig. 3 *A* and *B*). Reintroduction of MFN1 corrected the defect of *Mfn1*−/− MEFs in mitochondrial PEG fusion assays (Fig. 3*D*, compare open diamonds with open squares) and enabled the pro-fusion effect of OPA1 (Fig. 3*D*, compare filled diamonds with filled squares). Because the mitochondrial defect of *Mfn1*−/− MEFs is complemented by MFN2 (30), we assessed whether introduction of MFN2 could also correct OPA1-driven mitochondrial tubulation. Expression of MFN2 in *Mfn1*−/− cells restored mitochondrial shape but did not allow OPA1-driven mitochondrial elongation (Fig. 3 *A* and *B*). To further test functional interdependence between OPA1 and mitofusins, we turned to OPA1 knockdown MEFs. Although levels of OPA1 did not influence mitochondrial elongation induced by MFN2, they proved essential for MFN1, which caused tubulation only in control H4 cells (Fig. 2 *B* and *C*). In complex, failure of *Mfn1*−/− mitochondria to fuse in response to OPA1 is a specific consequence of MFN1 deficiency, which cannot be complemented by MFN2. Moreover, MFN1 but not MFN2 requires adequate levels of OPA1 to promote mitochondrial elongation, further substantiating a functional interdependence between OPA1 and MFN1.

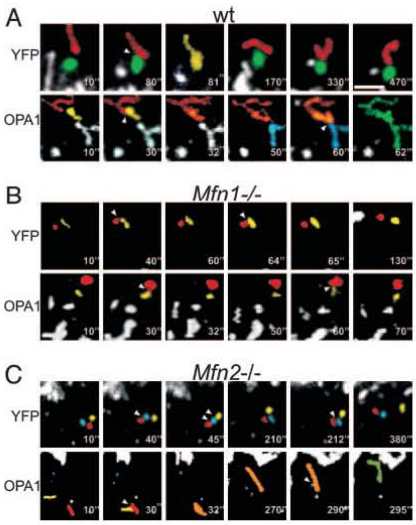

Fig. 4. The lack of MFN1 does not affect mitochondrial juxtaposition but blocks OPA1-induced mitochondrial tubulation. WT (*A*), *Mfn1*−/− (*B*), and *Mfn2*−/− (*C*) MEFs were cotransfected with mtYFP and empty vector (*Upper*) or with mtYFP and OPA1 (*Lower*), and, after 24 h, confocal *z*-stacks were acquired as described in *Supporting Materials and Methods*. Stacks were reconstructed and volume-rendered, and movements of individual mitochondria were tracked. Five-fold magnified portions of single *z*-planes corresponding to the indicated frames are shown. For the sake of clarity, mitochondria were individually labeled in different colors. Arrowheads indicate sites of mitochondrial contact. Colors of tubular mitochondria resulted from the merging of the colors of the individual mitochondria from which they originated. (Scale bar, 4 μm.)

Number of Intermitochondrial Contacts Is Not Affected by Levels of Mitofusins and OPA1. *Mfn1*−/− mitochondria are characterized by motion defects resulting in disordered, Brownian-like wandering of the organelles around the cytoplasm (30). If this phenotype resulted in fewer contacts between mitochondria, it might cause the inability of OPA1 to promote fusion in *Mfn1*−/− MEFs. To address whether contacts between *Mfn1*−/− mitochondria were impaired, we performed 4D imaging of mitochondria, i.e., time series of *z*-stacks of mitochondrial images. Yellow fluorescent protein-expressing WT mitochondria juxtaposed and merged in tubuli in which individual mitochondria were not recognizable (Fig. 4*A Upper*). These tubuli reverted then to the original elemental mitochondria, probably by fission (Fig. 4*A Upper*). *Mfn1*−/− (Fig. 4*B*) and *Mfn2*−/− mitochondria (Fig. 4*C*) juxtaposed closely, remaining in contact for seconds, even minutes, but did not fuse to constitute tubuli in any of the acquired planes. We cannot exclude the formation of tubuli that rapidly reverted by fission, albeit we never observed fission events completing in <500 msec (the acquisition time of one stack). We quantified contacts by following randomly chosen mitochondria in the volume of the *z*-stack for the entire acquisition sequence. The number of mitochondrial contacts was similar in WT, *Mfn1*−/−, and *Mfn2*−/− MEFs (8.5 ± 1.5 contacts in WT, 7 ± 0.9 in *Mfn1*−/−, and 7.5 ± 0.8 in *Mfn2*−/− MEFs; n = 16 in four different experiments). However, differences existed in the number of "productive" contacts, leading to the formation of mitochondrial tubuli, which were 2.3 ± 0.4 in WT, 0.7 ± 0.3 in *Mfn2*−/−, and 0.4 ± 0.3 in *Mfn1*−/− cells (n = 16 in four different experiments). Although OPA1 overexpression did not change the total number of contacts, in WT MEFs it caused a 2- to 3-fold increase in tubulation events (5.25 ± 1.25 productive events in a total of 9.75 ± 2.25 contacts; n = 16 in four different experiments) (Fig. 4*A*). A similar pattern was observed in *Mfn2*−/− MEFs (Fig. 4*C*), with 4.2 ± 1.1 productive events in a total of 8.1 ± 0.8 contacts (n = 16 in four different experiments). *Mfn1*−/− mitochondria also were unable to merge into tubuli after OPA1 overexpression (Fig. 4*B*). In this case, contacts were 7.25 ± 2.6, but only 0.5 ± 0.3 were productive. In summary, the total number of contacts between mitochondria is not affected by OPA1 overexpression or by MFN deficiency. OPA1 facilitates fusion after contacts between WT and *Mfn2*−/− but not *Mfn1*−/− mitochondria. Taken together, our results suggest that OPA1 requires MFN1 to fuse the membranes of two juxtaposed mitochondria and not to produce intermitochondrial contacts.

Discussion

OPA1 is so far the only mammalian mitochondria-shaping protein localized in the inner mitochondrial membrane (34, 37). Albeit it shares 30% homology with *S. cerevisiae* mgm1p, which in budding yeast is crucial to maintain fusion-competent mitochondria (22, 23), its biological function remains unclear. Overexpression of OPA1 has been reported to promote fission and perinuclear clustering of mitochondria (33–35). Conversely, ablation of OPA1 resulted in mitochondrial depolarization, derangement of the mitochondrial network, and release of cytochrome *c* (36), or in localized constrictions, followed by fragmentation (35). It is difficult to reconcile the proposed pro-fission role of OPA1 with the known function in mitochondrial fusion of its yeast orthologue mgm1p. To define the biological function of OPA1, we have used a combination of genetics and imaging. Overexpression of OPA1 in MEFs induces mitochondrial elongation and tubulation, in keeping with what was observed in 3T3 fibroblasts (37), but at a variance from the results obtained in HeLa and COS7 cells (33–35). OPA1 might cause fragmentation only when it is expressed at very high levels in cells such as HeLa and COS7, where mitochondria are already elongated. This interpretation is also consistent with the finding that in COS7 cells the inactive K301A mutant of OPA1, which does not hydrolyze GTP (35), also causes fragmentation (33). Stable reduction of OPA1 levels by RNAi results in mitochondrial fragmentation, often associated with clustering. A similar mitochondrial phenotype is observed in HeLa cells after transient RNAi (35, 36). Assays of mitochondrial fusion show that OPA1 controls the complex process of mitochondrial fusion, a direct correlation being observed between levels of OPA1 and fusion efficiency. PEG fusion assays are limited in that they measure not only mitochondrial fusion *per se*, but also the preparatory events of mitochondrial juxtaposition and docking, which therefore need to be measured. Real-time imaging experiments show that OPA1 does not promote mitochondrial docking. Taken together, our data suggest that OPA1 impinges on the fusion step to regulate mitochondrial morphology.

Function of OPA1 requires an intact GTPase and C-terminal coiled-coil domain, two hot spots for OPA1 mutations in dominant optic atrophy (31, 32, 39). Overexpression of the K301A mutant of OPA1 impairs mitochondrial fusion; interestingly, monocytes from dominant optic atrophy patients carrying mutations in OPA1 GTPase domain display fragmented mitochondria (32). The C-terminal coiled-coil domain is also necessary for mitochondrial fusion. Coiled-coil regions often participate in protein–protein interaction (42), and integrity of the C-terminal domain of the *S. cerevisiae* orthologue of OPA1, mgm1p, is required for its activity (23). Recent evidence supports a model in which mgm1p mediates mitochondrial fusion through a multiprotein complex with the outer membrane proteins fzo1p and ugo1p (23). Although the mammalian homologue of ugo1p is not yet identified, fzo1p orthologues have been characterized in

MFN1 and MFN2. Their ablation results in embryonic lethality, mitochondrial fragmentation, and heterogeneous mitochondrial dysfunction (30). We reasoned that OPA1 function might depend on other mitochondria shaping proteins, such as the outer membrane MFNs. In cells deficient in MFN1, OPA1 cannot promote mitochondrial fusion. This defect is complemented by reintroduction of MFN1 but not MFN2, unequivocally identifying outer membrane MFN1 as an essential functional partner of OPA1. Moreover, MFN1 is unable to promote mitochondrial elongation if OPA1 is ablated. Thus, OPA1 and MFN1 appear to functionally depend on each other.

A major dilemma is whether the two fzo1p homologues MFN1 and MFN2 are functionally redundant. Our genetic analysis provides evidence of a functional diversity between MFN1 and MFN2, suggesting a functional axis between OPA1 and MFN1. This finding might explain the morphological difference between mitochondria of *Mfn1*−/− and *Mfn2*−/− cells. In the absence of MFN2 the inner–outer membrane fusion machinery composed by OPA1 and MFN1 is still intact and can provide a low degree of fusion resulting in the few tubular mitochondria of *Mfn2*−/− MEFs. Because MFN1 appears to allow fusion of the inner and outer membrane, it will be interesting to assess whether during evolution MFN2 acquired other specialized functions like regulation of mitochondrial positioning and/or communication with other cellular structures.

It has been suggested that OPA1 could maintain cristae structure (36). During cell death mitochondrial fusion is inhibited (43); inactivation of OPA1 might therefore be a crucial step in mitochondrial remodeling during apoptosis. Because OPA1 is unable to promote fusion in the absence of MFN1, our results provide a framework to dissect specific effects of OPA1 during apoptosis on cristae structure vs. preservation of mitochondrial fusion.

We thank D. Chan (California Institute of Technology, Pasadena, CA) for the kind gift of WT, *mfn1*−/−, and *mfn2*−/− MEFs and for critical reading of the manuscript; V. Petronilli for helpful discussions; and P. Bernardi and M. Zaccolo for critical reading of the manuscript. O.M.d.B. is the recipient of a Bolsa de Doutoramento of the Fundação para a Ciência e Tecnologia (Lisbon). L.S. is an assistant Telethon scientist of the Dulbecco–Telethon Institute. This work was supported by Telethon Italy, the Glaucoma Research Foundation, and the Human Frontier Science Program Organization.

1. Jouaville, L. S., Ichas, F., Holmuhamedov, E. L., Camacho, P. & Lechleiter, J. D. (1995) *Nature* **377,** 438–441.
2. Wang, X. (2001) *Genes Dev.* **15,** 2922–2933.
3. Frey, T. G. & Mannella, C. A. (2000) *Trends Biochem. Sci.* **25,** 319–324.
4. Mannella, C. A., Pfeiffer, D. R., Bradshaw, P. C., Moraru, I. I., Slepchenko, B., Loew, L. M., Hsieh, C. E., Buttle, K. & Marko, M. (2001) *IUBMB Life* **52,** 93–100.
5. Bernardi, P. & Azzone, G. F. (1981) *J. Biol. Chem.* **256,** 7187–7192.
6. Scorrano, L., Ashiya, M., Buttle, K., Weiler, S., Oakes, S. A., Mannella, C. A. & Korsmeyer, S. J. (2002) *Dev. Cell* **2,** 55–67.
7. Griparic, L. & van der Bliek, A. M. (2001) *Traffic* **2,** 235–244.
8. Legros, F., Lombes, A., Frachon, P. & Rojo, M. (2002) *Mol. Biol. Cell* **13,** 4343–4354.
9. Amchenkova, A. A., Bakeeva, L. E., Chentsov, Y. S., Skulachev, V. P. & Zorov, D. B. (1988) *J. Cell Biol.* **107,** 481–495.
10. Pacher, P. & Hajnoczky, G. (2001) *EMBO J.* **20,** 4107–4121.
11. Collins, T. J., Berridge, M. J., Lipp, P. & Bootman, M. D. (2002) *EMBO J.* **21,** 1616–1627.
12. Catlett, N. L. & Weisman, L. S. (2000) *Curr. Opin. Cell Biol.* **12,** 509–516.
13. Frank, S., Gaume, B., Bergmann-Leitner, E. S., Leitner, W. W., Robert, E. G., Catez, F., Smith, C. L. & Youle, R. J. (2001) *Dev. Cell* **1,** 515–525.
14. Shaw, J. M. & Nunnari, J. (2002) *Trends Cell Biol.* **12,** 178–184.
15. Bleazard, W., McCaffery, J. M., King, E. J., Bale, S., Mozdy, A., Tieu, Q., Nunnari, J. & Shaw, J. M. (1999) *Nat. Cell Biol.* **1,** 298–304.
16. Sesaki, H. & Jensen, R. E. (1999) *J. Cell Biol.* **147,** 699–706.
17. Mozdy, A. D., McCaffery, J. M. & Shaw, J. M. (2000) *J. Cell Biol.* **151,** 367–380.
18. Tieu, Q., Okreglak, V., Naylor, K. & Nunnari, J. (2002) *J. Cell Biol.* **158,** 445–452.
19. Hermann, G. J., Thatcher, J. W., Mills, J. P., Hales, K. G., Fuller, M. T., Nunnari, J. & Shaw, J. M. (1998) *J. Cell Biol.* **143,** 359–373.
20. Rapaport, D., Brunner, M., Neupert, W. & Westermann, B. (1998) *J. Biol. Chem.* **273,** 20150–20155.
21. Sesaki, H. & Jensen, R. E. (2001) *J. Cell Biol.* **152,** 1123–1134.
22. Wong, E. D., Wagner, J. A., Gorsich, S. W., McCaffery, J. M., Shaw, J. M. & Nunnari, J. (2000) *J. Cell Biol.* **151,** 341–352.
23. Wong, E. D., Wagner, J. A., Scott, S. V., Okreglak, V., Holewinske, T. J., Cassidy-Stone, A. & Nunnari, J. (2003) *J. Cell Biol.* **160,** 303–311.
24. Sesaki, H., Southard, S. M., Yaffe, M. P. & Jensen, R. E. (2003) *Mol. Biol. Cell* **14,** 2342–2356.
25. Labrousse, A. M., Zappaterra, M. D., Rube, D. A. & van der Bliek, A. M. (1999) *Mol. Cell* **4,** 815–826.
26. Smirnova, E., Griparic, L., Shurland, D. L. & van der Bliek, A. M. (2001) *Mol. Biol. Cell* **12,** 2245–2256.
27. James, D. I., Parone, P. A., Mattenberger, Y. & Martinou, J. C. (2003) *J. Biol. Chem.* **278,** 36373–36379.
28. Santel, A. & Fuller, M. T. (2001) *J. Cell Sci.* **114,** 867–874.
29. Rojo, M., Legros, F., Chateau, D. & Lombes, A. (2002) *J. Cell Sci.* **115,** 1663–1674.
30. Chen, H., Detmer, S. A., Ewald, A. J., Griffin, E. E., Fraser, S. E. & Chan, D. C. (2003) *J. Cell Biol.* **160,** 189–200.
31. Alexander, C., Votruba, M., Pesch, U. E., Thiselton, D. L., Mayer, S., Moore, A., Rodriguez, M., Kellner, U., Leo-Kottler, B., Auburger, G., *et al.* (2000) *Nat. Genet.* **26,** 211–215.
32. Delettre, C., Lenaers, G., Griffoin, J. M., Gigarel, N., Lorenzo, C., Belenguer, P., Pelloquin, L., Grosgeorge, J., Turc-Carel, C., Perret, E., *et al.* (2000) *Nat. Genet.* **26,** 207–210.
33. Misaka, T., Miyashita, T. & Kubo, Y. (2002) *J. Biol. Chem.* **277,** 15834–15842.
34. Satoh, M., Hamamoto, T., Seo, N., Kagawa, Y. & Endo, H. (2003) *Biochem. Biophys. Res. Commun.* **300,** 482–493.
35. Griparic, L., van der Wel, N. N., Orozco, I. J., Peters, P. J. & van der Bliek, A. M. (2004) *J. Biol. Chem.* **279,** 18792–18798.
36. Olichon, A., Baricault, L., Gas, N., Guillou, E., Valette, A., Belenguer, P. & Lenaers, G. (2003) *J. Biol. Chem.* **278,** 7743–7746.
37. Olichon, A., Emorine, L. J., Descoins, E., Pelloquin, L., Brichese, L., Gas, N., Guillou, E., Delettre, C., Valette, A., Hamel, C. P., *et al.* (2002) *FEBS Lett.* **523,** 171–176.
38. Santel, A., Frank, S., Gaume, B., Herrler, M., Youle, R. J. & Fuller, M. T. (2003) *J. Cell Sci.* **116,** 2763–2774.
39. Delettre, C., Griffoin, J. M., Kaplan, J., Dollfus, H., Lorenz, B., Faivre, L., Lenaers, G., Belenguer, P. & Hamel, C. P. (2001) *Hum. Genet.* **109,** 584–591.
40. Delettre, C., Lenaers, G., Pelloquin, L., Belenguer, P. & Hamel, C. P. (2002) *Mol. Genet. Metab.* **75,** 97–107.
41. Wei, M. C., Zong, W. X., Cheng, E. H., Lindsten, T., Panoutsakopoulou, V., Ross, A. J., Roth, K. A., MacGregor, G. R., Thompson, C. B. & Korsmeyer, S. J. (2001) *Science* **292,** 727–730.
42. Lupas, A. (1996) *Trends Biochem. Sci.* **21,** 375–382.
43. Karbowski, M., Arnoult, D., Chen, H., Chan, D. C., Smith, C. L. & Youle, R. J. (2004) *J. Cell Biol.* **164,** 493–499.

Cell

Mitochondrial Rhomboid PARL Regulates Cytochrome c Release during Apoptosis via OPA1-Dependent Cristae Remodeling

Sara Cipolat,[1,7] Tomasz Rudka,[2,7] Dieter Hartmann,[2,7] Veronica Costa,[1] Lutgarde Serneels,[2] Katleen Craessaerts,[2] Kristine Metzger,[2] Christian Frezza,[1] Wim Annaert,[3] Luciano D'Adamio,[5] Carmen Derks,[2] Tim Dejaegere,[2] Luca Pellegrini,[6] Rudi D'Hooge,[4] Luca Scorrano,[1,*] and Bart De Strooper[2,*]

[1]Dulbecco-Telethon Institute, Venetian Institute of Molecular Medicine, Padova, Italy

[2]Neuronal Cell Biology and Gene Transfer Laboratory

[3]Membrane Trafficking Laboratory

Center for Human Genetics, Flanders Interuniversity Institute for Biotechnology (VIB4) and K.U.Leuven, Leuven, Belgium

[4]Laboratory of Biological Psychology, K.U.Leuven, Leuven, Belgium

[5]Albert Einstein College of Medicine, Bronx, NY 10461, USA

[6]Centre de Recherche Robert Giffard, Universitè Laval, G1J 2G3 Quebec, Canada

[7]These authors contribute equally to this work.

*Contact: luca.scorrano@unipd.it (L.S.); bart.destrooper@med.kuleuven.be (B.D.S.)

DOI 10.1016/j.cell.2006.06.021

SUMMARY

Rhomboids, evolutionarily conserved integral membrane proteases, participate in crucial signaling pathways. Presenilin-associated rhomboid-like (PARL) is an inner mitochondrial membrane rhomboid of unknown function, whose yeast ortholog is involved in mitochondrial fusion. *Parl*$^{-/-}$ mice display normal intrauterine development but from the fourth postnatal week undergo progressive multisystemic atrophy leading to cachectic death. Atrophy is sustained by increased apoptosis, both in and ex vivo. *Parl*$^{-/-}$ cells display normal mitochondrial morphology and function but are no longer protected against intrinsic apoptotic death stimuli by the dynamin-related mitochondrial protein OPA1. *Parl*$^{-/-}$ mitochondria display reduced levels of a soluble, intermembrane space (IMS) form of OPA1, and OPA1 specifically targeted to IMS complements *Parl*$^{-/-}$ cells, substantiating the importance of PARL in OPA1 processing. *Parl*$^{-/-}$ mitochondria undergo faster apoptotic cristae remodeling and cytochrome c release. These findings implicate regulated intramembrane proteolysis in controlling apoptosis.

INTRODUCTION

Rhomboid proteases constitute probably the most widely conserved polytopic-membrane-protein family identified until now (Koonin et al., 2003). Seven rhomboids have been identified in *D. melanogaster* (Freeman, 2004), where they function as essential activators of the epidermal growth factor (EGF) signaling pathway, proteolytically cleaving the EGF receptor ligands Spitz, Gurken, and Keren. Since all Rhomboids share a conserved serine protease catalytic dyad (Lemberg et al., 2005), it has been suggested that they are able to cleave proteins in the transmembrane domain. Therefore, together with the presenilin aspartyl proteases and the Site 2 metalloproteases, they have been functionally assigned to a previously unidentified class of highly hydrophobic proteases involved in "regulated intramembranous proteolytic cleavage," a novel cell-signaling mechanism (Brown et al., 2000). Our knowledge of the mammalian rhomboids is extremely scarce. For example, they are unlikely to be involved in EGF signaling, since TGFα, the major mammalian ligand of the EGFR pathway, is released by metalloproteases of the ADAM family (Freeman, 2004).

Recently, a mitochondrial rhomboid, *rbd1/pcp1*, was identified in *Saccharomyces cerevisiae* (Esser et al., 2002; Herlan et al., 2003; McQuibban et al., 2003; Sesaki et al., 2003). Δ*rbd1* cells display fragmented mitochondria and impaired growth on nonfermentable carbon sources, similar to the phenotype caused by deletion of the dynamin-related protein Mgm1p, which turned out to be a substrate for Rbd1p. The short isoform of Mgm1p produced by Rbd1p is required to maintain mitochondrial morphology and fusion (Herlan et al., 2003; McQuibban et al., 2003). Thus, rhomboids and intramembrane proteolysis appear to control mitochondrial dynamics and function in yeast.

Mitochondria are crucial organelles in intermediate metabolism and energy production (Danial et al., 2003), Ca^{2+} signaling (Rizzuto et al., 2000), and integration and amplification of apoptotic signals (Green and Kroemer, 2004). Such functional versatility is mirrored by their

complex and dynamic morphology, controlled by a growing family of "mitochondria-shaping" proteins that regulate fusion and fission events. In mammals, fission is controlled by the dynamin-related protein DRP-1 (Smirnova et al., 2001) and its outer membrane (OM) adaptor hFis1 (James et al., 2003; Yoon et al., 2003). Fusion is mediated by two OM proteins, mitofusin (MFN) -1 and -2. Optic atrophia 1 (OPA1), the homolog of *S. cerevisiae* Mgm1p, is the only dynamin-related protein identified in the inner membrane (IM) so far (Olichon et al., 2002). OPA1 promotes mitochondrial fusion by cooperating with MFN1 (Cipolat et al., 2004) and is mutated in dominant optic atrophy, the most common cause of inherited optic neuropathy (Alexander et al., 2000; Delettre et al., 2000). The homolog of yeast Rbd1p in mammals is the so-called "presenilin-associated rhomboid-like" (PARL). PARL is a rhomboid protease originally identified in a two-hybrid screen to interact with presenilin, the enzymatically active core protein of γ-secretase (Pellegrini et al., 2001), and later found to be mitochondrial (Sik et al., 2004). We used a genetic approach to investigate the function of PARL and its potential role in OPA1 processing.

RESULTS

Targeted Inactivation of the Mouse *Parl* Gene

Mice with loxP sites inserted in the *Parl* gene ($Parl^{flx/flx}$) were generated by homologous recombination (Figure 1A). They were crossed with a mouse strain expressing Cre from the PGK promoter, resulting in Cre-mediated excision of the region between the loxP sites in all tissues. The resulting *Parl* null allele ($Parl^{-/-}$) (Figure 1A) still generated a small amount of aberrantly migrating RNA (Figure 1C). RT-PCR and sequencing showed the absence of exon 2. Since this resulted in a frame shift and premature stop codon, the remaining RNA is no longer functional (Figures 1D and 1F). Immunoblotting confirmed the loss of PARL in fibroblasts derived from $Parl^{-/-}$ mice (Figure 1E).

Parl$^{-/-}$ Mice Prematurely Die of Progressive Cachexia

$Parl^{-/-}$ mice were born in a normal Mendelian frequency and developed normally up to 4 weeks. From then on, mice displayed severe growth retardation (Figures 2A and 2B). $Parl^{-/-}$ mice lost muscle mass (erector spinae, abdominal muscles, and diaphragm), leading to postural defects with hunchback deformity (Figure 2A). All animals died between 8 and 12 weeks (Figure 2C), most likely as a consequence of moving and breathing problems and general cachexia.

Microscopically, the diameter of individual muscle fibers was reduced (Figure 2O). Spinal motoneurons were normal, and AChE histochemistry failed to reveal signs of neurogenic atrophy (data not shown). At 8 weeks, thymus and spleen were massively atrophic, weighing 10% or less compared to controls (Figures 2D and 2I), with severe lymphocyte loss (Figures 2E and 2J). Uteri remained prepuberal, while ovaries were histologically

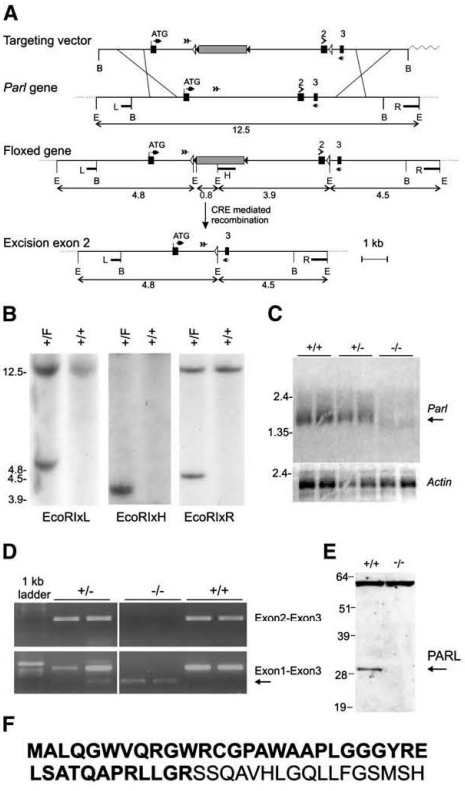

Figure 1. Generation of *Parl* Knockout Mice

(A) Maps of the targeting vector, the wild-type *Parl* allele, the conditional targeted allele (floxed allele), and the disrupted *Parl* allele. Exons (black boxes), LoxP and FRT recombination sites (white and black arrowheads, respectively), and locations of PCR primers are indicated. The expected sizes for restriction fragments detected by 5′ (L), 3′ (R) flanking or internal probes (H) (PCR fragments, black bars) from targeted and wild-type alleles are indicated with line diagrams. Positive selection marker is indicated as a gray box. Relevant restriction sites are shown (BglII, indicated as B and EcoRI as E).

(B) Examples of Southern blot of DNA isolated from ES cells, digested with EcoRI, and hybridized with the different probes (L, R, and internal [H]).

(C) Northern blot: the *Parl* transcript is detected in wt and heterozygous embryos. In $Parl^{-/-}$, a weak signal corresponding to an aberrant transcript is detected. The *β-actin* transcript is detected as control.

(D) RT-PCR analysis of *Parl* transcripts in wt and $Parl^{-/-}$ MEF cells. A shorter transcript of *Parl* is detected in the $Parl^{-/-}$ cells. Sequencing of the aberrant transcript confirmed a reading shift in remaining transcript.

(E) 100 μg of wt and $Parl^{-/-}$ MEFs lysate was resolved by SDS-PAGE and probed with anti-PARL antibody (specific band around 30 kDa). The unspecific upper band was used as loading control.

(F) Prediction of the maximal possible aberrant PARL protein. Bold amino acids are identical to wt PARL.

normal. Males showed cryptorchidism with size reduction of testes, epididymis, and accessory glands (data not shown). Fluoro-Jade (Figure 2N) staining and activated caspase-3 immunoreactivity (data not shown) indicated (mild) neurodegenerative changes and apoptotic cell death in thalamus and striatum. Latency of the acoustic startle response was increased in *Parl* $^{-/-}$ mice ($p < 0.001$), which could relate to defects in neural conduction, striatal dysfunction, and/or increased reaction time (data not shown).

Parl $^{-/-}$ mice have thus greatly reduced life span due to progressive cachexia and are characterized by severe atrophy of muscular tissue, spleen, and thymus and indications of increased apoptosis. We investigated the extent to which mitochondrial dysfunction and/or apoptotic dysregulation contributed to this multisystemic atrophy.

Parl Is Not Required for Mitochondrial Respiratory Function

Total ATP content in limb muscles isolated from *Parl* $^{-/-}$ and wild-type (wt) animals was comparable (67.5 ± 11.3 nmol ATP/μg protein in *wt* versus 62.6 ± 16.4 nmol ATP/μg protein in *Parl* $^{-/-}$ muscle). Basal (state 4), ADP-stimulated (state 3), and maximal (uncoupled) respiratory rates (J_{O2}) of wt and *Parl* $^{-/-}$ mitochondria isolated from liver (data not shown), fibroblasts (data not shown), or muscle (Figure 2P) were similar, irrespective of the substrates used to feed the respiratory chain. Moreover, uptake of the potentiometric dye tetramethyl rhodamine methyl ester (TMRM) was unaltered in *Parl* $^{-/-}$ mouse embryonic fibroblasts (MEFs) (see Figure S1A in the Supplemental Data available with this article online) and in primary myoblasts and myotubes isolated from *Parl* $^{-/-}$ diaphragms (Figure 6E). Mitochondrial depolarization in response to the F_1F_0ATPase inhibitor oligomycin is a sensitive test of latent mitochondrial dysfunction in intact cells (Irwin et al., 2003). Real-time imaging of mitochondrial TMRM fluorescence in response to oligomycin showed no depolarization in *Parl* $^{-/-}$ MEFs, myoblasts, or myotubes (Figures S1B–S1D). Thus, *Parl* $^{-/-}$ mitochondria do not display primary respiratory defects or latent mitochondrial dysfunction in hepatocytes, MEFs, myocytes, or myotubes. Mitochondrial dysfunction therefore does not explain *Parl* $^{-/-}$ muscular atrophy and multisystemic failure.

Absence of *Parl* Results in Massive Apoptosis of T and B Lymphocytes

Muscle atrophy can be caused by apoptosis, but apoptotic segments of muscle fibers are rapidly cleared, making them difficult to detect (Sandri and Carraro, 1999). We turned therefore to thymus and spleen, where apoptosis determines cellular content and fate. Severe cell depletion and marked TUNEL staining was evident in both organs of *Parl* $^{-/-}$ animals (Figures 2E and 2J). In the thymus, the great majority of T cells follow the normal developmental sequence CD4 CD8 (double negative, DN)→$CD4^+$ $CD8^+$(double positive, DP)→$CD4^+CD8^-$ or CD4 $CD8^+$ (single positive). Numerically, DN thymocytes were unchanged, while DP cells were reduced over 100-fold in *Parl* $^{-/-}$ mice (Figures 2F and 2G) as a result of massive apoptosis revealed by their counterstaining with annexin-V (Figure 2H, gray bars). Similarly, apoptosis depleted the $B220^+$ B cell population in *Parl* $^{-/-}$ spleens (Figures 2K–2M). *Parl* $^{-/-}$ thymocytes isolated from 7-week-old mice and cultured in complete media also displayed increased death (Figure 2H, hatched bars), suggesting a cell-autonomous effect (Hao et al., 2005). Overall our results show that in adult *Parl* $^{-/-}$ mouse, $B220^+$ B cells as well as DP T cells undergo increased apoptosis in and ex vivo. Together with the caspase-3 positivity of brain sections (data not shown) and the muscular atrophy, these results suggest that increased susceptibility to apoptosis could contribute to the multisystemic failure of *Parl* $^{-/-}$ mice.

Parl Regulates Cytochrome c Release from Mitochondria

To analyze the effects of PARL deficiency on apoptosis at the molecular level, we turned to MEFs. SV40-transformed *Parl* $^{-/-}$ MEFs proved very susceptible to a panoply of intrinsic apoptotic stimuli acting via mitochondria, including the "BH3-only" member of the BCL-2 family BID. Conversely, death by the extrinsic stimulus TNF-α was comparable in wt and *Parl* $^{-/-}$ MEFs (Figure 3A). Thus, PARL does not influence the extrinsic pathway of apoptosis induced by TNF-α in MEFs. Expression of BCL-2 did not protect (data not shown), demonstrating that MEFs behave like type I cells, bypassing mitochondria in this form of apoptosis (Scaffidi et al., 1998). This was confirmed in primary MEFs from a different clone (data not shown). Finally, primary myoblasts from *Parl* $^{-/-}$ mice also showed increased TUNEL-positive nuclei in response to H_2O_2 (Figure 3A). Reintroduction of active PARL in *Parl* $^{-/-}$ MEFs decreased death to wt levels, irrespective of the stimulus employed (Figures 3B–3D). Conversely, a catalytically inactive mutant of PARL, 335His→Gly ($PARL^{H335G}$), corrected PARL expression (Figure 3E) but was unable to rescue apoptosis of *Parl* $^{-/-}$ MEFs (Figure 3H).

Following treatment with H_2O_2, *Parl* $^{-/-}$ MEFs and primary myoblasts released cytochrome *c* more rapidly than their wt counterparts (Figures 4A–4D). Mitochondrial dysfunction, which accompanies cytochrome c release, also occurred faster in *Parl* $^{-/-}$ MEFs (Figures 4E and 4F), while multidomain proapoptotics BAK and BAX, required for release of cytochrome c through the outer membrane (Wei et al., 2001), were equally activated (data not shown). Isolated *Parl* $^{-/-}$ liver mitochondria also released cytochrome c faster than their wt counterparts upon treatment with recombinant caspase-8-cleaved BID (cBID) (Figure 4G). This was again not due to enhanced BAK activation, as higher-order BAK oligomers appeared with the same kinetics in wt and *Parl* $^{-/-}$ mitochondria (Figure 4H).

The major store of cytochrome c released during apoptosis is located in the mitochondrial cristae. We therefore measured cytochrome c redistribution following treatment of isolated wt and *Parl* $^{-/-}$ mitochondria with cBID using

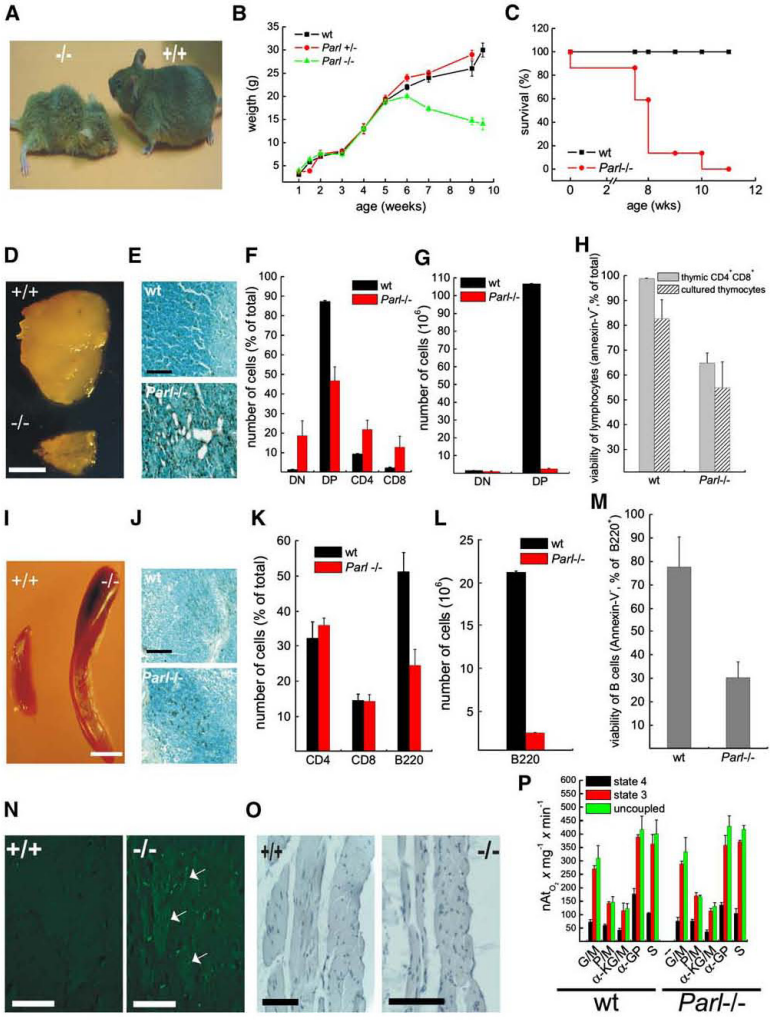

Figure 2. Wasting Phenotype of the *Parl*$^{-/-}$ Mice Is Characterized by Increased Apoptosis

(A) Representative photograph of wt (+/+) and *Parl* $^{-/-}$ (−/−) 8-week-old littermates.

(B) Growth curve of wt, *Parl*$^{+/-}$, and *Parl* $^{-/-}$ female littermates (mean ± SEM).

(C) Kaplan-Meier survival curve of wt and *Parl* $^{-/-}$ littermates.

(D) Images of thymuses dissected from 8-week-old wt (+/+) and *Parl* $^{-/-}$ (−/−) mice. Scale bar, 1 mm.

(E) TUNEL staining of wt and *Parl* $^{-/-}$ 7-week-old thymuses. Scale bar, 75 μm.

(F) Cumulative analysis of subset distribution of thymic lymphocytes of the indicated genotype, stained with anti-CD4-FITC and anti-CD8-PECy5 antibodies. Data represent mean ± SE of eight 7- to 9-week-old littermates.

(G) Numbers of DN and DP thymic lymphocytes (±SE) from eight different wt and *Parl* $^{-/-}$ littermates.

(H) Decreased viability of DP (gray bars) and cultured (hatched bars) *Parl* $^{-/-}$ thymic lymphocytes. Viability of DP was calculated as the percentage of annexin-V-Alexa 568-negative events in gated CD4-FITC, CD8-PECy5-positive thymic lymphocytes of the indicated genotype. Data represent mean ± SE of five wt and *Parl* $^{-/-}$ littermates.

(I) Images of spleens dissected from 8-week-old wt and *Parl* $^{-/-}$ littermates. Scale bar, 1 mm.

(J) TUNEL staining of wt and *Parl* $^{-/-}$ 7-week-old spleens. Scale bar, 75 μm.

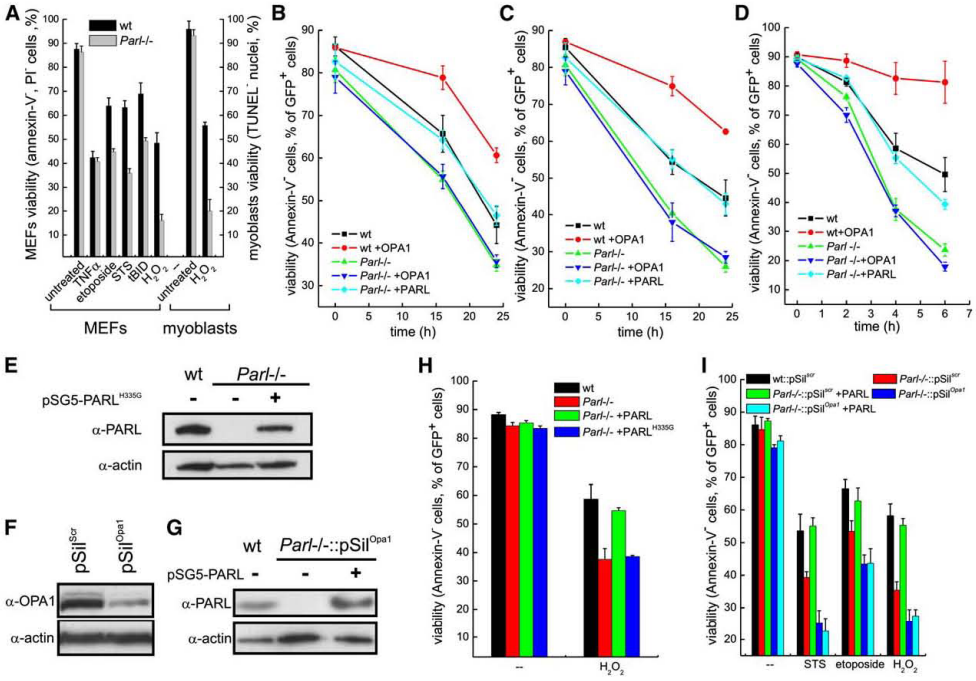

Figure 3. PARL Controls Apoptosis Induced by Intrinsic Stimuli and Is Required for Antiapoptotic Activity of OPA1

(A) MEFs (bars on the left) or primary myoblasts (bars on the right) of the indicated genotype were treated with TNF-α, etoposide, staurosporine, H_2O_2, or transfected with tBID-GFP. Viability was determined as the percentage of annexin-V-Fluos, PI-negative cells by flow cytometry, as the percentage of GFP-positive, annexin-V-Alexa 568-negative cells in the case of tBID, or as the number of TUNEL-negative nuclei by imaging in the case of myoblasts. Data represent mean ± SE of five independent experiments.

(B–D) MEFs of the indicated genotype transfected as indicated were treated with etoposide (B), staurosporine (C), or H_2O_2 (D). At the indicated times, viability was determined cytofluorimetrically as the percentage of GFP-positive, annexin-V-Alexa568-negative cells.

(E) MEFs were transfected as indicated and lysed after 24 hr. Protein (50 μg) was analyzed by SDS-PAGE/immunoblotting.

(F) *Parl*$^{-/-}$ MEFs stably expressing the indicated shRNA-generating pSilencer (pSil) plasmids (scr: scrambled) were lysed, and 40 μg of protein were analyzed by SDS-PAGE/immunoblotting.

(G) MEFs were transfected as indicated and lysed after 24 hr. Protein (40 μg) was analyzed by SDS-PAGE/immunoblotting.

(H) MEFs cotransfected with GFP and the indicated plasmids were treated after 24 hr with 1 mM H_2O_2, and viability was measured after further 4 hr as the percentage of GFP-positive, annexin-V-Alexa 568-negative cells. Data represent mean ± SE of five independent experiments.

(I) Cells of the indicated genotype were treated with H_2O_2, etoposide, or staurosporine, and viability was determined as the percentage of GFP-positive, annexin-V-Alexa 568-negative cells. Data represent mean ± SE of five independent experiments.

the differential ability of ascorbate and N,N,N',N'-tetramethyl-p-phenylenediamine (TMPD) to reduce free (intramembrane space located) and membrane-bound (cristae located) cytochrome c, respectively. The ratio of ascorbate-driven over TMPD-driven respiration increases when cytochrome c is mobilized from its binding sites on

(K) Cumulative analysis of subset distribution of splenic lymphocytes stained with CD4-FITC, CD8-PECy5, and B220-PE antibodies. Data represent mean ± SE of eight 7-week-old littermates.

(L) Absolute values of $B220^+$ splenic lymphocytes ±SE from eight different wt and *Parl*$^{-/-}$ littermates.

(M) Decreased viability of B lymphocytes in *Parl*$^{-/-}$ spleens. Viability was calculated as the percentage of annexin-V-Fluos-negative cells in gated $B220^+$ splenic lymphocytes. Data represent mean ± SE of five wt and *Parl*$^{-/-}$ littermates.

(N) Fluoro-Jade staining of *Capsula interna* from wt (+/+) and *Parl*$^{-/-}$ (−/−) 8-week-old littermates. Arrows indicate degenerating neurons. Scale bars, 100 μm.

(O) Hematoxylin staining of abdominal wall muscles of 8-week-old wt (+/+) and *Parl*$^{-/-}$ (−/−) littermates. Scale bars, 120 μm.

(P) Quantitative analysis of oxygen consumption in mitochondria isolated from limb muscles of 8-week-old littermates of the indicated genotype. Mitochondria were incubated with glutamate/malate (G/M), pyruvate/malate (P/M), α-ketoglutarate/malate (α-KG/M), α-glycerophosphate (α-GP), or succinate (S) into an oxygen electrode chamber. Data represent average ± SE of five independent experiments.

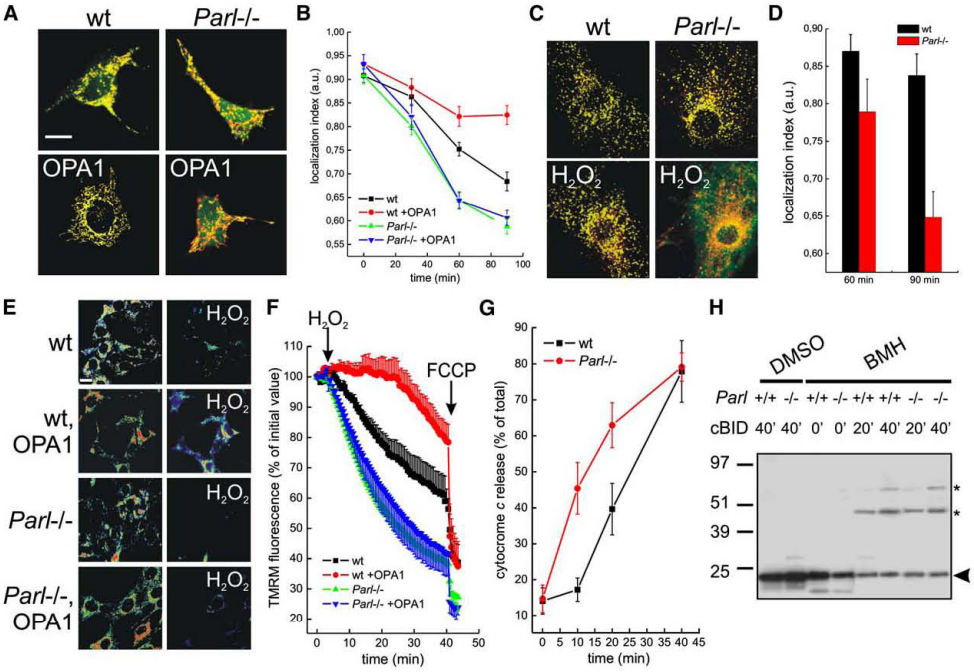

Figure 4. PARL Regulates the Mitochondrial Pathway of Apoptosis by Controlling OPA1-Dependent Mobilization of Cytochrome c

(A) Representative confocal images of wt and *Parl* $^{-/-}$ MEFs cotransfected with mtRFP (red) and empty vector or OPA1. Cells were treated for 90 min with 1 mM H_2O_2, fixed, and immunostained with a FITC-conjugated anti-cytochrome c antibody (green).

(B) Experiments as in (A), except that cells were fixed at the indicated times. Localization index was calculated from 30 randomly selected images. Data represent mean ± SE of five independent experiments.

(C) Representative confocal images of wt and *Parl* $^{-/-}$ primary myoblasts immunostained with anti-cytochrome c (green) and anti-TOM20 (red) antibodies. When indicated, cells were treated for 90 min with 1 mM H_2O_2.

(D) Localization index for cytochrome c in myoblasts. Experiments were performed as in (B). Data represent mean ± SE of three independent experiments.

(E) Representative pseudocolor-coded images of TMRM fluorescence in wt and *Parl* $^{-/-}$ MEFs transfected with GFP and empty vector or OPA1. Cells were loaded with 20 nM TMRM and real-time imaging sequences were acquired. Initial (left) and t = 35 min (right) frames are shown. Scale bar, 20 μm.

(F) Quantitative analysis of TMRM fluorescence changes over mitochondrial regions in transfected cells identified from their GFP fluorescence. Data represent mean ± SE of six independent experiments performed as in (E). Where indicated (arrows), 1 mM H_2O_2 and 2 μM FCCP were added.

(G) Liver mitochondria were treated with cBID and the amount of cytochrome c in the supernatant and in the pellet was determined by ELISA. Data represent the average ± SE of three independent experiments.

(H) Liver mitochondria were treated with cBID. DMSO or 10 mM BMH was added at the indicated time (Wei et al., 2000). Mitochondrial proteins (40 μg) were analyzed by SDS-PAGE/immunoblotting using anti-BAK antibody. Arrowhead, BAK; asterisks, BAK multimers.

cristae membranes (Scorrano et al., 2002). We also measured cytochrome b_5-mediated NADH oxidation, which is rate limited by free cytochrome c in the intermembrane space (IMS) (Bernardi and Azzone, 1981; Scorrano et al., 2002). Both assays showed that cytochrome c redistributed faster into the IMS in *Parl* $^{-/-}$ compared to wt mitochondria in response to cBID (Figures 5A–5C). Electron microscopy and morphometric analysis showed that remodeled class II morphology, which accounts for mobilized cytochrome c (Scorrano et al., 2002), appeared earlier in *Parl* $^{-/-}$ mitochondria following cBID (Figure 5D,E). Thus, PARL participates in the mechanism keeping in check cristae and cytochrome c redistribution during apoptosis.

Parl Is Dispensable for Mitochondrial Fusion

The yeast ortholog of *Parl*, *RBD1*, is required for maintenance of mitochondrial morphology, which in turn influences mitochondrial participation to apoptosis (Youle and Karbowski, 2005). Rbd1p cleaves Mgm1p, and expression of an Rbd1p-cleaved Mgm1p isoform in Δ*rbd1* cells partially complements mitochondrial shape defects (McQuibban et al., 2003). The mammalian ortholog of

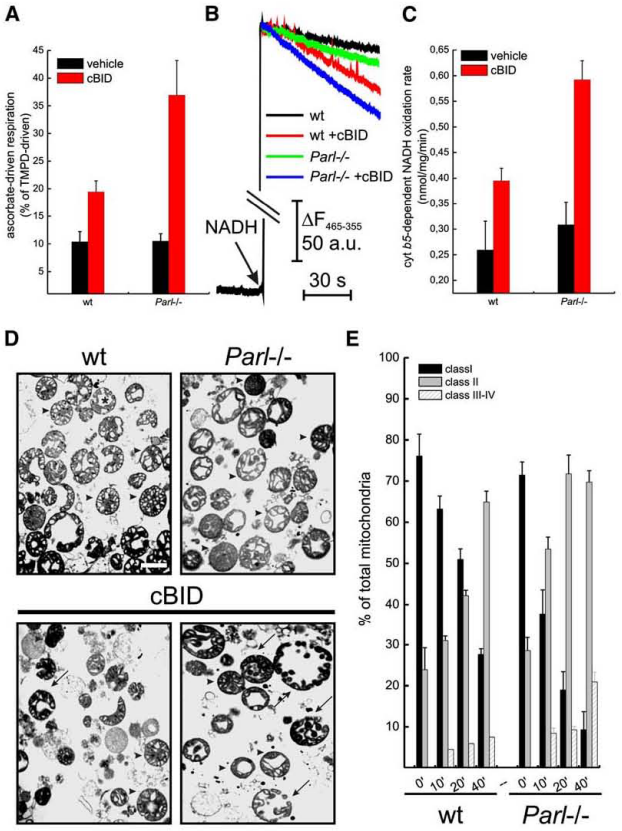

Figure 5. Kinetics of Cytochrome c Mobilization and Cristae Remodeling in Mitochondria Lacking PARL

(A) Liver mitochondria were treated with cBID or with vehicle, transferred into an oxygen electrode chamber, and ascorbate/TMPD respiratory ratio was determined. Data represent average ± SE of five independent experiments.

(B) Representative traces of NADH fluorescence changes caused by cytochrome b_5-dependent NADH oxidation. Liver mitochondria were incubated with cBID or with vehicle. Where indicated (arrow), 20 nmol NADH × mg protein $^{-1}$ were added.

(C) Experiment was performed as in (B). Data represent average ± SE of five independent experiments.

(D) Representative electron micrographs of wt and *Parl* $^{-/-}$ mitochondria. Mitochondria from livers were treated for the indicated time with cBID, fixed, and TEM images of randomly selected fields were acquired. Arrowheads denote class I (normal) mitochondria, arrows class II (remodelled) mitochondria. Scale bar, 500 nm.

(E) Morphometric analysis of wt and *Parl* $^{-/-}$ mitochondria treated with cBID for the indicated times. Experiments were performed as in (A). Data represent average ± SE of three independent experiments.

Mgm1p is OPA1, which requires MFN1 to promote fusion of mitochondria (Cipolat et al., 2004).

We decided therefore to investigate whether PARL, like its yeast homolog Rbd1p, controlled OPA1-dependent mitochondrial dynamics. Mitochondria of *Parl* $^{-/-}$ MEFs transfected with a mitochondrially targeted yellow fluorescent protein (mtYFP) appeared globular or rod-shaped, their elongation being visually (Figure 6A) and quantitatively (Figure 6B) undistinguishable from that of wt cells. Fusion rates of mitochondria were identical in wt and *Parl* $^{-/-}$ MEFs (Figures 6C and 6D). Mitochondrial morphology was similar in wt and *Parl* $^{-/-}$ primary myoblasts as well (Figure 6E). Levels of OPA1 were not changed in *Parl* $^{-/-}$ MEFs (Figure S2A), and its expression (Figure S2A) caused mitochondrial elongation (Figures 6A and 6B) comparable to that observed in wt cells (Cipolat et al., 2004). Thus, *Parl* is not required for the pro-fusion effect of OPA1. MFN1 and MFN2 also promoted equal mitochondrial elongation in wt and *Parl* $^{-/-}$ cells (Figures 6A and 6B), and expression of PARL had no effect on mitochondrial shape (Figures 6A and 6B) or fusion (data not shown) in wt MEFs. In total, these data indicate that *Parl* is not required for maintenance of mitochondrial shape and/or fusion, even in tissues severely affected by *Parl* ablation, like muscle, and that *Parl* is dispensable for regulation of mitochondrial dynamics by OPA1.

Parl and OPA1 Act in the Same Antiapoptotic Pathway

OPA1 regulates mitochondrial shape, but is also an antiapoptotic protein (Lee et al., 2004). We considered the possibility that both functions could be (partially) independent from each other and investigated whether *Parl* was required for the antiapoptotic function of OPA1. OPA1 protected wt but not *Parl* $^{-/-}$ MEFs from death by etoposide, staurosporine, and H_2O_2 (Figures 3B–3D). Furthermore, expression of OPA1 in *Parl* $^{-/-}$ MEFs did not reduce cytochrome c release (Figures 4A and 4B) or mitochondrial depolarization (Figures 4E and 4F) following intrinsic stimuli. Thus, in the absence of *Parl*, OPA1 is unable to

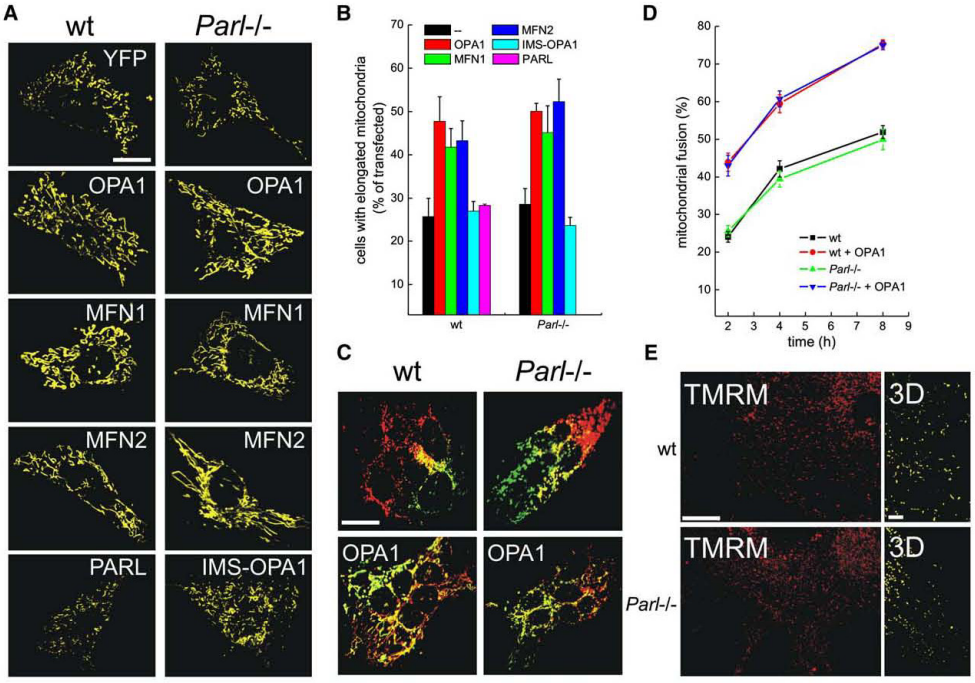

Figure 6. PARL Is Not Required for Mitochondrial Fusion

(A) MEFs were cotransfected with mtYFP and empty vector or the indicated plasmid. Confocal images of mtYFP fluorescence from randomly selected cells. Scale bar, 10 μm.

(B) Morphometric analysis of mitochondrial shape. Experiments were as in (A). Fifty randomly selected images of mtYFP fluorescence were acquired, stored, and classified as described. Data represent mean ± SE of five independent experiments.

(C) MEFs transfected with mtRFP and mtGFP or cotransfected with OPA1 were fused with PEG1500 and fixed after 4 hr. Scale bar, 20 μm.

(D) Time course of mitochondrial fusion in wt and *Parl*$^{-/-}$ MEFs. Experiments were performed as in (C), except that cells were fixed at the indicated times. Mitochondrial fusion was measured from 30 randomly selected polykaryons. Data represent mean ± SE of three independent experiments.

(E) Mitochondrial morphology in myoblasts isolated from diaphragm of wt and *Parl*$^{-/-}$ 7-week-old littermates. Myoblasts were loaded with 10 nM TMRM. Randomly selected confocal, 20 μm deep z axis stacks of TMRM fluorescence were acquired, stored, reconstructed, and volume rendered. Images on the left side are middle sections of the z-stacks, on the right, magnified (3×) volume-rendered 3D reconstructions of the stacks. Scale bars, 10 μm on the left, 3 μm on the right.

block apoptosis, placing PARL and OPA1 in the same genetic pathway. We next ablated OPA1 using short hairpin RNA interference (shRNAi) in wt and *Parl*$^{-/-}$ MEFs (Figure 3F). This rendered both cell types more susceptible to apoptosis (Figure 3I and Lee et al., 2004). Reintroduction of PARL in *Parl*$^{-/-}$ MEFs in which OPA1 was silenced (Figure 3G) did not rescue from enhanced apoptosis (Figure 3I). Thus, PARL is genetically positioned upstream of OPA1 in this pathway of death.

PARL Is Involved in the Production of Soluble, Antiapoptotic OPA1

PARL is apparently upstream of OPA1 in a pathway regulating cytochrome c release during apoptosis. Further experiments suggested that PARL and OPA1 interacted at the protein level as well. Subfractionation of mitochondria showed that both PARL and OPA1 were localized in the inner mitochondrial membrane (Figure 7A) and anti-PARL antibody specifically coimmunoprecipitated OPA1 in wt but not *Parl*$^{-/-}$ MEFs (Figure 7B). Finally, OPA1 interacted with PARL in a yeast two-hybrid interaction experiment (Table S1). As the proteins interact and the catalytic site of PARL is required to regulate cytochrome c release (Figure 3H), we investigated whether OPA1 could be a substrate of PARL. OPA1 is synthesized as an integral IM protein from one single gene. Alternative splicing generates at least eight different transcripts, all of them containing the transmembrane domain (Delettre et al., 2001). This complicated considerably the identification of potential processed OPA1 forms in immunoblots of mitochondrial

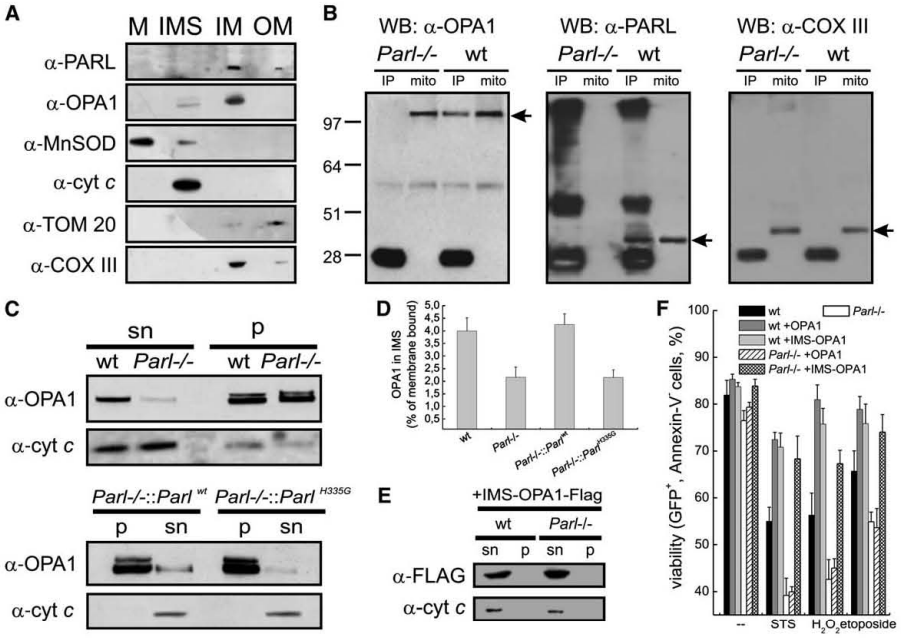

Figure 7. PARL Interacts with OPA1 and Participates in the Production of an Intermembrane Space Form Required to Protect from Apoptosis

(A) Mouse liver mitochondria were subfractionated, and 50 μg of matrix (M), intermembrane space (IMS), inner membrane (IM) and outer membrane (OM) proteins were separated by SDS-PAGE and immunoblotted with the indicated antibodies.

(B) Western blots (WB) using OPA1, PARL, and COXIII antibodies as indicated of mitochondrial proteins immunoprecipitated with PARL antibodies (IP) or present in total mitochondrial lysate (mito). Arrows indicate OPA1, PARL, and COX III, respectively.

(C) Pellet (p, 10 μg) and supernatant (sn, 100 μg) of hypotonically swollen, KCl-washed mitochondria isolated from MEFs of the indicated genotypes to release IMS proteins were analyzed by SDS-PAGE/immunoblotting using anti-OPA1 and anti-cytochrome c (cyt c) antibodies.

(D) Densitometric analysis of IMS OPA1. Experiments were as in (C). Data represent average ± SE of eight independent experiments.

(E) Cells were transfected with IMS-OPA1-FLAG, and the IMS and membrane fractions from isolated mitochondria were separated as in (D) and analyzed by SDS-PAGE/immunoblotting.

(F) MEFs cotransfected with GFP and empty vectors or with the indicated plasmids were treated with staurosporine, H_2O_2, and etoposide. Viability was determined cytofluorimetrically as the percentage of GFP-positive, annexin-V-Alexa 568-negative cells. Data represent mean ± SE of five independent experiments.

fractions isolated from different tissues (data not shown). In order to enrich for potential cleaved, soluble OPA1 forms, we generated membrane (pellet) and IMS (supernatant) fractions from mitochondria by hypotonic swelling and salt washes, a treatment that dissociates weakly bound proteins from the IM (Jacobs and Sanadi, 1960). An OPA1 form characterized by lower MW was found in the IMS (Figures 7A and 7C), and levels of this IMS OPA1 were reduced in *Parl* $^{-/-}$ mitochondria (Figure 7C and densitometry in 7D). Accordingly, stable reintroduction in *Parl* $^{-/-}$ MEFs of wt but not the catalytic dyad mutant H335G PARL restored levels of IMS OPA1 (Figure 7C and densitometry in 7D). This was not due to differences in expression of these reintroduced PARLs (Figure S2B), suggesting that the catalytic activity of PARL is involved in the generation of this soluble IMS form, although we cannot exclude at this point that the action of PARL on OPA1 could be indirect. Some OPA1 remained detectable in the IMS of *Parl* $^{-/-}$ mitochondria, suggesting the existence of at least one additional protease that cleaves OPA1.

The reduced levels of IMS OPA1 could explain increased susceptibility of *Parl* $^{-/-}$ cells to apoptosis. A FLAG-tagged OPA1 in which residues 1–229 were replaced with the IMS targeting signal of AIF (IMS-OPA1) (Otera et al., 2005) was targeted to the IMS (Figure 7E). IMS-OPA1 protected wt but notably also *Parl* $^{-/-}$ MEFs from apoptosis induced by all intrinsic stimuli tested (Figure 7F), substantiating a pivotal role for IMS-OPA1 in the regulation of cell death. IMS-OPA1 did not induce mitochondrial elongation (Figures 6A and 6B), dissociating even further the profusion effect from the antiapoptotic function of OPA1.

DISCUSSION

We demonstrate here that PARL is an antiapoptotic protein. Ablation of this gene causes faster release of the cytochrome c pool from the mitochondrial cristae. This function critically depends on a genetic interaction with OPA1 and involves the generation of a soluble, IMS-located form of OPA1. As demonstrated in the accompanying manuscript (Frezza et al., 2006), membrane bound and soluble IMS OPA1 participate in the formation of oligomers, and their disruption correlates with the tightness of the cristae junctions and cytochrome c release. The reduced levels of IMS-OPA1 in the *Parl* $^{-/-}$ cells could therefore represent a mechanistic explanation for the increased apoptosis observed in the *Parl* $^{-/-}$ mice.

Parl Deficiency Causes Increased Apoptosis, Resulting in Generalized Wasting and Premature Death

PARL was initially identified in a two-hybrid screen using the carboxy-terminal part of presenilin as bait (Pellegrini et al., 2001). We anticipated therefore that *Parl* ablation would cause embryonic phenotypes overlapping with those observed in presenilin-deficient animals (Marjaux et al., 2004). However, the phenotype of *Parl* $^{-/-}$ mice is completely different, being characterized by progressive cachexia from the fourth week on, eventually leading to death. In addition, APP is normally processed in *Parl* $^{-/-}$ mice (data not shown). It is reasonable to conclude that presenilin binds PARL only in vitro.

We next turned to rbd1p, the PARL ortholog in *S. cerevisiae*. Rbd1p deficiency causes mitochondrial fission, respiratory dysfunction, and growth arrest (Esser et al., 2002; Herlan et al., 2003; McQuibban et al., 2003; Sesaki et al., 2003). However, *Parl* $^{-/-}$ mitochondria from multiple tissues did not display overt or latent respiratory dysfunction in vitro or in situ or changes in mitochondrial morphology. Thus, the function of Rbdp1p in yeast seems not to be conserved in PARL in mice, an evolutionary divergence seen also with other rhomboids (Freeman, 2004).

Parl $^{-/-}$ mice shared several phenotypical characteristics with *Bcl-2* $^{-/-}$ mice, including early postnatal mortality with muscular atrophy and massive apoptotic involution of thymus and spleen (Veis et al., 1993). Muscle wasting is also compatible with increased apoptosis (Kujoth et al., 2005). *Parl* $^{-/-}$ primary myoblasts indeed displayed higher sensitivity to intrinsic stimuli of apoptosis, which together with analysis of other tissues and cells, further substantiates a role for PARL in the control of cell death.

PARL Is Epistatic to OPA1 in Controlling Cytochrome c Mobilization from Cristae during Apoptosis

Rbd1p interacts with Mgm1p in yeast to regulate mitochondrial fusion. We therefore evaluated whether PARL interacts with OPA1, the mammalian ortholog of Mgm1p. OPA1 has pro-fusion ability, which depends on MFN1 (Cipolat et al., 2004), and antiapoptotic activity, which could be dependent or separated from its fusion ability (Lee et al., 2004). PARL deficiency did not affect fusion by OPA1 or MFN1, but was clearly involved in the antiapoptotic function of OPA1. Furthermore, when *Opa1* was silenced by siRNA in *Parl* $^{-/-}$ cells, they were no longer rescued by reexpression of PARL, demonstrating that PARL is genetically positioned upstream of OPA1. Yeast two-hybrid and coimmunoprecipitation assays indicated a direct protein-protein interaction between PARL and OPA1. In the accompanying paper, we demonstrate that disruption of OPA1-containing oligomers correlates with mitochondrial cristae remodeling and completion of cytochrome c release (Frezza et al., 2006). Accordingly, we observed in *Parl* $^{-/-}$ fibroblasts and myoblasts, as well as in purified *Parl* $^{-/-}$ liver mitochondria, enhanced mitochondrial remodeling and mobilization of cristae stores of cytochrome c, corroborating the conclusion that PARL and OPA1 are part of the same molecular pathway of death.

PARL Participates in the Generation of Soluble IMS OPA1

Rbd1p regulates mitochondrial shape by proteolytic processing of Mgm1p, and PARL can rescue Rbd1p proteolytic processing of Mgm1p in yeast (McQuibban et al., 2003), indicating that PARL proteolytic activity, as opposed to its function in mitochondrial morphology, is maintained in evolution. However, multiple splice variants of OPA1 complicate the comparison of its electrophoretic migration pattern in mammalian wt and *Parl* $^{-/-}$ tissues. We therefore focused on the hypothesis that PARL could be involved in the generation of an IMS, soluble form of OPA1. We found indeed a small (~4%) fraction of IMS-OPA1 that decreased strongly in *Parl* $^{-/-}$ mitochondria. Expression of a version of OPA1 targeted to the IMS (Otera et al., 2005) protected *Parl* $^{-/-}$ fibroblasts from apoptosis like wt OPA1 did in wt cells. Finally, PARL^{H335G}, mutated in its catalytic dyad (Lemberg et al., 2005), did not rescue production of IMS OPA1 in *Parl* $^{-/-}$ mitochondria and also failed to rescue the apoptotic phenotype of *Parl* $^{-/-}$ cells, suggesting that OPA1 could indeed be a substrate for PARL. Obviously, we cannot exclude that PARL could act indirectly via activation of another, unknown protease (Arnoult et al., 2005) or that OPA1 is processed independently by multiple proteases. These possibilities are supported by the retrieval of traces of IMS-OPA1 in *Parl* $^{-/-}$ MEFs. Our overall analysis strongly supports, however, our conclusion that PARL has a crucial role in proteolytic processing of OPA1.

IMS and integral IM OPA1 both participate in oligomers that are disrupted during cristae remodeling and release of cytochrome c. These oligomers are greatly reduced in *Parl* $^{-/-}$ mitochondria (Frezza et al., 2006). We therefore suggest that the reduced OPA1 processing in *Parl* $^{-/-}$ tissues can account for the faster cristae remodeling and cytochrome c mobilization and ultimately for the increased apoptosis observed in the *Parl*-deficient mice.

It remains unclear why only a small fraction of OPA1 becomes cleaved by PARL (or by a yet unknown protease).

In other examples of intramembrane proteolysis, like Notch signaling (Mumm et al., 2000), the substrate is cleaved after a conformational switch induced by binding to a ligand and/or cleavage by a second protease. Alternatively, cleavage of OPA1 could be regulated by compartmentalization, a case exemplified by the couple Spitz/Rhomboid-1. Before cleavage, Spitz is kept at the endoplasmic reticulum, while Rhomboid-1 resides in Golgi. Since PARL and OPA1 are both located in the inner membrane, one has to speculate that the two proteins are sequestered in different domains and that only a small fraction of total OPA1 becomes available for cleavage, a possibility supported by the high level of compartmentalization of the IM (Perotti et al., 1983).

Intramembrane Proteolysis Involved in the Regulation of Apoptosis

In the last few years, several intramembrane cleaving proteases have been identified, overturning the dogma that proteolysis (a hydrolyzing reaction) occurs only in aqueous environments (Annaert and De Strooper, 2002; Brown et al., 2000; Freeman, 2004; Kopan and Ilagan, 2004). Intramembrane proteolysis often generates an active soluble protein fragment that translocates to the nucleus to activate gene transcription or acts as a soluble ligand in a paracrine way. In *Drosophila*, rhomboids are important regulators of the EGFR pathway (Freeman, 2004). In bacteria and parasites, rhomboids are involved in quorum sensing (Gallio et al., 2002) and in invasion of host cells (Brossier et al., 2005). In all eukaryotes, a mitochondrial rhomboid is present, which in yeast is involved in the regulation of mitochondrial fusion and respiration. Little is known about the function of rhomboids in mammals, but the analysis of the *Parl*-deficient mouse now implicates the mitochondrial rhomboid in the regulation of apoptosis. The fact that *Parl* deficiency affects mice only in their early adult life suggests that this rhomboid protease could become an important drug target to modulate apoptosis in diseases of adult life, like cancer and neurodegenerative disorders.

EXPERIMENTAL PROCEDURES

Generation of *Parl*-Deficient Mice

The hygromycin B resistance gene flanked with two FRT sequences and one loxP sequence was inserted into intron 2 of a 9.5 kb BglII DNA restriction fragment of *Parl* covering the ATG start codon, exons 2 and 3, and a part of intron 4. A second loxP sequence was inserted into the SmaI site in intron 3 (Figure 1A). Hygromycin B-resistant E14 ES colonies were screened by Southern blot analysis (Figure 1B). Two mutated ES cell lines were microinjected into blastocysts of C57Bl/6J mice. Animals carrying a null allele were obtained after breeding with transgenic females expressing a PGK-driven Cre-recombinase.

Antibodies

A Parl carboxy-terminal antibody was generated by immunizing rabbits with a synthetic peptide (HEIRTNGPKKGGGSK) coupled to keyhole limpet haemocyanin (KLH). Other antibodies used are described in the Supplemental Data.

Analysis of Cell Death

Thymic lymphocytes were stained with CD4-FITC, CD8-PECy5, and annexin-V-Alexa 568. Splenic lymphocytes were stained with B220-PE and annexin-V-Fluos (Roche). Viability was determined by the percentage of annexin-V-negative events in the gated CD4, CD8-positive or B220-positive population. 1×10^5 MEFs were treated with TNF-α (100 IU and 0.5 μg/mL actinomycin, 6 hr), etoposide (5 μM, 16 hr), staurosporine (1 μM, 16 hr), H_2O_2 (1 mM, 4 hr), or transfected with tBID-GFP (48 hr) and stained with propidium iodide (PI) and annexin-V-FLUOS. Viability was measured by flow cytometry as the percentage annexin-V, PI-negative cells or as the percentage of annexin-V-negative events in the GFP cotransfected positive population. TUNEL staining of myoblasts was performed using the Apop-Tag kit (Roche).

Mitochondrial Assays

MEFs, liver, and muscle mitochondria were isolated by differential centrifugation. Details can be found in the Supplemental Data.

Mitochondrial oxygen consumption in the presence of 5 mM glutamate/2.5 mM malate or 2.5 mM pyruvate/1 mM malate or α-ketoglutarate 15 mM/1 mM malate for the analysis of complex I-driven respiration; 5 mM succinate or 5 mM α-glycerophosphate in the presence of 2 μM rotenone for complex II-driven respiration; or 3 mM ascorbate plus 150 μM TMPD in the presence of 0.5 μg/ml antimycin A for complex IV-driven respiration was measured with a Clarke-type oxygen electrode (Hansatech).

Cytochrome c redistribution and release in response to recombinant cBID was determined as described (Scorrano et al., 2002). Unless specified, cBID was used at a concentration of 32 pmol × mg^{-1} of mitochondria.

PEG fusion assays were performed as described in Cipolat et al. (2004).

For protein cross-linking, mitochondria were treated with 10 mM BMH (Pierce) for 30 min, dissolved in gel loading buffer, and proteins were analyzed by SDS-PAGE.

Imaging

Transfected cells were analyzed with a Nikon Eclipse TE300 inverted microscope equipped with a Perkin Elmer Ultraview LCI, a piezoelectric z axis motorized stage (Pifoc), and an Orca ER 12-bit CCD camera (Hamamatsu). Morphometric analysis was performed as described in Cipolat et al. (2004). Stacks of 20 images separated by 1 μm along the z axis were acquired. 3D reconstruction and volume rendering were performed using a plug-in of ImageJ (NIH). For imaging of polykarions and of cytochrome c release, a Nikon Eclipse E600FN upright microscope equipped with a Biorad Radiance 2100 CLS was used. Colocalization index was calculated as described (Frezza et al., 2006). Details on objectives and excitation/emission wavelengths can be found in the Supplemental Data.

Electron Microscopy

Fixation, embedding, TEM, and morphometric analysis of isolated mitochondria was performed by the Telethon EM Core Facility (TEEMCoF) as described (Scorrano et al., 2002).

Submitochondrial Fractionation and Immunoblotting

For detection of IMS proteins, freeze-thawn mitochondria were hypotonically swollen in 10 mM Tris-Cl (pH 7.4), spun at 10,000 × g, and the pellet was further washed in 150 mM KCl, 10 mM Tris-Cl (pH 7.4). The supernatants were pooled, concentrated 10-fold using a Centricon-10 filter unit (Millipore), and constituted the IMS fraction. Proteins were dissolved in gel-loading buffer (NuPAGE, Invitrogen) and electrophoresed.

Submitochondrial fractionation was performed according to Sottocasa et al. (1967). Briefly, mitochondria (50 mg) were incubated in 10 mM KH_2PO_4. After centrifugation, the pellet was resuspended in 125 mM KCl, 10 mM Tris-MOPS (pH 7.4), and centrifuged again. The combined supernatants constituted the IMS fraction. The pellet was

then resuspended in 10 mM KH_2PO_4, 1.8 M sucrose, 2 mM ATP, 2 mM $MgSO_4$, and centifuged over a 1.18 M sucrose cushion at 90,000 × g. The upper clear layer corresponded to the matrix (M) fraction, the yellow interphase to the OM, and the pellet to the IM.

For immunoprecipitation, 200 μg of mitochondria isolated from MEFs were dissolved in RIPA buffer. Anti-PARL immunocomplexes were adsorbed on 50 μl agarose beads conjugated with protein-G and boiled in loading buffer.

Supplemental Data

The Supplemental Data for this article can be found online at http://www.cell.com/cgi/content/full/126/1/163/DC1/.

ACKNOWLEDGMENTS

Research in BDS laboratory is supported by a Freedom to Discover grant from Bristol-Myers-Squibb; a Pioneer award from the Alzheimer's Association; the Fund for Scientific Research, Flanders; K.U. Leuven (GOA); European Union (APOPIS: LSHM-CT-2003-503330); and Federal Office for Scientific Affairs, Belgium (IUAP P5/19). L.S. is an Assistant Telethon Scientist of the Dulbecco-Telethon Institute. This research was supported by Telethon Italy; AIRC Italy; Compagnia di San Paolo; Human Frontier Science Program Organization. We thank Dr. Katsuyoshi Mihara (Kyushu University, Fukuoka, Japan) for the kind gift of the p3xFLAG-CMV14-AIF-Opa1 (IMS-OPA1-FLAG) plasmid.

Received: June 30, 2005
Revised: March 8, 2006
Accepted: June 8, 2006
Published: July 13, 2006

REFERENCES

Alexander, C., Votruba, M., Pesch, U.E., Thiselton, D.L., Mayer, S., Moore, A., Rodriguez, M., Kellner, U., Leo-Kottler, B., Auburger, G., et al. (2000). OPA1, encoding a dynamin-related GTPase, is mutated in autosomal dominant optic atrophy linked to chromosome 3q28. Nat. Genet. *26*, 211–215.

Annaert, W., and De Strooper, B. (2002). A cell biological perspective on Alzheimer's disease. Annu. Rev. Cell Dev. Biol. *18*, 25–51.

Arnoult, D., Grodet, A., Lee, Y.J., Estaquier, J., and Blackstone, C. (2005). Release of OPA1 during apoptosis participates in the rapid and complete release of cytochrome c and subsequent mitochondrial fragmentation. J. Biol. Chem. *280*, 35742–35750.

Bernardi, P., and Azzone, G.F. (1981). Cytochrome c as an electron shuttle between the outer and inner mitochondrial membranes. J. Biol. Chem. *256*, 7187–7192.

Brossier, F., Jewett, T.J., Sibley, L.D., and Urban, S. (2005). A spatially localized rhomboid protease cleaves cell surface adhesins essential for invasion by Toxoplasma. Proc. Natl. Acad. Sci. USA *102*, 4146–4151.

Brown, M.S., Ye, J., Rawson, R.B., and Goldstein, J.L. (2000). Regulated intramembrane proteolysis: a control mechanism conserved from bacteria to humans. Cell *100*, 391–398.

Cipolat, S., Martins de Brito, O., Dal Zilio, B., and Scorrano, L. (2004). OPA1 requires mitofusin 1 to promote mitochondrial fusion. Proc. Natl. Acad. Sci. USA *101*, 15927–15932.

Danial, N.N., Gramm, C.F., Scorrano, L., Zhang, C.Y., Krauss, S., Ranger, A.M., Datta, S.R., Greenberg, M.E., Licklider, L.J., Lowell, B.B., et al. (2003). BAD and glucokinase reside in a mitochondrial complex that integrates glycolysis and apoptosis. Nature *424*, 952–956.

Delettre, C., Lenaers, G., Griffoin, J.M., Gigarel, N., Lorenzo, C., Belenguer, P., Pelloquin, L., Grosgeorge, J., Turc-Carel, C., Perret, E., et al. (2000). Nuclear gene OPA1, encoding a mitochondrial dynamin-related protein, is mutated in dominant optic atrophy. Nat. Genet. *26*, 207–210.

Delettre, C., Griffoin, J.M., Kaplan, J., Dollfus, H., Lorenz, B., Faivre, L., Lenaers, G., Belenguer, P., and Hamel, C.P. (2001). Mutation spectrum and splicing variants in the OPA1 gene. Hum. Genet. *109*, 584–591.

Esser, K., Tursun, B., Ingenhoven, M., Michaelis, G., and Pratje, E. (2002). A novel two-step mechanism for removal of a mitochondrial signal sequence involves the mAAA complex and the putative rhomboid protease Pcp1. J. Mol. Biol. *323*, 835–843.

Freeman, M. (2004). Proteolysis within the membrane: rhomboids revealed. Nat. Rev. Mol. Cell Biol. *5*, 188–197.

Frezza, C., Cipolat, S., de Brito, O.M., Micaroni, M., Beznoussenko, G.V., Rudka, T., Bartoli, D., Polishchuk, R.S., Danial, N.N., De Strooper, B., and Scorrano, L. (2006). OPA1 controls apoptotic cristae remodeling independently from mitochondrial fusion. Cell *126*, this issue, 177–189.

Gallio, M., Sturgill, G., Rather, P., and Kylsten, P. (2002). A conserved mechanism for extracellular signaling in eukaryotes and prokaryotes. Proc. Natl. Acad. Sci. USA *99*, 12208–12213.

Green, D.R., and Kroemer, G. (2004). The pathophysiology of mitochondrial cell death. Science *305*, 626–629.

Hao, Z., Duncan, G.S., Chang, C.C., Elia, A., Fang, M., Wakeham, A., Okada, H., Calzascia, T., Jang, Y., You-Ten, A., et al. (2005). Specific ablation of the apoptotic functions of cytochrome C reveals a differential requirement for cytochrome C and Apaf-1 in apoptosis. Cell *121*, 579–591.

Herlan, M., Vogel, F., Bornhovd, C., Neupert, W., and Reichert, A.S. (2003). Processing of Mgm1 by the rhomboid-type protease Pcp1 is required for maintenance of mitochondrial morphology and of mitochondrial DNA. J. Biol. Chem. *278*, 27781–27788.

Irwin, W.A., Bergamin, N., Sabatelli, P., Reggiani, C., Megighian, A., Merlini, L., Braghetta, P., Columbaro, M., Volpin, D., Bressan, G.M., et al. (2003). Mitochondrial dysfunction and apoptosis in myopathic mice with collagen VI deficiency. Nat. Genet. *35*, 367–371.

Jacobs, E.E., and Sanadi, D.R. (1960). The reversible removal of cytochrome c from mitochondria. J. Biol. Chem. *235*, 531–534.

James, D.I., Parone, P.A., Mattenberger, Y., and Martinou, J.C. (2003). hFis1, a novel component of the mammalian mitochondrial fission machinery. J. Biol. Chem. *278*, 36373–36379.

Koonin, E.V., Makarova, K.S., Rogozin, I.B., Davidovic, L., Letellier, M.C., and Pellegrini, L. (2003). The rhomboids: a nearly ubiquitous family of intramembrane serine proteases that probably evolved by multiple ancient horizontal gene transfers. Genome Biol. *4*, R19.

Kopan, R., and Ilagan, M.X. (2004). Gamma-secretase: proteasome of the membrane? Nat. Rev. Mol. Cell Biol. *5*, 499–504.

Kujoth, G.C., Hiona, A., Pugh, T.D., Someya, S., Panzer, K., Wohlgemuth, S.E., Hofer, T., Seo, A.Y., Sullivan, R., Jobling, W.A., et al. (2005). Mitochondrial DNA mutations, oxidative stress, and apoptosis in mammalian aging. Science *309*, 481–484.

Lee, Y.J., Jeong, S.Y., Karbowski, M., Smith, C.L., and Youle, R.J. (2004). Roles of the mammalian mitochondrial fission and fusion mediators Fis1, Drp1, and Opa1 in apoptosis. Mol. Biol. Cell *15*, 5001–5011.

Lemberg, M.K., Menendez, J., Misik, A., Garcia, M., Koth, C.M., and Freeman, M. (2005). Mechanism of intramembrane proteolysis investigated with purified rhomboid proteases. Embo J. *24*, 464–472.

Marjaux, E., Hartmann, D., and De Strooper, B. (2004). Presenilins in memory, Alzheimer's disease, and therapy. Neuron *42*, 189–192.

McQuibban, G.A., Saurya, S., and Freeman, M. (2003). Mitochondrial membrane remodelling regulated by a conserved rhomboid protease. Nature *423*, 537–541.

Mumm, J.S., Schroeter, E.H., Saxena, M.T., Griesemer, A., Tian, X., Pan, D.J., Ray, W.J., and Kopan, R. (2000). A ligand-induced

extracellular cleavage regulates gamma-secretase-like proteolytic activation of Notch1. Mol. Cell *5*, 197–206.

Olichon, A., Emorine, L.J., Descoins, E., Pelloquin, L., Brichese, L., Gas, N., Guillou, E., Delettre, C., Valette, A., Hamel, C.P., et al. (2002). The human dynamin-related protein OPA1 is anchored to the mitochondrial inner membrane facing the inter-membrane space. FEBS Lett. *523*, 171–176.

Otera, H., Ohsakaya, S., Nagaura, Z., Ishihara, N., and Mihara, K. (2005). Export of mitochondrial AIF in response to proapoptotic stimuli depends on processing at the intermembrane space. Embo J. *24*, 1375–1386.

Pellegrini, L., Passer, B.J., Canelles, M., Lefterov, I., Ganjei, J.K., Fowlkes, B.J., Koonin, E.V., and D'Adamio, L. (2001). PAMP and PARL, two novel putative metalloproteases interacting with the COOH-terminus of Presenilin-1 and -2. J. Alzheimers Dis. *3*, 181–190.

Perotti, M.E., Anderson, W.A., and Swift, H. (1983). Quantitative cytochemistry of the diaminobenzidine cytochrome oxidase reaction product in mitochondria of cardiac muscle and pancreas. J. Histochem. Cytochem. *31*, 351–365.

Rizzuto, R., Bernardi, P., and Pozzan, T. (2000). Mitochondria as all-round players of the calcium game. J. Physiol. *529*, 37–47.

Sandri, M., and Carraro, U. (1999). Apoptosis of skeletal muscles during development and disease. Int. J. Biochem. Cell Biol. *31*, 1373–1390.

Scaffidi, C., Fulda, S., Srinivasan, A., Friesen, C., Li, F., Tomaselli, K.J., Debatin, K.M., Krammer, P.H., and Peter, M.E. (1998). Two CD95 (APO-1/Fas) signaling pathways. EMBO J. *17*, 1675–1687.

Scorrano, L., Ashiya, M., Buttle, K., Weiler, S., Oakes, S.A., Mannella, C.A., and Korsmeyer, S.J. (2002). A distinct pathway remodels mitochondrial cristae and mobilizes cytochrome c during apoptosis. Dev. Cell *2*, 55–67.

Sik, A., Passer, B.J., Koonin, E.V., and Pellegrini, L. (2004). Self-regulated cleavage of the mitochondrial intramembrane-cleaving protease PARL yields Pbeta, a nuclear-targeted peptide. J. Biol. Chem. *279*, 15323–15329.

Sesaki, H., Southard, S.M., Hobbs, A.E., and Jensen, R.E. (2003). Cells lacking Pcp1p/Ugo2p, a rhomboid-like protease required for Mgm1p processing, lose mtDNA and mitochondrial structure in a Dnm1p-dependent manner, but remain competent for mitochondrial fusion. Biochem. Biophys. Res. Commun. *308*, 276–283.

Smirnova, E., Griparic, L., Shurland, D.L., and van der Bliek, A.M. (2001). Dynamin-related protein Drp1 is required for mitochondrial division in mammalian cells. Mol. Biol. Cell *12*, 2245–2256.

Sottocasa, G.L., Kuylenstierna, B., Ernster, L., and Bergstrand, A. (1967). An electron-transport system associated with the outer membrane of liver mitochondria. A biochemical and morphological study. J. Cell Biol. *32*, 415–438.

Veis, D.J., Sorenson, C.M., Shutter, J.R., and Korsmeyer, S.J. (1993). Bcl-2-deficient mice demonstrate fulminant lymphoid apoptosis, polycystic kidneys, and hypopigmented hair. Cell *75*, 229–240.

Wei, M.C., Lindsten, T., Mootha, V.K., Weiler, S., Gross, A., Ashiya, M., Thompson, C.B., and Korsmeyer, S.J. (2000). tBID, a membrane-targeted death ligand, oligomerizes BAK to release cytochrome c. Genes Dev. *14*, 2060–2071.

Wei, M.C., Zong, W.X., Cheng, E.H., Lindsten, T., Panoutsakopoulou, V., Ross, A.J., Roth, K.A., MacGregor, G.R., Thompson, C.B., and Korsmeyer, S.J. (2001). Proapoptotic BAX and BAK: a requisite gateway to mitochondrial dysfunction and death. Science *292*, 727–730.

Yoon, Y., Krueger, E.W., Oswald, B.J., and McNiven, M.A. (2003). The mitochondrial protein hFis1 regulates mitochondrial fission in mammalian cells through an interaction with the dynamin-like protein DLP1. Mol. Cell. Biol. *23*, 5409–5420.

Youle, R.J., and Karbowski, M. (2005). Mitochondrial fission in apoptosis. Nat. Rev. Mol. Cell Biol. *6*, 657–663.

Cell

OPA1 Controls Apoptotic Cristae Remodeling Independently from Mitochondrial Fusion

Christian Frezza,[1] Sara Cipolat,[1] Olga Martins de Brito,[1] Massimo Micaroni,[2] Galina V. Beznoussenko,[2] Tomasz Rudka,[3] Davide Bartoli,[1] Roman S. Polishuck,[2] Nika N. Danial,[4] Bart De Strooper,[3] and Luca Scorrano[1,*]
[1]Dulbecco-Telethon Institute, Venetian Institute of Molecular Medicine, Padova, Italy
[2]Department of Cell Biology and Oncology, Consorzio "Mario Negri Sud," Santa Maria Imbaro, Italy
[3]Neuronal Cell Biology and Gene Transfer Laboratory, Center for Human Genetics, Flanders Interuniversity Institute for Biotechnology (VIB4) and K.U. Leuven, Belgium
[4]Department of Cancer Biology, Dana-Farber Cancer Institute, Harvard Medical School, Boston, MA 02115, USA
*Contact: luca.scorrano@unipd.it
DOI 10.1016/j.cell.2006.06.025

SUMMARY

Mitochondria amplify activation of caspases during apoptosis by releasing cytochrome c and other cofactors. This is accompanied by fragmentation of the organelle and remodeling of the cristae. Here we provide evidence that Optic Atrophy 1 (OPA1), a profusion dynamin-related protein of the inner mitochondrial membrane mutated in dominant optic atrophy, protects from apoptosis by preventing cytochrome c release independently from mitochondrial fusion. OPA1 does not interfere with activation of the mitochondrial "gatekeepers" BAX and BAK, but it controls the shape of mitochondrial cristae, keeping their junctions tight during apoptosis. Tightness of cristae junctions correlates with oligomerization of two forms of OPA1, a soluble, intermembrane space and an integral inner membrane one. The proapoptotic BCL-2 family member BID, which widens cristae junctions, also disrupts OPA1 oligomers. Thus, OPA1 has genetically and molecularly distinct functions in mitochondrial fusion and in cristae remodeling during apoptosis.

INTRODUCTION

Mitochondria amplify apoptosis induced by several stimuli (Green and Kroemer, 2004). They release cytochrome c and other proapoptotic proteins activating a postmitochondrial pathway that culminates in cell demise (Wang, 2001). Proteins of the BCL-2 family control the release of cytochrome c from mitochondria required for the activation of effector caspases (Adams and Cory, 2001). The "BH3-only" proapoptotic members of the family transmit the different apoptotic signals to the multidomain members BAX and BAK that are required for cytochrome c release and mitochondrial dysfunction (Scorrano and Korsmeyer, 2003). In a widely accepted model, these proteins can form a channel for the efflux of cytochrome c across the outer mitochondrial membrane (Green and Kroemer, 2004). Additional pathways downstream of the BH3-only proteins ensure complete release of cytochrome c and mitochondrial dysfunction. They include fragmentation of the mitochondrial network and remodeling of the cristae characterized by fusion of individual cristae and opening of the cristae junctions (Frank et al., 2001; Scorrano et al., 2002).

Mitochondrial morphology is controlled by a growing family of "mitochondria-shaping" proteins (Griparic and van der Bliek, 2001). Mitofusin (MFN) -1 and -2 are dynamin-related proteins of the outer membrane (OM) essential for mitochondrial tethering and fusion (Santel and Fuller, 2001; Legros et al., 2002; Santel et al., 2003; Chen et al., 2003). MFN2 is presumed to have mostly a regulatory role (Ishihara et al., 2004), while MFN1 tethers two juxtaposed organelles (Koshiba et al., 2004) and cooperates with Optic Atrophy 1 (OPA1) in the fusion process (Cipolat et al., 2004). OPA1 is also a dynamin-related protein that resides in the inner mitochondrial membrane (IM). Dynamin-related protein 1 (DRP-1) is located in the cytoplasm but during fission translocates to mitochondria where it binds to hFis1, its adaptor in the OM (Smirnova et al., 2001; Yoon et al., 2003; James et al., 2003). It is presumed that DRP-1 can sever both membranes either directly or by recruiting other IM proteins.

A growing body of evidence suggests that mitochondria-shaping proteins participate in cell death. Dnm1p, the yeast ortholog of DRP-1, mediates mitochondrial fragmentation and apoptosis-like death in *S. cerevisiae* (Fannjiang et al., 2004). Blocking Drp-1 in *C. elegans* inhibits apoptotic mitochondrial fragmentation and results in the accumulation of supernumerary cells during development (Jagasia et al., 2005). Expression of a dominant negative mutant of DRP-1 or downregulation of hFis1 in

mammalian cells delays cytochrome c release and apoptosis (Frank et al., 2001; Lee et al., 2004). MFN1 and MFN2, alone or in combination, prevent death by some intrinsic stimuli (Sugioka et al., 2004; Neuspiel et al., 2005), consistent with early inhibition of MFN1-dependent fusion during apoptosis (Karbowski et al., 2004). Following several death stimuli, including the BH3-only proteins BID and BIK, mitochondria remodel their internal structure: individual cristae fuse and cristae junctions widen, allowing complete cytochrome c release (Scorrano et al., 2002; Germain et al., 2005). While the molecular details of mitochondrial fragmentation during apoptosis have been partially unraveled, little is known about the mechanisms controlling cristae remodeling, and we wished to further elucidate this process. OPA1 protects from apoptosis and is so far the only mitochondria-shaping protein associated with the IM (Olichon et al., 2003), making it a potential candidate to control cristae remodeling. Downregulation of OPA1 not only causes mitochondrial fragmentation but also alters the shape of the cristae (Olichon et al., 2003). Since cristae contain the bulk of cytochrome c, the regulation of this process could explain the known antiapoptotic effect of OPA1. Alternatively, OPA1 could act by counteracting mitochondrial fission (Lee et al., 2004). Here we genetically dissect the role of OPA1 in apoptosis and find that this can be separated from its role in mitochondrial fusion.

RESULTS

OPA1 Protects from Apoptosis by Preventing Cytochrome c Release and Mitochondrial Dysfunction

Expression of wild-type (wt) OPA1 protected mouse embryonic fibroblasts (MEFs) from death induced by apoptotic stimuli that activate the mitochondrial pathway like H_2O_2, etoposide, staurosporine, and truncated, active BID (tBID) (Wei et al., 2001; Scorrano et al., 2003) (Figures 1A–1D). OPA1 did not affect the extrinsic pathway of apoptosis recruited by TNFα since MEFs used in these experiments behave like type I cells not safeguarded by expression of BCL-2 (not shown). In type I cells, death receptors directly activate effector caspases, bypassing the mitochondrial amplificatory loop (Scaffidi et al., 1998). Mutation of a conserved Lys of the GTPase domain to Ala ($OPA1^{K301A}$), or truncation of a part of the C-terminal coiled-coil domain ($OPA1^{R905^*}$) impair OPA1 pro-fusion activity (Cipolat et al., 2004). When these mutants were expressed at similar levels to wt OPA1 (data not shown and Cipolat et al., 2004), they failed to protect from all the stimuli tested (Figure 1). Thus, the GTPase and the C-terminal coiled-coil domains of OPA1 are required for protection from apoptosis.

OPA1 delayed release of cytochrome c following H_2O_2 (Figure 2A; quantification in Figure 2B), staurosporine (Figure S1B), etoposide, and tBID (not shown). Release of cytochrome c is accompanied by mitochondrial dysfunction and loss of mitochondrial membrane potential.

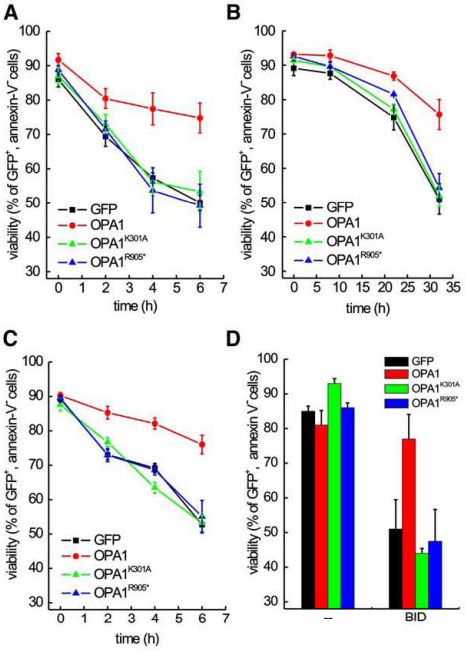

Figure 1. OPA1 Protects Against Apoptosis by Intrinsic Stimuli

wt MEFs were cotransfected with GFP and the indicated plasmids and after 24 hr treated with 1 mM H_2O_2 (A) (mean ± SEM of 12 independent experiments), 2 μM etoposide (B) (mean ± SEM of 12 independent experiments), or 2 μM staurosporine (C) (mean ± SEM of 12 independent experiments) for the indicated times. In (D) cells were cotransfected with GFP and pcDNA3.1 or with pcDNA3.1-tBID and after 24 hr viability was determined. Data represent average ± SEM of 7–12 independent experiments.

We followed in real time changes in the mitochondrial fluorescence of the potentiometric probe tetramethylrhodamine methylester (TMRM). OPA1 prevented depolarization induced by H_2O_2 (Figures 2C and 2D). Conversely, $OPA1^{K301A}$ had no such protective effects on cytochrome c release and mitochondria depolarization (Figures 2C and 2D). These results indicate that functional OPA1 decreases release of cytochrome c and loss of mitochondrial membrane potential during apoptosis.

OPA1 Does Not Require Mitofusins to Protect from Apoptosis

OPA1 requires *Mfn1* for its profusion activity (Cipolat et al., 2004). To check whether OPA1 protects against apoptosis by promoting fusion, we expressed OPA1 in MEFs lacking *Mfn1*. OPA1 protected *Mfn1*$^{-/-}$ cells from apoptosis induced by all the intrinsic stimuli tested to an extent similar to that observed in wt cells (Figures 3A–3C). Since residual mitochondrial fusion is still observed in *Mfn1*$^{-/-}$ MEFs, we

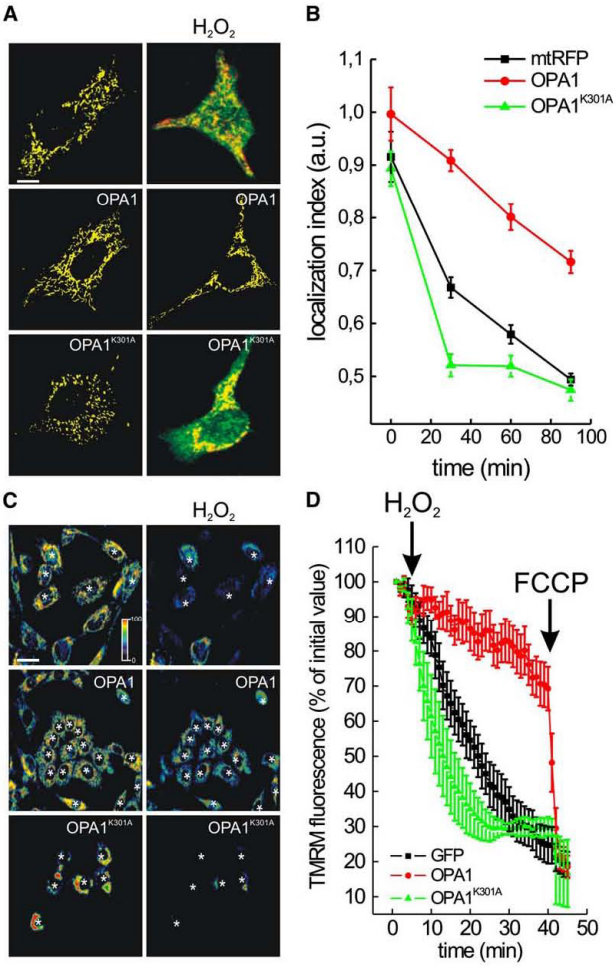

Figure 2. OPA1 Delays Release of Cytochrome c and Mitochondrial Dysfunction during Apoptosis

(A) Representative images of subcellular cytochrome c distribution. wt MEFs were cotransfected with mtRFP (red), and the indicated plasmids were left untreated or treated for 30 min with 1 mM H_2O_2, fixed and immunostained for cytochrome c (green). Bar, 15 μm.

(B) Localization index of cytochrome c. Experiments were performed as in (A), but cells were fixed at the indicated times. Data represent mean ± SEM of five independent experiments.

(C) Pseudocolor-coded images of TMRM fluorescence in wt MEFs cotransfected with GFP and the indicated plasmids. Left images represent the initial frame of the real-time sequence, while right ones were acquired at time = 40 min. Asterisks indicate GFP-positive cells. The pseudocolor scale is shown. Bar, 40 μm.

(D) Quantitative analysis of TMRM fluorescence changes over mitochondrial regions. When indicated (arrows), 1 mM H_2O_2, and 2 μM FCCP were added. Data represent average ± SEM of eight independent experiments performed as in (C).

turned to cells doubly deficient for *Mfn1* and *Mfn2* (DMF), where fusion is completely blocked (Chen et al., 2005). DMF cells appeared as sensitive to staurosporine and H_2O_2 as wt and single *Mfn1*$^{-/-}$ cells, and OPA1 was effective in protecting them from apoptosis (Figures 3D and 3E). We confirmed that OPA1 inhibited release of cytochrome c in *Mfn1*$^{-/-}$ and in DMF cells induced by H_2O_2 (Figures 3F and 3G) or by staurosporine (Figures S1C and S1D). Of note, *Mfn1*$^{-/-}$ and DMF mitochondria expressing OPA1 remained completely fragmented, yet they retained cytochrome c, further dissociating blockage of cytochrome c release from mitochondrial fusion. Thus, OPA1 protects from apoptosis in the absence of MFN1 and MFN2. The profusion activity of OPA1 is therefore not necessary for its antiapoptotic activity.

OPA1 Controls Cytochrome c Mobilization from Mitochondrial Cristae

We verified whether OPA1 influenced the release of cytochrome c in an in vitro quantitative assay using purified organelles and recombinant proteins. Cytochrome c release from mitochondria isolated from control MEF clones carrying an empty vector with a Puromycin resistance gene (wt::*Puro* and *Mfn1*$^{-/-}$::*Puro*) in response to recombinant, caspase-8-cleaved p7/p15 BID (cBID) was almost complete after 15 min. We generated clones expressing high levels of OPA1 (wt::*Opa1* and *Mfn1*$^{-/-}$::*Opa1*) as confirmed by immunoblotting (Figure S2). Mitochondria isolated from these cells conversely retained a significant fraction of cytochrome c even after 15 min (Figures 4A–4D). Release was extremely fast in mitochondria isolated

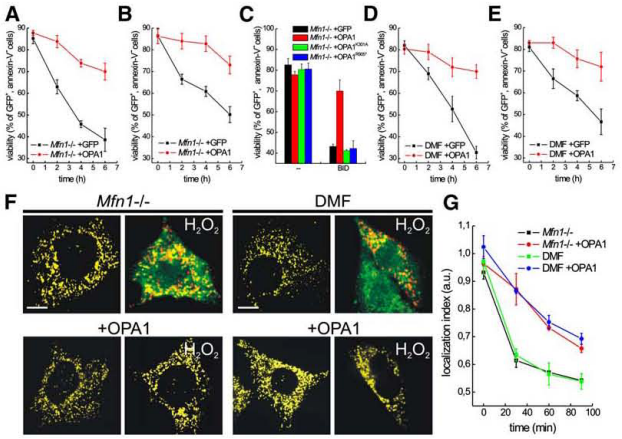

Figure 3. Mitofusins Are Not Required for the Antiapoptotic Effect of OPA1

(A–E) Cells of the indicated genotype were cotransfected with GFP and the indicated plasmids and treated with 1 mM H_2O_2 (A and D) or 2 μM staurosporine (B and E). At the indicated times, cells were harvested and viability was determined. In (C), *Mfn1*$^{-/-}$ MEFs were cotransfected with GFP and pcDNA3.1 or pcDNA3.1-tBID and after 24 hr viability was determined. Data represent average ± SEM of ten independent experiments.

(F) Representative images of subcellular cytochrome c distribution. Cells of the indicated genotype cotransfected with mtRFP (red) and the indicated plasmid were left untreated or treated for 30 min with 1 mM H_2O_2, fixed, and immunostained for cytochrome c (green). Bar, 10 μm.

(G) Localization index of cytochrome c. Experiments were performed as in (F), except that cells were fixed at the indicated times. Data represent average ± SEM of five independent experiments.

from MEFs expressing high levels of OPA1^{K301A} (wt::*Opa1*^{K301A}) or a short hairpin RNA interference targeting OPA1 (wt::*shOpa1*) (Figure S2), reaching ~85% of the total pool of cytochrome c after only 5 min (Figures 4B and 4C). Thus, levels of active OPA1 regulate the release of cytochrome c from mitochondria. The final step of cytochrome c release from mitochondria requires activation and oligomerization of the multidomain proapoptotic BCL-2 family members BAX and BAK. We found that OPA1 did not delay activation and translocation of BAX to mitochondria in response to staurosporine (Figure S1A). Furthermore, BAK activation, measured by its oligomerization in purified mitochondria upon BID stimulation, was also unaltered (Figures 4F and 4G). Thus, OPA1 does not interfere with activation of proapoptotic members of the BCL-2 family, crucial for the permeabilization of the OM.

A small fraction of cytochrome c, corresponding to ~15%–20% of the total, is found free in the IMS, while most is located in the cristae (Scorrano et al., 2002). The OM of mitochondria can be selectively permeabilized

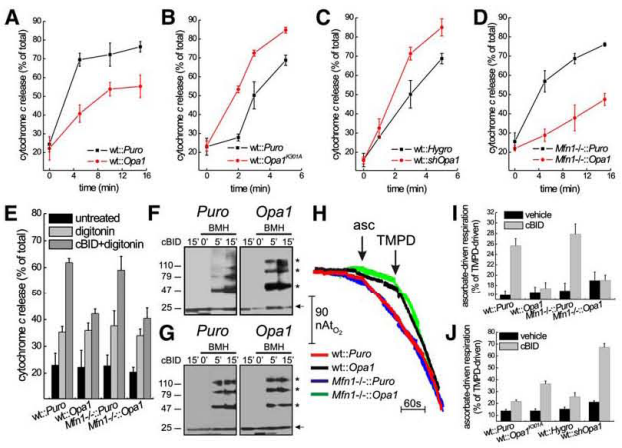

Figure 4. OPA1 Controls Mobilization of Cytochrome c from Mitochondrial Cristae in Response to BID

(A–D) Mitochondria isolated from MEFs of the indicated genotype were treated for the indicated times with cBID. After centrifugation the amount of cytochrome c in supernatant and pellet was determined by a specific ELISA. Data represent average ± SEM of four independent experiments.

(E) Mitochondria isolated from MEFs of the indicated genotype were incubated with cBID for 3 min. The OM was then permeabilized with 40 pmol digitonin × mg^{-1} mitochondria for 5 min. After centrifugation, cytochrome c content in supernatant and pellet was measured as in (A).

(F and G) wt (F) and *Mfn1*$^{-/-}$ (G) mitochondria of the indicated genotype were treated with cBID for the indicated times. DMSO or 10 mM BMH was then added and after 30 min the crosslinking reaction was quenched (Wei et al., 2000). Equal amounts (40 μg) of mitochondrial proteins were analyzed by SDS-PAGE/immunoblotting using anti-BAK antibody. Asterisks: BAK multimers.

(H) Representative traces of ascorbate-driven respiration following BID treatment. Mitochondria of the indicated genotype were treated for 5 min with cBID and then transferred into an oxygen electrode chamber. Where indicated (arrows), 6 mM ascorbate-Tris and 300 μM TMPD were added.

(I and J) Quantitative analysis of the effect of OPA1 levels and function on BID-induced cytochrome c mobilization. Mitochondria of the indicated genotype were treated with cBID for 5 (I) or 3 min (J), and cytochrome c in the supernatant was assayed as in (D). Data represent average ± SEM of five independent experiments.

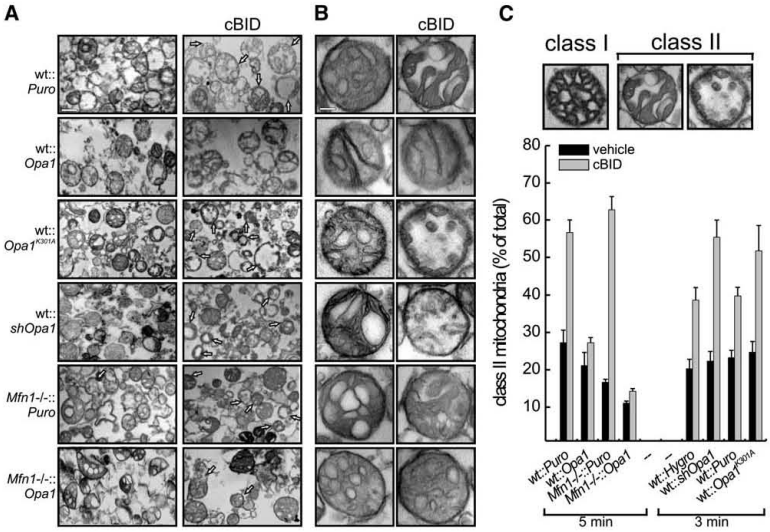

Figure 5. Mitochondrial Morphological Changes in Response to BID: Regulation by OPA1

(A) Representative EM fields of mitochondria of the indicated genotype. Where indicated, mitochondria were treated for 5 min with cBID, except for wt::*shOpa1* and wt::*Opa1*^{K301A} mitochondria, which were treated for 3 min. Arrows indicate class II mitochondria. Bar, 600 nm.

(B) Magnifications of representative transmission EM of mitochondria. Experiments were performed as in (A). Bar, 200 nm.

(C) Blind morphometric analysis of randomly selected EM fields of mitochondria of the indicated genotype. The experiments were performed as in (A). Inset shows representative class I and class II (remodeled) morphologies (Scorrano et al., 2002). Data represent average ± SEM of three independent experiments.

using titrated amounts of digitonin to selectively release the IMS pool of cytochrome c (Scorrano et al., 2002). Approximately 15% of total cytochrome c was released upon permeabilization of the outer membrane in wt and *Mfn1*$^{-/-}$ mitochondria, irrespective of OPA1. When wt and *Mfn1*$^{-/-}$ mitochondria were pretreated with cBID for 3 min, ~60% of total cytochrome c was recovered in the supernatant, confirming that at this early timepoint cBID promotes mobilization of cytochrome c from cristae to the IMS (Scorrano et al., 2002). This increase in digitonin-releasable cytochrome c upon cBID treatment was not observed in mitochondria from cells expressing OPA1 (Figure 4E). Thus, OPA1 appears to selectively stabilize the pool of cytochrome c that cBID mobilizes towards the IMS.

We therefore measured cytochrome c mobilization from cristae using a specific assay. Given the different redox potential and accessibility of membrane bound and free cytochrome c, these two pools can be specifically reduced by ascorbate and N,N,N′,N′-tetramethyl-p-phenylenediamine (TMPD) (Scorrano et al., 2002; Nicholls et al., 1980). The ratio of ascorbate over TMPD-driven O_2 consumption (asc/TMPD) therefore provides an estimate of the pool of free cytochrome c in the IMS relative to the total mitochondrial cytochrome c. An increase in asc/TMPD ratio reflects the mobilization of cytochrome c from the cristae stores towards the IMS (Scorrano et al., 2002). cBID almost doubled this ratio in wt and *Mfn1*$^{-/-}$ mitochondria (Figures 4H and 4I). OPA1 did not affect basal asc/TMPD ratio, but it blocked the increase in the ratio observed upon cBID treatment in wt and *Mfn1*$^{-/-}$ mitochondria (Figures 4H and 4I). Conversely, OPA1^{K301A} and downregulation of OPA1 levels augmented the effect of cBID on the asc/TMPD ratio (Figure 4J). Of note, lower OPA1 levels resulted in a small but significant increase in basal asc/TMPD ratio (Figure 4J, $p < 0.05$ compared to control wt::*Hygro* mitochondria). Thus, OPA1 regulates apoptotic redistribution of cytochrome c from the cristae.

OPA1 Controls Apoptotic Remodeling of Mitochondrial Cristae

The changes in mitochondrial ultrastructure defined as "cristae remodeling" correlate with redistribution of cytochrome c from the cristae (Scorrano et al., 2002). Using conventional transmission electron microscopy (TEM), it is possible to identify remodeled "class II" mitochondria and normal "class I" mitochondria based on the appearance of the electron transparent cristae (see Figure 5C for representative images). We therefore turned to TEM of mitochondria isolated from the generated cellular models to investigate whether OPA1 influenced remodeling of the cristae. OPA1 promoted juxtaposition of the cristae membranes, generating extremely narrow structures not seen in control mitochondria (Figures 5A and 5B).

In contrast, cristae appeared wider and in wt::*Opa1*^{K301A} and wt::*shOpa1* mitochondria (Figures 5A and 5B). *Mfn1* $^{-/-}$::*Puro* and *Mfn1* $^{-/-}$::*Opa1* mitochondria displayed hyperconvex, balloon-like cristae, connected by narrow, tubular, elongated junctions to the intermembrane space (Figures 5A and 5B). cBID induced the appearance of several class II organelles in control populations (arrows in Figure 5A; magnification in Figure 5B). These remodeled mitochondria were predominant in wt::*Opa1*^{K301A} or wt::*shOpa1* as soon as 3 min after cBID (arrows in Figure 5A; magnification in Figure 5B). On the other hand, cristae of wt::*Opa1* and *Mfn1* $^{-/-}$::*Opa1* mitochondria remained narrow, and mainly class I mitochondria were retrieved following cBID (Figure 5A; magnification in Figure 5B). These observations were further corroborated by a morphometric analysis (Figure 5C).

The effect of OPA1 on mitochondrial morphology and remodeling warranted a more detailed structural investigation by electron tomography. Cristae of wt::*Puro* mitochondria appeared as pleomorphic individual structures connected to the IMS by a narrow tubular junction of 16.2 ± 2.1 nm (n = 9 in two different tomograms). wt OPA1 promoted close juxtaposition of the cristae membranes, and some cristae spanned the diameter of the reconstructed mitochondrion. The cristae junction was extremely narrow, measuring 15.2 ± 2.3 nm (n = 9 in two different tomograms) (Figure 6A). Conversely, wt::*Opa1*^{K301A} and wt::*shOpa1* cristae protruded in the matrix for less than the radius of the organelle. The narrow tubular junction was unaltered in wt::*Opa1*^{K301A} (17.1 ± 2.1 nm, n = 9 in two different tomograms) and in wt::*shOpa1* mitochondria (20.2 ± 1.6 nm, n = 9 in two different tomograms) (Figure 6A).

In wt::*Puro* mitochondria cBID promoted fusion of cristae in few intercommunicating compartments and widened the cristae junctions (45.4 ± 3.2 nm, n = 9 in two different tomograms). In wt::*Opa1* mitochondria, in contrast, cristae fused following cBID, but they retained an extremely narrow aspect, and the diameter of the tubular junction remained small (20.2 ± 3.1 nm, n = 9 in two different tomograms). Cristae junction diameter increased extremely in wt::*Opa1*^{K301A} mitochondria (65.3 ± 4.2 nm, n = 9 in two different tomograms) and in wt::*shOpa1* (73.3 ± 2.1 nm, n = 9 in two different tomograms) (Figure 6A). Rotation of a volume-rendered 3D reconstruction where the outer membrane had been peeled out allowed clear visualization of the cristae junctions (Figure 6B). In untreated mitochondria, these narrow structures were unaffected by expression of OPA1. Following cBID they became greatly enlarged, and this enlargement was entirely prevented by OPA1 expression (Figure 6B). To investigate whether OPA1 required *Mfn1* to control shape and remodeling of the cristae, we turned to *Mfn1* $^{-/-}$ mitochondria. *Mfn1* $^{-/-}$::*Puro* mitochondria showed balloon-like, hyperconvex, individual cristae coexisting with more conventional pleomorphic ones. Independently from their shape, cristae had narrow junctions of 19.0 ± 2.1 nm (n = 9 in two different tomograms). *Mfn1* $^{-/-}$::*Opa1* mitochondria showed balloon cristae with some aspects of close juxtaposition of cristae membranes similar to those observed in wt::*Opa1* organelles. The narrow tubular junction of these cristae measured 18.3 ± 2.2 nm (n = 9 in two different tomograms). cBID caused fusion of *Mfn1* $^{-/-}$::*Puro* cristae and widening of their tubular junctions (41.4 ± 2.2 nm, n = 9 in two different tomograms). Conversely, junctions remained tight in *Mfn1* $^{-/-}$::*Opa1* cristae, their diameter measuring 18.5 ± 2.0 nm (n = 9 in two different tomograms) (Figure 6A). Thus, OPA1 counteracts the widening of the tubular junctions induced by cBID independently of MFN1.

Oligomers of Soluble and Membrane Bound OPA1 Are Disrupted by BID Early during Apoptosis

We turned to a biochemical approach to determine how OPA1 could control cristae shape. OPA1 is synthesized as an integral IM protein from one single gene. Alternative splicing generates eight different transcripts, all of them containing the transmembrane domain (Delettre et al., 2001), but a minor fraction of OPA1 is released in the IMS in a process that is regulated by the IM rhomboid protease PARL (Cipolat et al, 2006). The IMS form is crucial for OPA1 antiapoptotic activity (Cipolat et al., 2006). We verified whether expression of OPA1 in wt and *Mfn1* $^{-/-}$ cells resulted in an increase in IMS OPA1. Immunoblotting of membrane (pellet) and IMS (supernatant) fractions generated by hypotonic swelling and salt washes of mitochondria revealed that following expression, levels of IMS OPA1 were increased (Figure 7A). OPA1 in the membrane-enriched fraction was resistant to carbonate extraction, further indicating that this OPA1 form is integrally inserted in the IM (not shown). Consistent with this, only a minor fraction of OPA1 was released from mitochondria treated with cBID, even when cytochrome c release was complete (Figure S3). Thus, complete release of OPA1 does not occur in isolated mitochondria upon cBID treatment and can therefore not explain cristae remodeling, as previously suggested (Arnoult et al., 2005).

We therefore analyzed in greater detail OPA1 in normal and apoptotic mitochondria. Percoll-purified normal and cBID-treated, CHAPS-solubilized mouse liver mitochondria displayed very similar elution patterns from Superose 6 columns (not shown) (Danial et al., 2003). Fractions were pooled according to their size exclusion properties, designated B to E4 in descending order of molecular weight, and analyzed by SDS-PAGE and immunoblot. OPA1 was revealed in the high-molecular-weight fractions B to E2, indicating that OPA1 was part of a multimolecular complex. The matrix protein cyclophilin D used as a control was found only in fractions E3 and E4. Another OPA1 immunoreactive band with a MW corresponding to that of the soluble IMS form (Figure 7A) was found in fractions E2 (~180–230 kDa), E1 (~230–440 kDa), and D (~440–670 kDa), indicating that IMS OPA1 is also part of a multiprotein complex (Figure 7B). Following cBID, OPA1 was retrieved in fractions D, E2, and E3. p15 fragment of BID was specifically enriched in this last fraction and to a lower extent in

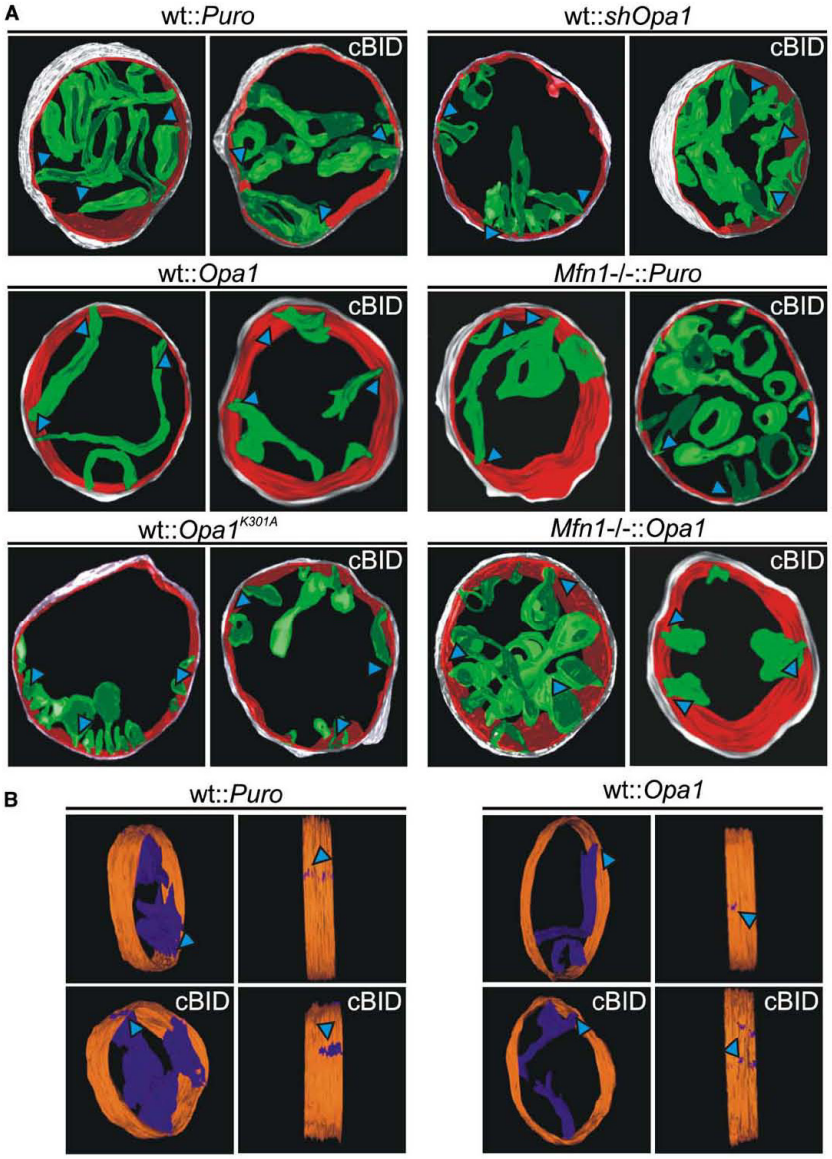

Figure 6. Electron Tomography of Mitochondrial Morphological Changes in Response to BID: Regulation by OPA1

(A) Surface-rendered views of tomographic reconstructions of mitochondria of the indicated genotype. Where indicated, mitochondria were treated with cBID for 5 min before fixation. wt::*shOpa1* and wt::$Opa1^{K301A}$ mitochondria were treated for 3 min. Outer membrane is depicted in light gray, inner boundary membrane in red, and cristae in green. Cyan arrowheads point to cristae junctions. Note that selected, representative cristae were traced when their degree of interconnectivity allowed it.

(B) Rotations of representative surface rendered views of tomographic reconstructions of mitochondria. Experiment was as in (A). Cristae are depicted in purple and inner boundary membrane in orange. Outer membrane has been peeled out to highlight individual openings of the cristae junctions (arrowheads).

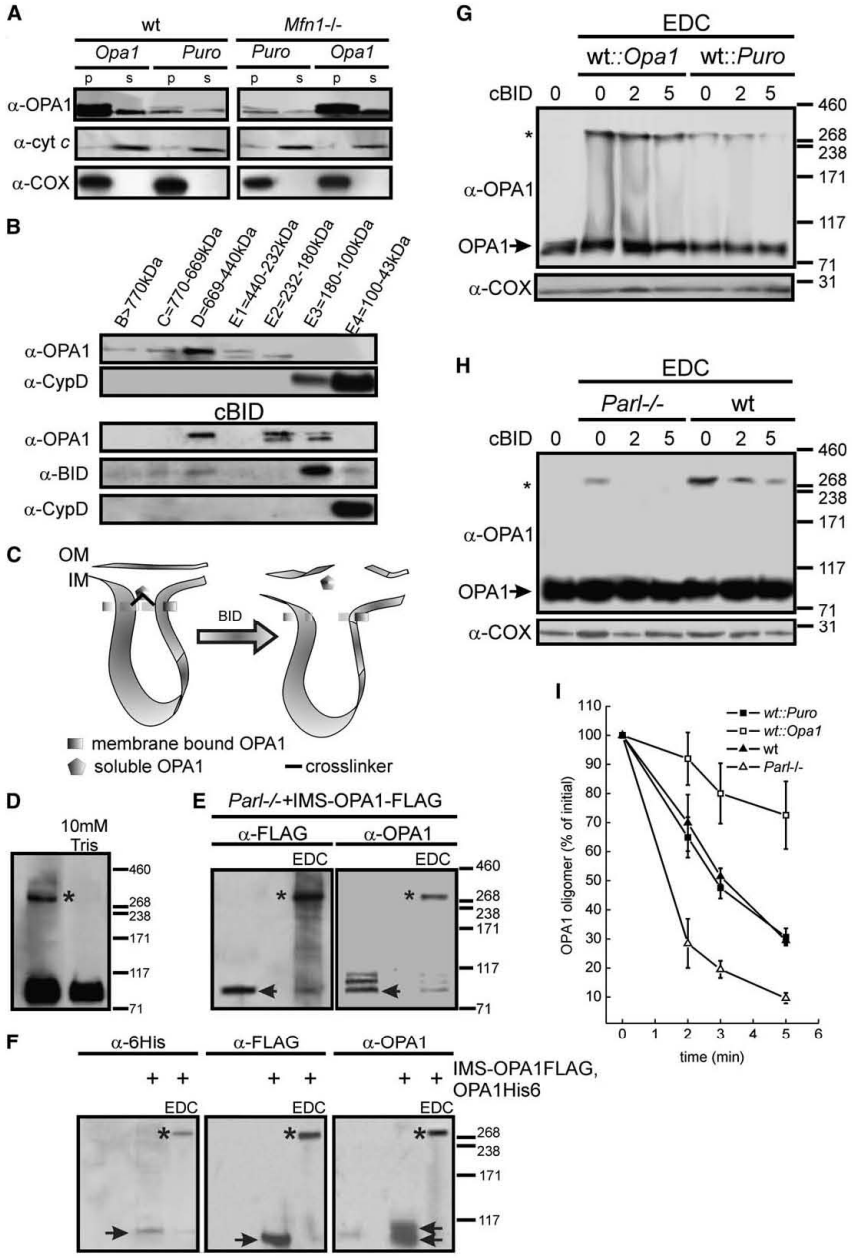

Figure 7. Oligomers Comprising IMS and Transmembrane OPA1 Are Early Targets of BID

(A) Mitochondria of the indicated genotype were hypotonically swollen and membrane (p) and soluble (intermembrane space, s) fractions were recovered. Proteins were separated by SDS-PAGE and immunoblotted with the indicated antibodies. COX indicates cytochrome c oxidase III.

fractions D, C, and E4. The matrix protein cyclophilin D was selectively enriched in low MW fraction E4 (Figure 7B). Thus, OPA1 is mainly found in high MW complexes; the lower MW form of OPA1, corresponding to IMS OPA1, is specifically enriched in fractions D to E2; and OPA1 is mainly found in lower MW fractions in apoptotic mitochondria, corresponding to smaller protein complexes.

Dynamin-related proteins are known to homo-hetero oligomerize (Danino and Hinshaw, 2001). We asked whether OPA1 could also form oligomers containing IMS and/or transmembrane forms. Such a structure could represent a molecular staple that juxtaposes the cristae membranes and could participate in the formation of the narrow tubular junction (Figure 7C). We tested whether chemical crosslinking revealed higher-order complexes immunoreactive for OPA1. A complex of OPA1 of ~290 kDa was indeed identified in mitochondria treated with the zero-length crosslinker 1-ethyl-3-(3-dimethylaminopropyl)carbodiimide (EDC) (Figure 7D). Identical results were observed with the 16 Å crosslinker bismaleimidohexane (not shown). This complex was absent in mitochondria whose cristae had been mechanically distended by osmotic swelling (asterisk in Figure 7D). Thus, OPA1 can be crosslinked into a high-order complex only when cristae are intact. In order to understand the composition of this complex, we turned to *Parl*$^{-/-}$ mitochondria where IMS OPA1 is greatly reduced (Cipolat et al., 2006). Levels of OPA1 complex were also reduced, suggesting a role for IMS OPA1 in its formation (Figure 7H). A FLAG-tagged version of OPA1 selectively targeted to the IMS (IMS-OPA1-FLAG) (Otera et al., 2005; Cipolat et al., 2006) expressed in *Parl*$^{-/-}$ mitochondria was retrieved in the EDC-crosslinked complex by specific anti-FLAG immunoblotting (asterisk in Figure 7E). Reprobing of the membrane with an anti-OPA1 antibody revealed that IMS-OPA1-FLAG displayed an apparent MW of ~88 kDa (arrowhead in Figure 7E), while endogenous OPA1 run at ~100 kDa. Following crosslinking, levels of 100 kDa endogenous and of 88 kDa IMS-OPA1-FLAG were decreased, while the levels of the larger complex increased, suggesting that both IMS and transmembrane forms of OPA1 constitute an oligomer. We further tested this by coexpressing a His-tagged version of OPA1 (OPA1-6His) with IMS-OPA1-FLAG in *Parl*$^{-/-}$ MEFs. As expected, ~98% of OPA1-6His remained transmembrane in mitochondria lacking PARL, as judged by immunoblotting of membrane and IMS fractions (not shown). Transmembrane OPA1-6His and IMS OPA1-FLAG were both found in the oligomer by specific immunoblotting (Figure 7F). Thus, the oligomer contains both transmembrane and IMS OPA1.

We next assessed the fate of this OPA1 oligomer during apoptosis. The oligomer rapidly disappeared following cBID, becoming almost undetectable after 5 min (Figures 7G and 7H). Expression of OPA1 augmented levels of this oligomer and, more importantly, stabilized it in cBID-treated mitochondria (Figure 7G). In *Parl*$^{-/-}$ mitochondria with greatly reduced IMS-OPA1 (Cipolat et al., 2006), OPA1 oligomer was weakly represented and early disrupted by cBID (Figure 7H). A quantitative, densitometric analysis confirmed faster disappearance of the oligomer in *Parl*$^{-/-}$ mitochondria and its stabilization following expression of OPA1 in wt organelles (Figure 7I). Of note, destabilization of OPA1 oligomer is an initial event following cBID, occurring before the complete release of cytochrome c. In as early as 5 min, levels in the oligomer are reduced by ~70%. This almost complete destabilization correlates with the release of approximately 80% of the cytochrome c observed at the same timepoint (Figure 4A). OPA1 oligomer is therefore an early target during cytochrome c release induced by BID. Expression of IMS-OPA1-FLAG protected *Parl*$^{-/-}$ MEFs from apoptosis (Cipolat et al., 2006) and prevented the enhanced cristae remodeling observed in response to cBID (Figure S4), substantiating the role of OPA1 oligomerization in this pathway.

DISCUSSION

The initial assumption that mitochondrial structure is not affected during apoptosis has been challenged during the last years. Mitochondrial fragmentation (Frank et al., 2001; Jagasia et al., 2005) and cristae remodeling (Scorrano et al., 2002; Germain et al., 2005) augment

(B) Mouse liver mitochondria were treated when indicated with cBID for 10 min, solubilized in 6 mM CHAPS, and subjected to gel filtration on Superose 6, and fractions were collected according to the indicated size exclusion properties, pooled, and concentrated. Fifty micrograms of proteins from the indicated fractions were separated by SDS-PAGE and immunoblotted with the indicated antibodies. CypD indicates cyclophilin D.
(C) Cartoon depicting the effect of BID-induced cristae remodeling on putative OPA1 oligomers; OM and IM indicate outer and inner mitochondrial membrane.
(D) Mitochondria left untreated or osmotically swollen for 10 min were incubated with 10 mM EDC for 30 min followed by centrifugation. Proteins in the pellets were separated by SDS-PAGE and immunoblotted using anti-OPA1 antibodies; the asterisk indicates OPA1 oligomer.
(E) Mitochondria were isolated from *Parl*$^{-/-}$ MEFs transfected with IMS-OPA1-FLAG and treated with the crosslinker EDC as in (D). Proteins were separated by SDS-PAGE and immunoblotted using the indicated antibodies; arrows indicate IMS-OPA1-FLAG, while asterisks denote OPA1 oligomer.
(F) *Parl*$^{-/-}$ MEFs were cotransfected with GFP and where indicated with IMS-OPA1-FLAG and OPA1-6His, sorted, and mitochondria were isolated. Where indicated, mitochondria were treated with EDC as in (D). Equal amounts of protein were separated by SDS-PAGE and immunoblotted using the indicated antibodies. Arrows indicate IMS-OPA1-FLAG and OPA1-6His, while asterisks denote OPA1 oligomer.
(G and H) Mitochondria of the indicated genotype were treated with cBID for the indicated times and then crosslinked with EDC as in (D). Proteins were separated by SDS–PAGE and immunoblotted using the indicated antibodies. Asterisk denotes OPA1 oligomer. Arrow indicates nonoligomerized OPA1. COX is cytochrome c oxidase III.
(I) Kinetics of OPA1 oligomer destabilization by cBID. OPA1 oligomer was analyzed by densitometry on immunoblots following normalization for loading based on levels of COX. Data were normalized to levels of OPA1 oligomer in untreated mitochondria and represent average ± SEM of five independent experiments.

cytochrome c release and complete the program of mitochondrial dysfunction (Green and Kroemer, 2004). Little is known about the molecular mechanisms behind this remodeling process, but a likely candidate protein is OPA1, a dynamin-related protein of the IM, which mediates fusion of the organelle. We demonstrate here that mitochondrial remodeling and cytochrome c mobilization are regulated by levels of functional OPA1 and that this occurs independently from mitochondrial fusion. We also show that IMS and transmembrane OPA1 form oligomers that are early targets of BID during cristae remodeling.

OPA1 reduces cytochrome c release, mitochondrial dysfunction, and cell death induced by intrinsic stimuli without interfering with activation of the mitochondrial gatekeepers, the multidomain proapoptotics BAX and BAK (Scorrano and Korsmeyer, 2003). Given its function in mitochondrial fusion, one could predict that OPA1 protects by counteracting apoptotic fragmentation of mitochondria, a process observed in several paradigms of cell death (Youle and Karbowski, 2005). This appeared not to be the case since OPA1 efficiently protects cells lacking *Mfn1*, essential for OPA1-mediated mitochondrial fusion (Cipolat et al., 2004), and doubly *Mfn* null MEFs where fusion is completely abolished (Chen et al., 2005). Active OPA1 on the other hand blocks intramitochondrial cytochrome c redistribution that follows cristae remodeling (Scorrano et al., 2002; Germain et al., 2005). Previous approaches using conventional EM of mitochondria in cells with downregulated OPA1 or mgm1p (its yeast homolog) showed a gross disruption of the overall cristae morphology (Olichon et al., 2003; Amutha et al., 2004; Griparic et al., 2004). Loss of mitochondrial DNA and therefore of components of the respiratory chain contributed to this phenotype in yeast (Amutha et al., 2004). In mammalian cells, the remodeling of the cristae observed in situ can follow the activation of apoptosis caused by ablation of *Opa1* (Olichon et al., 2003). We therefore reinvestigated the role of OPA1 in biogenesis and remodeling of the cristae using tomography of mitochondria isolated from cellular models with defined levels of this protein. Electron tomography showed that OPA1 regulates shape and length of mitochondrial cristae and more importantly cristae remodeling during apoptosis. OPA1 keeps tight the cristae junction, which is likely to regulate mobilization of cytochrome c to the IMS following BID treatment. *Mfn1*$^{-/-}$ cristae appeared hyperconvex. Nevertheless, they were still connected by a narrow tubular junction to the IMS, and this junction widened following BID treatment. OPA1 did not change curvature of *Mfn1*$^{-/-}$ cristae but, significantly, blocked enlargement of the cristae junction. Thus, curvature of the cristae is not the determining factor in cytochrome c release.

How does OPA1 regulate remodeling of the cristae? One possibility is that OPA1 is released completely during apoptosis, as it has been previously reported (Arnoult et al., 2005). On the other hand, OPA1 has been found to be mainly an integral IM protein (Griparic et al., 2004; Satoh et al., 2003). We indeed observed the release of only a small pool of OPA1 corresponding to a fraction of the protein that is present in the IMS of untreated mitochondria. OPA1 exists in multiple splicing variants. Nevertheless, a transmembrane domain is present in all eight different variants and ensures integral insertion in the IM. So, how is this IMS pool of OPA1 produced? In yeast, pcp1p/rbd1p, a rhomboid protease of the IM, cleaves the transmembrane domain of mgm1p, the yeast homolog of OPA1, to generate a short form soluble in the IMS (McQuibban et al., 2003; Herlan et al., 2003). In an accompanying manuscript, evidence is provided that formation of IMS OPA1 in mammalian mitochondria appears to depend on PARL, the ortholog of rbd1p. *Parl* is also a prerequisite for the antiapoptotic function of OPA1 (Cipolat et al., 2006). This correlates with decreased levels of soluble IMS OPA1 and can be rescued by IMS OPA1 expression (Cipolat et al., 2006). We therefore investigated the potential role of IMS OPA1 at the molecular level. An indication came from studies on dynamin I, which tubulates membranes and assembles in oligomers that are crucial to sever membranes (Sweitzer and Hinshaw, 1998). OPA1 is, however, located inside the bilayer on which it should act. It therefore was unlikely that OPA1 could operate in a similar way as dynamin I. We therefore tested an alternative hypothesis in which transmembrane OPA1 uses the soluble, IMS form to oligomerize. These oligomers could "staple" the membranes of the cristae. We found support for this hypothesis in a series of experiments. First, gel filtration chromatography showed that OPA1 was found in fractions containing high MW complexes (also in HeLa mitochondria [Satoh et al., 2003]). Second, cBID destabilized these oligomers, correlating with increased cytochrome c release and apoptosis. Third, chemical crosslinking identified an ~290 kDa OPA1 immunoreactive band that disappeared when membranes of cristae were separated by osmotic swelling. This oligomer contained the soluble IMS form and the transmembrane IM form of OPA1, as demonstrated using tagged versions of IMS and IM OPA1. Fourth, the presence and disappearance of this oligomer correlates with protection against and induction of apoptosis and cytochrome c release, respectively. Fifth, levels of IMS OPA1 are crucial for the formation of the oligomer to protect from apoptosis (Cipolat et al., 2006) and to prevent cristae remodeling. Taken together, these results suggest that OPA1 oligomers participate in formation and maintenance of the cristae junction.

The size of the OPA1 oligomer as determined by crosslinking and the retrieval of tagged versions of IMS and IM OPA1 in this oligomer suggest the hypothesis of at least a trimer comprising two IM and one IMS OPA1. However, OPA1 is also found in fractions of higher MW in both normal and apoptotic mitochondria. Thus, we cannot exclude the possibility that other proteins participate in this complex. The fact that we found OPA1 in a ~230 to ~180 kDa fraction following treatment with cBID would indeed suggest that OPA1 can associate with other proteins during apoptosis. This is a next challenge requiring copurification experiments and proteomic approaches in normal and apoptotic mitochondria.

Our work shows that OPA1 is a bifunctional protein. On one hand it in promotes mitochondrial fusion, depending on MFN1. On the other, it regulates apoptosis by controlling cristae remodeling and cytochrome c redistribution. This correlates with OPA1 oligomerization and is dependent on its cleavage by PARL. In conclusion, oligomerization of OPA1 appears to be a mechanism that regulates apoptosis by maintaining the tightness of cristae junctions. This unexpected role of OPA1 needs to be further explored. This mechanism could, for example, contribute to the pathogenesis of dominant optic atrophy since mutations causing this disease cluster in the GTPase and coiled-coil domains of OPA1, possibly impairing assembly and/or function of the OPA1 oligomer.

EXPERIMENTAL PROCEDURES

Cell Culture, Transfection, Sorting, and Generation of Stable Clones

SV40 transformed wt and *Mfn1*$^{-/-}$ MEFs were cultured as described in Cipolat et al. (2004); DMF MEFs were cultured as described in Chen et al. (2005). Cells were transfected using Transfectin (Biorad) following manufacturer's instructions.

For sorting, 1×10^8 cotransfected MEFs were analyzed by light forward and side scatter and for GFP fluorescence through a 530 nm band pass filter as they traversed the beam of an argon ion laser (488 nm, 100 mW) of an FACSAria (BD). Nontransfected MEFs were used to set the background fluorescence. Sorted cells were checked for viability by Trypan Blue exclusion.

The single clones were generated by limited dilution following transfection and antibiotic selection of expressing cells.

Analysis of Cell Death

1×10^5 MEFs of the indicated genotype grown in 12-well plates were cotransfected with pEGFP and the indicated vector. After 24 hr cells were treated as described and stained with Annexin-V-Alexa568 (Roche) according to manufacturer's protocol. Apoptosis was measured by flow cytometry (FACSCalibur) as the percentage of annexin-V-positive events in the GFP-positive population.

Transmission Electron Microscopy, Tomographic Reconstruction, and Mitochondrial Morphometry

Mitochondria were fixed for 1 hr at 25°C using glutaraldehyde at a final concentration of 2.5% (V/V). Thin sections were imaged on a Tecnai-12 electron microscope (Philips-FEI) at the Telethon EM Core Facility (TeEMCoF, Istituto Mario Negri Sud). For tomography, colloidal gold particles were applied to one side of 200 nm-thick sections as alignment markers. Tilt series of 122 images were recorded around one tilt axis, over an angular range of 120° with a 1° tilt interval. Images were aligned and reconstructed as previously described (Scorrano et al., 2002). The reconstructed volumes had dimensions of 512 × 512 × 80–100 pixels depending on section thickness, with a pixel size range of 2.5–4.1 nm. Surface-rendered models were produced using IMOD (Mironov et al., 2001) or Reconstruct (Fiala, 2005). Measurements were made directly on 1 pixel-thick tomogram slices.

Molecular Biology

p3 × FLAG-CMV14-AIF-Opa1 (IMS-OPA1-FLAG) and pCDNA3-OPA1-HA-HisTag (OPA1-6His) were kind gifts from K. Mihara (Kyushu University, Fukuoka, Japan) and P. Belenguer (U. of Toulouse, France), respectively. shRNAi were constructed to target the nucleotide region 1813–1831 of murine OPA1. All other plasmids are described in Cipolat et al. (2004).

Imaging

For cytochrome c immunolocalization, cells grown on coverslips were transfected with mtRFP and after 24 hr incubated as detailed. Immunostaining for cytochrome c was performed as described in Scorrano et al. (2003). For cytochrome c and mtRFP detection, green and red channel images were acquired simultaneously using two separate color channels on the detector assembly of a Nikon Eclipse E600 microscope equipped with a Biorad MRC-1024 laser scanning confocal imaging system. The localization index was calculated as described in Petronilli et al. (2001).

For imaging of mitochondrial membrane potential, MEFs grown on coverslips were cotransfected as indicated and after 24 hr loaded with 10 nM TMRM (Molecular Probes) in the presence of 2 μg/ml cyclosporine H, a P-glycoprotein inhibitor (30 min at 37°C). Clusters of GFP-positive cells were identified and sequential images of TMRM fluorescence were acquired every 30 s using an Olympus IMT-2 inverted microscope equipped with a CellR Imaging system.

Recombinant Proteins

p7/p15 recombinant BID was produced, purified, and cleaved with caspase-8 as described in Scorrano et al. (2002). Unless noted, it was used at a final concentration of 32 pmol × mg^{-1}.

In Vitro Mitochondrial Assays

Mitochondria were isolated by standard differential centrifugation in isolation buffer (IB). Oxygen consumption of mitochondria incubated in experimental buffer (EB) was measured using a Clarke-type oxygen electrode (Hansatech Instruments) (Scorrano et al., 2002). Cytochrome c redistribution and release in response to recombinant cBID was determined as described in Scorrano et al. (2002).

Biochemistry

For protein crosslinking, mitochondria were treated with 10 mM BMH (Pierce) or with 10 mM EDC (Pierce) for 30 min at 37°C. Samples were centrifuged for 10 min at 12000 × g at 4°C, and the mitochondrial pellets were resuspended in SDS-PAGE sample loading buffer. DTT in the sample buffer quenched the crosslinking reaction. Proteins were separated by 3%–8% Tris-Acetate or 4%–12% Tris-MES SDS-PAGE (NuPage, Invitrogen), transferred onto PVDF membranes (Millipore), and probed using the indicated primary antibodies and isotype matched secondary antibodies conjugated to horseradish peroxidase. Signals were detected using ECL (Amersham). Details on the antibodies used can be found in Supplemental Data. Densitometry was performed using a GS170 Calibrated Imaging densitometer, and data were analyzed using Quantity One software (Biorad).

For Superose 6 filtration, purified mouse liver mitochondria (50 mg) were solubilized in the presence of 6 mM CHAPS passed onto a Superose 6 column, and fractions were collected, pooled, and concentrated as described (Danial et al., 2003).

Additional details on the experimental procedures can be found in Supplemental Data available with this article online.

Supplemental Data

Supplemental Data include four figures and can be found with this article online at http://www.cell.com/cgi/content/full/126/1/177/DC1/.

ACKNOWLEDGMENTS

L.S. is an Assistant Telethon Scientist of the Dulbecco-Telethon Institute. This research is supported by Telethon; AIRC; Compagnia di San Paolo; and the Human Frontier Science Program Organization. The TeEMCoF is supported by Telethon Italy (GTF03006). We thank Drs. K. Mihara and P. Belenguer for the gift of plasmids and D. Chan for *Mfn1*$^{-/-}$ and DMF cells. Research in BDS laboratory is supported by a Freedom to Discover grant from Bristol Myers Squib, a Pioneer award from the Alzheimer's Association, the Fund for Scientific Research, Flanders; K.U.Leuven (GOA); European Union (APOPIS:

LSHM-CT-2003-503330); and Federal Office for Scientific Affairs, Belgium.

Received: July 11, 2005
Revised: March 8, 2006
Accepted: June 8, 2006
Published: July 13, 2006

REFERENCES

Adams, J.M., and Cory, S. (2001). Life-or-death decisions by the Bcl-2 protein family. Trends Biochem. Sci. *26*, 61–66.

Amutha, B., Gordon, D.M., Gu, Y., and Pain, D. (2004). A novel role of Mgm1p, a dynamin-related GTPase, in ATP synthase assembly and cristae formation/maintenance. Biochem. J. *381*, 19–23.

Arnoult, D., Grodet, A., Lee, Y.J., Estaquier, J., and Blackstone, C. (2005). Release of OPA1 during apoptosis participates in the rapid and complete release of cytochrome c and subsequent mitochondrial fragmentation. J. Biol. Chem. *280*, 35742–35750.

Chen, H., Detmer, S.A., Ewald, A.J., Griffin, E.E., Fraser, S.E., and Chan, D.C. (2003). Mitofusins Mfn1 and Mfn2 coordinately regulate mitochondrial fusion and are essential for embryonic development. J. Cell Biol. *160*, 189–200.

Chen, H., Chomyn, A., and Chan, D.C. (2005). Disruption of fusion results in mitochondrial heterogeneity and dysfunction. J. Biol. Chem. *280*, 26185–26192.

Cipolat, S., de Brito, O.M., Dal Zilio, B., and Scorrano, L. (2004). OPA1 requires mitofusin 1 to promote mitochondrial fusion. Proc. Natl. Acad. Sci. USA *101*, 15927–15932.

Cipolat, S., Rudka, T., Hartmann, D., Costa, V., Serneels, L., Craessaerts, K., Metzger, K., Frezza, C., Annaert, W., D'Adamio, L., Derks, C., Dejaegere, T., Pellegrini, L., D'Hooge, R., Scorrano, L., and De Strooper, B. (2006). Mitochondrial rhomboid PARL regulates cytochrome c release during apoptosis via OPA1-dependent cristae remodelling. Cell *126*, this issue, 163–175.

Danial, N.N., Gramm, C.F., Scorrano, L., Zhang, C.Y., Krauss, S., Ranger, A.M., Datta, S.R., Greenberg, M.E., Licklider, L.J., Lowell, B.B., et al. (2003). BAD and glucokinase reside in a mitochondrial complex that integrates glycolysis and apoptosis. Nature *424*, 952–956.

Danino, D., and Hinshaw, J.E. (2001). Dynamin family of mechanoenzymes. Curr. Opin. Cell Biol. *13*, 454–460.

Delettre, C., Griffoin, J.M., Kaplan, J., Dollfus, H., Lorenz, B., Faivre, L., Lenaers, G., Belenguer, P., and Hamel, C.P. (2001). Mutation spectrum and splicing variants in the OPA1 gene. Hum. Genet. *109*, 584–591.

Fannjiang, Y., Cheng, W.C., Lee, S.J., Qi, B., Pevsner, J., McCaffery, J.M., Hill, R.B., Basanez, G., and Hardwick, J.M. (2004). Mitochondrial fission proteins regulate programmed cell death in yeast. Genes Dev. *18*, 2785–2797.

Fiala, J.C. (2005). Reconstruct: a free editor for serial section microscopy. J. Microsc. *218*, 52–61.

Frank, S., Gaume, B., Bergmann-Leitner, E.S., Leitner, W.W., Robert, E.G., Catez, F., Smith, C.L., and Youle, R.J. (2001). The role of dynamin-related protein 1, a mediator of mitochondrial fission, in apoptosis. Dev. Cell *1*, 515–525.

Germain, M., Mathai, J.P., McBride, H.M., and Shore, G.C. (2005). Endoplasmic reticulum BIK initiates DRP1-regulated remodelling of mitochondrial cristae during apoptosis. EMBO J. *24*, 1546–1556.

Green, D.R., and Kroemer, G. (2004). The pathophysiology of mitochondrial cell death. Science *305*, 626–629.

Griparic, L., and van der Bliek, A.M. (2001). The many shapes of mitochondrial membranes. Traffic *2*, 235–244.

Griparic, L., van der Wel, N.N., Orozco, I.J., Peters, P.J., and van der Bliek, A.M. (2004). Loss of the intermembrane space protein Mgm1/OPA1 induces swelling and localized constrictions along the lengths of mitochondria. J. Biol. Chem. *279*, 18792–18798.

Herlan, M., Vogel, F., Bornhovd, C., Neupert, W., and Reichert, A.S. (2003). Processing of Mgm1 by the rhomboid-type protease Pcp1 is required for maintenance of mitochondrial morphology and of mitochondrial DNA. J. Biol. Chem. *278*, 27781–27788.

Ishihara, N., Eura, Y., and Mihara, K. (2004). Mitofusin 1 and 2 play distinct roles in mitochondrial fusion reactions via GTPase activity. J. Cell Sci. *117*, 6535–6546.

Jagasia, R., Grote, P., Westermann, B., and Conradt, B. (2005). DRP-1-mediated mitochondrial fragmentation during EGL-1-induced cell death in C. elegans. Nature *433*, 754–760.

James, D.I., Parone, P.A., Mattenberger, Y., and Martinou, J.C. (2003). hFis1, a novel component of the mammalian mitochondrial fission machinery. J. Biol. Chem. *278*, 36373–36379.

Karbowski, M., Arnoult, D., Chen, H., Chan, D.C., Smith, C.L., and Youle, R.J. (2004). Quantitation of mitochondrial dynamics by photolabeling of individual organelles shows that mitochondrial fusion is blocked during the Bax activation phase of apoptosis. J. Cell Biol. *164*, 493–499.

Koshiba, T., Detmer, S.A., Kaiser, J.T., Chen, H., McCaffery, J.M., and Chan, D.C. (2004). Structural basis of mitochondrial tethering by mitofusin complexes. Science *305*, 858–862.

Lee, Y.J., Jeong, S.Y., Karbowski, M., Smith, C.L., and Youle, R.J. (2004). Roles of the mammalian mitochondrial fission and fusion mediators Fis1, Drp1, and Opa1 in apoptosis. Mol. Biol. Cell *15*, 5001–5011.

Legros, F., Lombes, A., Frachon, P., and Rojo, M. (2002). Mitochondrial fusion in human cells is efficient, requires the inner membrane potential, and is mediated by mitofusins. Mol. Biol. Cell *13*, 4343–4354.

McQuibban, G.A., Saurya, S., and Freeman, M. (2003). Mitochondrial membrane remodelling regulated by a conserved rhomboid protease. Nature *423*, 537–541.

Mironov, A.A., Beznoussenko, G.V., Nicoziani, P., Martella, O., Trucco, A., Kweon, H.S., Di Giandomenico, D., Polishchuk, R.S., Fusella, A., Lupetti, P., et al. (2001). Small cargo proteins and large aggregates can traverse the Golgi by a common mechanism without leaving the lumen of cisternae. J. Cell Biol. *155*, 1225–1238.

Neuspiel, M., Zunino, R., Gangaraju, S., Rippstein, P., and McBride, H.M. (2005). Activated Mfn2 signals mitochondrial fusion, interferes with Bax activation and reduces susceptibility to radical induced depolarization. J. Biol. Chem. *26*, 25060–25070.

Nicholls, P., Hildebrandt, V., Hill, B.C., Nicholls, F., and Wrigglesworth, J.M. (1980). Pathways of cytochrome c oxidation by soluble and membrane-bound cytochrome aa3. Can. J. Biochem. *58*, 969–977.

Olichon, A., Baricault, L., Gas, N., Guillou, E., Valette, A., Belenguer, P., and Lenaers, G. (2003). Loss of OPA1 perturbates the mitochondrial inner membrane structure and integrity, leading to cytochrome c release and apoptosis. J. Biol. Chem. *278*, 7743–7746.

Otera, H., Ohsakaya, S., Nagaura, Z., Ishihara, N., and Mihara, K. (2005). Export of mitochondrial AIF in response to proapoptotic stimuli depends on processing at the intermembrane space. EMBO J. *24*, 1375–1386.

Petronilli, V., Penzo, D., Scorrano, L., Bernardi, P., and Di Lisa, F. (2001). The mitochondrial permeability transition, release of cytochrome c and cell death. Correlation with the duration of pore openings in situ. J. Biol. Chem. *276*, 12030–12034.

Santel, A., and Fuller, M.T. (2001). Control of mitochondrial morphology by a human mitofusin. J. Cell Sci. *114*, 867–874.

Santel, A., Frank, S., Gaume, B., Herrler, M., Youle, R.J., and Fuller, M.T. (2003). Mitofusin-1 protein is a generally expressed mediator of mitochondrial fusion in mammalian cells. J. Cell Sci. *116*, 2763–2774.

Satoh, M., Hamamoto, T., Seo, N., Kagawa, Y., and Endo, H. (2003). Differential sublocalization of the dynamin-related protein OPA1

isoforms in mitochondria. Biochem. Biophys. Res. Commun. *300*, 482–493.

Scaffidi, C., Fulda, S., Srinivasan, A., Friesen, C., Li, F., Tomaselli, K.J., Debatin, K.M., Krammer, P.H., and Peter, M.E. (1998). Two CD95 (APO-1/Fas) signaling pathways. EMBO J. *17*, 1675–1687.

Scorrano, L., and Korsmeyer, S.J. (2003). Mechanisms of cytochrome c release by proapoptotic BCL-2 family members. Biochem. Biophys. Res. Commun. *304*, 437–444.

Scorrano, L., Ashiya, M., Buttle, K., Weiler, S., Oakes, S.A., Mannella, C.A., and Korsmeyer, S.J. (2002). A distinct pathway remodels mitochondrial cristae and mobilizes cytochrome c during apoptosis. Dev. Cell *2*, 55–67.

Scorrano, L., Oakes, S.A., Opferman, J.T., Cheng, E.H., Sorcinelli, M.D., Pozzan, T., and Korsmeyer, S.J. (2003). BAX and BAK regulation of endoplasmic reticulum Ca^{2+}: a control point for apoptosis. Science *300*, 135–139.

Smirnova, E., Griparic, L., Shurland, D.L., and van der Bliek, A.M. (2001). Dynamin-related protein Drp1 is required for mitochondrial division in mammalian cells. Mol. Biol. Cell *12*, 2245–2256.

Sugioka, R., Shimizu, S., and Tsujimoto, Y. (2004). Fzo1, a protein involved in mitochondrial fusion, inhibits apoptosis. J. Biol. Chem. *279*, 52726–52734.

Sweitzer, S.M., and Hinshaw, J.E. (1998). Dynamin undergoes a GTP-dependent conformational change causing vesiculation. Cell *93*, 1021–1029.

Wang, X. (2001). The expanding role of mitochondria in apoptosis. Genes Dev. *15*, 2922–2933.

Wei, M.C., Lindsten, T., Mootha, V.K., Weiler, S., Gross, A., Ashiya, M., Thompson, C.B., and Korsmeyer, S.J. (2000). tBID, a membrane-targeted death ligand, oligomerizes BAK to release cytochrome c. Genes Dev. *14*, 2060–2071.

Wei, M.C., Zong, W.X., Cheng, E.H., Lindsten, T., Panoutsakopoulou, V., Ross, A.J., Roth, K.A., MacGregor, G.R., Thompson, C.B., and Korsmeyer, S.J. (2001). Proapoptotic BAX and BAK: a requisite gateway to mitochondrial dysfunction and death. Science *292*, 727–730.

Yoon, Y., Krueger, E.W., Oswald, B.J., and McNiven, M.A. (2003). The mitochondrial protein hFis1 regulates mitochondrial fission in mammalian cells through an interaction with the dynamin-like protein DLP1. Mol. Cell. Biol. *23*, 5409–5420.

Youle, R.J., and Karbowski, M. (2005). Mitochondrial fission in apoptosis. Nat. Rev. Mol. Cell Biol. *6*, 657–663.

Cell Death and Differentiation (2006) 13, 1833–1834
© 2006 Nature Publishing Group All rights reserved 1350-9047/06 $30.00
www.nature.com/cdd

News and Commentary

To fuse and to protect. A novel role for CED-9 in mitochondrial morphology reveals an ancient function

S Cipolat[1] and L Scorrano*,[1]

[1] Dulbecco-Telethon Institute, Venetian Institute of Molecular Medicine, Via Orus 2, Padova 35129, Italy
* Corresponding author: L Scorrano, Dulbecco-Telethon Institute, Venetian Institute of Molecular Medicine, Via Orus 2, Padova 35129, Italy. Tel: +39 049 792 3221; Fax +39 049 792 3271; E-mail: luca.scorrano@unipd.it

Cell Death and Differentiation (2006) **13,** 1833–1834.
doi:10.1038/sj.cdd.4402005; published online 14 July 2006

Imagine that while walking in your Campus behind an old, gigantic tree you find the Magic Lamp; imagine that the Genius of the Lamp is willing to satisfy only one of your (many) desires; imagine that you are a scientist, that you are working on apoptosis, more specifically on the role of mitochondria in cell death. Well, won't you ask the Genius to let you know 'Why and when'? Why did Nature choose mitochondria as the main actor of programmed cell death, and when during evolution this happened? Of course you would, but unfortunately Geniuses are on strike for the next two hundred years (at least here in Italy...). So you must stick to Science and look out for experimental evidences that can provide an answer to your question. Apparently this is your lucky day, because a recent paper by Seamus Martin and co-workers is here to help you out.[1]

Mitochondria are key organelles in apoptosis. In mammalian cells they orchestrate the amplification of death signals by releasing cytochrome *c* into the cytosol, where it forms the so-called apoptosome together with the adapter Apaf-1 and procaspase 9. This complex, in cooperation with other factors released from mitochondria, is required for the complete activation of effector caspases.[2] Anti- and proapoptotic members of the Bcl-2 family negatively or positively regulate this release, ultimately defining the fate of the cell.[3] The fine mechanisms controlling the egress of cytochrome *c* remain a matter of intense debate. A current model postulates that the 'BH3-only' subset of proapoptotic Bcl-2 family members senses death signals and transmits them to the 'multidomain' proapoptotics like Bax and Bak. These ultimately oligomerize in the mitochondrial outer membrane to generate pathways that grant the physical efflux of cytochrome *c* and of the other mitochondrial apoptotic cofactors. While such a model appears substantiated by several evidences, how antiapoptotic Bcl-2 family members oppose their proapoptotic counterparts is less clear. It has been proposed that Bcl-2 and Bcl-X_L sequester BH3-only molecules, preventing activation of the multidomain proapoptotics.[4] Alternatively, antiapoptotic proteins could keep Bax and Bak in an inactive conformation, antagonizing binding to the incoming BH3-only proteins.[5] Even more debated is how the activation of multidomain proapoptotics results in the release of cytochrome *c*. It remains unclear whether this process involves only the outer membrane, or also changes in the inner; whether it requires additional mitochondrial cofactors, or Bax and/or Bak are self-sufficient; whether it requires, or it is followed by mitochondrial dysfunction.[3]

This picture appears complex enough, but as usual it represents just our attempt to simplify the much more complicated pathways organized by Nature. To deepen our understanding of these mechanisms, we think that we should try to look backwards, that is we should understand two unresolved issues: what was the ancient function of the members of the Bcl-2 family, and why they ultimately chose mitochondria as their playground. These two key questions are probably intermingled. A recent paper by S Martin and co-workers suggest a 'morphological' answer to these conundrums.[1]

We should start by pointing out that the mammalian system is rather peculiar. If we go back to simpler multicellular organisms like *Caenorhabditis elegans* and *Drosophila melanogaster*, we would see that despite conservation of Bcl-2 family members, mitochondria appear to be dispensable or just platforms where the reactions that regulate apoptosis happen to take place. For example, in *C. elegans* the BH-3 only orthologue EGL-1 displaces CED-4, the Apaf-1 homologue, from CED-9, which is homologue to Bcl-2.[6] Similarly, in *Drosophila* the proapoptotic Debcl and the antiapoptotic Buffy/dBorg-2 Bcl-2 family members appear to play a limited role in a cell death pathway mainly regulated by inhibitor of apoptosis (IAP) proteins.[7] Nevertheless, mitochondria undergo previously overlooked changes in their shape during developmental apoptosis in the worm as well as following expression of Debcl in *Drosophila* cells. Jagasia *et al.*[8] showed that the fragmentation of the mitochondrial network during developmental apoptosis of *C. elegans* is enhanced by EGL-1 and independent of caspase activation, suggesting that it occurs before of, or simultaneously to caspase activation. Expression of Debcl in *Drosophila* as well as in mammalian cells causes a similar fragmentation of the mitochondrial network.[9] These probably represent the only mitochondrial changes that we found conserved during apoptosis of invertebrate and mammalian cells. Early in the course of programmed cell death, mammalian mitochondria coordinately fragment and undergo a reorganization of their cristae, called 'remodelling', in order to release most of their cytochrome *c* content.[10–12] Mitochondrial fission is an early trait of apoptosis, occurring simultaneously to Bax translocation from the cytosol, and before activation of caspases.[10] The fragmented appearance of mitochondria is caused by a combination of activation of the fission machinery and inhibition of the fusion one.[13–15]

Mitochondrial shape results from the equilibrium between fusion and fission processes. Fusion is mediated by mitofusin

(Mfn) 1 and 2, large GTPases of the outer membrane; and by Opa1, a GTPase anchored to the inner membrane.[16,17] Conversely, fission results from the translocation of the dynamin-related protein Drp-1 from the cytosol to the outer mitochondrial membrane, where it reportedly binds to hFis1.[18,19] The importance of these proteins and of mitochondrial shape changes in regulating mammalian apoptosis, is substantiated by genetic evidences showing that inhibition of fission, as well as promotion of fusion counteract apoptosis by intrinsic, mitochondria utilizing stimuli (reviewed in Youle and Karbowski[20]).

While mitochondrial fragmentation during apoptosis appears to be conserved from worms to mammals, it remains unclear whether other Bcl-2 orthologues, besides EGL-1, display any effect on morphology of the organelle. A positive answer to this question would open the possibility that regulators of cell death have at least some functional similarities with regulators of mitochondrial shape. This conclusion would be reinforced by recent experiments performed in yeast. Programmed cell death of yeast is controlled by the Drp-1 orthologue dnm1p and fis1p (the homologue of mammalian Fis1) blocks this pro-death activity of dnm1p. Unexpectedly, human Bcl-2 and Bcl-X_L can substitute fis1p in this process.[21] Delivani *et al.* show that CED-9 can impinge on the morphology of mitochondrial network in several mammalian cell types, where its expression results in clustering of the organelle. On the other hand, CED-9 does not block mitochondrial outer membrane permeabilization and apoptosis induced by enforced Bax oligomerization in HeLa cells. CED-9 conversely retains its ability to suppress apoptosis mediated by CED-4-dependent activation of CED-3 also in the context of these mammalian cells. As human Bcl-2 inhibits developmental apoptosis in *C. elegans*, it is reasonable to think that the apoptotic pathway diverged during evolution, acquiring specific mammalian features (like release of cytochrome *c*) that are not blocked by early regulators like CED-9.[6] What conversely appears to be conserved between CED-9 and Bcl-X_L is their ability to change mitochondrial morphology. CED-9, as well as Bcl-X_L promote fusion and antagonize fragmentation associated with apoptosis. CED-9 does not block death induced by actinomycin or daunorubicin, suggesting that fission is not required for apoptosis by these stimuli. Fusion induced by CED-9 is efficiently antagonized by coexpression of EGL-1. As this occurs in the absence of cytochrome *c* release and apoptosis, it is reasonable to speculate that EGL-1 might fragment worm mitochondria as a consequence of the inhibition of CED-9 pro-fusion activity rather than of the induction of apoptosis. In the search for a molecular mechanism, Delivani *et al.* show that CED-9, Bcl-2 and Bcl-X_L physically interact with Mfn2. This interaction could provide an explanation for the observed pro-fusion effect of the antiapoptotic Bcl-2 family members of worm and mammals. Genetic experiments could be designed to test whether Mfn2 is required for fusion promoted by CED-9. These would allow unraveling a specific pro-fusion activity of CED-9, which is independent from its interaction with Mfn2. This possibility is further suggested by the notion that the bulk of mitochondrial fusion is granted by the Opa1-Mfn1 axis,[17] Mfn2 playing a more regulatory role.[22] Should this be the case, we would have found for the first time a specific, additional feature of antiapoptotic Bcl-2 family members conserved throughout evolution: regulation of mitochondrial morphology. Probably we should then consider that the primordial role of this CED-9/Bcl-2 family was to regulate morphology of the mitochondrial network, and that the control of apoptosis emerged as an additional feature later during evolution. The work by Martin and co-workers opens our eyes on this rather unexpected possibility: proteins were not made up for what we think they are for.

1. Delivani P *et al.* (2006) Mol Cell 21: 761–773.
2. Green DR and Kroemer G (2004) Science 305: 626–629.
3. Danial NN and Korsmeyer SJ (2004) Cell 116: 205–219.
4. Cheng EH *et al.* (2001) Mol Cell 8: 705–711.
5. Willis SN *et al.* (2005) Genes Dev 19: 1294–1305.
6. Lettre G and Hengartner MO (2006) Nat Rev Mol Cell Biol. 7: 97–108.
7. Kornbluth S and White K (2005) J Cell Sci 118: 1779–1787.
8. Jagasia R *et al.* (2005) Nature 433: 754–760.
9. Igaki T *et al.* (2000) Proc Natl Acad Sci USA 97: 662–667.
10. Frank S *et al.* (2001) Dev Cell 1: 515–525.
11. Scorrano L *et al.* (2002) Dev Cell 2: 55–67.
12. Germain M *et al.* (2005) EMBO J 24: 1546–1556.
13. Karbowski M *et al.* (2004) J Cell Biol 164: 493–499.
14. Arnoult D *et al.* (2005) Curr Biol 15: 2112–2118.
15. Arnoult D *et al.* (2005) J Biol Chem 280: 35742–35750.
16. Chen H *et al.* (2003) J Cell Biol 160: 189–200.
17. Cipolat S *et al.* (2004) Proc Natl Acad Sci USA 101: 15927–15932.
18. Smirnova E *et al.* (2001) Mol Biol Cell 12: 2245–2256.
19. James DI *et al.* (2003) J Biol Chem 278: 36373–36379.
20. Youle RJ and Karbowski M (2005) Nat Rev Mol Cell Biol 6: 657–663.
21. Fannjiang Y *et al.* (2004) Genes Dev 18: 2785–2797.
22. Ishihara N, Eura Y and Mihara K (2004) J Cell Sci 117: 6535–6546.

OPA1 participates in differentiation of embryonic stem cells into cardiomyocytes.

Sara Cipolat and Luca Scorrano

Dulbecco-Telethon Institute, Venetian Institute of Molecular Medicine, Padova, Italy

Summary

The dynamin-related protein OPA1 regulates adult homeostasis by controlling mitochondrial fusion and apoptosis, but it is essential also during embryogenesis. The lack of *Opa1* impairs early stages of embryonic development: *Opa1*$^{-/-}$ embryos die during the late gastrulation stage, showing a fundamental role for OPA1 in early embryonic survival. Genetic manipulation and *in vitro* differentiation of ES cells allows to pinpoint individual differentiation processes that are affected by manipulation of a single gene, without the compensatory or adverse influence of the whole animal environment. To address whether OPA1 regulates a genetic pathway that control embryonic development, we studied whether ablation of OPA1 influenced differentiation of embryonic stem (ES) cells *in vitro*. A murine ES cell where *Opa*1 has been gene-trapped after exon 5b had reduced OPA1 levels. These did not affect mitochondrial function or pluripotency, yet they resulted in fragmented mitochondrial network and in a surprising selective block in cardiomyocyte differentiation, while neuronal one was completely unaffected.

Introduction

Mitochondria are essential organelles for life and death of the cell: they produce most of the cellular ATP (Danial et al., 2003), regulate cytosolic Ca^{2+} signalling (Rizzuto et al., 2000), and integrate and amplify different apoptotic stimuli (Green and Kroemer, 2004). Defects in any of these processes can be detrimental for the cell: several diseases are indeed consequences of, or are aggravated by, mitochondrial dysfunction (Schapira, 2006). This functional versatility of mitochondria is mirrored by their complex and dynamic morphology, controlled by a growing family of "mitochondria-shaping" proteins that regulate fusion and fission events. OPA1 is the only component of this family located in the inner mitochondrial membrane (Olichon et al., 2002) and is mutated in dominant optic atrophy (Alexander et al., 2000). In mammalian cells OPA1 plays two genetically distinct roles in promoting mitochondrial fusion by cooperating with MFN1 (Cipolat et al., 2004), a large GTPase of the outer mitochondrial membrane; and in regulating apoptosis, controlled by the mitochondrial rhomboid protease PARL (Frezza et al., 2006; Cipolat et al., 2006). Thus, OPA1 affects complex cellular functions, as substantiated in overexpression studies showing a role for this protein in movement of leukocytes (Campello et al., 2006) and formation of dendritic spines (Li et al., 2004). Furthermore, homozygous mutant mice die in uterus at 13.5 dpc, with first notable developmental delay at E 8.5, showing that OPA1 is required for a complete embryonic development. (Davies et al., 2007; Alavi et al., 2007). Analysis of *Mfn1* and *Mfn2* knockout mice demonstrated that they die in midgestation, similar to *Opa1* homozygous mutant mice (Chen et al., 2003), demonstrating an essential role of mitochondria-shaping protein in early development. Moreover it has been recently demonstrated that levels of expression of mitochondria-shaping proteins are tightly regulated during *in vitro* differentiation of murine embryonic stem cells into cardiomyocytes (Chung et al., 2007)

We therefore reasoned that levels of OPA1 are likely to affect development, by regulating mitochondrial fusion or apoptosis. We addressed the effects of OPA1 ablation during *in vitro* differentiation of ES cells into cardiac and neuronal lineages using a hanging-drop differentiation system (Keller, 1995)

Results

Characterization of Opa1^{gt} *ES cells*

In order to address whether *Opa1* can be a candidate gene that regulates stem cells self-renewal and differentiation, we analyzed an ES cell line where *Opa1* had been gene trapped (*Opa1*^{gt}).

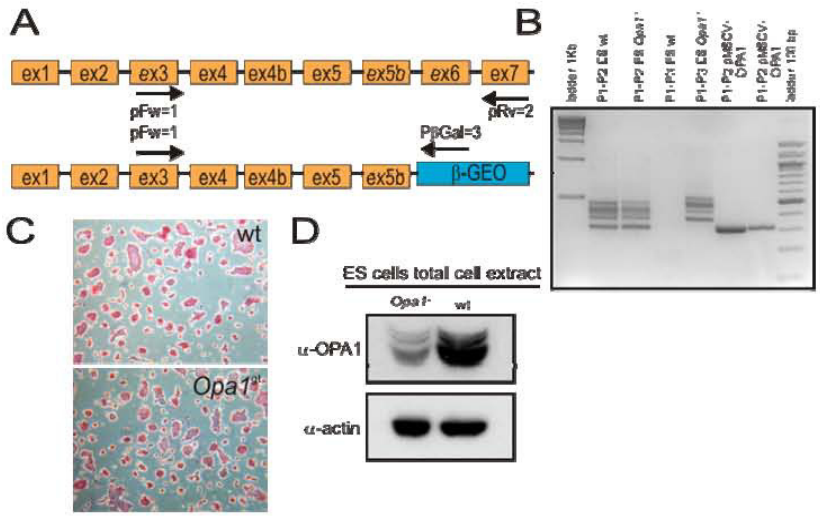

Figure 1: ***Characterization of Opa1^{gt} ES cells***. (**A**) Schematic representation of the 5' end of *Opa1* gene in wild type and gene-trapped allele. Insertion of the βGEO cassette and position of the relative primers are indicated. (**B**) 1% agarose gel of RT-PCR products of wt and *Opa1*^{gt} transcripts, using the indicated primers. (**C**) Staminality of *wt* and *Opa1*^{gt} ES cells. Representative images of *wt* and *Opa1*^{gt} ES cells stained with alkaline phosphatase, a marker of undifferentiated status. (**D**) Wt and *Opa1*^{gt} ES cells were lysed and equal amounts of protein (30 ug) were separated by SDS-PAGE and immunoblotted with the indicated antibodies.

The *Opa1* gene trapped cell line XK328 was generated by the Sanger Institute Gene Trap Resource (SIGTR). The gene trapped cell line was derived from the parental 129P2 (formerly 129/Ola) ES cell line, subclone E14Tg2A.4, upon viral transduction with a specific gene trapping vector followed by G418 selection and sequence confirmation.

Upon thawing the XK328 cell line, we performed RT-PCR to confirm that the cell line contains the insertion in the *Opa1* gene and to detect the exact position of this insertion. The RT-PCR reaction was designed to detect the fusion transcript generated by splicing of endogenous gene exons upstream of the insertion site to the gene trap vector. For this purpose, we designed three primers: one forward primer positioned in exon 3 and two reverse primers, complementary to *Opa1* exon 7 and the beginning of the βGEO cassette, respectively (Figure 1, A). From the analysis of the RT-PCR results appeared that all OPA1 mRNAs variant have been gene trapped by the βGEO cassette (Figure 1, B), resulting in an *Opa1*$^{+/-}$ genotype and in 50% down regulation of the OPA1 levels of expression, as confirmed by immunoblotting (Figure 1, D).

Both wt and *Opa1*^{gt} ES cells displayed good level of alkaline phosphatase staining, a specific maker of totipotency (Figure 1, C). We could conclude that both cell lines were undifferentiated and maintain pluripotent properties.

Cardiomyocytes differentiation capacity of Opa1^{gt} ES

We compared the differentiation potential into cardiomyocytes of the *Opa1*^{gt} ES cell line with the relative *wt*. Using the hanging drop technique in the presence of specifically tested serum it was possible to follow changing in morphology of derived EB and detect their beating activity (Fig 2, A). Single *wt* and *Opa1*^{gt} differentiated EBs were plated (1 EB/well) and the number of wells containing beating areas were counted and normalized to the total number of wells containing EBs. Interestingly, after 14 days of differentiation *Opa1*^{gt} ES cells displayed a decreased capacity to differentiate into beating embryoid bodies (EBs). While almost all the EBs derived from the E14Tg2A.4 wt cell line showed a beating activity after 14 days, it was impossible to detect beating activity in EB derived from *Opa1*^{gt} cell line (Fig. 2, B). We confirmed our results by repeating the differentiation procedure several times and by checking beating activity at prolonged time point (data not shown). Moreover, *Opa1*^{gt} cardiac differentiated EBs did not overexpress MF-20, a late marker of cardiomyocytes differentiation, compared with the relative wt differentiated EB, 14 days after differentiation, while they retained decreased OPA1 level of expression (Fig. 2, C).

These preliminary results indicated that OPA1 is a good candidate to regulate differentiation of ES cells *in vitro*.

Neural differentiation capacity of Opa1^{gt} ES

Since OPA1 had a crucial role on controlling differentiation of ES cells in cardiomyocytes we

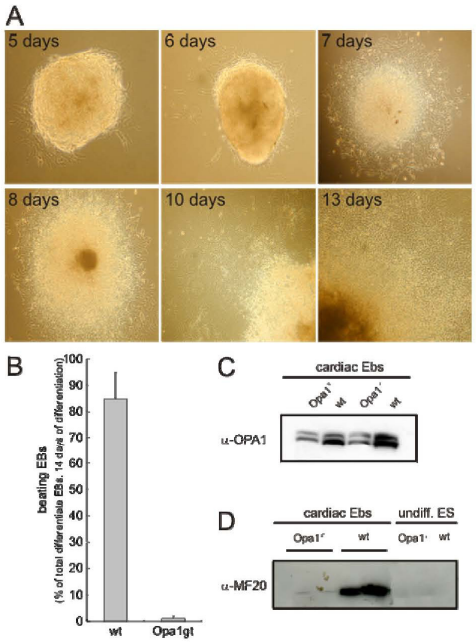

Figure 2: **Cardiomyocyte differentiation of wt and *Opa1*^{gt} ES cells.** (**A**) Representative images of wt Embryoid bodies during cardiac differentiation. (**B**) Effect of *Opa1*^{gt} on cardiomyocyte differentiation. Single wt and *Opa1*^{gt} differentiated EBs were plated (1 EB/well) and the number of wells containing beating areas were counted and normalized to the total number of wells containing EBs.. Data represent average ± SE of 7 independent experiments. (**C**) Wt and *Opa1*^{gt} cardiac differentiated EBs and the relative undifferentiated ES cells were lysed and equal amounts of protein (30 µg) were separated by SDS-PAGE and immunoblotted with the indicated antibodies

hypothesized that it could be a candidate gene that regulates stem cells self-renewal and differentiation. We decided to investigate whether the modulation of OPA1 expression levels could influence the differentiation of embryonic stem cells into a different lineage, the neuronal one. In order to analyze the role of OPA1 in controlling *in vitro* neuronal differentiation of ES cells, we compared the ability of *Opa1*^{gt} ES cells and the relative wt to differentiate in neuronal EBs using the hanging drop method in the presence of retinoic acid (Figure. 3, A). Single *wt* and *Opa1*^{gt} differentiated EBs, obtained using the hanging drop method in the presence of retinoic acid (Okada et al., 2004), were plated (1 EB/well) and the number of wells containing neuronal-like EBs were counted and normalized to the total number of wells containing EBs. *Opa1*^{gt} and the relative wt ES cell displayed comparable ability to differentiate into neuronal like EB after 14 days of differentiation (Fig 3, B) and both overexpressed a late marker of neuronal differentiation, β-tubulin isotype III (Fig 3, C).

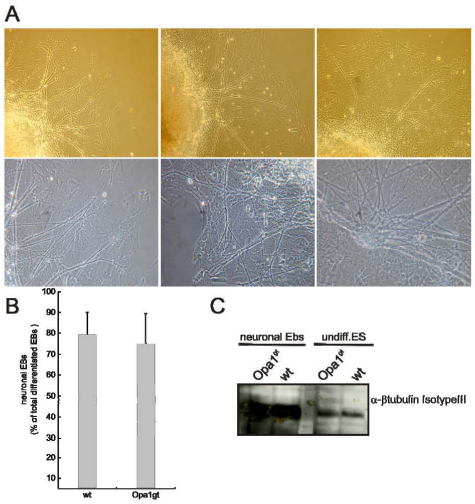

Figure 3: **Neuronal differentiation of wt and *Opa1*^{gt} ES cells.** (**A**) Representative images of wt EBs during neuronal differentiation. (**B**) Effect of *Opa1*^{gt} on neuronal differentiation. Single wt and *Opa1*^{gt} differentiated EBs were plated (1 EB/well) and the number of wells containing neuronal-like EBs were counted and normalized to the total number of wells containing EBs. Data represent average ± SE of 7 independent experiments. (**C**) Wt and *Opa1*^{gt} neuronal differentiated EBs and the relative undifferentiated ES cells were lysed and equal amounts of protein (30 ug) were separated by SDS-PAGE and immunoblotted with β-tubulin antibody (marker of neuronal differentiation)

Molecular mechanism by which levels of OPA1 influence differentiation into cardiomyocytes

Since *Opa1*^{gt} ES cells displayed a decreased capacity to differentiate into beating cardiomyocytes, while they retained a normal neuronal differentiation potential we wished to understand why the down regulation of OPA1 levels specifically impairs cardiomyocytes differentiation. It has been recently demonstrated that differentiation of embryonic stem cells into energetically competent, contracting cardiomyocytes requires a switch from an anaerobic, glycolytic metabolism to a mitochondrial oxidative one (Chung et al., 2007). We wanted to verify whether the absence of cardiomyocytes differentiation in *Opa1*^{gt} ES cells could be caused by a deficit in mitochondrial function. We measured mitochondrial oxygen consumption in *Opa1*^{gt} and the relative wt embryonic stem cells permeabilzed in the presence of digitonin. Basal (state 4), ADP-stimulated (state 3) and maximal (uncoupled) respiratory rates (JO2) of wt and *Opa1*^{gt} cells were comparable (Fig 4, A). Moreover, uptake of the potentiometric dye tetramethyl rhodamine methyl ester (TMRM) was unaltered and real-time imaging of mitochondrial TMRM fluorescence in

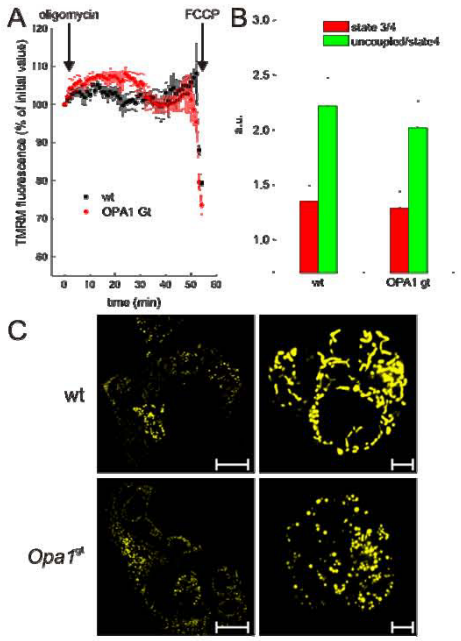

Figure 4: **Analysis of mitochondrial function and morphology in wt and *Opa1*^{gt} ES cells** (**A**) Cells of the indicated genotype were loaded with 10 nM TMRM and real time imaging sequences were acquired. Quantitative analysis of TMRM fluorescence changes over mitochondrial region. Data represent mean ± SE of 3 independent experiments. Where indicated (arrows), 2 μM oligomycin and 2 μM FCCP were added. (**B**) Quantitative analysis of oxygen consumption in permeabilizated embryonic stem cells of the indicated genotype. ES cells were incubated with succinate in the presence of rotenone into an oxygen electrode chamber. Data represent average ± SE of 5 independent experiments. (**C**) Representative confocal images of wt and *Opa1*^{gt} ES electroporated with mtYFP. Images on the left side are pictures acquired with a 60X objective, on the right, magnified (3X) pictures. Bars, 10 μm on the left, 3 μm on the right.

response to oligomycin showed no depolarization (Fig 4, B). Thus, *Opa1*^{gt} did not display primary respiratory defects or latent mitochondrial dysfunction.

It has been recently demonstrated that the genetic reprogramming associated with cardiac differentiation of stem cells is reflected in the modulation of genes involved in mitochondrial structural organization and network formation (Chung et al., 2007). Since OPA1 levels of expression regulate mitochondrial morphology, we compared mitochondrial structure in *Opa1*^{gt} ES and the relative wt. We analyzed morphology of ES cells electroporated with a mitochondrially targeted yellow fluorescence protein (mtYFP) by using confocal microscopy (Fig 4, C, left panel). Mitochondria of undifferentiated wt and *Opa1*^{gt} ES cells appeared globular or rod-shaped, dispersed through the cytosol. High power magnification revealed that mitochondria of *Opa1*^{gt} ES appeared more fragmented and shorter compare with the relative wt ES cells (Fig. 4, C, right panel).

Discussion

Here we describe that ES cells where *Opa1* has been gene trapped are unable to differentiate into cardiomyocytes, while they retain their normal neuronal differentiation potential. Our preliminary in vitro analysis reveals that specific differentiation pathways are affected by the ablation of 50% of a mitochondria-shaping protein.

Gene trapping is a method of randomly generating embryonic stem cells with well-characterized insertional mutations, by inserting a gene trap construct into an intronic or coding region of genomic DNA with a promoter-less reporter gene and a selectable marker used to identify cell lines where the vector has successfully interrupted a gene. In our system, the insertion of the promoter-less reporter cassette β-GEO occurred after the exon 5b of *Opa1* gene, resulting in the ablation of one of the two alleles. The application of the gene trapping technique in ES cells and the subsequent *in vitro* differentiation of these pluripotent cells permits modification of the mammalian genome without concern for adverse effects on overall embryonic development. For this reason the *Opa1*^{gt} demonstrated to be a good tool to study the possible role of OPA1 in controlling developmental differentiation.

The comparison of the differentiation potential into cardiomyocytes and neurons of the *Opa1*^{gt} ES cell line with its wt counterpart showed that down regulation of OPA1 decreased capacity to differentiate into contractile embryoid bodies (EBs), while it did not alter the ability to differentiate into neuronal-like EBs. These preliminary results indicated that OPA1 is a good candidate to regulate differentiation of ES cells *in vitro*. We reasoned that one of the possible causes of this developmental block could reside in functional or morphological alterations in Opa1-deficient mitochondria. Confocal microscopy showed increased fragmentation in the *Opa1*^{gt} ES cells, while basal and stimulated respiration, as well as basal or stressed membrane potential resulted normal. This morphological derangement could be the explanation for the impaired cardiomyocytes differentiation potential: disruption of mitochondrial network, or an increased fragmentation leads to a dramatic reduction in the number of beating embryoid bodies and sarcomere content of differentiating cardiomyocytes (Chung et al., 2007).

The data presented here, albeit preliminary, suggest that mitochondria-shaping proteins are also essential in certain differentiation pathways. To address whether the impairment in cardiomyocytes differentiation is specifically due to the down regulation of OPA1 levels, we will re-express the protein in the *Opa1*^{gt} cells at the same level of the relative wt cells. Clones of *Opa1*^{gt} ES cells stable overexpressing OPA1 will be differentiated *in vitro* ability to differentiate in

cardiomyocytes will be compared with the relative wt ES cells. Moreover we wish to analyze at which stage of the cardiomyocytes differentiation pathway OPA1 plays a role. The differentiation of mouse ES cells to cardiomyocytes *via* EBs recapitulates many of the developmental profiles seen in normal fetal heart development , with the orderly appearance of cardiac-associated gene products, including transcription factors (Nkx2.5, GATA 4) and contractile proteins (α-MHC, MLC). In order to understand whether cardiac differentiation in *Opa1*^{gt} ES cells is blocked at an early or a late stage, we will analyze the expression of specific markers of differentiation stages in EBs derived from *Opa1*^{gt} ES cells.

Experimental procedures

ES cells culture and electroporation

Opa1^{gt} and the relative E14Tg2A.4 murine embryonic stem cells were cultured on top of a monolayer of STO feeders at a density of $1x10^5$ cells per square centimeter. The ES cell culture medium was renewed daily, and the ES cells were subcultured onto new feeders every 2 to 3 days. Culture medium for the undifferentiated ES cells consisted of Dulbecco's Modified Eagle Medium with high glucose (Invitrogen), supplemented with 15% heat-inactivated FCS (ES cells defined, Hyclone SH30070), 1 mM sodium pyruvate (Invitrogen), 2 mM glutamine (Invitrogen), 1X nonessential amino acids (Invitrogen), 0.1 mM β-mercaptoethanol, and 10^3U/ml leukemia inhibitory factor (ESGRO 10^7 Units/mL, Chemicon International,Temecula, CA, USA; cat. no. ESG1107).
For electroporation, 1 $X10^7$ ES cells were seeded into a 4 mm electroporation cuvette (Biorad 165-2088) with 0.5 ml medium and 10µg DNA, electroporated twice at 200 V, 960 µF.
Alkaline phosphatase staining of *Opa1*^{gt} and E14Tg2A.4 ES cells (grown in the absence of feeder layer for two days on 60mm Petri dish) was performed using the AP staining kit (Chemicon international SCR004) according to Manifacturer's instruction.

Preparation of feeder layers

STO cells were cultured in Dulbecco's Modified Eagle's Medium (DMEM) (Gibco) supplemented with 10% fetal bovine serum (FBS) (Gibco), 50 U/mL Penicillin, 50 µg/mL Streptomycin, 100 µM non essential aminoacids (MEM, Gibco/Invitrogen) and 2 mM glutamine (Gibco). To prepare feeder layer, STO cells at confluence stage were treated with 0.01 mg/ml of Mitomycin *c* (Sigma, M-0503) to inhibit the division for 30 minutes. Cells were trypsinized, collected and plated at a density of $5x10^4$ cells per square centimetre onto gelatin-coated tissue culture plates. To prepare gelatin-coated tissue culture dishes, a thin layer of 0.1% gelatine solution (Sigma; G9391) was distributed to cover the bottom of the plate and incubate 1 hr at room temperature.

Western blot and antibodies

For analyses of protein of whole cell lysates ES cell or EBs were harvested and disrupted in RIPA buffer [150 mM NaCl, 1% (V/V) Nonidet P-40 (NP40), 0.25% (w/V) deoxycholate, 1 mM EDTA, 50 mM Tris, pH 7.4] in the presence of complete protease-inhibitor mixture (5 µg/ml aprotinin, 5 µg/ml leupeptin, 5 µg/ml pepstatin, Sigma), kept on ice for 30 min and centrifuged for 10 min at 15,000 g to remove nuclei, membranes and unsolubilized proteins. The concentration of proteins in solution was estimated with by using the BCA™ assay (Pierce). Equal amounts of proteins from undifferentiated *Opa1*^{gt} and wt ES and differentiated EBs were dissolved in gel loading buffer (NuPAGE, Invitrogen) and electrophoresed. For immunoblotting experiments, the following antibodies were employed: monoclonal anti-OPA1 (1:500, BD Biosciences), anti-tubulin isotype III (Sigma; cat. no. T-8660), anti-sarcomeric myosin (MF-20, monoclonal supernatant obtained from the Developmental Studies Hybridoma Bank, Iowa, IA, USA), horseradish peroxidase conjugated secondary antibodies (Amersham) were used followed by detection by chemiluminescence (Amersham).

Differentiation procedure

For in vitro differentiation, ES cells were cultured in DMEM with high glucose (Invitrogen), supplemented with 15% heat-inactivated FCS (tested for differentiation of Embryo Bodies, EuroClone, Celbio), 1 mM sodium pyruvate, 2 mM glutamine, 1X nonessential amino acids, 0.1 mM β-mercaptoethanol. ES cells were differentiated by EB formation. As a standard method for EB formation the hanging drop method was performed. Hanging drops (one drop of 35 µl contains 100 cells) were placed on the lid of a 100mm bacterial grade dish filled with a solution composed of 30% FBS, 70% sterile water, and incubated a 37 °C, 5% CO_2 for 2 days. The formed EBs were collected and transferred to a 60mm bacterial-grade dish. After 3 days of culture in suspension 30-50 EBs were transferred to a 60mm culture dish or single EBs was placed in each well of a 24-well plate. Differentiation medium was changed every two days. Periodically, microscopy was performed to detect the generation of spontaneously contracting cells in the population derived from an EB in each well. For the neuronal differentiation procedure, retinoic acid (Sigma; cat. no. R-2625) was added to the differentiation medium to a final concentration of 10^{-6} M from the fifth day of differentiation.

Confocal imaging

For imaging of mitochondrial network, $6x10^4$ cells of the indicated genotype were seeded onto 25 mm-round glass coverslips and electroporated with the mtYFP. After 24 hrs cells were incubated in Hank's Balanced Salt Solution (HBSS) supplemented with 10 mM Hepes and coverslips were placed on the stage of a Nikon Eclipse TE300 inverted microscope equipped with a spinning-disk Perkin Elmer Ultraview LCI confocal system, a piezoelectric *z*-axis motorized stage (Pifoc) and a Orca ER 12-bit CCD camera (Hamamatsu). Cells expressing mtYFP were excited using the 488 nm line of the He-Ne laser (Perkin Elmer) with exposure times of 50 msec using a 60X 1.4 NA Plan Apo objective (Nikon). For quantitative real-time analysis of changes in mitochondrial membrane potential $6x10^4$ ES cells of the indicated genotype grown on 24 mm round coverslips were incubated with 10 nM TMRM (Molecular Probes) and 2 µg/mL CsH, a P-glycoprotein inhibitor, dissolved in HBSS for 30 minutes at 37°C and subsequently placed on the stage of an Olympus IMT-2 inverted microscope equipped with a CellR Imaging systems. Sequential images of TMRM fluorescence were acquired every 60 s using exposure times of 30 ms with a 40x, 1.4 NA Plan Apo objective (Olympus) by exciting cells using a 525±20 excitation filter and collecting emitted light using a 570 LP filter. Images were stored for subsequent analysis, background subtraction and normalization which was performed exactly as described in (Frezza et al., 2007).

Mitochondrial functional assay

Mitochondrial oxygen consumption was measured by using a Clarke-type oxygen electrode (Hansatech Instruments). ES cells of the indicated genotype were incubated in experimental buffer (EB, 125 mM KCl, 10 mM Tris-MOPS, 1 mM KPi, 10 µM EGTA-Tris, pH 7.4, 25°C) 5 mM succinate in the presence of 2 µM rotenone.

Reference list:

Alavi,M.V., Bette,S., Schimpf,S., Schuettauf,F., Schraermeyer,U., Wehrl,H.F., Ruttiger,L., Beck,S.C., Tonagel,F., Pichler,B.J., Knipper,M., Peters,T., Laufs,J., and Wissinger,B. (2007). A splice site mutation in the murine Opa1 gene features pathology of autosomal dominant optic atrophy. Brain *130*, 1029-1042.

Alexander,C., Votruba,M., Pesch,U.E., Thiselton,D.L., Mayer,S., Moore,A., Rodriguez,M., Kellner,U., Leo-Kottler,B., Auburger,G., Bhattacharya,S.S., and Wissinger,B. (2000). OPA1, encoding a dynamin-related GTPase, is mutated in autosomal dominant optic atrophy linked to chromosome 3q28. Nat. Genet. *26*, 211-215.

Campello,S., Lacalle,R.A., Bettella,M., Manes,S., Scorrano,L., and Viola,A. (2006). Orchestration of lymphocyte chemotaxis by mitochondrial dynamics. J. Exp. Med. *203*, 2879-2886.

Chen,H., Detmer,S.A., Ewald,A.J., Griffin,E.E., Fraser,S.E., and Chan,D.C. (2003). Mitofusins Mfn1 and Mfn2 coordinately regulate mitochondrial fusion and are essential for embryonic development. J. Cell Biol. *160*, 189-200.

Chung,S., Dzeja,P.P., Faustino,R.S., Perez-Terzic,C., Behfar,A., and Terzic,A. (2007). Mitochondrial oxidative metabolism is required for the cardiac differentiation of stem cells. Nat. Clin. Pract. Cardiovasc. Med. *4 Suppl 1*, S60-S67.

Cipolat,S., de Brito,O.M., Dal Zilio,B., and Scorrano,L. (2004). OPA1 requires mitofusin 1 to promote mitochondrial fusion. Proc. Natl. Acad. Sci. U. S. A *101*, 15927-15932.

Cipolat,S., Rudka,T., Hartmann,D., Costa,V., Serneels,L., Craessaerts,K., Metzger,K., Frezza,C., Annaert,W., D'Adamio,L., Derks,C., Dejaegere,T., Pellegrini,L., D'Hooge,R., Scorrano,L., and De Strooper,B. (2006). Mitochondrial Rhomboid PARL Regulates Cytochrome c Release during Apoptosis via OPA1-Dependent Cristae Remodeling. Cell *126*, 163-175.

Danial,N.N., Gramm,C.F., Scorrano,L., Zhang,C.Y., Krauss,S., Ranger,A.M., Datta,S.R., Greenberg,M.E., Licklider,L.J., Lowell,B.B., Gygi,S.P., and Korsmeyer,S.J. (2003). BAD and glucokinase reside in a mitochondrial complex that integrates glycolysis and apoptosis. Nature *424*, 952-956.

Davies,V.J., Hollins,A.J., Piechota,M.J., Yip,W., Davies,J.R., White,K.E., Nicols,P.P., Boulton,M.E., and Votruba,M. (2007). Opa1 deficiency in a mouse model of autosomal dominant optic atrophy impairs mitochondrial morphology, optic nerve structure and visual function. Hum. Mol. Genet. *16*, 1307-1318.

Frezza,C., Cipolat,S., and Scorrano,L. (2007). Measuring mitochondrial shape changes and their consequences on the mitochondrial involvement during apoptosis. In Mitochondria Practical Protocols, D.Leister and J.M.Herrmann, eds. (Totowa, NJ: Humana Press), pp. 405-420.

Frezza,C., Cipolat,S., Martins,d.B., Micaroni,M., Beznoussenko,G.V., Rudka,T., Bartoli,D., Polishuck,R.S., Danial,N.N., De Strooper,B., and Scorrano,L. (2006). OPA1 Controls Apoptotic Cristae Remodeling Independently from Mitochondrial Fusion. Cell *126*, 177-189.

Green,D.R. and Kroemer,G. (2004). The pathophysiology of mitochondrial cell death. Science *305*, 626-629.

Keller,G.M. (1995). In vitro differentiation of embryonic stem cells. Curr. Opin. Cell Biol. *7*, 862-869.

Li,Z., Okamoto,K., Hayashi,Y., and Sheng,M. (2004). The importance of dendritic mitochondria in the morphogenesis and plasticity of spines and synapses. Cell *119*, 873-887.

Okada,Y., Shimazaki,T., Sobue,G., and Okano,H. (2004). Retinoic-acid-concentration-dependent acquisition of neural cell identity during in vitro differentiation of mouse embryonic stem cells. Dev. Biol. *275*, 124-142.

Olichon,A., Emorine,L.J., Descoins,E., Pelloquin,L., Brichese,L., Gas,N., Guillou,E., Delettre,C., Valette,A., Hamel,C.P., Ducommun,B., Lenaers,G., and Belenguer,P. (2002). The human dynamin-related protein OPA1 is anchored to the mitochondrial inner membrane facing the inter-membrane space. FEBS Lett. *523*, 171-176.

Rizzuto,R., Bernardi,P., and Pozzan,T. (2000). Mitochondria as all-round players of the calcium game. J. Physiol. *529 Pt 1:37-47*., 37-47.

Schapira,A.H. (2006). Mitochondrial disease. Lancet *368*, 70-82.

5. Conclusions

The work presented in this Thesis sheds new light on the functions of the mitochondria-shaping protein OPA1 and in particular, it contributes to elucidate how the genetic basis of its functional regulation.

Our results revealed that OPA1 controls the process of mitochondrial fusion, with a direct correlation observed between levels of OPA1 and fusion efficiency. Wild type, but not mutated OPA1 promotes mitochondrial fusion with the exchange of matricial content. This function of OPA1 requires an intact GTPase and C-terminal coiled coil domain, two hot-spots for OPA1 mutations in DOA. We performed a genetic analysis to elucidate the role of the putative outer membrane partners (the two mitofusins) in fusion driven by OPA1. Our results showed that OPA1 required Mitofusin 1, but not its close homologue Mitofusin 2. The generation of cells knocked down for OPA1 allowed us to further test the functional interdependence between OPA1 and MFN1. While MFN1 required adequate levels of OPA1, MFN2 could drive fusion independently of these. Our results unequivocally identify OPA1 as a player in the fusion of mammalian mitochondria and reveal a functional difference between MFN1 and MFN2 (Cipolat et al., 2004).

Since OPA1 is unable to promote fusion in the absence of MFN1, our results provide a framework to dissect specific effects of OPA1 during apoptosis on *cristae* structure *vs.* preservation of mitochondrial fusion. We demonstrated that mitochondrial remodelling and cytochrome *c* mobilization are regulated by levels of functional OPA1 and that this occurs independently from mitochondrial fusion. We also reveled that IMS and transmembrane OPA1 form oligomers that are early targets of BID during cristae remodeling (Frezza et al., 2006).

We therefore extended our investigation to the regulation of the antiapoptotic function of OPA1. In yeast the orthologue of OPA1 Mgm1p is cleaved and functionally activated by Rbd1p. PARL (Presenilin associated rhomboid-like) is the mammalian orthologue of Rbd1p and can functionally replace it in yeast cells, thus emerging as an attractive candidate for the regulation of the multiple functions of OPA1. We again decided to use the tools of genetics and we investigated the phenotype of a *Parl*$^{-/-}$ mouse. This mouse has a complex phenotype of multisystemic apoptosis, leading to premature death. By analyzing multiple primary and transformed cell types, we could rule out a role for mitochondrial dysfunction or loss of fusion in this phenotype of the *Parl*$^{-/-}$ mouse. Conversely, we demonstrated that it results from a specific defect in the *cristae*-remodelling pathway controlled by OPA1. Using a combination of genetics, physiology and biochemistry, we show that PARL regulates the mitochondrial pathway of apoptosis. We further demonstrate that OPA1 is cleaved in a process that requires the rhomboid protease PARL, to generate a relatively scarce soluble, IMS form. This soluble OPA1 has a role in apoptosis but not in the regulation of mitochondrial morphology (Frezza et al.,

2006; Cipolat et al., 2006). We did not proof that PARL cleaves OPA1 directly. PARL could act indirectly *via* activation of another, unknown protease. Alternatively, OPA1 can be independently processed by multiple proteases, PARL being just one of them. These possibilities are supported by the retrieval of traces of IMS-OPA1 also in *Parl*$^{-/-}$ MEFs. Along this line, it has been reported by Mihara and colleagues demonstrated that in mammalian cells Opa1 can be cleaved by the m-AAA protease paraplegin. The m-AAA protease is known to mediate the ATP-dependent dislocation of proteins from the membrane to allow their complete proteolysis in a hydrophilic environment (Leonhard et al., 2000). Interestingly, the ATP-dependent membrane dislocation of cytochrome *c* peroxidase by the m-AAA protease in yeast was recently found to facilitate maturation by the rhomboid protease Pcp1 (Tatsuta et al., 2007; Esser et al., 2002). In case of OPA1 processing in yeast cells, Pcp1 and m-AAA protease might be involved independently but not sequentially, as the processing intermediate was not detected in Δpcp1 cells in contrast to the case for yeast cytochrome *c* peroxidise (Ishihara et al., 2006). In yeast mAAA is a hetero-multimeric complex composed of Yta10/Afg3 and Yta12/Rca1. While OPA1 processing was almost completely blocked in Δyta10 and Δyta12 strains, processing of endogenous Mgm1p was not affected. In human two m-AAA proteases, paraplegin and AFG3L2, are expressed and form a high molecular weight complex in the mitochondrial inner membrane (Atorino et al., 2003). Although mutation in paraplegin causes an autosomal recessive form of hereditary spastic paraplegia, HSP, characterized by oxidative phosphorylation defects and neuronal degeneration, (Casari et al., 1998; Ferreirinha et al., 2004) its specific substrates are not fully understood. The function of AFG3L2 is not known (Banfi et al., 1999). In mouse mAAA is composed of Paraplegin, which forms only hetero-oligomers with the other components, Afg3L1 and Afg3l2, which can form both homo and hetero-oligomers. It should be noted that Paraplegin faces the matrix and that the mitochondrial processing peptidase already trims most of the matrix residues of Opa1 (Olichon et al., 2002).
More recently the group of D. Chan demonstrated that the cleavage of Opa1 is regulated by the i-AAA protease Yme1L (Griparic et al., 2007; Song et al., 2007).
Further investigation are required to better understand which protease cleave OPA1, where, and which function of the protein is regulated by the cleavage.
In conclusion the work presented in this Thesis elucidates that in mammalian cells OPA1 plays two genetically distinct roles in promoting mitochondrial fusion by cooperating with MFN1 (Cipolat et al., 2004), a large GTPase of the outer mitochondrial membrane; and in regulating apoptosis, controlled by the mitochondrial rhomboid protease PARL (Frezza et al., 2006; Cipolat et al., 2006). These distinct and differently regulated functions of OPA1 could have major consequences on the ability of OPA1 to regulated *in vitro* differentiation of embryonic stem cells.

6. Reference list:

Alavi,M.V., Bette,S., Schimpf,S., Schuettauf,F., Schraermeyer,U., Wehrl,H.F., Ruttiger,L., Beck,S.C., Tonagel,F., Pichler,B.J., Knipper,M., Peters,T., Laufs,J., and Wissinger,B. (2007). A splice site mutation in the murine Opa1 gene features pathology of autosomal dominant optic atrophy. Brain *130*, 1029-1042.

Alexander,C., Votruba,M., Pesch,U.E., Thiselton,D.L., Mayer,S., Moore,A., Rodriguez,M., Kellner,U., Leo-Kottler,B., Auburger,G., Bhattacharya,S.S., and Wissinger,B. (2000). OPA1, encoding a dynamin-related GTPase, is mutated in autosomal dominant optic atrophy linked to chromosome 3q28. Nat. Genet. *26*, 211-215.

Alirol,E., James,D., Huber,D., Marchetto,A., Vergani,L., Martinou,J.C., and Scorrano,L. (2006). The mitochondrial fission protein hFis1 requires the endoplasmic reticulum gateway to induce apoptosis. Mol. Biol. Cell *17*, 4593-4605.

Allen,J.F., Puthiyaveetil,S., Strom,J., and Allen,C.A. (2005). Energy transduction anchors genes in organelles. Bioessays *27*, 426-435.

Amchenkova,A.A., Bakeeva,L.E., Chentsov,Y.S., Skulachev,V.P., and Zorov,D.B. (1988). Coupling membranes as energy-transmitting cables. I. Filamentous mitochondria in fibroblasts and mitochondrial clusters in cardiomyocytes. J. Cell Biol. *107*, 481-495.

Amutha,B., Gordon,D.M., Gu,Y., and Pain,D. (2004). A novel role of Mgm1p, a dynamin-related GTPase, in ATP synthase assembly and cristae formation/maintenance. Biochem J *381*, 19-23.

Anderson,L. (1981). Identification of mitochondrial proteins and some of their precursors in two-dimensional electrophoretic maps of human cells. Proc. Natl. Acad. Sci. U. S. A *78*, 2407-2411.

Atorino,L., Silvestri,L., Koppen,M., Cassina,L., Ballabio,A., Marconi,R., Langer,T., and Casari,G. (2003). Loss of m-AAA protease in mitochondria causes complex I deficiency and increased sensitivity to oxidative stress in hereditary spastic paraplegia. J. Cell Biol. *163*, 777-787.

Attardi,G. and Schatz,G. (1988). Biogenesis of mitochondria. Annu. Rev. Cell Biol. *4*, 289-333.

Bach,D., Pich,S., Soriano,F.X., Vega,N., Baumgartner,B., Oriola,J., Daugaard,J.R., Lloberas,J., Camps,M., Zierath,J.R., Rabasa-Lhoret,R., Wallberg-Henriksson,H., Laville,M., Palacin,M., Vidal,H., Rivera,F., Brand,M., and Zorzano,A. (2003). Mitofusin-2 determines mitochondrial network architecture and mitochondrial metabolism. A novel regulatory mechanism altered in obesity. J. Biol. Chem. *278*, 17190-17197.

Banfi,S., Bassi,M.T., Andolfi,G., Marchitiello,A., Zanotta,S., Ballabio,A., Casari,G., and Franco,B. (1999). Identification and characterization of AFG3L2, a novel paraplegin-related gene. Genomics *59*, 51-58.

Baricault,L., Segui,B., Guegand,L., Olichon,A., Valette,A., Larminat,F., and Lenaers,G. (2007). OPA1 cleavage depends on decreased mitochondrial ATP level and bivalent metals. Exp. Cell Res. *313*, 3800-3808.

Berger,K.H. and Yaffe,M.P. (1996). Mitochondrial distribution and inheritance. Experientia *52*, 1111-1116.

Bernardi,P. and Azzone,G.F. (1981). Cytochrome c as an electron shuttle between the outer and inner mitochondrial membranes. J. Biol. Chem. *256*, 7187-7192.

Bernardi,P., Petronilli,V., Di,L.F., and Forte,M. (2001). A mitochondrial perspective on cell death. Trends Biochem. Sci. *26*, 112-117.

Bouhon,I.A., Joannides,A., Kato,H., Chandran,S., and Allen,N.D. (2006). Embryonic stem cell-derived neural progenitors display temporal restriction to neural patterning. Stem Cells *24*, 1908-1913.

Breckenridge,D.G., Stojanovic,M., Marcellus,R.C., and Shore,G.C. (2003). Caspase cleavage product of BAP31 induces mitochondrial fission through endoplasmic reticulum calcium signals, enhancing cytochrome c release to the cytosol. J. Cell Biol. *160*, 1115-1127.

Brown,M.S., Ye,J., Rawson,R.B., and Goldstein,J.L. (2000). Regulated intramembrane proteolysis: a control mechanism conserved from bacteria to humans. Cell *100*, 391-398.

Calvo,S., Jain,M., Xie,X., Sheth,S.A., Chang,B., Goldberger,O.A., Spinazzola,A., Zeviani,M., Carr,S.A., and Mootha,V.K. (2006). Systematic identification of human mitochondrial disease genes through integrative genomics. Nat. Genet. *38*, 576-582.

Campello,S., Lacalle,R.A., Bettella,M., Manes,S., Scorrano,L., and Viola,A. (2006). Orchestration of lymphocyte chemotaxis by mitochondrial dynamics. J. Exp. Med. *203*, 2879-2886.

Carelli,V., Ross-Cisneros,F.N., and Sadun,A.A. (2004). Mitochondrial dysfunction as a cause of optic neuropathies. Prog. Retin. Eye Res. *23*, 53-89.

Casari,G., De,F.M., Ciarmatori,S., Zeviani,M., Mora,M., Fernandez,P., De,M.G., Filla,A., Cocozza,S., Marconi,R., Durr,A., Fontaine,B., and Ballabio,A. (1998). Spastic paraplegia and OXPHOS impairment caused by mutations in paraplegin, a nuclear-encoded mitochondrial metalloprotease. Cell *93*, 973-983.

Castellani,R., Hirai,K., Aliev,G., Drew,K.L., Nunomura,A., Takeda,A., Cash,A.D., Obrenovich,M.E., Perry,G., and Smith,M.A. (2002). Role of mitochondrial dysfunction in Alzheimer's disease. J. Neurosci. Res. *70*, 357-360.

Catlett,N.L. and Weisman,L.S. (2000). Divide and multiply: organelle partitioning in yeast. Curr. Opin. Cell Biol. *12*, 509-516.

Cerveny,K.L. and Jensen,R.E. (2003). The WD-repeats of Net2p interact with Dnm1p and Fis1p to regulate division of mitochondria. Mol Biol Cell *14*.

Chang,C.R. and Blackstone,C. (2007). Cyclic AMP-dependent protein kinase phosphorylation of Drp1 regulates its GTPase activity and mitochondrial morphology. J. Biol. Chem. *282*, 21583-21587.

Chen,H., Detmer,S.A., Ewald,A.J., Griffin,E.E., Fraser,S.E., and Chan,D.C. (2003). Mitofusins Mfn1 and Mfn2 coordinately regulate mitochondrial fusion and are essential for embryonic development. J. Cell Biol. *160*, 189-200.

Chen,H., McCaffery,J.M., and Chan,D.C. (2007). Mitochondrial Fusion Protects against Neurodegeneration in the Cerebellum. Cell *130*, 548-562.

Chen,K.H., Guo,X., Ma,D., Guo,Y., Li,Q., Yang,D., Li,P., Qiu,X., Wen,S., Xiao,R.P., and Tang,J. (2004). Dysregulation of HSG triggers vascular proliferative disorders. Nat. Cell Biol. *6*, 872-883.

Cheng,E.H., Wei,M.C., Weiler,S., Flavell,R.A., Mak,T.W., Lindsten,T., and Korsmeyer,S.J. (2001). Bcl-2, bcl-x(l) sequester bh3 domain-only molecules preventing bax- and bak-mediated mitochondrial apoptosis. Mol. Cell *8*, 705-711.

Cho,Y.M., Kwon,S., Pak,Y.K., Seol,H.W., Choi,Y.M., Park,d.J., Park,K.S., and Lee,H.K. (2006). Dynamic changes in mitochondrial biogenesis and antioxidant enzymes during the spontaneous differentiation of human embryonic stem cells. Biochem. Biophys. Res. Commun. *348*, 1472-1478.

Choi,S.Y., Huang,P., Jenkins,G.M., Chan,D.C., Schiller,J., and Frohman,M.A. (2006). A common lipid links Mfn-mediated mitochondrial fusion and SNARE-regulated exocytosis. Nat. Cell Biol. *8*, 1255-1262.

Chung,S., Dzeja,P.P., Faustino,R.S., Perez-Terzic,C., Behfar,A., and Terzic,A. (2007). Mitochondrial oxidative metabolism is required for the cardiac differentiation of stem cells. Nat. Clin. Pract. Cardiovasc. Med. *4 Suppl 1*, S60-S67.

Cipolat,S., de Brito,O.M., Dal Zilio,B., and Scorrano,L. (2004). OPA1 requires mitofusin 1 to promote mitochondrial fusion. Proc. Natl. Acad. Sci. U. S. A *101*, 15927-15932.

Cipolat,S., Rudka,T., Hartmann,D., Costa,V., Serneels,L., Craessaerts,K., Metzger,K., Frezza,C., Annaert,W., D'Adamio,L., Derks,C., Dejaegere,T., Pellegrini,L., D'Hooge,R., Scorrano,L., and De Strooper,B. (2006). Mitochondrial Rhomboid PARL Regulates Cytochrome c Release during Apoptosis via OPA1-Dependent Cristae Remodeling. Cell *126*, 163-175.

Collins,T.J., Berridge,M.J., Lipp,P., and Bootman,M.D. (2002). Mitochondria are morphologically and functionally heterogeneous within cells. EMBO J. *21*, 1616-1627.

D'Herde,K., De Prest,B., Mussche,S., Schotte,P., Beyaert,R., Coster,R.V., and Roels,F. (2001). Ultrastructural localization of cytochrome c in apoptosis demonstrates mitochondrial heterogeneity. Cell Death. Differ. *7*, 331-337.

Danial,N.N., Gramm,C.F., Scorrano,L., Zhang,C.Y., Krauss,S., Ranger,A.M., Datta,S.R., Greenberg,M.E., Licklider,L.J., Lowell,B.B., Gygi,S.P., and Korsmeyer,S.J. (2003). BAD and glucokinase reside in a mitochondrial complex that integrates glycolysis and apoptosis. Nature *424*, 952-956.

Danial,N.N. and Korsmeyer,S.J. (2004). Cell death: critical control points. Cell *116*, 205-219.

Davies,V.J., Hollins,A.J., Piechota,M.J., Yip,W., Davies,J.R., White,K.E., Nicols,P.P., Boulton,M.E., and Votruba,M. (2007). Opa1 deficiency in a mouse model of autosomal dominant optic atrophy impairs mitochondrial morphology, optic nerve structure and visual function. Hum Mol Genet *16*, 1307-1318.

Dawson,T.M. and Dawson,V.L. (2003). Molecular pathways of neurodegeneration in Parkinson's disease. Science *302*, 819-822.

de Brito,O.M. and Scorrano,L. (2007). Mitofusin-2, A Mitochondria-Shaping Protein with Signaling Roles Beyond Fusion. Antioxid. Redox. Signal.

De Strooper,B., Annaert,W., Cupers,P., Saftig,P., Craessaerts,K., Mumm,J.S., Schroeter,E.H., Schrijvers,V., Wolfe,M.S., Ray,W.J., Goate,A., and Kopan,R. (1999). A presenilin-1-dependent gamma-secretase-like protease mediates release of Notch intracellular domain. Nature *398*, 518-522.

De Strooper,B., Saftig,P., Craessaerts,K., Vanderstichele,H., Guhde,G., Annaert,W., Von Figura,K., and Van Leuven,F. (1998). Deficiency of presenilin-1 inhibits the normal cleavage of amyloid precursor protein. Nature *391*, 387-390.

Del Rio,A., Dutta,K., Chavez,J., Ubarretxena-Belandia,I., and Ghose,R. (2007). Solution structure and dynamics of the N-terminal cytosolic domain of rhomboid intramembrane protease from Pseudomonas aeruginosa: insights into a functional role in intramembrane proteolysis. J. Mol. Biol. *365*, 109-122.

Delettre,C., Griffoin,J.M., Kaplan,J., Dollfus,H., Lorenz,B., Faivre,L., Lenaers,G., Belenguer,P., and Hamel,C.P. (2001). Mutation spectrum and splicing variants in the OPA1 gene. Hum. Genet. *109*, 584-591.

Delettre,C., Lenaers,G., Griffoin,J.M., Gigarel,N., Lorenzo,C., Belenguer,P., Pelloquin,L., Grosgeorge,J., Turc-Carel,C., Perret,E., Astarie-Dequeker,C., Lasquellec,L., Arnaud,B., Ducommun,B., Kaplan,J., and Hamel,C.P. (2000). Nuclear gene OPA1, encoding a mitochondrial dynamin-related protein, is mutated in dominant optic atrophy. Nat. Genet. *26*, 207-210.

Delettre,C., Lenaers,G., Pelloquin,L., Belenguer,P., and Hamel,C.P. (2002). OPA1 (Kjer type) dominant optic atrophy: a novel mitochondrial disease. Mol. Genet. Metab. *75*, 97-107.

Dimmer,K.S., Fritz,S., Fuchs,F., Messerschmitt,M., Weinbach,N., Neupert,W., and Westermann,B. (2002). Genetic basis of mitochondrial function and morphology in Saccharomyces cerevisiae. Mol. Biol. Cell *13*, 847-853.

Dimmer,K.S., Jakobs,S., Vogel,F., Altmann,K., and Westermann,B. (2005). Mdm31 and Mdm32 are inner membrane proteins required for maintenance of mitochondrial shape and stability of mitochondrial DNA nucleoids in yeast. J. Cell Biol. *168*, 103-115.

Dimmer,K.S., Navoni,F., Casarin,A., Trevisson,E., Endele,S., Winterpacht,A., Salviati,L., and Scorrano,L. (2008). LETM1, deleted in Wolf Hirschhorn syndrome is required for normal mitochondrial morphology and cellular viability. Hum. Mol. Genet. *17*, 201-214.

Dudkina,N.V., Heinemeyer,J., Keegstra,W., Boekema,E.J., and Braun,H.P. (2005). Structure of dimeric ATP synthase from mitochondria: an angular association of monomers induces the strong curvature of the inner membrane. FEBS Lett. *579*, 5769-5772.

Dumollard,R., Duchen,M., and Carroll,J. (2007). The role of mitochondrial function in the oocyte and embryo. Curr. Top. Dev. Biol. *77*, 21-49.

Duvezin-Caubet,S., Jagasia,R., Wagener,J., Hofmann,S., Trifunovic,A., Hansson,A., Chomyn,A., Bauer,M.F., Attardi,G., Larsson,N.G., Neupert,W., and Reichert,A.S. (2006). Proteolytic processing of OPA1 links mitochondrial dysfunction to alterations in mitochondrial morphology. J. Biol. Chem.

Escobar-Henriques,M., Westermann,B., and Langer,T. (2006). Regulation of mitochondrial fusion by the F-box protein Mdm30 involves proteasome-independent turnover of Fzo1. J. Cell Biol. *173*, 645-650.

Esser,K., Tursun,B., Ingenhoven,M., Michaelis,G., and Pratje,E. (2002). A novel two-step mechanism for removal of a mitochondrial signal sequence involves the mAAA complex and the putative rhomboid protease Pcp1. J Mol Biol *323*, 835-843.

Eura,Y., Ishihara,N., Yokota,S., and Mihara,K. (2003). Two mitofusin proteins, mammalian homologues of FZO, with distinct functions are both required for mitochondrial fusion. J. Biochem. (Tokyo) *134*, 333-344.

Evans,M.J. and Kaufman,M.H. (1981). Establishment in culture of pluripotential cells from mouse embryos. Nature *292*, 154-156.

Facucho-Oliveira,J.M., Alderson,J., Spikings,E.C., Egginton,S., and St John,J.C. (2007). Mitochondrial DNA replication during differentiation of murine embryonic stem cells. J. Cell Sci. *120*, 4025-4034.

Fannjiang,Y., Cheng,W.C., Lee,S.J., Qi,B., Pevsner,J., McCaffery,J.M., Hill,R.B., Basanez,G., and Hardwick,J.M. (2004). Mitochondrial fission proteins regulate programmed cell death in yeast. Genes Dev. *18*, 2785-2797.

Fehrenbacher,K.L., Yang,H.C., Gay,A.C., Huckaba,T.M., and Pon,L.A. (2004). Live cell imaging of mitochondrial movement along actin cables in budding yeast. Curr. Biol. *14*, 1996-2004.

Fernandez-Silva,P., Enriquez,J.A., and Montoya,J. (2003). Replication and transcription of mammalian mitochondrial DNA. Exp. Physiol *88*, 41-56.

Ferre,M., Amati-Bonneau,P., Tourmen,Y., Malthiery,Y., and Reynier,P. (2005). eOPA1: an online database for OPA1 mutations. Hum. Mutat. *25*, 423-428.

Ferreirinha,F., Quattrini,A., Pirozzi,M., Valsecchi,V., Dina,G., Broccoli,V., Auricchio,A., Piemonte,F., Tozzi,G., Gaeta,L., Casari,G., Ballabio,A., and Rugarli,E.I. (2004). Axonal degeneration in paraplegin-deficient mice is associated with abnormal mitochondria and impairment of axonal transport. J. Clin. Invest *113*, 231-242.

Feuerhake,F., Sigg,W., Hofter,E.A., Dimpfl,T., and Welsch,U. (2000). Immunohistochemical analysis of Bcl-2 and Bax expression in relation to cell turnover and epithelial differentiation markers in the non-lactating human mammary gland epithelium. Cell Tissue Res. *299*, 47-58.

Frank,S., Gaume,B., Bergmann-Leitner,E.S., Leitner,W.W., Robert,E.G., Catez,F., Smith,C.L., and Youle,R.J. (2001). The role of dynamin-related protein 1, a mediator of mitochondrial fission, in apoptosis. Dev. Cell *1*, 515-525.

Frederick,R.L., McCaffery,J.M., Cunningham,K.W., Okamoto,K., and Shaw,J.M. (2004). Yeast Miro GTPase, Gem1p, regulates mitochondrial morphology via a novel pathway. J. Cell Biol. *167*, 87-98.

Frey,T.G. and Mannella,C.A. (2000). The internal structure of mitochondria. Trends. Biochem. Sci. *25*, 319-324.

Frezza,C., Cipolat,S., Martins,d.B., Micaroni,M., Beznoussenko,G.V., Rudka,T., Bartoli,D., Polishuck,R.S., Danial,N.N., De Strooper,B., and Scorrano,L. (2006). OPA1 Controls Apoptotic Cristae Remodeling Independently from Mitochondrial Fusion. Cell *126*, 177-189.

Frieden,M., James,D., Castelbou,C., Danckaert,A., Martinou,J.C., and Demaurex,N. (2004). Ca^{2+} homeostasis during mitochondrial fragmentation and perinuclear clustering induced by hFis1. J. Biol. Chem. *279*, 22704-22714.

Fritz,S., Weinbach,N., and Westermann,B. (2003). Mdm30 is an F-box protein required for maintenance of fusion-competent mitochondria in yeast. Mol. Biol. Cell *14*, 2303-2313.

Gakh,O., Cavadini,P., and Isaya,G. (2002). Mitochondrial processing peptidases. Biochim Biophys Acta *1592*, 63-77.

Gallop,J.L., Butler,P.J., and McMahon,H.T. (2005). Endophilin and CtBP/BARS are not acyl transferases in endocytosis or Golgi fission. Nature *438*, 675-678.

Gallop,J.L., Jao,C.C., Kent,H.M., Butler,P.J., Evans,P.R., Langen,R., and McMahon,H.T. (2006). Mechanism of endophilin N-BAR domain-mediated membrane curvature. EMBO J. *25*, 2898-2910.

Germain,M., Mathai,J.P., McBride,H.M., and Shore,G.C. (2005). Endoplasmic reticulum BIK initiates DRP1-regulated remodelling of mitochondrial cristae during apoptosis. EMBO J. *24*, 1546-1556.

Glater,E.E., Megeath,L.J., Stowers,R.S., and Schwarz,T.L. (2006). Axonal transport of mitochondria requires milton to recruit kinesin heavy chain and is light chain independent. J. Cell Biol. *173*, 545-557.

Gorsich,S.W. and Shaw,J.M. (2004). Importance of mitochondrial dynamics during meiosis and sporulation. Mol. Biol. Cell *15*, 4369-4381.

Gossler,A., Doetschman,T., Korn,R., Serfling,E., and Kemler,R. (1986). Transgenesis by means of blastocyst-derived embryonic stem cell lines. Proc. Natl. Acad. Sci. U. S. A *83*, 9065-9069.

Green,D.R. and Kroemer,G. (2004). The pathophysiology of mitochondrial cell death. Science *305*, 626-629.

Griffin,E.E., Graumann,J., and Chan,D.C. (2005). The WD40 protein Caf4p is a component of the mitochondrial fission machinery and recruits Dnm1p to mitochondria. J Cell Biol *170*.

Griparic,L., Kanazawa,T., and van der Bliek,A.M. (2007). Regulation of the mitochondrial dynamin-like protein Opa1 by proteolytic cleavage. J. Cell Biol *178*, 757-764.

Griparic,L. and van der Bliek,A.M. (2001). The many shapes of mitochondrial membranes. Traffic *2*, 235-244.

Guillery,O., Malka,F., Landes,T., Guillou,E., Blackstone,C., Lombes,A., Belenguer,P., Arnoult,D., and Rojo,M. (2007). Metalloprotease-mediated OPA1 processing is modulated by the mitochondrial membrane potential. Biol. Cell.

Guo,X., Macleod,G.T., Wellington,A., Hu,F., Panchumarthi,S., Schoenfield,M., Marin,L., Charlton,M.P., Atwood,H.L., and Zinsmaier,K.E. (2005). The GTPase dMiro is required for axonal transport of mitochondria to Drosophila synapses. Neuron *47*, 379-393.

Hackenbrock,C.R. (1966). Ultrastructural bases for metabolically linked mechanical activity in mitochondria. I. Reversible ultrastructural changes with change in metabolic steady state in isolated liver mitochondria. J. Cell Biol. *30*, 269-297.

Hacker,G. (2000). The morphology of apoptosis. Cell Tissue Res. *301*, 5-17.

Hajek,P., Chomyn,A., and Attardi,G. (2007). Identification of a novel mitochondrial complex containing mitofusin 2 and stomatin-like protein 2. J. Biol. Chem. *282*, 5670-5681.

Hales,K.G. and Fuller,M.T. (1997). Developmentally regulated mitochondrial fusion mediated by a conserved, novel, predicted GTPase. Cell *90*, 121-129.

Hanahan,D. and Weinberg,R.A. (2000). The hallmarks of cancer. Cell *100*, 57-70.

Harder,Z., Zunino,R., and McBride,H. (2004). Sumo1 conjugates mitochondrial substrates and participates in mitochondrial fission. Curr. Biol. *14*, 340-345.

Hengartner,M.O. (2000). The biochemistry of apoptosis. Nature *407*, 770-776.

Herlan,M., Bornhovd,C., Hell,K., Neupert,W., and Reichert,A.S. (2004). Alternative topogenesis of Mgm1 and mitochondrial morphology depend on ATP and a functional import motor. J Cell Biol *165*, 167-173.

Herlan,M., Vogel,F., Bornhovd,C., Neupert,W., and Reichert,A.S. (2003). Processing of Mgm1 by the rhomboid-type protease Pcp1 is required for maintenance of mitochondrial morphology and of mitochondrial DNA. J. Biol. Chem. *278*, 27781-27788.

Hermann,G.J. and Shaw,J.M. (1998). Mitochondrial dynamics in yeast. Annu. Rev. Cell Dev. Biol. *14*, 265-303.

Hermann,G.J., Thatcher,J.W., Mills,J.P., Hales,K.G., Fuller,M.T., Nunnari,J., and Shaw,J.M. (1998). Mitochondrial fusion in yeast requires the transmembrane GTPase Fzo1p. J. Cell Biol. *143*, 359-373.

Hinshaw,J.E. (1999). Dynamin spirals. Curr. Opin. Struct. Biol *9*, 260-267.

Hobbs,A.E., Srinivasan,M., McCaffery,J.M., and Jensen,R.E. (2001). Mmm1p, a mitochondrial outer membrane protein, is connected to mitochondrial DNA (mtDNA) nucleoids and required for mtDNA stability. J. Cell Biol. *152*, 401-410.

Hollenbeck,P.J. and Saxton,W.M. (2005). The axonal transport of mitochondria. J. Cell Sci. *118*, 5411-5419.

Huang,T.T. and D'Andrea,A.D. (2006). HAUSP hunting the FOX(O). Nat. Cell Biol. *8*, 1043-1045.

Igaki,T., Kanuka,H., Inohara,N., Sawamoto,K., Nunez,G., Okano,H., and Miura,M. (2000). Drob-1, a Drosophila member of the Bcl-2/CED-9 family that promotes cell death. Proc. Natl. Acad. Sci U. S. A *97*, 662-667.

Ishihara,N., Eura,Y., and Mihara,K. (2004). Mitofusin 1 and 2 play distinct roles in mitochondrial fusion reactions via GTPase activity. J. Cell Sci. *117*, 6535-6546.

Ishihara,N., Fujita,Y., Oka,T., and Mihara,K. (2006). Regulation of mitochondrial morphology through proteolytic cleavage of OPA1. EMBO J. *25*, 2966-2977.

Jacobs,H.T., Lehtinen,S.K., and Spelbrink,J.N. (2000). No sex please, we're mitochondria: a hypothesis on the somatic unit of inheritance of mammalian mtDNA. Bioessays *22*, 564-572.

Jagasia,R., Grote,P., Westermann,B., and Conradt,B. (2005). DRP-1-mediated mitochondrial fragmentation during EGL-1-induced cell death in C. elegans. Nature *433*, 754-760.

James,D.I., Parone,P.A., Mattenberger,Y., and Martinou,J.C. (2003). hFis1, a novel component of the mammalian mitochondrial fission machinery. J. Biol. Chem. *278*, 36373-36379.

Jeyaraju,D., Xu,L., Letellier,M.C., Bandaru,S., Zunino,R., Berg,E.A., McBride,H., and Pellegrini,L. (2006). Phosphorylation and cleavage of a vertebrate-specific domain of the rhomboid protease PARL regulate mitochondrial morphology. Proc Natl Acad Sci U S A. 2006 103(49):18562-7.

John,G.B., Shang,Y., Li,L., Renken,C., Mannella,C.A., Selker,J.M., Rangell,L., Bennett,M.J., and Zha,J. (2005). The mitochondrial inner membrane protein mitofilin controls cristae morphology. Mol. Biol. Cell *16*, 1543-1554.

Johnson,E.S. (2004). Protein modification by SUMO. Annu. Rev Biochem *73*, 355-382.

Jones,B.A. and Fangman,W.L. (1992). Mitochondrial DNA maintenance in yeast requires a protein containing a region related to the GTP-binding domain of dynamin. Genes Dev. *6*, 380-389.

Jouaville,L.S., Ichas,F., Holmuhamedov,E.L., Camacho,P., and Lechleiter,J.D. (1995). Synchronization of calcium waves by mitochondrial substrates in Xenopus laevis oocytes. Nature *377*, 438-441.

Kang,D., Kim,S.H., and Hamasaki,N. (2007). Mitochondrial transcription factor A (TFAM): roles in maintenance of mtDNA and cellular functions. Mitochondrion. *7*, 39-44.

Kanki,T., Nakayama,H., Sasaki,N., Takio,K., Alam,T.I., Hamasaki,N., and Kang,D. (2004). Mitochondrial nucleoid and transcription factor A. Ann. N. Y. Acad. Sci. *1011*, 61-68.

Karbowski,M., Arnoult,D., Chen,H., Chan,D.C., Smith,C.L., and Youle,R.J. (2004a). Quantitation of mitochondrial dynamics by photolabeling of individual organelles shows that mitochondrial fusion is blocked during the Bax activation phase of apoptosis. J. Cell Biol. *164*, 493-499.

Karbowski,M., Jeong,S.Y., and Youle,R.J. (2004b). Endophilin B1 is required for the maintenance of mitochondrial morphology. J. Cell Biol. *166*, 1027-1039.

Karbowski,M., Neutzner,A., and Youle,R.J. (2007). The mitochondrial E3 ubiquitin ligase MARCH5 is required for Drp1 dependent mitochondrial division. J. Cell Biol *178*, 71-84.

Karbowski,M., Norris,K.L., Cleland,M.M., Jeong,S.Y., and Youle,R.J. (2006). Role of Bax and Bak in mitochondrial morphogenesis. Nature *443*, 658-662.

Karbowski,M. and Youle,R.J. (2003). Dynamics of mitochondrial morphology in healthy cells and during apoptosis. Cell Death. Differ. *10*, 870-880.

Karren,M.A., Coonrod,E.M., Anderson,T.K., and Shaw,J.M. (2005). The role of Fis1p-Mdv1p interactions in mitochondrial fission complex assembly. J Cell Biol *171*, 291-301.

Kay,B.K., Williamson,M.P., and Sudol,M. (2000). The importance of being proline: the interaction of proline-rich motifs in signaling proteins with their cognate domains. FASEB J. *14*, 231-241.

Kerr,J.F., Wyllie,A.H., and Currie,A.R. (1972). Apoptosis: a basic biological phenomenon with wide-ranging implications in tissue kinetics. Br. J. Cancer *26*, 239-257.

Kijima,K., Numakura,C., Izumino,H., Umetsu,K., Nezu,A., Shiiki,T., Ogawa,M., Ishizaki,Y., Kitamura,T., Shozawa,Y., and Hayasaka,K. (2005). Mitochondrial GTPase mitofusin 2 mutation in Charcot-Marie-Tooth neuropathy type 2A. Hum. Genet. *116*, 23-27.

Kim,J.Y., Hwang,J.M., Ko,H.S., Seong,M.W., Park,B.J., and Park,S.S. (2005). Mitochondrial DNA content is decreased in autosomal dominant optic atrophy. Neurology *64*, 966-972.

Kjer,B., Eiberg,H., Kjer,P., and Rosenberg,T. (1996). Dominant optic atrophy mapped to chromosome 3q region. II. Clinical and epidemiological aspects. Acta Ophthalmol Scand *74*.

Koehler,C.M. (2004). New developments in mitochondrial assembly. Annu Rev Cell Dev Biol *20*.

Koehler,C.M., Leuenberger,D., Merchant,S., Renold,A., Junne,T., and Schatz,G. (1999). Human deafness dystonia syndrome is a mitochondrial disease. Proc. Natl. Acad. Sci U. S. A *96*, 2141-2146.

Kondoh,H., Lleonart,M.E., Nakashima,Y., Yokode,M., Tanaka,M., Bernard,D., Gil,J., and Beach,D. (2007). A high glycolytic flux supports the proliferative potential of murine embryonic stem cells. Antioxid. Redox. Signal. *9*, 293-299.

Koonin,E.V., Makarova,K.S., Rogozin,I.B., Davidovic,L., Letellier,M.C., and Pellegrini,L. (2003). The rhomboids: a nearly ubiquitous family of intramembrane serine proteases that probably evolved by multiple ancient horizontal gene transfers. Genome Biol. *4*, R19.

Koshiba,T., Detmer,S.A., Kaiser,J.T., Chen,H., McCaffery,J.M., and Chan,D.C. (2004). Structural basis of mitochondrial tethering by mitofusin complexes. Science *305*, 858-862.

Krammer,P.H. (2000). CD95's deadly mission in the immune system. Nature *407*, 789-795.

Kroemer,G. and Zitvogel,L. (2007). Death, danger, and immunity: an infernal trio. Immunol. Rev. *220*, 5-7.

Labrousse,A.M., Zappaterra,M.D., Rube,D.A., and van der Bliek,A.M. (1999b). C. elegans dynamin-related protein DRP-1 controls severing of the mitochondrial outer membrane. Mol. Cell *4*, 815-826.

Labrousse,A.M., Zappaterra,M.D., Rube,D.A., and van der Bliek,A.M. (1999a). C. elegans dynamin-related protein DRP-1 controls severing of the mitochondrial outer membrane. Mol. Cell *4*, 815-826.

Langer,T., Kaser,M., Klanner,C., and Leonhard,K. (2001). AAA proteases of mitochondria: quality control of membrane proteins and regulatory functions during mitochondrial biogenesis. Biochem. Soc. Trans. *29*, 431-436.

Lawson,V.H., Graham,B.V., and Flanigan,K.M. (2005). Clinical and electrophysiologic features of CMT2A with mutations in the mitofusin 2 gene. Neurology *65*, 197-204.

Leahy,A., Xiong,J.W., Kuhnert,F., and Stuhlmann,H. (1999). Use of developmental marker genes to define temporal and spatial patterns of differentiation during embryoid body formation. J. Exp. Zool. *284*, 67-81.

Lee,Y.J., Jeong,S.Y., Karbowski,M., Smith,C.L., and Youle,R.J. (2004). Roles of the mammalian mitochondrial fission and fusion mediators Fis1, Drp1, and Opa1 in apoptosis. Mol. Biol. Cell *15*, 5001-5011.

Legros,F., Lombes,A., Frachon,P., and Rojo,M. (2002). Mitochondrial fusion in human cells is efficient, requires the inner membrane potential, and is mediated by mitofusins. Mol Biol Cell *13*, 4343-4354.

Legros,F., Malka,F., Frachon,P., Lombes,A., and Rojo,M. (2004). Organization and dynamics of human mitochondrial DNA. J Cell Sci *117*, 2653-2662.

Lemberg,M.K., Menendez,J., Misik,A., Garcia,M., Koth,C.M., and Freeman,M. (2005). Mechanism of intramembrane proteolysis investigated with purified rhomboid proteases. EMBO J *24*.

Leonhard,K., Guiard,B., Pellecchia,G., Tzagoloff,A., Neupert,W., and Langer,T. (2000). Membrane protein degradation by AAA proteases in mitochondria: extraction of substrates from either membrane surface. Mol. Cell *5*, 629-638.

Lettre,G. and Hengartner,M.O. (2006). Developmental apoptosis in C. elegans: a complex CEDnario. Nat Rev Mol Cell Biol *7*, 97-108.

Li,Z., Okamoto,K., Hayashi,Y., and Sheng,M. (2004). The importance of dendritic mitochondria in the morphogenesis and plasticity of spines and synapses. Cell *119*, 873-887.

Liu,S., Dontu,G., and Wicha,M.S. (2005). Mammary stem cells, self-renewal pathways, and carcinogenesis. Breast Cancer Res. *7*, 86-95.

Liu,X., Kim,C.N., Yang,J., Jemmerson,R., and Wang,X. (1996). Induction of apoptotic program in cell-free extracts: requirement for dATP and cytochrome c. Cell *86*, 147-157.

Lodi,R., Tonon,C., Valentino,M.L., Iotti,S., Clementi,V., Malucelli,E., Barboni,P., Longanesi,L., Schimpf,S., Wissinger,B., Baruzzi,A., Barbiroli,B., and Carelli,V. (2004). Deficit of in vivo mitochondrial ATP production in OPA1-related dominant optic atrophy. Ann. Neurol. *56*, 719-723.

Lonergan,T., Brenner,C., and Bavister,B. (2006). Differentiation-related changes in mitochondrial properties as indicators of stem cell competence. J. Cell Physiol *208*, 149-153.

Malka,F., Lombes,A., and Rojo,M. (2006). Organization, dynamics and transmission of mitochondrial DNA: focus on vertebrate nucleoids. Biochim. Biophys. Acta *1763*, 463-472.

Mannella,C.A., Marko,M., Penczek,P., Barnard,D., and Frank,J. (1994). The internal compartmentation of rat-liver mitochondria: tomographic study using the high-voltage transmission electron microscope. Microsc Res Tech *27*.

Margulis,L. (1971). The origin of plant and animal cells. Am. Sci. *59*, 230-235.

Martin,G.R. (1980). Teratocarcinomas and mammalian embryogenesis. Science *209*, 768-776.

mati-Bonneau,P., Valentino,M.L., Reynier,P., Gallardo,M.E., Bornstein,B., Boissiere,A., Campos,Y., Rivera,H., de la Aleja,J.G., Carroccia,R., Iommarini,L., Labauge,P., Figarella-Branger,D., Marcorelles,P., Furby,A., Beauvais,K., Letournel,F., Liguori,R., La,M.C., Montagna,P., Liguori,M., Zanna,C., Rugolo,M., Cossarizza,A., Wissinger,B., Verny,C., Schwarzenbacher,R., Martin,M.A., Arenas,J.I., Ayuso,C., Garesse,R., Lenaers,G., Bonneau,D., and Carelli,V. (2007). OPA1 mutations induce mitochondrial DNA instability and optic atrophy 'plus' phenotypes. Brain.

McQuibban,G.A., Lee,J.R., Zheng,L., Juusola,M., and Freeman,M. (2006). Normal mitochondrial dynamics requires rhomboid-7 and affects Drosophila lifespan and neuronal function. Curr Biol *16*, 537-541.

McQuibban,G.A., Saurya,S., and Freeman,M. (2003). Mitochondrial membrane remodelling regulated by a conserved rhomboid protease. Nature *423*, 537-541.

Meeusen,S., McCaffery,J.M., and Nunnari,J. (2004). Mitochondrial fusion intermediates revealed in vitro. Science *305*, 1747-1752.

Meier,P., Finch,A., and Evan,G. (2000). Apoptosis in development. Nature *407*, 796-801.

Messerschmitt,M., Jakobs,S., Vogel,F., Fritz,S., Dimmer,K.S., Neupert,W., and Westermann,B. (2003). The inner membrane protein Mdm33 controls mitochondrial morphology in yeast. J. Cell Biol. *160*, 553-564.

Minauro-Sanmiguel,F., Wilkens,S., and Garcia,J.J. (2005). Structure of dimeric mitochondrial ATP synthase: novel F0 bridging features and the structural basis of mitochondrial cristae biogenesis. Proc. Natl. Acad. Sci. U. S. A *102*, 12356-12358.

Misaka,T., Miyashita,T., and Kubo,Y. (2002). Primary structure of a dynamin-related mouse mitochondrial GTPase and its distribution in brain, subcellular localization, and effect on mitochondrial morphology. J Biol Chem *277*.

Mitchell,P. (1979). Keilin's respiratory chain concept and its chemiosmotic consequences. Science *206*, 1148-1159.

Morris,R.L. and Hollenbeck,P.J. (1995). Axonal transport of mitochondria along microtubules and F-actin in living vertebrate neurons. J. Cell Biol. *131*, 1315-1326.

Nakamura,N., Kimura,Y., Tokuda,M., Honda,S., and Hirose,S. (2006). MARCH-V is a novel mitofusin 2- and Drp1-binding protein able to change mitochondrial morphology. EMBO Rep. *7*, 1019-1022.

Neutzner,A. and Youle,R.J. (2005). Instability of the mitofusin Fzo1 regulates mitochondrial morphology during the mating response of the yeast Saccharomyces cerevisiae. J Biol Chem *280*.

Nosek,J. and Tomaska,L. (2003). Mitochondrial genome diversity: evolution of the molecular architecture and replication strategy. Curr. Genet. *44*, 73-84.

Nowikovsky,K., Froschauer,E.M., Zsurka,G., Samaj,J., Reipert,S., Kolisek,M., Wiesenberger,G., and Schweyen,R.J. (2004). The LETM1/YOL027 gene family encodes a factor of the mitochondrial K+ homeostasis with a potential role in the Wolf-Hirschhorn syndrome. J. Biol. Chem. *279*, 30307-30315.

Okamoto,K. and Shaw,J.M. (2005). Mitochondrial morphology and dynamics in yeast and multicellular eukaryotes. Annu. Rev. Genet. *39*, 503-536.

Olichon,A., Baricault,L., Gas,N., Guillou,E., Valette,A., Belenguer,P., and Lenaers,G. (2003). Loss of OPA1 perturbates the mitochondrial inner membrane structure and integrity, leading to cytochrome c release and apoptosis. J. Biol. Chem. *278*, 7743-7746.

Olichon,A., Emorine,L.J., Descoins,E., Pelloquin,L., Brichese,L., Gas,N., Guillou,E., Delettre,C., Valette,A., Hamel,C.P., Ducommun,B., Lenaers,G., and Belenguer,P. (2002). The human dynamin-related protein OPA1 is anchored to the mitochondrial inner membrane facing the inter-membrane space. FEBS Lett. *523*, 171-176.

Olichon,A., Landes,T., Arnaune-Pelloquin,L., Emorine,L.J., Mils,V., Guichet,A., Delettre,C., Hamel,C., Amati-Bonneau,P., Bonneau,D., Reynier,P., Lenaers,G., and Belenguer,P. (2007). Effects of OPA1 mutations on mitochondrial morphology and apoptosis: relevance to ADOA pathogenesis. J. Cell Physiol *211*, 423-430.

Pacher,P. and Hajnoczky,G. (2001). Propagation of the apoptotic signal by mitochondrial waves. EMBO J. *20*, 4107-4121.

Palade,G.E. (1952). The fine structure of mitochondria. Anat. Rec. *114*, 427-451.

Paumard,P., Vaillier,J., Coulary,B., Schaeffer,J., Soubannier,V., Mueller,D.M., Brethes,D., di Rago,J.P., and Velours,J. (2002). The ATP synthase is involved in generating mitochondrial cristae morphology. EMBO J. *21*, 221-230.

Pellegrini,L., Passer,B.J., Canelles,M., Lefterov,I., Ganjei,J.K., Fowlkes,B.J., Koonin,E.V., and D'Adamio,L. (2001). PAMP and PARL, two novel putative metalloproteases interacting with the COOH-terminus of Presenilin-1 and -2. J. Alzheimers. Dis. *3*, 181-190.

Pelloquin,L., Belenguer,P., Menon,Y., Gas,N., and Ducommun,B. (1999). Fission yeast Msp1 is a mitochondrial dynamin-related protein. J. Cell Sci. *112*.

Perkins,G.A., Renken,C.W., Frey,T.G., and Ellisman,M.H. (2001). Membrane architecture of mitochondria in neurons of the central nervous system. J Neurosci Res *66*.

Perotti,M.E., Anderson,W.A., and Swift,H. (1983). Quantitative cytochemistry of the diaminobenzidine cytochrome oxidase reaction product in mitochondria of cardiac muscle and pancreas. J. Histochem. Cytochem. *31*, 351-365.

Peters,R., Leyvraz,S., and Perey,L. (1998). Apoptotic regulation in primitive hematopoietic precursors. Blood *92*, 2041-2052.

Pevny,L.H., Sockanathan,S., Placzek,M., and Lovell-Badge,R. (1998). A role for SOX1 in neural determination. Development *125*, 1967-1978.

Poyton,R.O. and McEwen,J.E. (1996). Crosstalk between nuclear and mitochondrial genomes. Annu. Rev. Biochem. *65*, 563-607.

Prokisch,H., Scharfe,C., Camp,D.G., Xiao,W., David,L., Andreoli,C., Monroe,M.E., Moore,R.J., Gritsenko,M.A., Kozany,C., Hixson,K.K., Mottaz,H.M., Zischka,H., Ueffing,M., Herman,Z.S., Davis,R.W., Meitinger,T., Oefner,P.J., Smith,R.D., and Steinmetz,L.M. (2004). Integrative analysis of the mitochondrial proteome in yeast. PLoS. Biol. *2*, e160.

Rapaport,D., Brunner,M., Neupert,W., and Westermann,B. (1998). Fzo1p is a mitochondrial outer membrane protein essential for the biogenesis of functional mitochondria in Saccharomyces cerevisiae. J. Biol. Chem. *273*, 20150-20155.

Rawson,R.B., Zelenski,N.G., Nijhawan,D., Ye,J., Sakai,J., Hasan,M.T., Chang,T.Y., Brown,M.S., and Goldstein,J.L. (1997). Complementation cloning of S2P, a gene encoding a putative metalloprotease required for intramembrane cleavage of SREBPs. Mol Cell *1*, 45-57.

Reiter,R.E., Gu,Z., Watabe,T., Thomas,G., Szigeti,K., Davis,E., Wahl,M., Nisitani,S., Yamashiro,J., Le Beau,M.M., Loda,M., and Witte,O.N. (1998). Prostate stem cell antigen: a cell surface marker overexpressed in prostate cancer. Proc. Natl. Acad. Sci. U. S. A *95*, 1735-1740.

Reya,T., Morrison,S.J., Clarke,M.F., and Weissman,I.L. (2001b). Stem cells, cancer, and cancer stem cells. Nature *414*, 105-111.

Reya,T., Morrison,S.J., Clarke,M.F., and Weissman,I.L. (2001a). Stem cells, cancer, and cancer stem cells. Nature *414*, 105-111.

Rizzuto,R., Bernardi,P., and Pozzan,T. (2000). Mitochondria as all-round players of the calcium game. J Physiol *529 Pt 1*, 37-47.

Robertson,E., Bradley,A., Kuehn,M., and Evans,M. (1986). Germ-line transmission of genes introduced into cultured pluripotential cells by retroviral vector. Nature *323*, 445-448.

Rodriguez,J. and Lazebnik,Y. (1999). Caspase-9 and APAF-1 form an active holoenzyme. Genes Dev. *13*, 3179-3184.

Rojo,M., Legros,F., Chateau,D., and Lombes,A. (2002). Membrane topology and mitochondrial targeting of mitofusins, ubiquitous mammalian homologs of the transmembrane GTPase Fzo. J. Cell Sci. *115*, 1663-1674.

Rolletschek,A., Chang,H., Guan,K., Czyz,J., Meyer,M., and Wobus,A.M. (2001). Differentiation of embryonic stem cell-derived dopaminergic neurons is enhanced by survival-promoting factors. Mech. Dev. *105*, 93-104.

Santel,A., Frank,S., Gaume,B., Herrler,M., Youle,R.J., and Fuller,M.T. (2003). Mitofusin-1 protein is a generally expressed mediator of mitochondrial fusion in mammalian cells. J. Cell Sci. *116*, 2763-2774.

Santel,A. and Fuller,M.T. (2001). Control of mitochondrial morphology by a human mitofusin. J. Cell Sci. *114*, 867-874.

Satoh,M., Hamamoto,T., Seo,N., Kagawa,Y., and Endo,H. (2003). Differential sublocalization of the dynamin-related protein OPA1 isoforms in mitochondria. Biochem. Biophys. Res. Commun. *300*, 482-493.

Schapira,A.H. (2006). Mitochondrial disease. Lancet *368*, 70-82.

Schmidt,A., Wolde,M., Thiele,C., Fest,W., Kratzin,H., Podtelejnikov,A.V., Witke,W., Huttner,W.B., and Soling,H.D. (1999). Endophilin I mediates synaptic vesicle formation by transfer of arachidonate to lysophosphatidic acid. Nature *401*, 133-141.

Scorrano,L., Ashiya,M., Buttle,K., Weiler,S., Oakes,S.A., Mannella,C.A., and Korsmeyer,S.J. (2002). A Distinct Pathway Remodels Mitochondrial Cristae and Mobilizes Cytochrome c during Apoptosis. Dev. Cell *2*, 55-67.

Scorrano,L. and Korsmeyer,S.J. (2003). Mechanisms of cytochrome c release by proapoptotic BCL-2 family members. Biochemical and Biophysical Research Communications *304*, 437-444.

Sesaki,H., Dunn,C.D., Iijima,M., Shepard,K.A., Yaffe,M.P., Machamer,C.E., and Jensen,R.E. (2006). Ups1p, a conserved intermembrane space protein, regulates mitochondrial shape and alternative topogenesis of Mgm1p. J. Cell Biol. *173*, 651-658.

Sesaki,H. and Jensen,R.E. (2001). UGO1 encodes an outer membrane protein required for mitochondrial fusion. J. Cell Biol. *152*, 1123-1134.

Sesaki,H. and Jensen,R.E. (2004). Ugo1p links the Fzo1p and Mgm1p GTPases for mitochondrial fusion. J Biol Chem. *279*, 28298-28303.

Sesaki,H., Southard,S.M., Hobbs,A.E., and Jensen,R.E. (2003a). Cells lacking Pcp1p/Ugo2p, a rhomboid-like protease required for Mgm1p processing, lose mtDNA and mitochondrial structure in a Dnm1p-dependent manner, but remain competent for mitochondrial fusion. Biochem. Biophys. Res. Commun. *308*, 276-283.

Sesaki,H., Southard,S.M., Yaffe,M.P., and Jensen,R.E. (2003b). Mgm1p, a dynamin-related GTPase, is essential for fusion of the mitochondrial outer membrane. Mol. Biol. Cell *14*, 2342-2356.

Shaw,J.M. and Nunnari,J. (2002). Mitochondrial dynamics and division in budding yeast. Trends Cell Biol. *12*, 178-184.

Shoubridge,E.A. and Wai,T. (2007). Mitochondrial DNA and the mammalian oocyte. Curr. Top. Dev. Biol. *77*, 87-111.

Sickmann,A., Reinders,J., Wagner,Y., Joppich,C., Zahedi,R., Meyer,H.E., Schonfisch,B., Perschil,I., Chacinska,A., Guiard,B., Rehling,P., Pfanner,N., and Meisinger,C. (2003). The proteome of Saccharomyces cerevisiae mitochondria. Proc. Natl. Acad. Sci. U. S. A *100*, 13207-13212.

Sik,A., Passer,B.J., Koonin,E.V., and Pellegrini,L. (2004). Self-regulated cleavage of the mitochondrial intramembrane-cleaving protease PARL yields Pbeta, a nuclear-targeted peptide. J Biol Chem. *279*, 15323-15329.

Smirnova,E., Griparic,L., Shurland,D.L., and van der Bliek,A.M. (2001). Dynamin-related protein Drp1 is required for mitochondrial division in mammalian cells. Mol. Biol. Cell *12*, 2245-2256.

Smithies,O., Gregg,R.G., Boggs,S.S., Koralewski,M.A., and Kucherlapati,R.S. (1985). Insertion of DNA sequences into the human chromosomal beta-globin locus by homologous recombination. Nature *317*, 230-234.

Song,Z., Chen,H., Fiket,M., Alexander,C., and Chan,D.C. (2007). OPA1 processing controls mitochondrial fusion and is regulated by mRNA splicing, membrane potential, and Yme1L. J. Cell Biol *178*, 749-755.

Spitkovsky,D., Sasse,P., Kolossov,E., Bottinger,C., Fleischmann,B.K., Hescheler,J., and Wiesner,R.J. (2004). Activity of complex III of the mitochondrial electron transport chain is essential for early heart muscle cell differentiation. FASEB J. *18*, 1300-1302.

St John,J.C., Ramalho-Santos,J., Gray,H.L., Petrosko,P., Rawe,V.Y., Navara,C.S., Simerly,C.R., and Schatten,G.P. (2005). The expression of mitochondrial DNA transcription factors during early cardiomyocyte in vitro differentiation from human embryonic stem cells. Cloning Stem Cells *7*, 141-153.

Staub,O. and Rotin,D. (2006). Role of ubiquitylation in cellular membrane transport. Physiol Rev. *86*, 669-707.

Stojanovski,D., Koutsopoulos,O.S., Okamoto,K., and Ryan,M.T. (2004). Levels of human Fis1 at the mitochondrial outer membrane regulate mitochondrial morphology. J Cell Sci *117*.

Stowers,R.S., Megeath,L.J., Gorska-Andrzejak,J., Meinertzhagen,I.A., and Schwarz,T.L. (2002). Axonal transport of mitochondria to synapses depends on milton, a novel Drosophila protein. Neuron *36*, 1063-1077.

Sugioka,R., Shimizu,S., and Tsujimoto,Y. (2004). Fzo1, a protein involved in mitochondrial fusion, inhibits apoptosis. J. Biol. Chem. *279*, 52726-52734.

Suzuki,M., Jeong,S.Y., Karbowski,M., Youle,R.J., and Tjandra,N. (2003). The solution structure of human mitochondria fission protein Fis1 reveals a novel TPR-like helix bundle. J. Mol. Biol. *334*, 445-458.

Szabadkai,G., Simoni,A.M., Chami,M., Wieckowski,M.R., Youle,R.J., and Rizzuto,R. (2004). Drp-1-dependent division of the mitochondrial network blocks intraorganellar Ca^{2+} waves and protects against Ca^{2+}-mediated apoptosis. Mol Cell *16*, 59-68.

Taguchi,N., Ishihara,N., Jofuku,A., Oka,T., and Mihara,K. (2007). Mitotic phosphorylation of dynamin-related GTPase Drp1 participates in mitochondrial fission. J. Biol. Chem. *282*, 11521-11529.

Tatsuta,T., Augustin,S., Nolden,M., Friedrichs,B., and Langer,T. (2007). m-AAA protease-driven membrane dislocation allows intramembrane cleavage by rhomboid in mitochondria. EMBO J. *26*, 325-335.

Terskikh,A.V., Easterday,M.C., Li,L., Hood,L., Kornblum,H.I., Geschwind,D.H., and Weissman,I.L. (2001). From hematopoiesis to neuropoiesis: evidence of overlapping genetic programs. Proc. Natl. Acad. Sci. U. S. A *98*, 7934-7939.

Thomas,K.R. and Capecchi,M.R. (1987). Site-directed mutagenesis by gene targeting in mouse embryo-derived stem cells. Cell *51*, 503-512.

Thompson,S., Clarke,A.R., Pow,A.M., Hooper,M.L., and Melton,D.W. (1989). Germ line transmission and expression of a corrected HPRT gene produced by gene targeting in embryonic stem cells. Cell *56*, 313-321.

Thundathil,J., Filion,F., and Smith,L.C. (2005). Molecular control of mitochondrial function in preimplantation mouse embryos. Mol. Reprod. Dev. *71*, 405-413.

Tieu,Q., Okreglak,V., Naylor,K., and Nunnari,J. (2002). The WD repeat protein, Mdv1p, functions as a molecular adaptor by interacting with Dnm1p and Fis1p during mitochondrial fission. J. Cell Biol. *158*, 445-452.

Tondera,D., Czauderna,F., Paulick,K., Schwarzer,R., Kaufmann,J., and Santel,A. (2005). The mitochondrial protein MTP18 contributes to mitochondrial fission in mammalian cells. J Cell Sci *118*.

Tondera,D., Santel,A., Schwarzer,R., Dames,S., Giese,K., Klippel,A., and Kaufmann,J. (2004). Knockdown of MTP18, a novel phosphatidylinositol 3-kinase-dependent protein, affects mitochondrial morphology and induces apoptosis. J Biol Chem *279*.

Trimmer,P.A., Swerdlow,R.H., Parks,J.K., Keeney,P., Bennett,J.P., Jr., Miller,S.W., Davis,R.E., and Parker,W.D., Jr. (2000). Abnormal mitochondrial morphology in sporadic Parkinson's and Alzheimer's disease cybrid cell lines. Exp. Neurol. *162*, 37-50.

Urban,S. and Freeman,M. (2003). Substrate specificity of rhomboid intramembrane proteases is governed by helix-breaking residues in the substrate transmembrane domain. Mol. Cell *11*, 1425-1434.

Urban,S. and Freeman,M. (2002). Intramembrane proteolysis controls diverse signalling pathways throughout evolution. Curr Opin Genet Dev *12*.

Urban,S., Lee,J.R., and Freeman,M. (2001). Drosophila rhomboid-1 defines a family of putative intramembrane serine proteases. Cell *107*, 173-182.

Urban,S. and Wolfe,M.S. (2005). Reconstitution of intramembrane proteolysis in vitro reveals that pure rhomboid is sufficient for catalysis and specificity. Proc Natl Acad Sci U S A *102*, 1883-1888.

van der Bliek,A.M. (2000). A mitochondrial division apparatus takes shape. J. Cell Biol. *151*, F1-F4.

Votruba,M., Moore,A.T., and Bhattacharya,S.S. (1997). Genetic refinement of dominant optic atrophy (OPA1) locus to within a 2 cM interval of chromosome 3q. J. Med. Genet. *34*, 117-121.

Votruba,M., Moore,A.T., and Bhattacharya,S.S. (1998). Clinical features, molecular genetics, and pathophysiology of dominant optic atrophy. J. Med. Genet. *35*, 793-800.

Wang,X. (2001). The expanding role of mitochondria in apoptosis. Genes Dev. *15*, 2922-2933.

Wang,Y., Zhang,Y., and Ha,Y. (2006). Crystal structure of a rhomboid family intramembrane protease. Nature *444*, 179-180.

WARBURG,O. (1956). On respiratory impairment in cancer cells. Science *124*, 269-270.

Waterham,H.R., Koster,J., van Roermund,C.W., Mooyer,P.A., Wanders,R.J., and Leonard,J.V. (2007). A lethal defect of mitochondrial and peroxisomal fission. N. Engl. J. Med. *356*, 1736-1741.

Weiss,M.J. and Orkin,S.H. (1996). In vitro differentiation of murine embryonic stem cells. New approaches to old problems. J. Clin. Invest *97*, 591-595.

Welchman,R.L., Gordon,C., and Mayer,R.J. (2005). Ubiquitin and ubiquitin-like proteins as multifunctional signals. Nat. Rev. Mol. Cell Biol. *6*, 599-609.

Wilkinson,D.G., Bhatt,S., and Herrmann,B.G. (1990a). Expression pattern of the mouse T gene and its role in mesoderm formation. Nature *343*, 657-659.

Wilkinson,D.G., Bhatt,S., and Herrmann,B.G. (1990b). Expression pattern of the mouse T gene and its role in mesoderm formation. Nature *343*, 657-659.

Willis,S.N., Chen,L., Dewson,G., Wei,A., Naik,E., Fletcher,J.I., Adams,J.M., and Huang,D.C. (2005). Proapoptotic Bak is sequestered by Mcl-1 and Bcl-xL, but not Bcl-2, until displaced by BH3-only proteins. Genes Dev. *19*, 1294-1305.

Wong,E.D., Wagner,J.A., Gorsich,S.W., McCaffery,J.M., Shaw,J.M., and Nunnari,J. (2000). The dynamin-related GTPase, Mgm1p, is an intermembrane space protein required for maintenance of fusion competent mitochondria. J. Cell Biol. *151*, 341-352.

Wong,E.D., Wagner,J.A., Scott,S.V., Okreglak,V., Holewinske,T.J., Cassidy-Stone,A., and Nunnari,J. (2003). The intramitochondrial dynamin-related GTPase, Mgm1p, is a component of a protein complex that mediates mitochondrial fusion. J. Cell Biol. *160*, 303-311.

Yonashiro,R., Ishido,S., Kyo,S., Fukuda,T., Goto,E., Matsuki,Y., Ohmura-Hoshino,M., Sada,K., Hotta,H., Yamamura,H., Inatome,R., and Yanagi,S. (2006). A novel mitochondrial ubiquitin ligase plays a critical role in mitochondrial dynamics. EMBO J. *25*, 3618-3626.

Yoon,Y., Krueger,E.W., Oswald,B.J., and McNiven,M.A. (2003). The mitochondrial protein hFis1 regulates mitochondrial fission in mammalian cells through an interaction with the dynamin-like protein DLP1. Mol. Cell Biol. *23*, 5409-5420.

Youle,R.J. and Karbowski,M. (2005). Mitochondrial fission in apoptosis. Nat Rev Mol Cell Biol *6*, 657-663.

Zhou,S., Schuetz,J.D., Bunting,K.D., Colapietro,A.M., Sampath,J., Morris,J.J., Lagutina,I., Grosveld,G.C., Osawa,M., Nakauchi,H., and Sorrentino,B.P. (2001). The ABC transporter Bcrp1/ABCG2 is expressed in a wide variety of stem cells and is a molecular determinant of the side-population phenotype. Nat. Med. *7*, 1028-1034.

Zou,H., Li,Y., Liu,X., and Wang,X. (1999). An APAF-1.cytochrome c multimeric complex is a functional apoptosome that activates procaspase-9. J Biol Chem *274*.

Zuchner,S., Mersiyanova,I.V., Muglia,M., Bissar-Tadmouri,N., Rochelle,J., Dadali,E.L., Zappia,M., Nelis,E., Patitucci,A., Senderek,J., Parman,Y., Evgrafov,O., Jonghe,P.D., Takahashi,Y., Tsuji,S., Pericak-Vance,M.A., Quattrone,A., Battologlu,E., Polyakov,A.V., Timmerman,V., Schroder,J.M., and Vance,J.M. (2004). Mutations in the mitochondrial GTPase mitofusin 2 cause Charcot-Marie-Tooth neuropathy type 2A. Nat. Genet.

Zuchner,S. and Vance,J.M. (2006). Mechanisms of disease: a molecular genetic update on hereditary axonal neuropathies. Nat. Clin. Pract. Neurol. *2*, 45-53.